rAAV-based gene therapy for molybdenum cofactor deficiency type B

Doctoral thesis

In partial fulfilment of the requirements for the degree

"Doctor rerum naturalium (Dr. rer. nat.)"

in the Molecular Medicine Study Program

at the Georg-August University Göttingen

submitted by

Joanna Jakubiczka-Smorag

born in

Czestochowa, Poland

Göttingen, 2015

Members of the Thesis Committee:

Supervisor

Prof. Dr. rer. nat. Peter Burfeind

Institute of Human Genetics, University Medical Centre Göttingen

Second member of the Thesis Committee

Prof. Dr. rer. nat. Peter Schu

Department of Cellular Biochemistry, University Medical Centre Göttingen

Third member of the Thesis Committee

Prof. Dr. med. Wolfgang Brück

Institute of Neuropathology, University Medical Centre Göttingen

Date of Disputation: 03.06.2015

AFFIDAVIT

Herewith I declare that my doctoral thesis entitled: "rAAV-based gene therapy for molybdenum cofactor deficiency type B" has been written independently with no other sources and aids than quoted.

Göttingen, 24.04.2015   …………………………………..

TABLE OF CONTENTS

LIST OF ABBREVIATIONS

ABBREVIATION / SYMBOL	EXPLANATION
♀	Female
♂	Male
Δ	Delta
μ	Micro = 10^{-6}
Ø	Without
129Sv	Name of the mouse strain
A	Ampere
AAV	Adeno-associated virus
Ab	Antibody
ABC	ATP-Binding Cassette
Acr	Acrosin
Ad	Adenovirus
AMP	Adenosine monophosphate
Amp	Ampicillin
AO	Aldehyde oxidase
AP	Alkaline phosphatase
ATP	Adenosine triphosphate
BF	Bright field
bGH	Bovine growth hormone
BLAST	Basic Local Alignment Search Tool
bp	Base pair(s)
BSA	Bovine serum albumin
°C	Celsius grad
C57BL, C57BL/6N	Names of the mouse strains
CA	*Cornu Ammonis*
Cap	Capsid
Casp3	Caspase 3
CBA	Chicken β-actin

VI

cDNA	Complementary DNA
cm	Centimetre
CMV	*Cytomegalovirus*
CNS	Central nervous system
cPMP	Cyclic pyranopterin monophosphate
CT	Computed tomography
dATP	Deoxyadenosine Triphosphate
DAPI	Diamidino-2-phenylindole dihydrochloride
dATP	Deoxyadenosine-5'-triphosphate
DEPC	Diethylpyrocarbonate
dH_2O	Distilled Water
ddH_2O	Double-distilled water
DG	*Dentate gyrus*
DLBCL	Diffuse large B-cell lymphoma
DMEM	Dulbecco's Modified Eagle Medium
DMSO	Dimethyl Sulphoxide
DNA	Deoxyribonucleic acid
Dnajc24	DnaJ (Hsp40) homologue, subfamily C, member 24
DNAse	Deoxyribonuclease
dNTP	Deoxynucleotidetriphosphate
DKO	Double knockout
DPBS	Dulbecco's phosphate-buffered saline
ds	Double-stranded
dT	Deoxythymidinate
DTT	Dithiothreitol
E.coli	*Escherichia coli*
EDTA	Ethylene Diamine Tetraacetic Acid
EGFP/eGFP	Enhanced green fluorescent protein
En2	Engrailed-2
EPB	Epidermal permeability barrier

ES	Embryonic stem
ESC	Embryonic stem cell
et al	And others
EtBr	Ethidium Bromide
EtOH	Ethanol
Ex	Exon
F	Forward
F	Farad
F.IX	Factor IX
FAD	Flavin adenine dinucleotide
FBS	Fetal bovine serum
FCS	Fetal calf serum
FGFR1	Fibroblast growth factor receptor 1
Fig.	Figure
Flp	Flippase
FRT	FLP recognition target
G	Gravitational constant
g	Gram
Gapdh	Glyceraldehyde 3-phosphate dehydrogenase
GC	Genome copy
GFAP	Glial fibrillary acidic protein
GFP	Green fluorescent protein
GPHN	Gephyrin
GTP	Guanosine-5'-triphosphate
h	Hour
hAAT	Human alpha 1-antitrypsin
hßActin	Human beta-actin
HCA	Hepatocellular adenoma
HCC	Hepatocellular carcinoma
HE	Hematoxylin-eosin

HPLC	High-performance liquid chromatography
HPRT	Hypoxanthine-guanine phosphoribosyltransferase
HSPG	Heparan sulfate proteoglycan
IBA1	Ionised calcium binding adaptor molecule 1
IgG	Immunoglobulin G
IHC	Immunohistochemistry
IPTG	Isopropyl-ß-thiogalactopyranoside
IRES	Internal ribosome entry site
ITR	Inverted terminal repeat
Kan	Kanamycin
Kb	Kilobase
KCl	Potassium chloride
kDa	Kilodalton
KO	Knockout
KOMP	Knockout Mouse Project
LacZ	Beta-galactosidase
LB	Luria-Bertani
M	Molar
m	Milli = 10^{-3}
m	Meter
mARC	Mitochondrial amidoxime reducing component
$MgCl_2$	Magnesium chloride
MGI	Mouse Genome Informatics
Min	Minute
Mo	Molybdenum
MoCo	Molybdenum cofactor
MOCS/Mocs	Molybdenum cofactor synthesis
MOCODB	Molybdenum cofactor deficiency complementation group B
MOT	Molybdate transporter

MPI	Max Planck Institute
MPT	Molybdopterin
MRI	Magnetic resonance imaging
mRNA	Messenger RNA
n	Nano = 10^{-9}
n.a.	Not analysed
NaAc	Sodium acetate
NAb	Neutralising antibody
NaCl	Sodium chloride
NCBI	National Centre for Biotechnology Information
Neo	Neomycin
NeuN	Neuronal nuclei
NPC	Nuclear pore complex
nt	Nucleotide
Oligo (dT)	Oligodeoxythymidylic acid
ORF	Open reading frame
Ori	Origin
p	Promoter
p	Pico = 10^{-12}
pA	Polyadenylation
PAGE	Polyacrylamide gel electrophoresis
PBS	Phosphate-buffered saline
PCR	Polymerase chain reaction
pelo	Pelota homologue
PFA	Paraformaldehyde
pH	Negative logarithm of the hydrogen ion concentration
polyA	Polyadenylation
PVDF	Polyvinylidene difluoride
qPCR	Quantitative PCR
qRT-PCR	Quantitative Reverse Transcription PCR

R	Reverse
rAAV	Recombinant AAV
rcf	Relative centrifugal force
Rep	Replication initiator protein
RNA	Ribonucleic acid
RNase	Ribonuclease
Rpm	Rounds per minute
RT	Room Temperature
Rtl1	Retrotransposon-like 1
RT-PCR	Reverse Transcription PCR
SAM	S-adenosyl-L-methionine
SDS	Sodium dodecyl sulphate
Sec.	Second
Sry	Sex determining region Y
SUOX	Sulphite oxidase
ss	Single-stranded
T	Transgene
Tab.	Table
Taq	*Thermus aquaticus*
TBE	Tris/Borate/EDTA
TBG	Thyroxine binding globulin
TEWL	Transepidermal Water Loss
TIGEM	Telethon Institute of Genetics and Medicine
tu	Transfecting units
U	Unit
UMG	University Medical Centre Göttingen
UTR	Untranslated region
UV	Ultraviolet
V	Volt
VP	Viral Protein

WB	Western blot
w/o	Without
WT	Wild type
XDH	Xanthine dehydrogenase
x	Multiple
X-Gal	5-brom-4-chlor-3-indolyl-ß-Dgalactopyranoside
XOD	Xanthine oxidase
XOR	Xanthine oxidoreductase
Zfyve27	Zinc finger, FYVE domain containing 27

1   INTRODUCTION

1.1   Molybdenum cofactor (MoCo) deficiency

Molybdenum cofactor (MoCo) deficiency (complementation group A, B and C; OMIM# 252150, #252160 and #615501) is a rare, autosomal recessive disease leading to a combined deficiency of all MoCo-dependent enzymes. The usual phenotype includes untreatable neonatal seizures, mental retardation in association with elevated levels of xanthine in the plasma and urine, and elevated urine sulphites, particularly S-sulphocysteine (Macaya *et al.*, 2005), as well as feeding difficulties and dysmorphic facial features. Most infants die in early childhood, those who survive the neonatal period have a profound developmental delay with abnormal tone, lens dislocation, and renal stones (Carmi-Nawi *et al.*, 2011). Additionally, computed tomography (CT) and magnetic resonance imaging (MRI) often reveals dramatic and progressive loss of white matter in the brain (Reiss and Johnson, 2003). Although in MoCo deficiency all MoCo-dependent enzymes are inactive, the clinical findings are attributable to the loss of sulphite oxidase activity and the subsequent neurotoxic effect of sulphite accumulation (Reiss *et al.*, 2005). Both diseases MoCo deficiency and sulphite oxidase (SUOX) deficiency are clinically indistinguishable, and only biochemical tests can differentiate these two disorders. Besides an elevated sulphite level, MoCo-deficient patients present a diminished uric acid level, and an elevated xanthine concentration in the plasma and urine caused by the loss of xanthine dehydrogenase activity (Reiss and Johnson, 2003). In contrast to SUOX deficiency, therapy for type A of MoCo deficiency is available so the appropriate diagnosis increases the chances to rescue MoCo-deficient patients. Since MoCo is synthesised in a multi-step biosynthesis pathway, disease-causing mutations can occur in different genes. Dependent on the mutated gene, one can distinguish between three types of MoCo deficiency: type A, B and C **(Fig. 1.1)**. In type A deficiency, mutations are present in the *MOCS1* gene and abolish the formation of cyclic pyranopterin monophosphate (cPMP). The type B deficiency of the disease is characterised by mutations present in the *MOCS2* gene, thus blocking the conversion of cPMP to molybdopterin (MPT). In the last type of the deficiency, type C, the *GPHN* gene is affected preventing MPT from adenylation and further incorporation of molybdate to the pterin moiety (Arenas *et al.*, 2009). To date, mutations in the *MOCS3* gene have not been described (Reiss and Hahnewald, 2011). As

type A of the disease is the most frequent form (Reiss *et al.*, 1998), a murine *Mocs1* knockout mouse model was developed. *Mocs1* knockout mice represent a similar phenotype observed in MoCo deficiency type A patients, but without morphological changes in the brain and ectopic lenses. In addition, the *Mocs1* knockout animals reflected biochemical abnormalities typical for MoCo deficiency type A such as elevated level of sulphite and xanthine, and also exhibited early postnatal death (Lee *et al.*, 2002).

1.2   Molybdenum cofactor (MoCo)

Molybdenum (Mo) is an essential trace element for several enzymes important for metabolism processes in almost all living organisms (Zhang *et al.*, 2011). To date, more than 50 molybdenum-containing enzymes have been described. The vast majority of these enzymes have been found in bacteria and only seven in eukaryotes (Zhang and Gladyshev, 2008; Hille *et al.*, 2011). Bacteria as well as eukaryotic cells take up Mo in the form of its oxyanion molybdate (MoO_4^{2-}) (Bortels, 1930). The mechanism of this action is well studied in bacteria, where ABC- (ATP-binding cassette) type transporters consisting of three proteins encoded by *modA*, *modB*, and *modC* genes are required (Hagen, 2011). In eukaryotes, the molecular nature of the transporters is not well studied. The first molybdate transporter, MOT1, was identified in algae (*Chlamydomonas reinhardtii*) and plants (*Arabidopsis thaliana*) (Tejada-Jimenez *et al.*, 2007; Tomatsu *et al.*, 2007); however, it is not present in the animal kingdom. Recently, the MOT2 protein has been identified as a putative Mo transporter present in all eukaryotes, including human (Tejada-Jimenez *et al.*, 2011). **Figure 1.1** presents the summary of biosynthesis of human MoCo. Once molybdenum entered the cell as oxyanion, it has to be coordinated by a unique scaffold to become biologically active. This special function is performed by molybdopterin (MPT), a tricyclic pyranopterin containing a *cis*-dithiolene group needed for molybdenum ligation (Daniels *et al.*, 2008). Together the metal and pterin moiety form the molybdenum cofactor (MoCo) (Mendel, 2013). Cofactors are non-protein compounds required for the catalytic activity of enzymes (Eagleson, 1993). In contrast to bacteria, there are only four molybdenum cofactor-dependent enzymes in humans: [1] aldehyde oxidase (Mahler *et al.*, 1954), [2] xanthine oxidoreductase (De Renzo *et al.*, 1954), [3] sulphite oxidase (Cohen *et al.*, 1971) and [4] mitochondrial amidoxime reducing

component (mARC) (Wahl *et al.*, 2010). The biosynthetic pathway of MoCo is evolutionary conserved, and can be divided into four steps, according to the biosynthetic intermediates: cPMP (cyclic pyranopterin monophosphate), MPT (molybdopterin), adenylated MPT and MoCo (Mendel, 2013). This pathway begins in mitochondria with 5'-guanosine triphosphate (GTP), which is converted by products of *MOCS1A* and *MOCS1AB* genes to cPMP. The gene *MOCS1A* belongs to the superfamily of S-adenosylmethionine (SAM)-dependent radical enzymes. It catalyses the formation of radicals by a protein bound [4Fe-4S] cluster (Hanzelmann *et al.*, 2004), while the B domain of MOCS1AB fusion protein might function as a radical acceptor (Teschner *et al.*, 2010). Furthermore, cPMP has to pass the mitochondrial membranes, as all subsequent steps are localised in the cytosol (Kaufholdt *et al.*, 2013). A heterotetrameric complex of two small sulphur carriers and two large catalytic subunits of MPT-synthase (MOCS2A and MOCS2B, respectively) catalyses the sulphur transfer into cPMP leading to MPT formation. The sulphur group is delivered by the product of the *MOCS3* gene, which is believed to catalyse both the adenyl transfer, and subsequent thiocarboxylation at the C-terminus of the MOCS2A subunit within MPT-synthase (Matthies *et al.*, 2004). Once the MPT moiety is synthesised, the chemical backbone is ready to bind and coordinate the molybdenum atom. This step is subdivided into two separate steps. In bacteria each step is catalysed by separate MogA and MoeA proteins (Nichols and Rajagopalan, 2002), which were combined during evolution to form a single two-domain molybdenum insertase (Cnx1 in plant and Gephyrin in mammals) (Mendel, 2013). In the first step, MPT has to be activated by adenylation, which is carried out by the *MogA* or G-domain of the *Gephyrin* (*GPHN*) gene in a Mg^{2+} and ATP-dependent manner (Llamas *et al.*, 2004). Furthermore, the MPT-AMP serves as a substrate for the molybdenum insertion, which is catalysed by MoeA or the E-domain of *GPHN* (Llamas et al., 2006).
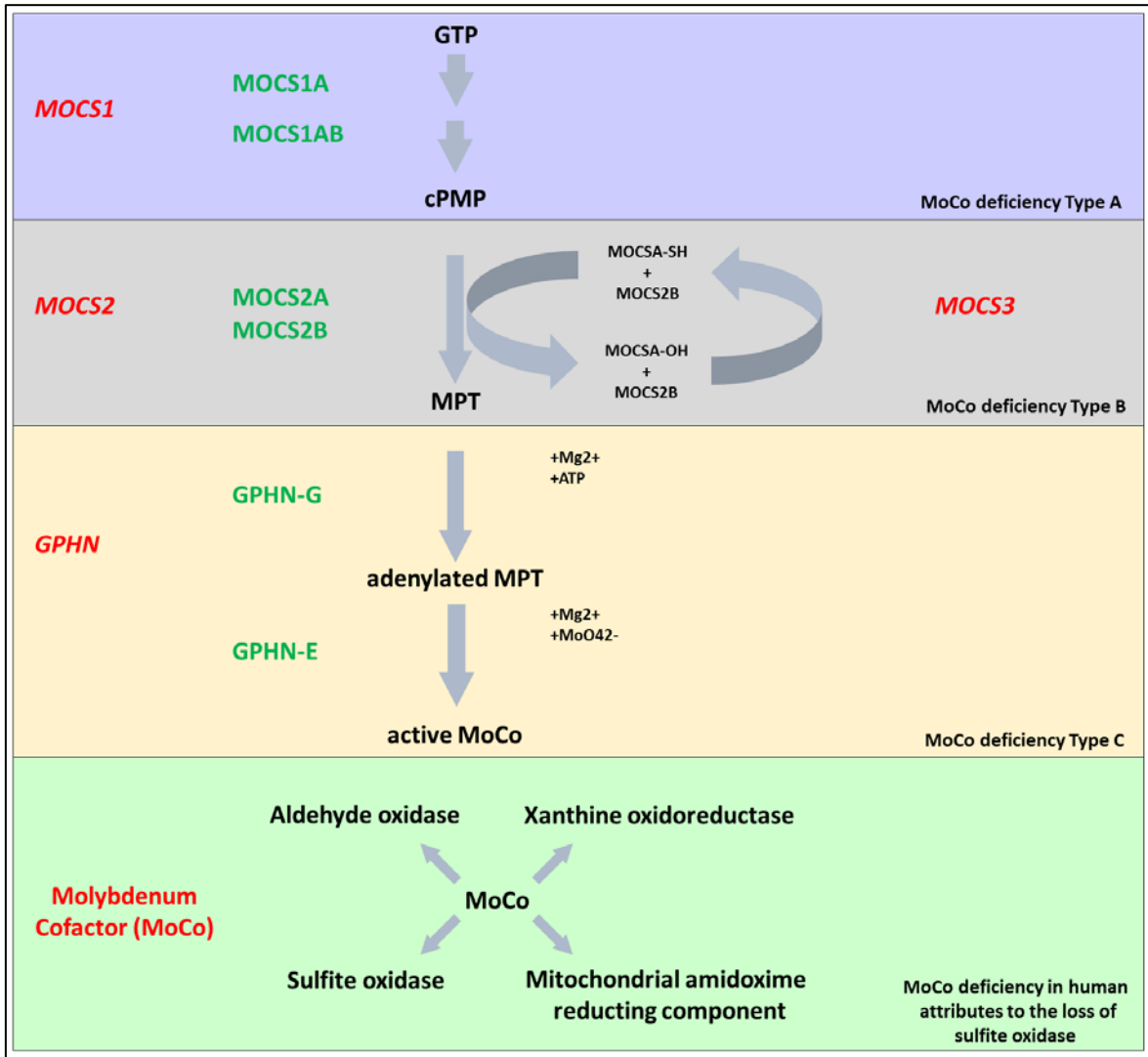
Fig. 1.1. Schematic representation of the molybdenum cofactor (MoCo) biosynthesis pathway and function in human cells. The biosynthesis pathway is divided into four steps, presented in violet (1st step), grey (2nd step) and yellow (3rd and 4th steps) squares, respectively. In the first step, guanosine thriphosphate (GTP) is converted to cyclic pyranopterin monophosphate (cPMP) by products of *MOCS1A* and *MOCS1AB* genes. Subsequently, molybdopterin-synthase consisting of two MOCS2A and two MOCS2B subunits catalyses sulphur incorporation into cPMP, leading to the formation of molybdopterin (MPT). The sulphur group required for this reaction is provided by the product of the *MOCS3* gene. Finally, MPT is converted into MoCo. This process is performed by Gephyrin (GPHN). In eukaryotes G domain of GPHN activates MPT by adenylation, while the E domain catalyses molybdenum incorporation. The first reaction occurs in a Mg^{2+} and ATP-dependent manner, while the second reaction requires only Mg^{2+}. The lack of MoCo leads to molybdenum cofactor deficiency disease. Depending on the mutation affecting MoCo synthesis, MoCo deficiency was classified into three types: A, B and C, as shown on the right site of the squares. The last, green square presents the function of MoCo in human. So far, four MoCo-dependent enzymes were characterised: aldehyde oxidase, xanthine oxidoreductase, sulphite oxidase and mitochondrial amidoxime

reducing component. MoCo deficiency in human attributes to the loss of sulphite oxidase. Scheme modified from Reiss and Hahnewald (2011).

1.3 Characteristics of the *MOCS2* gene

1.3.1 Genomic structure of the human *MOCS2* and mouse *Mocs2* genes

Products of the human *MOCS2* gene, involved in the second step of the MoCo biosynthesis pathway, form a complex called molybdopterin synthase, an enzyme required for the conversion of cyclic pyranopterin monophosphate (cPMP) to molybdopterin (MPT). It is a heterotetrameric complex consisting of two small MOCS2A (10 kDa) and two large MOCS2B (21 kDa) subunits. In humans, the *MOCS2* gene is localised on the long arm of chromosome 5 (5q11.2) and it encodes two transcripts corresponding to spliceform I (*MOCS2A*) and spliceform III (*MOCS2B*), respectively (Reiss and Hahnewald, 2011). Each transcript contains seven exons, with overlapping open reading frames (ORFs) in exon 3. Both ORFs are shifted relative to each other, thus do not share identical codons (Stallmeyer *et al.*, 1999). The translation start of the *MOCS2A* transcript is localised in exon 1a and the stop codon in exon 3. The *MOCS2B* transcription start site is localised in the alternative exon 1b, although the ORF for the MOCS2B protein starts in exon 3 and it is terminated in exon 7 **(Fig. 1.2a)**. The murine *Mocs2* gene is localised on chromosome 13 (13D2.2). In contrast to the human *MOCS2* gene, the mouse *Mocs2* gene encodes for three spliceforms: I-III. Spliceform I consists of 7 exons, while both spliceforms II and III contain 6 exons. **Figure 1.2b** presents the genomic structure of the mouse *Mocs2* gene together with the corresponding splice variants. Spliceform I, encodes the *Mocs2a* subunit or both *Mocs2a* and *Mocs2b* subunits of molybdopterin-(MPT) synthase. It expands on exons 1-7 with the start codon localised in exon 1 and the stop codon in exon 3 for *Mocs2a* or with the start codon in exon 3 and stop codon in exon 7 for *Mocs2b*, respectively. The gene products of *Mosc2a* and *Mocs2b* are evolutionary conserved, with 91% and 90% homology between mouse and human (Stallmeyer *et al.*, 1999). The *Mocs2b* transcript encoded by spliceform II includes exons 1 and 3-7. The translation start is localised in exon 3 and is terminated in exon 7, leading to Mocs2b protein formation. Analogous to the human *MOCS2* transcripts, mouse spliceforms I, II and III overlap in exon 3, and their ORFs are shifted relative to each other, thereby not sharing identical amino acids.
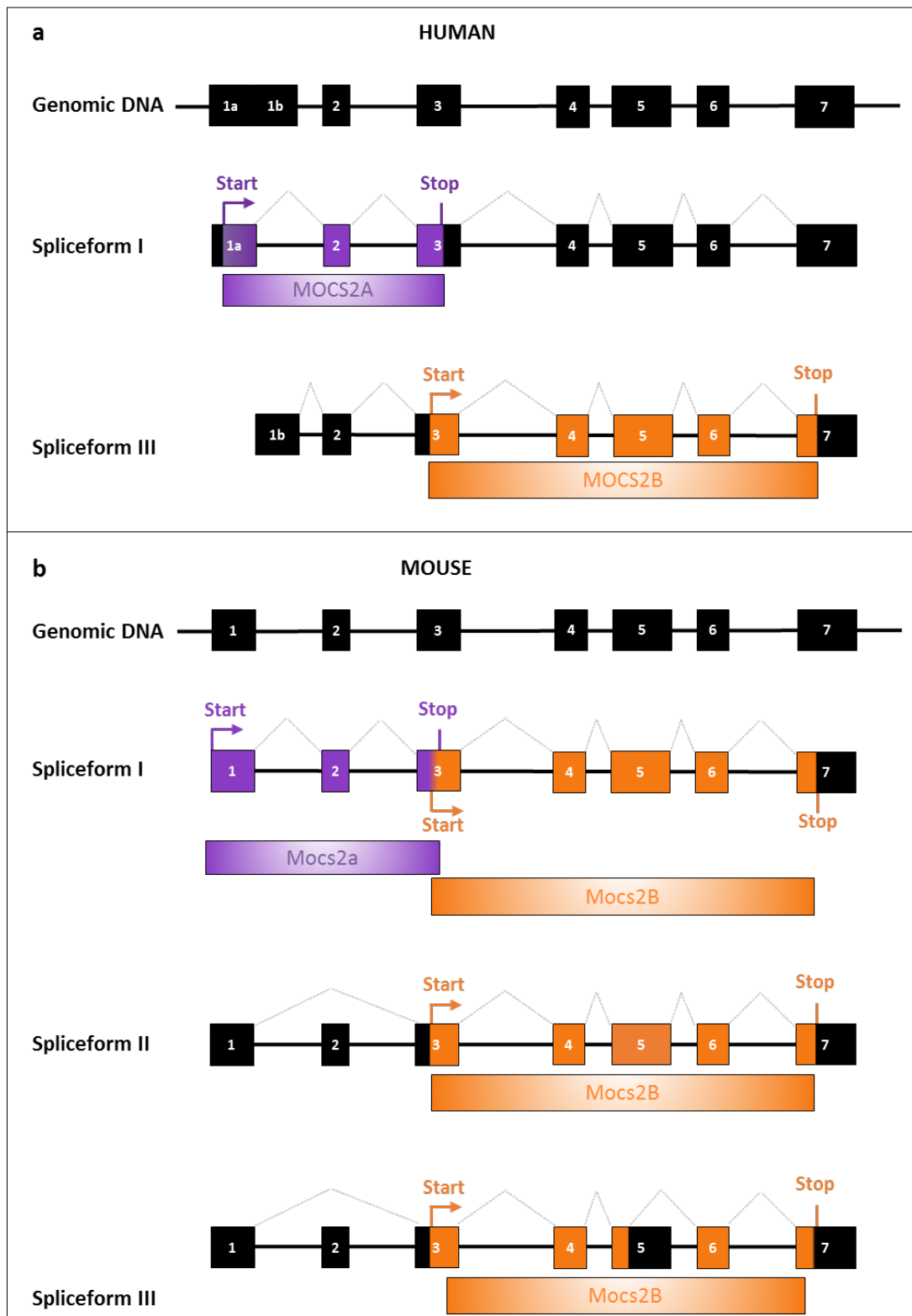
Fig. 1.2. Genomic structures of human *MOCS2* and mouse *Mocs2* genes and their alternative splicing products. (a) Gene structure of the human *MOCS2* gene together with corresponding transcripts encoding MOCS2A and MOCS2B proteins. Exons 1a and 1b of the human *MOCS2* gene are mutually exclusive and lead to the expression of two distinct proteins via spliceforms I (MOCS2A) and III (MOCS2B), respectively.

Spliceform I contains 7 exons, with the start codon (Start) localised in exon 1a and the stop codon in exon 3 (Stop). The ORF of spliceform I (presented in violet) expands on exons 1-3 and encodes the MOCS2A protein. Spliceform III comprises also 7 exons; however, the transcription start point is located in the alternative exon 1b. In contrast, its translation starts (Start) in exon 3 and is terminated (Stop) in exon 7. It expands on exons 3-7 (shown in orange) and encodes for the MOCS2B protein. The ORFs of *MOCS2A* and *MOCS2B* transcripts overlap in exon 3 by 77 nucleotides (nt), and they are shifted relative to each other, thereby not encoding for identical amino acids. **(b)** Genomic structure of the murine *Mocs2* gene together with alternative spliceforms. Spliceform I contains 7 exons, with start codon in exon 1 and stop codon in exon 3 for *Mocs2a* or with start codon in exon 3 and stop codon in exon 7 for *Mocs2b* transcripts, respectively. ORFs of these spliceforms encode Mocs2a protein (presented in violet) or Mocs2b protein (shown in orange). Both ORFs overlap in exon 3 by 77 nucleotides (nt). Spliceform II and III comprise 6 exons, as exon 2 is spiced out. The transcription starts in exon 1, however its translation begins in exon 3 and is terminated in exon 7. Additionally, in spliceform III part of the exon 5 is spliced out leading to a smaller isoform of the Mocs2b protein. Scheme modified from Hahnewald (2009), Reiss and Hahnewald (2011).

1.3.2 *MOCS2* expression pattern

The expression profiles of mouse *Mocs2* transcripts and proteins have not been studied so far. Besides a single Northern blot analysis performed on a human RNA library, little is known about the specific localisation of human *MOCS2* transcripts and proteins (Stallmeyer *et al.*, 1999). This former study has shown ubiquitous expression of *MOCS2* transcripts with the strongest expression detected in human skeletal muscle, kidney, pancreas and heart (Reiss *et al.*, 1998).

1.4 MoCo-dependent enzymes

In humans, there are four MoCo-dependent enzymes described so far: aldehyde oxidase, xanthine oxidoreductase, sulphite oxidase and mitochondrial amidoxime reducing component (Reiss and Hahnewald, 2011).

1.4.1 Aldehyde oxidase (AO)

AO is a flavoenzyme present ubiquitously in the cytosol in all vertebrates (Garattini *et al.*, 2008). It is a homodimer composed of two subunits of about 150 kDa. Each subunit has a typical tripartite structure, in which the N-terminal domain of 20 kDa includes two iron-containing clusters, the central domain corresponding to 40 kDa and harbours a flavin adenine dinucleotide (FAD) binding-site, and the last 85 kDa C-terminal domain

accommodates the molybdenum cofactor (Garattini *et al.*, 2008) **(Fig. 1.3)**. As soon as MoCo binds to the apoenzyme, AO becomes biologically active (Rajagopalan and Johnson, 1992). However, prior to that MoCo requires post-translational sulphuration to become catalytically active (Sagi *et al.*, 2002; Heidenreich *et al.*, 2005; Mendel and Bittner, 2006). The reaction is catalysed by sulphurase (Ichida *et al.*, 2001), which substitutes one of the oxo groups with the sulpho double bound in MoCo (Bittner *et al.*, 2001; Xiong *et al.*, 2001). AO proteins are present throughout evolution, from bacteria to man (Kurosaki *et al.*, 2013). In the human genome, AO is encoded by the *AOX1* gene. It is located on chromosome 2 (2q33.1), and consists of 35 exons (Terao *et al.*, 1998). In contrast, rodents have four *Aox* genes (*Aox1-4*) clustered on chromosome 1 (1C1.3) in mice, and chromosome 9 (9q31) in rats (Kurosaki *et al.*, 2004).
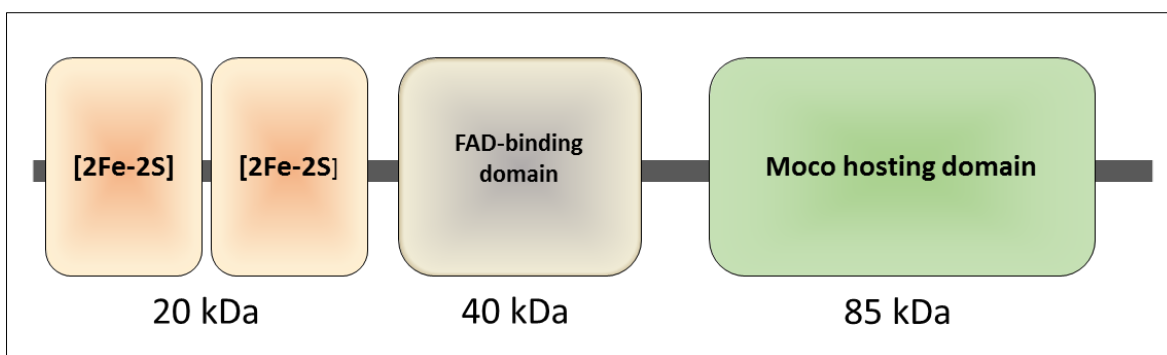
Fig. 1.3. Structure of the human aldehyde oxidase (AO) and the xanthine oxidoreductase (XOR) monomer. Each AO/XOR subunit consists of three domains: a 20 kDa N-terminal domain with two iron-containing [2Fe-2S] redox clusters, a 40 kDa FAD-binding domain with a flavin adenine dinucleotide (FAD) binding site, and a 85 kDa C-terminal domain hosting the molybdenum cofactor (MoCo) site adjacent to the substrate binding pocket. Domains were determined using Simple Modular Architecture Research Tool (http://smart.embl-heidelberg.de).

The biological function of the enzyme is not well known. It has been described to oxidise a broad range of substrates, mainly aldehydes, nitro/nitroso compounds or N-heterocycles (Beedham, 1985; Kitamura *et al.*, 2006). Recently, it has been recognised as regulator of drug metabolism (Pryde *et al.*, 2010; Garattini and Terao, 2012). AO is ubiquitously expressed, although the highest expression occurs in the liver (Garattini *et al.*, 2008). The activity of AO differs between species, e.g. it is high in monkeys and human, low in rats and absent in dogs (Kitamura *et al.*, 1999). Moreover, the activity varies within the same

species, like in different mouse or rat strains (Al-Salmy, 2002). Furthermore, in human, AO activity is detected in the trachea and bronchium epithelia and also in alveolar cells. In the gastrointestinal tract AO is active primarily in the epithelia of small and large intestines, while in the kidney the highest AO activity was shown in the proximal, distal and collecting tubules (Moriwaki *et al.*, 2001). To date, a gender-related difference in AO activity has not been reported in humans, but male mice present 2- to 4-fold higher AO activity than females (Al-Salmy, 2002). Additionally, other factors such as age, cigarette smoking, drug usage, and disease (e.g. cancer), may also alter AO activity (Beedham, 1985). To date, 5 mutations have been described in the human *AOX1* gene (Human Gene Mutation Database (HGMD) Professional 2015.1). Although these mutations influence AO catalytic efficiency, patients do not present a correlated phenotype (Hartmann *et al.*, 2012).

1.4.2   Xanthine oxidoreductase (XOR)

XOR, another MoCo-dependent enzyme, is a homolog of AO and belongs to the same family of flavoenzymes. Similar to AO, XOR exists as a homodimer composed of two 150 kDa subunits. Each subunit consists of three redox centres: a MoCo binding site, a FAD binding site, and a Fe/S cluster **(Fig. 1.3)**. The enzyme is active only in the presence of MoCo, however, MoCo must be first activated by sulphuration (Sagi *et al.*, 2002; Heidenreich *et al.*, 2005; Mendel and Bittner, 2006). Like AO, XOR is also present in the cytosol of all vertebrates (Garattini *et al.*, 2008). It exists in two interconvertible forms, xanthine oxidase (XOD) and xanthine dehydrogenase (XDH) which transfer electrons to both oxygen and nicotinamide adenine dinucleotides (NAD), respectively. Both act on the same substrates, hypoxanthine and xanthine, but XOD utilises substrates and O_2 as a cofactor to produce superoxide (O_2^-) and uric acid, and XDH acts on the same substrates utilising NAD as a cofactor to produce NADH instead of $\cdot O_2^-$ and uric acid (Chung *et al.*, 1997).

The XOR gene is localised on the short arm of human chromosome 2 (2p23.1) and on chromosome 17 (17E2) in mice. In both cases the XOR gene is composed of 36 exons. In mammals, the presence of XOR has been demonstrated in many organs, albeit at different levels and most cells show little enzyme activity. In humans the highest activity

is present in the intestine (Riario-Sforza *et al.*, 1969; Auscher *et al.*, 1979) and liver (Sarnesto *et al.*, 1996). Additionally, it can be found in human milk (Abadeh *et al.*, 1992). It has been shown that in mice *Xor* expression occurs in the mammary gland, where it is necessary as a structural component for milk fat droplet envelopment and secretion (McManaman *et al.*, 2002). XOR is one of the best-studied flavoproteins which catalyses two terminal reactions in purine degradation in primates: oxidation of hypoxanthine to xanthine and the subsequent oxidation of xanthine to uric acid (Hille and Nishino, 1995). These reactions and presumably other metabolic reactions of XOR have a far-reaching impact on cellular homeostasis, cellular protection from toxic compounds and also systemic protection, known as innate immunity.

The disease associated with XOR dysfunction in humans is termed xanthinuria, because of the excretion of xanthine in the urine (Dent and Philpot, 1954). Xanthinuria can be classified into two subtypes: type I (isolated form) in which XOR deficiency is observed due to a genetic defect in the *XOR* gene, and type II which involves dual deficiency of XOR and the homolog enzyme AO, due to a genetic defect in the MoCo or sulphurase required for MoCo activation (Peretz *et al.*, 2007; Ichida *et al.*, 2012). In higher animals other than primates, xanthinuria is lethal due to kidney damage, caused by the formation of xanthine stones (urolithiasis) in the urinary track (Kucera *et al.*, 1997; van Zuilen *et al.*, 1997; Tsuchida *et al.*, 2007; Miranda *et al.*, 2010). *Xor* knockout mice fail to thrive after 10 to 14 days, and die within the first month due to renal failure caused by the accumulation of triglyceride-rich substances as well as xanthine and hypoxanthine in the renal tubules (Ohtsubo *et al.*, 2009). The first month of life is a period, when the murine kidney undergoes maturation and remodelling, and is characterised by elevated activity of renal Xor (Ohtsubo *et al.*, 2004). In contrast to this report, another group showed that $Xor^{+/-}$ female mice, although with healthy appearance and normal fertility, are unable to maintain lactation and their pups die within two weeks after birth (Vorbach *et al.*, 2002). In human, xanthine urolithiasis is usually benign and easy to prevent or cure by appropriate alkalisation, forced hydration and restriction of dietary purines (Gargah *et al.*, 2010).

1.4.3 Sulphite oxidase (SO)

SO is an enzyme encoded by the *SUOX* gene, which is localised on human chromosome 12q13.2 and contains 3 exons, while in mice it is found on chromosome 10 with 4 exons. The enzyme is a homodimer complex where each subunit contains three domains: a N-terminal cytochrome b(5) domain (8.5 kDa), a central domain harbouring the molybdenum cofactor (MoCo) binding site (20 kDa), and a C-terminal dimerisation domain (14 kDa) (Rudolph *et al.*, 2003) **(Fig. 1.4)**.
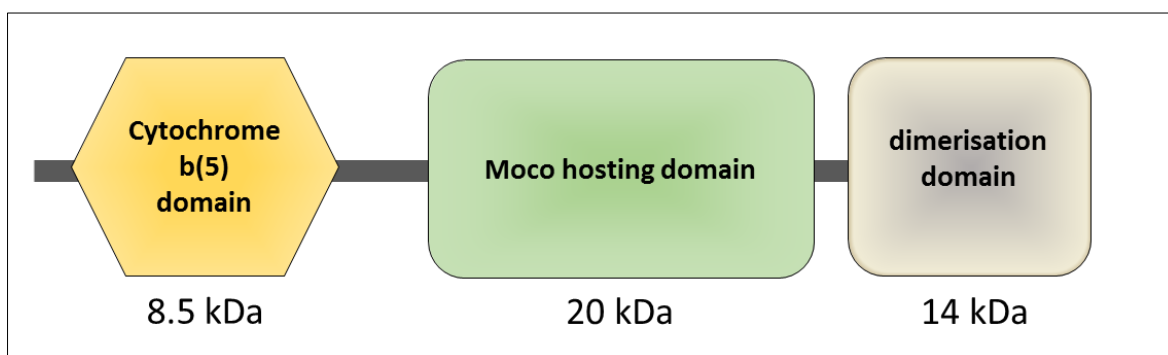
Fig. 1.4. Structure of the human sulphite oxidase monomer. The monomer of the sulphite oxidase consists of three domains: a 8.5 kDa N-terminal cytochrome b(5) domain, a 20 kDa MoCo-hosting domain, and a 14 kDa C-terminal dimerisation domain. Domains were determined using Simple Modular Architecture Research Tool (http://smart.embl-heidelberg.de).

The enzyme is localised in the intermembrane space of mitochondria, and catalyses the oxidation of sulphite to sulphate, the terminal reaction in the pathway of degradation of sulphur-containing amino acids (Johnson, 2003). In humans, the highest expression of *SUOX* occurs in the liver, kidney, skeletal muscles, heart, placenta, and brain (with the strongest signal in the cerebral cortex), while the thymus, spleen, peripheral blood leukocytes, colon, small intestine, and lung show little expression. In rats, the highest expression is present in the liver, kidney, heart, brain, and lung, but not in the skeletal muscle. Additionally, weak expression is present in the spleen and testis (Woo *et al.*, 2003). An isolated sulphite oxidase deficiency is a rare (25 cases described worldwide), autosomal recessive disorder with a very poor prognosis. The clinical symptoms, usually present in the neonatal period, include neurological abnormalities such as refractory seizures, abnormal muscle tone, abnormal movements, marked developmental delay and dislocation of ocular lenses (Lam *et al.*, 2002; Basheer *et al.*, 2007; Westerlinck *et al.*,

2014). In accordance with these studies, the rat model of the disease shows loss of pyramidal neurons in the hippocampus due to a neurotoxic effect of sulphite (Kocamaz *et al.*, 2012).

1.4.4 Mitochondrial amidoxime reducing component (mARC)

Recently, mitochondrial amidoxime reducing component (mARC) was discovered as a molybdenum-containing enzyme in mammals. All mammalian genomes studied to date contain two *mARC* genes: *MARC1* and *MARC2*. In humans, they are localised on chromosome 1q. The proteins encoded by these genes are mARC-1 and mARC-2, respectively (Ott *et al.*, 2014). Each protein contains three domains: a mitochondrial targeting signal (~2 kDa), a transmembrane domain (~13.5 kDa) and a catalytic core (~16 kDa) **(Fig. 1.5)**. It has been shown that mARC1 is localised in the outer mitochondrial membrane, with its catalytic domain facing to the cytosol (Klein *et al.*, 2012).
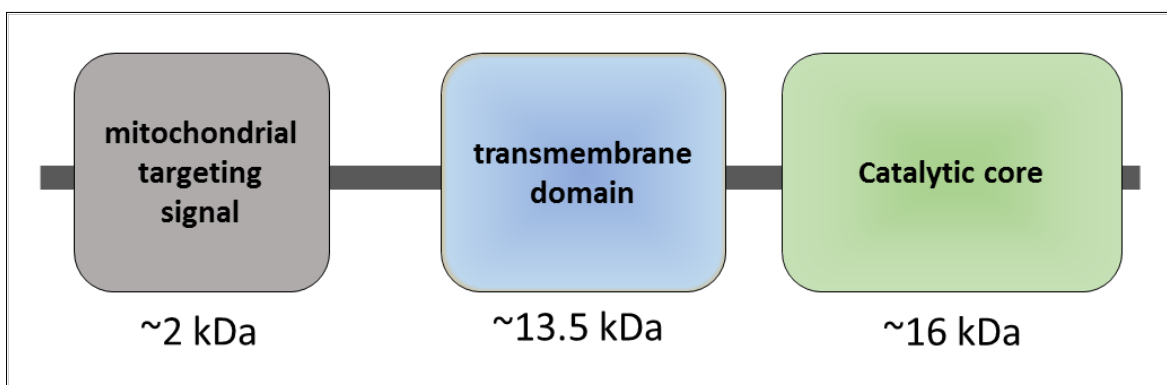
Fig. 1.5. Schematic representation of the human mitochondrial amidoxime reducing component (mARC). The enzyme consists of three domains: a 2 kDa transmembrane region, a 13.5 kDa central domain with unknown function, and a 16 kDa MoCo-sulphurase domain (catalytic core). Domains were determined using Simple Modular Architecture Research Tool (http://smart.embl-heidelberg.de).

In mammals, the highest mARC activity was found in the liver, kidney, thyroid and pancreas (Krompholz *et al.*, 2012). Although the endogenous function of the mARC protein is not fully understood, it was shown that the enzyme is linked with drug and lipid metabolism (Havemeyer *et al.*, 2014; Jakobs *et al.*, 2014).

12

1.5 **Substitution therapy for Molybdenum Cofactor Deficiency Type A**

Since MoCo is extremely unstable (Kramer *et al.*, 1987), a substitution therapy using a synthetic cofactor is not possible. However, cyclic pyranopterin monophosphate (cPMP), the first intermediate of the MoCo biosynthesis pathway, is a more stable one with a half-life of several hours at low pH (Fay *et al.*, 2007). Due to the fact that the biosynthesis pathway is conserved in plants, bacteria and humans it was possible to isolate large quantities of cPMP from *Escherichia coli* by a high-performance liquid chromatography (HPLC) procedure. Repeated intrahepatic injections of cPMP into *Mocs1* knockout mice normalised the phenotype and reconstituted MoCo biosynthesis as well as an activity of MoCo-dependent enzymes (Schwarz *et al.*, 2004). In 2009 the first MoCo-deficient patient suffering from type A of the disease, received intravenous injections with cPMP isolated from *E. coli*. Shortly after that, all markers of MoCo deficiency were normalised, including sulphite, S-sulphocysteine, thiosulphate, xanthine and uric acid. Clinically, the infant became more alert, convulsions and twitching disappeared within the first 2 weeks, and an electroencephalogram showed the return of rhythmic elements and markedly reduced epileptic form discharges (Veldman *et al.*, 2010).

1.6 **Gene therapy**

Although, an effective therapy for MoCo deficiency type A has already been established, all other types of the deficiency remain incurable. Instability of intermediates other than cyclic pyranopterin monophosphate (cPMP) excludes them as potential drugs in substitution therapies. To overcome this problem a gene therapy approach could be employed. Gene therapy is designed to introduce a functional copy of the gene into the appropriate cells of the patient, in order to produce sufficient amounts of the missing protein, and rescue the phenotype of the disorder. The gene of interest can be delivered into the target cells by physical, chemical or viral vectors. It can target somatic cells (only the recipient's genome is changed), as well as germ cells (the changes passing to the offspring through modified parent's egg or sperm). However, the second scenario is not being actively investigated, at least in larger animals and humans, because of the associated ethical controversy (Sharma *et al.*, 2004). To date, two different approaches for gene therapy exist: the *ex vivo* therapy and the *in vivo* therapy **(Fig 1.6)**. In the *ex vivo*

therapy approach cells are modified outside the patient's body and subsequently cells with the corrected gene of interest are transplanted back into the patient. In case of the *in vivo* therapy approach, genetic material is directly introduced to the recipient (Mulligan, 1993; Flotte and Ferkol, 1997).
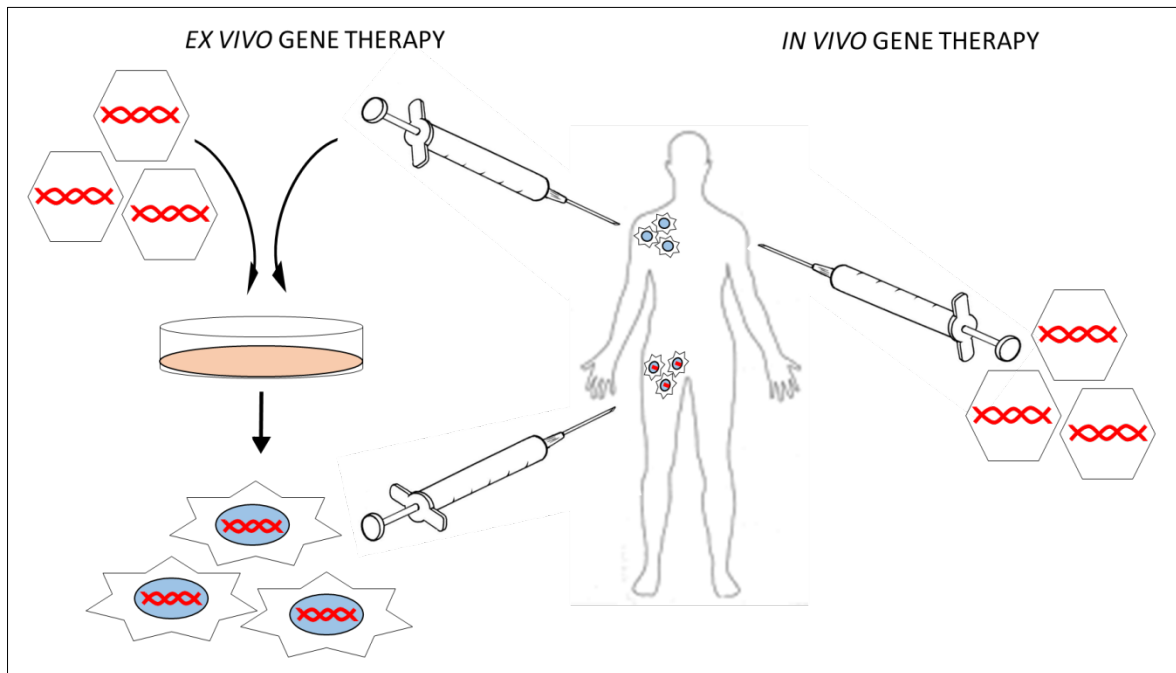
Fig. 1.6. Schematic illustration of *ex vivo* and *in vivo* techniques used in gene therapy approaches. The *ex vivo* technique involves tissue/cell biopsies, *in vitro* genetic manipulations, and re-implantation of corrected cells. The *in vivo* gene therapy is based on the direct introduction of genetically modified material to the recipient. Scheme modified from Kaji and Leiden (2001).

Generally, there are three methods used for gene therapy approaches: [1] a physical method which refers to the delivery of the gene via the application of physical force to increase the permeability of the cell membrane. The most common methods include microinjection, electroporation, ultrasound, gene gun and hydrodynamic application. [2] a chemical method utilising natural or synthetic carriers to deliver genes into cells. Here, calcium phosphate, DEAE-dextran, liposomes and lipoplexes are used for oral gene delivery, and surfactants and perflurochemical liquids for aerosol gene delivery (Sharma *et al.*, 2004; Miyazaki *et al.*, 2006; Prokop and Davidson, 2007). The last gene delivery system [3] is viral-based, where the therapeutic gene is delivered by modified, replication-deficient viruses, including retroviruses, adenoviruses (Ad), lentiviruses and adeno-associated viruses (AAV) (Escors and Breckpot, 2010). AAV vectors are currently

among the most frequently used viral vectors, and seem to be the most promising tool for gene therapy applications (Gauttier *et al.*, 2013).

1.6.1 Adeno-associated virus (AAV)

The first AAV was discovered in 1965 as a contaminant during adenovirus (Ad) preparation (Atchison *et al.*, 1965). It is a small, non-enveloped, single-stranded DNA (~4.7 kb) virus, with an icosahedral capsid of approximately 22 nm in diameter. It belongs to the family of *Parvoviridae*, placed in the genus *Dependovirus*, as its infection occurs only in the presence of a helper virus (adenovirus or herpesvirus). AAV integrates into the human genome in a site-specific manner on chromosome 19q14.4 (Daya and Berns, 2008). It can infect dividing and non-dividing cells (Samulski *et al.*, 1999). Although 80% of the human population is seropositive for AAV2 (the most extensively examined serotype), the virus has not been linked with any disease (Goncalves, 2005). The genome of the virus consists of two open reading frames (ORFs) flanked by 145 bp long inverted terminal repeats (ITRs) which are important for replication, genome packaging, transcription and site-specific integration of the viral DNA. The first ORF encodes for replication-associated protein (Rep) proteins, and is transcribed giving rise to four proteins: two larger Rep78 and Rep68 proteins expressed from the P5 promoter, and two smaller Rep52 and Rep40 proteins expressed from the P19 promoter. The larger Rep proteins positively and negatively regulate AAV gene expression in the presence or absence of a helper virus, respectively, and are required for DNA replication (Pereira *et al.*, 1997). Products of *Rep52* and *Rep40* genes are required for efficient packaging of the AAV genome into the capsid. All Rep proteins possess helicase/ATP-activity and additionally, the larger proteins possess a strand- and site-specific endonuclease activity, plus a site-specific DNA binding activity (Young *et al.*, 2000; King *et al.*, 2001). The second ORF encodes two proteins, driven by the P40 promoter. As a result of alternative spicing, three viral capsid (Cap) proteins, VP1, VP2, and VP3, are produced. All three proteins are necessary for the generation of infectious particles; however, VP2 and VP3 are sufficient for capsid formation, while VP1 is required for viral infection (Hermonat and Muzyczka, 1984; Tratschin *et al.*, 1984; Smuda and Carter, 1991). **Figure 1.7** shows a schematic representation of the AAV genome together with encoded proteins.
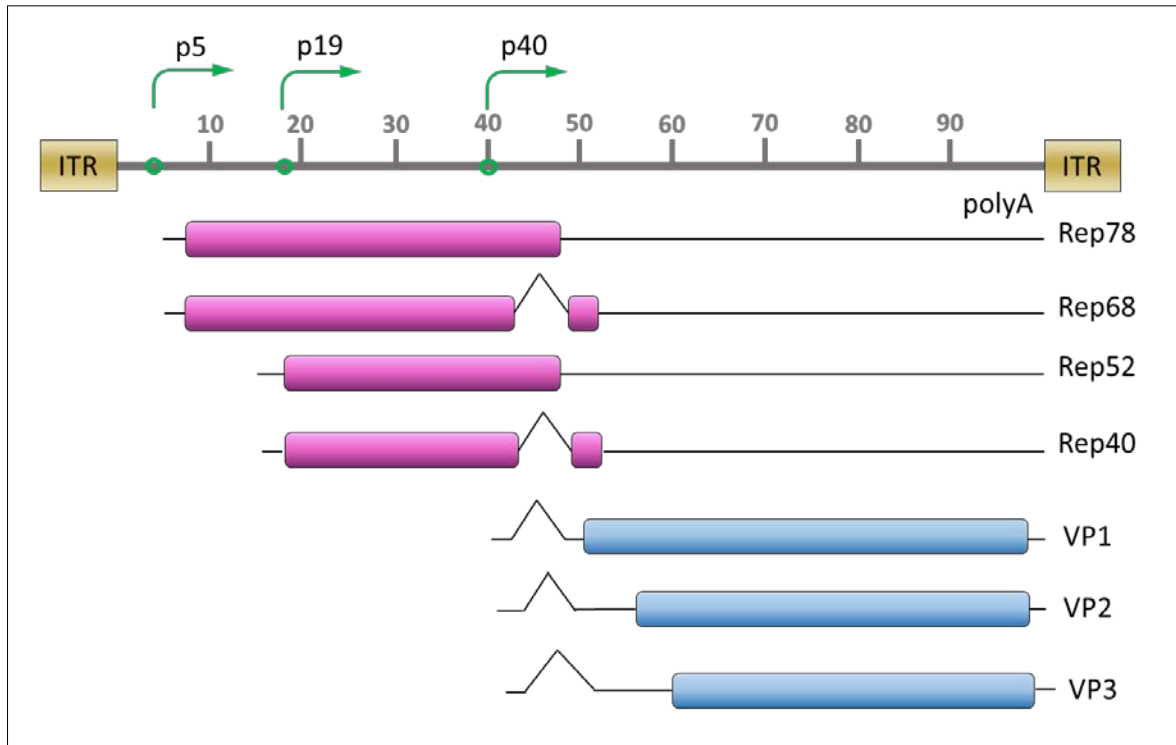
Fig. 1.7. Map of the wild type adeno-associated virus (AAV) genome. The AAV genome, flanked by two inverted terminal repeats (ITRs), contains 4680 nucleotides and is divided into 100 map units. Position p5, p19, and p40 represent promoters' localisation, and position 96 corresponds to the polyadenylation signal (polyA). Transcripts of replication-associated protein (Rep) genes driven by p5 and p19 promoters give rise to four different Rep proteins (shown in violet). Rep68 and Rep78 are transcribed from the p5 promoter, while Rep40 and Rep52 are transcribed from the p19 promoter. Three capsid (Cap) proteins, termed VP1, VP2, and VP3 (shown in blue) are transcribed from the p40 promoter. ITR elements are important for replication, packaging and integration of AAV (Dent and Philpot, 1954). Rep proteins are essential for targeted integration (McManaman *et al.*, 2002), while Cap proteins are important for viral packaging (Gargah *et al.*, 2010). Scheme modified from Merten *et al.* (2005).

The infection of AAV is a multistep process. First, the AAV attaches to the cell surface using its putative primary receptor, heparin sulphate proteoglycan (HSPG) (Summerford and Samulski, 1998). In addition, $\alpha_v\beta_5$ integrin and fibroblast growth factor receptor 1 (FGFR1) were suggested as co-receptors (Qing *et al.*, 1999; Summerford *et al.*, 1999). FGFR1 is believed to enhance the attachment process, while $\alpha_v\beta_5$ integrin is probably involved in endocytosis via clathrin-coated pits. VP-receptor interaction initiates the internalisation process. So far several genes were characterised to regulate this process, including cytosolic GTP-ase, dynamin, whose oligomerisation into a ring structure is necessary for the formation of clathrin-coated vesicles and further pinching them from

the cell membrane (Baba *et al.*, 1995; Hinshaw and Schmid, 1995; Sever *et al.*, 2000). In addition, integrin clustering facilitates the internalisation via the GTP-binding protein Rac1, whose activation leads in turn to activation of the phosphatidylinositol-3 kinase (PI3K) signalling pathway that transports the virus encapsulated in the endosomal vesicles along microfilaments and microtubules (Sanlioglu *et al.*, 2000). Furthermore, the AAV particles are delivered to the late endosomes and are released into the cytoplasm (Douar *et al.*, 2001). Little is known about the process how the virus enters the nucleus, as well as the exact place of viral uncoating. The transport occurs presumably through the nuclear pore complex (NPC), while the uncoating seems to take place in the nucleus (Sonntag *et al.*, 2006; Nonnenmacher and Weber, 2012). **Figure 1.8** shows a schematic representation of the AAV infection mechanism.
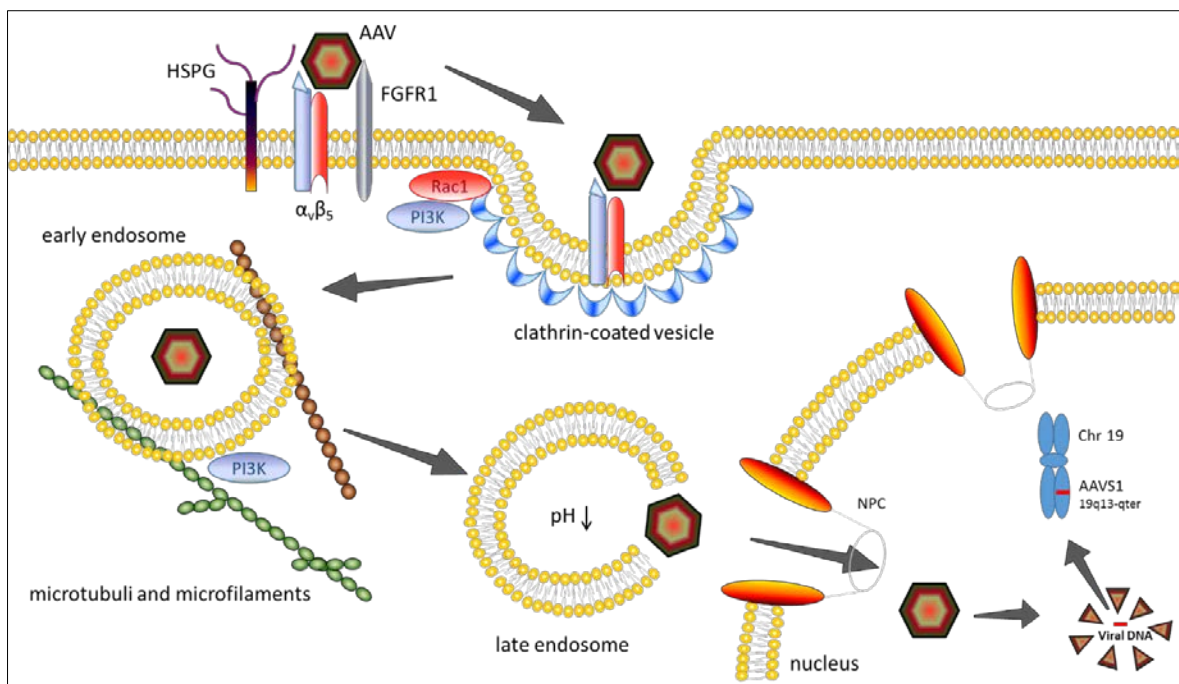
Fig. 1.8. Schematic representation of the AAV infection pathway. After the AAV binds to its primary attachment receptor (HSPG) and co-receptors (FGFR1 and $\alpha_v\beta_5$ integrin) the virus is rapidly internalised via clathrin-coated pits through a process involving $\alpha_v\beta_5$ integrin and in a dynamin-dependent manner. The internalisation is facilitated by the action of Rac1 which subsequently stimulates the PI3K pathway. These in turn control endosome trafficking along the cytoskeleton. The AAV particles are delivered to the late endosome where a progressive drop of pH changes the conformation of the viral capsid, leading to the disruption of the endosomal membrane. This leads to a release of viral particles to the cytoplasm and further transport to the nucleus most probably through the nuclear pore complex (NPC). Uncoating and subsequent releasing of the vector genome takes place in the nucleus. The DNA of the wild type AAV

integrates in a site-specific manner in a region on the long arm of human chromosome 19 (19q13-qter), termed the AAVS1 site. Scheme modified from Huttner (2003).

1.6.2 Recombinant adeno-associated virus (AAV)-based gene therapy

In order to produce a recombinant adeno-associated virus (rAAV), which will be suitable for gene therapy applications, most of the AAV genome has to be removed. Three different plasmids are required: [1] the therapeutic plasmid, which contains the therapeutic expression cassette flanked by inverted terminal repeats (ITRs), which are the only viral *cis* elements required for DNA replication and packaging (McLaughlin *et al.*, 1988). [2] The AAV *Rep* and *Cap* genes are provided in *trans* by a helper plasmid (Grimm *et al.*, 1998). These two plasmids are co-transfected together with a third plasmid [3], providing the capsid information necessary for AAV replication. After transcription and translation of Rep and Cap proteins, the ITR flanked transgene cassette is replicated, and single-stranded DNA molecules are capsulated to form viral particles. Furthermore, the particles have to be harvested, purified and titred (Wright, 2009). The usefulness of AAV in gene therapy approaches can be attributed to its lack of pathogenicity due to its replication failure. It can mediate long-term expression in a variety of tissues. However, the genetic modifications in the AAV genome affect the ability for site-specific integration (Lai *et al.*, 2002). During infection the rAAV genome enters the cell nucleus and persists there predominantly as an episome. However, the integration of the rAAV genome to the host chromosome is possible (Clark *et al.*, 1999; Nakai *et al.*, 2001; Inagaki *et al.*, 2007). Since it was shown that neonatal mice injected with rAAV developed hepatocellular carcinoma (HCC) (Donsante *et al.*, 2007; Chandler *et al.*, 2015), the investigation of potential tumour induction after rAAV-based gene therapy should be elucidated. Another very important determinant of the outcome of gene transfer is the immune response against the vector capsid and transgene product (Mingozzi and High, 2013). Due to this fact there are many factors which have to be taken into consideration during rAAV-based gene therapy designing, e.g. serotype of the virus, promoter under which the therapeutic gene is expressed, amount of the virus as well as route and time-point of injection. rAAVs have been already used in preclinical applications with animal models such as those for haemophilia (Niemeyer *et al.*, 2009), lysosomal storage diseases (Hu *et al.*, 2012) and vision deficiency (Acland *et al.*, 2005), all of these approaches have shown therapeutic

benefits through the viral treatment. Clinical trials using rAAV2 for the treatment of haemophilia B, cystic fibrosis, alpha-1-antitrypsin deficiency or Canavan disease have started already, and reports from phase I trials support the results of preclinical trials (Grieger and Samulski, 2005). Although a substitution therapy for molybdenum cofactor (MoCo) deficiency type A has already been established, a lifelong treatment with cPMP is required to rescue the phenotype. Therefore, a rAAV-based therapy could be an attractive alternative for an expensive and oppressive substitution therapy. A preliminary study has shown that an early treatment with rAAV carrying the expression cassette for the human *MOCS1* gene can completely suppress the phenotype in the *Mocs1* knockout mouse model of MoCo-deficiency type A (Kugler *et al.*, 2007).

1.7 AIMS

The main aim of the present thesis was the generation and characterisation of a mouse model for molybdenum cofactor (MoCo) deficiency supplementation group B, as well as investigating the efficiency and drawbacks of a rAAV-based gene therapy.

The main aims were as follows:

- **Generation of a mouse model for MoCo deficiency type B (*Mocs2*$^{-/-}$)**
  - o Confirmation of the homologous recombination
  - o Design of a genotyping strategy

- **Characterisation of *Mocs2*$^{-/-}$ animals**
  - o Analysis of *Mocs2* isoforms expression on the RNA and protein level by qRT-PCR, LacZ staining and Western blot, respectively
  - o Survival rate and body weight analyses of *Mocs2*$^{-/-}$ mice
  - o Biochemical analysis of the urine parameters
  - o Immunohistochemical analysis of the brain
  - o Histochemical analysis of the kidneys

- **Generation and characterisation of *MOCS2A* and *MOCS2B* transgenic mice**
  - o Generation of *MOCS2A* and *MOCS2B* constructs
  - o Pro-nucleus injection of *MOCS2A* or *MOCS2B* transgene constructs

- o Evaluation of transgene copy numbers in founder animals

- o Verification of the integration site(s)

- o Development of a genotyping strategy

- o Generation of *MOCS2A* and *MOCS2B* transgenic lines

- o Characterisation of the phenotype

- **Development of rAAV therapy for MoCo deficiency type B**
  - o Generation of recombinant adeno-associated virus (rAAV)
  - o Investigation of efficiency of rAAV transduction
  - o Investigation of specificity of rAAV transduction
  - o Investigation of the therapeutic potential of designed rAAV
  - o Investigation of expression persistence of the *MOCS2B* therapeutic gene after rAAV injections
  - o Investigation of the potential risk of mutagenesis after rAAV injections

2 MATERIALS AND METHODS

2.1 MATERIALS

2.1.1 Chemicals and reagents

CHEMICALS	MANUFACTURER
1 kb plus DNA Ladder	Life Technologies, Karlsruhe, Germany
100 bp DNA Ladder	Life Technologies, Karlsruhe, Germany
2-Mercaptoethanol	Life Technologies, New York, USA
3,3'-Diaminobenzidine (*DAB*)	Sigma-Aldrich GmbH, Steinheim, Germany
5-Bromo-4-chloro-3-indolyl phosphate (BCIP)	Sigma-Aldrich GmbH, Steinheim, Germany
5-Brom-4-chlor-3-indoxyl-β-D-galactopyranosid (X-Gal)	Biomol, Hamburg, Germany
Agar	Carl Roth GmbH, Karlsruhe, Germany
Agarose	Carl Roth GmbH, Karlsruhe, Germany
Ammonium chloride (NH_4Cl)	Sigma-Aldrich, Deisenhofen, Germany
Ampicillin	Sigma-Aldrich, Deisenhofen, Germany
Ampuwa (dH_2O)	Fresenius, Bad Homburg, Germany
Boric acid (H_3BO_3)	Scharlau Chemie S.A., Barcelona, Spain
Bradford Reagent	Sigma-Aldrich GmbH, Steinheim, Germany
Chloroform ($CHCl_3$)	Sigma-Aldrich, Steinheim, Germany
Cryo-Embedding Compound	Medite, Winter garden, USA
DePeX Mounting medium	Serva, Heidelberg, Germany
Dimethyl pyrocarbonate (DEPC)	Sigma-Aldrich, Deisenhofen, Germany
Dimethyl sulfoxid (DMSO)	Merck, Darmstadt, Germany
dNTPs	Life Technologies, Karlsruhe, Germany
Dulbecco's Modified Eagle Medium (DMEM)	PAN Biotech GmbH, Aidenbach, Germany
Ethanol (C_2H_5OH)	Baker, Deventer, Netherlands
Ethidium bromide (EtBr)	Sigma-Aldrich, Deisenhofen, Germany
Ethylendiamine-tetraacetic acid (EDTA)	ICN, Aurora, USA
Eukitt quick-hardening mounting medium	Sigma-Aldrich, Deisenhofen, Germany
Fetal bovine serum (FBS)	PAN Biotech GmbH, Aidenbach, Germany

Ficoll 400	Amersham Pharmalia, Freiburg, Germany
Formaldehyde solution 4%	Otto-Fischar GmbH, Saarbrucken, Germany
Gelatin	Sigma-Aldrich, Deisenhofen, Germany
Glacial acetic acid (CH_3COOH)	Life Technologies, Karlsruhe, Germany
Glucose ($C_6H_{12}O_6$)	Carl Roth GmbH, Karlsruhe, Germany
Glycerol ($C_3H_8O_3$)	Life Technologies, Karlsruhe, Germany
Glycin ($C_2H_5NO_2$)	Carl Roth GmbH, Karlsruhe, Germany
Glycerin ($C_3H_8O_3$)	Carl Roth GmbH, Karlsruhe, Germany
Hydrochloric acid (HCl)	Merck, Darmstadt, Germany
Igepal	Sigma-Aldrich, Deisenhofen, Germany
Igepal-CA-360 (Np-40)	Sigma-Aldrich, Deisenhofen, Germany
Isopropanol (C_3H_8O)	Baker, Deventer, Netherlands
Isopropyl β-D-1-thiogalactopyranoside (IPTG)	Biomol, Hamburg, Germany
Kanamycin	Sigma-Aldrich, Deisenhofen, Germany
Ketamin	Medistar Aschenberg, Germany
Leukemia Inhibitor factor (LIF)	Millipore, Billerica, USA
L-Glutamine	PAN Biotech GmbH, Aidenbach, Germany
Lipofectamine 2000	Life Technologies, Karlsruhe, Germany
Magnesium chloride ($MgCl_2$)	Merck, Darmstadt, Germany
Mayer's Hämalaun	Merck, Darmstadt, Germany
Medetomidin (Domitor)	Janssen Animal Health, Germany
Methanol (CH_4O)	Baker, Deventer, Netherlands
Milk powder	Carl Roth GmbH, Karlsruhe, Germany
Mitomycin C	Sigma-Aldrich GmbH, Steinheim, Germany
Natriumchloride (NaCl)	Merck, Darmstadt, Germany
Natrium deoxycholat ($C_{24}H_{39}NaO_4$)	Sigma-Aldrich GmbH, Steinheim, Germany
N, N-Dimethylfloramide (C_3H_7NO)	Sigma-Aldrich GmbH, Steinheim, Germany
Nitro Blue Tetrazolium (NBT)	Sigma-Aldrich GmbH, Steinheim, Germany
Non-essential aminoacid (NEAA)	Life Technologies, Karlsruhe, Germany

Nuclear Fast Red	Sigma-Aldrich GmbH, Steinheim, Germany
NuPAGE MES SDS running buffer	Life Technologies, Darmstadt, Germany
NuPAGE LDS sample buffer (4×)	Life Technologies, Karlsruhe, Germany
Orange G	Merck, Darmstadt, Germany
Opti-MEM	Life Technologies, Karlsruhe, Germany
Paraffin pellets	Carl Roth GmbH, Karlsruhe, Germany
Paraformaldehyde	Merck, Darmstadt, Germany
PBS	PAN-Systems, Nürnberg, Germany
Penicillin/Streptomycin	PAN-Systems, Nürnberg, Germany
Phenol	Biomol, Hamburg, Germany
Potasium acetate ($C_2H_3KO_2$)	Sigma-Aldrich GmbH, Steinheim, Germany
Potassium hexacyanoferrate (II) trihydrate $K_4[Fe(CN)_6]\cdot 3H_2O$	Sigma-Aldrich GmbH, Steinheim, Germany
Potassium hexacyanoferrate (III) $K_3[Fe(CN)_6]$	Sigma-Aldrich GmbH, Steinheim, Germany
RNase A	Qiagen, Hilden, Germany
RNase away	Biomol, Hamburg, Germany
Roti-Mount FluoroCare DAPI	Carl Roth GmbH, Karlsruhe, Germany
Roti Safe	Carl Roth GmbH, Karlsruhe, Germany
SeeBlue Plus2 Pre-Stained Standard	Life Technologies, Karlsruhe, Germany
S.O.C Medium	Life Technologies, Karlsruhe, Germany
Sodium acetate (NaAc)	Merck, Darmstadt, Germany
Sodium citrate ($Na_3C_6H_5O_7$)	Merck, Darmstadt, Germany
Sodium Deoxycholate ($C_{24}H_{39}NaO_4$)	Sigma-Aldrich GmbH, Steinheim, Germany
Sodium dodecyl sulphate (SDS)	Sigma-Aldrich GmbH, Steinheim, Germany
Sodium hydroxide (NaOH)	Merck, Darmstadt, Germany
Sodium pyruvate	Life Technologies, Karlsruhe, Germany
Streptavidin	Sigma-Aldrich GmbH, Steinheim, Germany
SuperSignal™ West Pico Chemiluminescent Substrate	Life Technologies, Karlsruhe, Germany
Tri Fast	PeqLab, Erlangen, Germany

Tris (hydroxymethyl) aminomethane	AppliChem GmbH, Darmstadt, Germany
Tris	Sigma, Deisenhofen, Germany
Triton X-100	Serva, Heidelberg, Germany
Tryptone/Peptone	Roth, Karlsruhe, Germany
Tween-20	Sigma, Steinheim, Germany
Xylene	Baker, Deventer, Germany
Yeast Extract	Carl Roth GmbH, Karlsruhe, Germany

2.1.2 Biochemical enzymes

ENZYMES	MANUFACTURER
Antarctic Phosphatase	New England Biolabs, Ibswich, USA
BigDye	Life technologies, Darmstadt, Germany
Complete Mini Protease Inhibitor Cocktail Tablets	Roche, Manheim, Germany
Direct PCR Lysis Reagent	Peqlab, Erlangen, Germany
DNAse	Sigma-Aldrich, Deisenhofen, Germany
Proteinase K	Carl Roth GmbH, Karlsruhe, Germany
Restriction Enzymes (with supplied buffers)	New England Biolabs, Ibswich, USA
Reverse Transcriptase SuperScript II	Life Technologies, Darmstadt, Germany
RNAse A	AppliChem GmbH, Darmstadt, Germany
Platinum Taq polymerase	Life Technologies, Karlsruhe, Germany
T4 DNA Ligase	Life Technologies, Darmstadt, Germany
TrypLE Express	Life Technologies, Darmstadt, Germany

2.1.3 Ready-to-use reaction systems

REACTION SYSTEM	MANUFACTURER
DNasy Blood and Tissue Kit	Qiagen, Hilden, Germany
DNA Walking Speed Up Kit	Seegene, USA
Direct PCR Tail Reagent	Peqlab, Erlangen, Germany
Endo Free Plasmid Maxi Kit	Qiagen, Hilden, Germany

Genome Walker Universal Kit	Clontech, Mountain View, CA, USA
Platinum SYBR-Green qPCR Super Mix-UDG	Life Technologies, Darmstadt, Germany
QIAquick Gel Extraction Kit	Qiagen, Hilden, Germany
RNAeasy Kit	Qiagen, Hilden, Germany

2.1.4 Plasmids

PLASMID	PROVIDED BY
pAAV2.1TBGeGFP3	Telethon Institute of Genetics and Medicine (*TIGEM*), Napoli, Italy
pCAAG-FLPe	Prof. I. Adham, Institute of Human Genetics Goettingen
pGEMTeasy	Promega, Wisconsin, USA
pWajaII	Waja Wegner
pWajaIII	Waja Wegner

2.1.5 Usage ware

USAGE WARE	MANUFACTURER
12 well cell culture plates	Cellstar, USA
6-, 24-well cell culture plates	Sarstedt, Numbrecht, Germany
	Corning Inc., New York, USA
384 wells-plates, white	AB-gene, Hamburg, Germany
13, 15, 50 ml tubes	Greiner-bio-one, Kremsmunster, Austria
Blotting Paper GB 002, 003, 004	Schleicher & Schuell, Dassel, Germany
Butterfly needle	Terumo, Leuven, Belgium
Cell culture flasks	Sarstedt, Nurnbrecht, Germany
Cover Glass 24x60mm	Menzel Glaser, Braunschweig, Germany
e-cup homogenisers	Sartorius, Goettingen, Germany
Electroporation cuvettes	Peqlab, Erlangen, Germany
Flat-bottomed Nuclon^{TM} surface 96 well	Nunc A/S, Denmark

cell culture plates	
Hybond C	Amersham, Braunschweig, Germany
Hybond N	Amersham, Braunschweig, Germany
Membrane filter	Millipore, Billerica, USA
Microcentrifuge Tubes	Sarstedt, Nurnbrecht, Germany
NuPAGE^{TM} 4-12%, 10% Bis-Tris Gel	Life Technologies, Darmstedt
Para-film M	Pechiney, Chicago, USA
Petri dishes	Greiner Nunc., Nurntingen, Germany
Pipet tips	Sarstedt, Nurnbrecht, Germany
PVDF-Membrane	GE Healthcare, Munich, Germany
QIAfilter Cartrige	Qiagen, Hilden, Germany
Qiagen-tip 100	Qiagen, Hilden, Germany
QIA quick column	Qiagen, Hilden, Germany
Single-use needle	B. Broun Sterican, Melsungen, Germany
Single-use syringe	Norm-Ject, Tuttingen, Germany
Sterile-single use filter Minisart	Sartorius, Goettingen, Germany
Sterile Corning Filter System	Sarstedt, Newton, USA
Superfrost slides	Thermo Scientific, Braunschweig, Germany
Syringe filters Minisart NML	Sartorius, Goettingen, Germany
Transfections tubes	Lab-Tek/Nalge, Nunc, USA
Whatman blotting paper	Schleicher and Schüll, Dassel, Germany
X-ray films	Amersham, Braunschweig, Germany

2.1.6 Technical equipment

TECHNICAL EQUIPMENT	MANUFACTURER
Autoclave Systec DX-150	Systec GmbH Wettenberg, Germany
BioRad gene pulser TM apparatus Electroporation	BioRad laboratories, München, Germany
Centrifuge 5415R	Eppendorf AG, Hamburg, Germany
Centrifuge, Megafuge 16R	Thermo Scientific, Osterode, Germany

Centrifufe, Multifuge X3R	Thermo Scientific, Osterode, Germany
Cryostat	Leica Microsystems, Nussloch, Germany
FluorChem Q	Alpha Innotech, Logan, Utah, USA
Freezer-152°C	GFL mbH, Burgwedel, Germany
Histocentre 2 embedding machine	Shandon, Pittsburg, USA
HT7900 Fast Real-Time PCR System	Applied Biosystems GmbH, Darmstadt, Germany
Incubator	Incubat Melag OHG, Berlin, Germany
Incubator	MWG-Biotech mini 10, Ebersberg,Germany
Incubator CO_2, MOCO-20AIC	Sanyo, Japan
Incubator Innova shaker-Series	New Brunschwick Scientific
Microtome Jung RM2035	Leica Instruments GmbH, Nussloch, Germany
Laminar Heraeus Instruments	HeraSafe, Hanau, Germany
Microscope BX60	Olympus, München, Germany
Microscope PrimoVert Zeiss	Microimaging GmbH, Goettingen, Germany
Monochrome Printer Mitsubishi P95	Biometra, Malaysia
NanoDrop 2000C Spectrophotometer	PeqLab Thermo Scientific, Erlangen, Germany
Roller RM5	Assistant, M.Zipperer GmbH, Etzenbach, Germany
Semi dry transfer machine (blotter)	Biometra An Analitik Jena, Germany
Sequencer 3500XL	Applied Biosystems, Darmstadt, Germany
Sonifier 250 Ultrasonic Cell Homogeniser	Branson, Danburg, USA
Spectrophotometer Ultraspec 3000	Amersham, Freiburg, Germany
Thermal Cycler 2720	Applied Biosystems, Singapore
Thermomixer 5436	Eppendorf-Netheler-Hinz GmbH, Hamburg, Germany
Thermomixer comfort	Eppendorf AG, Hamburg, Germany
UV Kontaktlampe Chroma42	Vetter GmbH, Wiesloch, Germany
UV Solo TS Imaging System (gel imaging)	Biometra Analytic Jena, Germany
Vortex Bibby Stuart	Bibby Sterilin LTD, Stone, Staffordshiere,

	England
Water bath	Kottermann, Hanigsen, Germany
Weighing Instrument MC1	Laboratory LC Sartorius, Goettingen, Germany

2.1.7   Solutions

SOLUTIONS	COMPONENTS
AE Buffer	10 mM Tris-HCl
	0.5 mM EDTA, pH 9
Animal anesthesia solution	0.25 ml Medetomidin (Domitor)
	1 ml Ketamin
	8.75 ml Sodium Chloride 0.9%
AP Buffer	100 mM NaCl
	50 mM $MgCl_2$
	100 mM Tris/HCl, pH 9.5
AP Staining Solution	45 µl NBT (75 mg/ml in DMF)
	35 µl BCIP (50 mg/ml in DMF)
	in 10 ml AP Buffer
Blocking Buffer (Western Blot)	1x TBS-Tween
	5% low-fat dry milk
Detergent rinse (LacZ staining)	0.02% Igepal
	0.01% Sodium Deoxycholate
	2mM $MgCl_2$ in 0.1M phosphate buffer, pH 7.5
Lysis Buffer I	50 mM Tris/HCl, pH 8.0
	100 mM EDTA
	0.5% SDS
Lysis Buffer II	100 mM Tris/HCl, pH 8.0
	5 mM EDTA
	200 mM NaCl
	0.2% SDS

28

	100 µg/ml Proteinase K
P1 Buffer (Plasmid Preparation)	50 mM Tris-HCl, pH 8.0
	10 mM EDTA
	100 µg/ml RNAse A
P2 Buffer (Plasmid Preparation)	200 mM NaOH
	1% SDS
P3 Buffer (Plasmid Preparation)	3 mM Potassium acetate, pH 5.5
PE Buffer	20 ml NaCl
	2 mM Tris-HCl, pH 7.5
	80% EtOH
Protein Lysis Buffer	150 mM NaCl
	1 mM EDTA
	50 mM Tris-HCl, pH 7.4
	1% IGEPAL-CA-360 (NP-40)
	0.25% Natriumdeoxycholat
	1 Tablet/ 10 ml Complete Mini protease inhibitor
	10 µl/10 ml Phosphatase-Inhibitor-Mix II
QBT Buffer	750 mM Sodium chloride
	50 mM MOPS, pH 7.0
	15 % Ethanol
	0.5 % Triton X-100
QC Buffer	1 mM Sodium chloride
	50 mM MOPS, pH 7.0
	15 % Ethanol
QF Buffer	1.25 M Sodium chloride
	50 mM Tris/HCl, pH 8.5
Stop Mix	15% Ficoll 400
	200 mM EDTA
	0.1 % Orange G

5 × TBE	450 mM Tris base
	450 mM Boric acid
	20 mM EDTA, pH 8
10 × TBS	1.37 M NaCl
	100 mM Tris
	Adjusted to pH 7.6 with HCl
TE Buffer	10 mM Tris/HCl, pH 8.0
	1 mM EDTA
Transfer Buffer (Western Blot)	25 mM Tris, pH 8.3
	150 mM Glycin
	20% Methanol
Washing Buffer (Western blot)	1 × TBS-Tween
	2% low-fat dry milk
X-Gal staining solution (LacZ staining)	0.02% Igepal
	0.01% Sodium Deoxycholate
	5mM Potassium hexacyanoferrate (II) trihydrate
	5mM Potassium hexacyanoferrate (III)
	2mM $MgCl_2$ in 0.1M phosphate buffer, pH 7.5
	1mg/ml X-Gal in N,N-dimethyl-formamide (prior to use)
X-Gal Stock Solution	20 mg X-Gal/ml N.N.-Dimethyl-formamide

2.1.8 Culture media antibiotics and agar plates

2.1.8.1 Culture media for bacteria

Luria-Bertani medium (LB medium)	10g/l Trypton/Pepton
	5g/l Yeast Extract
	10g/l NaCl
	pH 7.0

The LB medium was prepared with dH_2O, autoclaved and stored at 4°C.

2.1.8.2 Culture media for eukaryotic cells

Embryonic stem (ES) cell medium	DMEM
	1 mM Non-essential amino acids
	1 mM Sodium pyruvate
	10 µM ß-Mercaptoethanol
	2 mM L-Glutamine
	20% FBS
	1000 U/ml Recombinant leukaemia inhibitory factor (LIF)
Fibroblast cells medium (MEFs)	DMEM
	2 mM L-Glutamine
	10% FCS
	1% penicillin/streptomycin
Freezing medium	50% FCS
	20% DMSO
	30% culture medium

2.1.8.3 Antibiotics

For the antibiotics stock solutions were prepared. They were filtered through sterile disposable filters and stored at -20°C.

ANTIBIOTIC	STOCK SOLUTION	WORKING SOLUTION
Ampicillin	50 mg/ml	50 µg/ml
Kanamycin	50 mg/ml	50 µg/ml
Puromycin	50 mg/ml	50 µg/ml

2.1.8.4 IPTG/X-Gal plates

IPTG/X-Gal plates	LB-agar (1.5% Agar in the LB medium)
	50 µg/ml ampicillin
	100 µM IPTG
	0.4% X-Gal

The medium was autoclaved. After it had cooled down to a temperature lower than 55°C, the antibiotic, IPTG and X-Gal was added. Finally, the medium was poured into Petri dishes and stored at 4°C.

2.1.9 Biological material

2.1.9.1 Bacterial strains

Plasmids were transformed into the *Escherichia coli* strain DH5α, provided by Life Technologies, Karlsruhe, Germany.

2.1.9.2 Eukaryotic cell lines

NIH3T3	Mouse embryonic fibroblast cell line, ATCC, Rockville, USA
HepG2	Human hepatocellular liver carcinoma *cell* line, ATCC, Rockville, USA
HeLa	Human cervix adenocarcinoma cell line, ATCC, Rockville, USA
R1 ES	Mouse embryonic stem cell line, ATCC, Rockville, USA

2.1.9.3 Mouse strains

C57Bl/6N as well as 129sv mice were obtained from a colony of our own department. The animals were kept in sterile conditions, at a 12 hours light/dark cycle at 22° C and $55 \pm 5\%$ relative humidity. All experiments were performed according to the European and German protection of animals act. The number of sacrificed animals, the stress and pain they were suffering was reduced to a minimum. Euthanasia was performed either by cranial dislocation or CO_2 asphyxiation.

2.1.10 Synthetic DNA oligonucleotides

The synthetic oligonucleotide primers used in this study were obtained from Eurofins MWG Operon (Ebersberg, Germany), and dissolved in dH_2O (Ampuwa) to a final concentration of 100 pmol/µl. Sequences are listed below, starting from 5'- to 3'- end.

2.1.10.1 Vector-specific primer

PRIMER NAME	SEQUENCE
T7	TAATACGACTCACTATAGGG
Sp6	ATTTAGGTGACACTATAGAAT

2.1.10.2   Human-specific primers

PRIMER NAME	SEQUENCE
qMOCS2AEx1a_F	TCGGTCCCGCTGTCCTAG
qMOCS2AEx2_R	AAATGGTCTCTGAACGAACTCCT
qMOCS2BEx5_F	GGCAGAAATGGCCAGTCAA
qMOCS2BEx6_R	GCTGAGGACACAGCAATGATTA
nest.humF1_Ex3	AGCTCCTCGTGCTTCAGCCT
nest.hum.R1_Ex6	ATATGGGCACCTTGGCTTTTAAAGT
nest.humF2_Ex3	CCCCATTAGTGGAGGATAGTGCT
nest.hum.R2_Ex6	GAACCAAGCCAAGTCTATGGAAC
F_NotIEx3	GCGGCCGCATGTCGAGCTTGGAGATCAGCTCC
R_NotISTOPEx7	GCGGCCGCTTAACTGTTGGATGCCCAAAAGCA
R_NotIEx7	GCGGCCGCACTGTTGGATGCCCAAAAGCACTC

2.1.10.3   Mouse-specific primers

PRIMER NAME	SEQUENCE
Zfyve27_F	GCTCTCTGCACCCAGCTAAG
Zfyve27_R	ATAGAGGACCTGGGCACCTT
Sry_F	TCATGAGACTGCCAACCACAG
Sry_R	CATGACCACCACCACCACCAAA
HPRT_F	CGTCGTGATTAGCGATGATG
HPRT_R	TATGTCCCCCGTTGACTGAT
Mocs2aF_In2-3	GGCTTCATACGAAAAGGCTGT
Mocs2aR_In2-3	GTGCGTGGGGTTTGTTATTCT
Mocs2bF_Ex5	CGTATGTACCGATGGCAGAAA
Mocs2bR_In5-6	ACCTGAAGGTCTTGGCACATT
Mocs2aF_Ex1	GTGTAGCGGGATGGTTCCTA
Mocs2aR_Ex3	ACATCAGCCAACCCAGGAT
Mocs2bF_Ex5	CGTATGTACCGATGGCAGAA
Mocs2bR_Ex6	TATGGGCACCTTGGCTTTTA

Dnajc24_F	CATGGAGGAGTGTATGCAGAAGTT
Dnajc24_R	ATCTACTGGCCCCACATTTCTTAG
qF_Mocs2Ex4	CCTCTGTGTGGTGCAGTGTC
qR_Mocs2Ex5	ACCAAGCCGATGGAATACTG
Gapdh_F	CGTCCCGTAGACAAAATGGT
Gapdh_R	TTGATGGCAACAATCTCCAC

2.1.10.4 Genotyping primers

PRIMER NAME	SEQUENCE
MOCS2-5'arm	CCTCTGTCACTTACTTGGTTTGAGC
LAR3	CAACGGGTTCTTCTGTTAGTCC
MOCS2-3'arm	CGACTTACACATTGTTTCCATGTCC
Mocs2KOGeno_F1	GGGAATCCAGTCCACCCTTTCTCTT
Neo_F	GCAGCCTCTGTTCCACATACACTTCA
GeneSpec_R1	ACAATCTCCTCAAGCAATTGTGGGC
Mocs2_5'F	AATAAGAACCCGGATCCCACACT
Mocs2KO_R	CCCGTTCAAAGATCTGAGTTGCT
Mocs2KO_F	GGGAATCCAGTCCACCCTTTCTCTT
Mocs2_3'R	CATGTTAATCGTCTGGGTTGTGACGA
Mouse#56_T1F	ACATGGAAATGTCAAGTGCACAG
TransgeneA_F	ATGCCTCTTCCGACCATCAA
Mouse#56_T1R	TACCAGCAGCATGTAATTTTCCAG
Mouse#56_T2F	GAGACCATGAAGGAAAAGTACACACA
Mouse#56_T2R	GTGGAAGATGTTGGGTTCTGGTATAA
Mouse#44_F	CCAGTACCCCAGAACTTGTGT
TransgeneA_R	CCGGTTGCATTCGATTCCTG
Mouse#44_R	AAACTTCCTACCCCTTACCCC
Mouse#84_F	CTAGCATTTCCCAAGGGTCA
TransgeneB_F	GATGCGCCAGAGTTGTTTCT
Mouse#84_R	GGTCCCCGTTTTTGTAAACC

2.1.10.5 cDNA synthesis primers

PRIMER NAME	SEQUENCE
oligo (dT)$_{12-18}$ primer	$(T)_{12}$ and $(T)_{18}$

2.1.11 Antibodies

2.1.11.1 Primary antibodies

The MOCS2A and MOCS2B antibodies were produced by Eurogentec (Seraing, Belgium), based on protein sequences provided by us. The peptide sequences used for immunisations were specific either for mice or for human.

PRIMARY ANTIBODY	MANUFACTURER
Anti-Mocs2a (EP130014) polyclonal antibody, rabbit	Eurogentec, Seraing, Belgium
Anti-Mocs2b (EP113633) polyclonal antibody, rabbit	Eurogentec, Seraing, Belgium
Anti-MOCS2B (EP113635) polyclonal antibody, rabbit	Eurogentec, Seraing, Belgium
Anti-α-tubulin, monoclonal antibody, mouse	Sigma-Aldrich, Deisenhofen, Germany
Anti-NeuN, Clone A60, monoclonal antibody, mouse	Merck-Millipore, Darmstadt, Germany
Anti-IBA1, polyclonal antibody, rabbit	Wako, Neuss, Germany
Anti-Caspase3, rabbit	BD Pharmingen, Germany
Anti-GFAP, monoclonal, mouse	Sigma-Aldrich, USA

2.1.11.2 Secondary antibodies

SECONDARY ANTIBODY	MANUFACTURER
Alexa Fluor 546 goat anti-rabbit IgG	Life Technologies, USA
Alexa Fluor 555 goat anti-mouse IgG	Life Technologies, USA
Anti-Rabbit IgG, Cy3	Sigma-Aldrich, USA
Anti-Mouse IgG-Peroxidase antibody produced in	Sigma-Aldrich, USA

rabbit	
Anti-Rabbit IgG-Peroxidase antibody produced in goat	Sigma-Aldrich, USA
Anti-Rabbit IgG (whole molecule)-Alkaline Phosphatase antibody produced in goat	Sigma-Aldrich, USA
Anti-Mouse IgG (whole molecule)-Alkaline Phosphatase antibody produced in goat	Sigma-Aldrich, USA
Anti-Mouse IgG-Peroxidase antibody produced in sheep	Amersham, Freiburg, Germany
Anti-Rabbit IgG-Peroxidase antibody produced in goat	Dianova, Hamburg, Germany

2.1.12 Databases

USAGE	PROGRAMM
Bioinformatics	Ensembl (http://www.ensembl.org/index.html)
	Nation Center for Biotechnology Information (NCBI) (http://www.ncbi.nlm.nih.gov/)
	ExPASy (http://www.expasy.org/)
	Online Mendelian Inheritance in Man (OMIM) (http://www.omim.org/)
	Human Gene Mutation Database (HGMD) (http://www.biobase-international.com/product/hgmd
	SnapGene Viewer (http://www.snapgene.com/products/snapgene_viewer/)
Cell counting	Image Processing and Analysis in JAVA (ImageJ) (http://imagej.nih.gov/ij/)
Primer design	Primer 3 (http://primer3.ut.ee/)
Protein sequence analysis	Simple Modular Architecture Research Tool (SMART) (http://smart.embl-heidelberg.de/)

Restriction site analysis	NEB Cutter 2.0 (http://nc2.neb.com/NEBcutter2/)
	WEB Cutter 2.0 (http://bio.lundberg.gu.se/cutter2/)

2.1.13   Statistical methods

STATISTICAL METHOD	APLICATION
Student's t-test	Calculation of differences between WT and KO animals
Chi-square test	Calculation of differences between F1 genotype frequencies and the Mendelian frequencies that would be expected after breading of heterozygous *Mocs2*$^{+/-}$ animals

2.1.14   Sterilisation of solutions and equipment

Heat-sensitive solutions were filtered using disposable sterile filter units (0.2 to 0.45 µm pore size). All solutions which were not heat-sensitive and the plastic equipment were sterilised at 121°C, 105 Pa for 60 min in an autoclave. Glass wares were sterilised overnight in an oven at 180°C.

2.2   METHODS

2.2.1   Isolation and purification of nucleic acids

2.2.1.1   Minipreparation of plasmid DNA

A single bacterial colony was inoculated into 5 ml LB medium, containing an antibiotic (ampicillin or kanamycin) (50 µg/ml), and incubated at 37°C overnight in the shaker with a shaking speed of 160 rpm. 0.6 ml of the overnight-culture was used for glycerol stock preparation. The rest was centrifuged at 13000 rpm for 5 min at RT. The bacteria pellet was resuspended in 100 µl of resuspension buffer P1 (Qiagen). The bacterial cells were lysed with 200 µl of P2 lysis solution (Qiagen), incubated at RT for 5 min, and then neutralised with 150 µl of buffer P3 (Qiagen). The precipitated solution was centrifuged at 13000 rpm at RT for 20 min. The supernatant was transferred into a fresh tube and centrifuged again under the same condition for 10 min. Finally, the supernatant (~450 µl) was transferred to fresh tube and mixed with an equal volume of ice-cold isopropanol to precipitate the DNA. After 30 min of incubation on ice, it was centrifuged at 13000 rpm at

4°C for 30 min. The DNA pellet was washed with 1ml of 70% ethanol, and after air-drying, dissolved in 30 µl of dH$_2$O (Ampuwa).

2.2.1.1.1 Preparation of bacterial glycerol stocks

200 µl of 80% sterile glycerol was added to 600 µl of a bacterial suspension, well mixed and stored at -80°C.

2.2.1.2 Large-scale preparation of Endotoxin-free plasmid DNA using the Qiagen Maxi Kit

A single colony was inoculated into 5 ml LB medium, containing an appropriate antibiotic (50 µg/ml). The pre-culture was incubated overnight at 37°C with shaking (160 rpm). Further, the pre-culture was diluted 500-fold in 100 ml of the LB medium and incubated 12 hours at 37°C with shaking (160 rpm). On the next day the overnight culture was centrifuged at 4000 rpm for 15 min at 4°C. The bacterial pellet was resuspended in 4 ml of P1 solution. Further, the cells were lysed with 4 ml of P2 buffer, neutralised with 4 ml of buffer P3 and immediately poured into the barrel of the QIAfilter Cartridge, provided by the company. After 10 min of incubation, the lysate was filtered to a 50 ml tube. Further, 1 ml of buffer ER was added to the filtered lysate and mixed. It was incubated on ice for 30 min. Before the lysate was applied to the supplied QIAGEN-tip 100, the column was equilibrated with buffer QBT. After the lysate passed through the resin by gravity flow, the QIAGEN-tip was washed twice with 10 ml of buffer QC, and the DNA was eluted using 5 ml of QN solution. To precipitate the DNA, 3.5 ml of isopropanol was added, mixed thoroughly and then centrifuged at 13000 rpm for 30 min at 4°C. The obtained DNA pellet was washed with 70% endotoxin-free ethanol, air-dried and dissolved in 100 µl of TE buffer.

2.2.1.3 Isolation of genomic DNA

2.2.1.3.1 Isolation of genomic DNA from tissue samples

Mouse tissue was homogenised and incubated in 700 µl of lysis buffer I, containing 35 µl proteinase K (100 µg/ml), overnight at 55°C in a thermomixer. The tissue lysate was centrifuged at 13000 rpm for 15 min and the supernatant was transferred into a fresh reaction tube. Further, genomic DNA was precipitated by adding an equal volume of

isopropanol, mixed by inverting and centrifuged at 13000 rpm at RT for 15 min. The DNA pellet was washed with 1 ml of 70% ethanol, dissolved in 50-100 µl of dH_2O (Ampuwa) and incubated at 60°C for 10 min.

2.2.1.3.2 Isolation of genomic DNA from cells

Cells were washed with DPBS, trypsinised and collected by centrifugation. The supernatant was removed by aspiration; the cell pellet was resuspended in DPBS and subsequently transferred into a reaction tube. After centrifugation at 1000 rpm for 5 min, the supernatant was removed, and cells were incubated overnight in 105 µl of lysis buffer II at 55^oC. After inactivation of proteinase K, an equal volume of isopropanol was added, mixed by inverting several times, and incubated for 10 min at RT. After centrifugation for 15 min at 13000 rpm, the DNA pellet was washed with 70% ethanol. The genomic DNA was dissolved in 50-100 µl of dH_2O (Ampuwa) and incubated at 55^oC for 10 min.

2.2.1.3.3 Isolation of genomic DNA from sperm

To collect the sperm, the chimeric male was bred with a wild type female. Once the vaginal plug was confirmed, the female was sacrificed and spermatozoa were flushed out from the uterus into DPBS and pelleted by centrifugation at 13000 rpm. The DNA from spermatozoa was isolated using the DNeasy Blood and Tissue Kit (Qiagen). The sperm was incubated for 1 hour at 56°C in the 100 µl of buffer X_2. Further, 200 µl of buffer AL was added and mixed. After the 200 µl of 100% ethanol was added and mixed, the mixture was loaded into DNeasy Mini spin column, placed in a 2 ml collection tube and centrifuged at 6000 rcf for 1 min. The flow through was discarded. The column was washed with 500 µl of buffer AW1, and centrifuged at 6000 rcf for 1 min. Again, the flow through was discarded, while the column was placed in a new 2 ml tube, and washed with 500 µl of buffer AW2 and subsequently centrifuged 3 min at 14000 rpm to dry the membrane. Next, the column was placed in a 1.5 ml tube, and the DNA was eluted with 50 µl of buffer AE. After 1 min of incubation, the tube was centrifuged for 1 min at 8000 rpm. The isolated DNA was used for PCR analysis.

2.2.1.3.4 **Isolation of genomic DNA from recombinant adeno-associated virus (rAAV)**

To extract DNA from rAAV, 10 µl of the viral sample was boiled at 90°C for 10 min in 90 µl DPBS, and subsequently centrifuged for 15 min at 13000 rpm at RT. 150 µl of lysis buffer containing proteinase K was added and the solution was incubated for 30 min at RT. After 5 min of centrifugation at 13000 rpm, 200 µl of isopropanol was added, and the solution was incubated 15 min at -20°C. After incubation, the sample was centrifuged for 5 min at 13000 rpm. The DNA pellet was washed with 70% ethanol, air-dried, and resuspended in 10-20 µl of dH$_2$O (Ampuwa). The DNA was stored at -20°C.

2.2.1.4 **Isolation of total RNA from tissue samples**

100-200 mg of tissue sample was homogenised in 0.5 ml of Tri Fast Reagent using an e-cup homogeniser. After 5 min incubation at RT, 100 µl of chloroform was added, mixed vigorously, and incubated 10 min at RT. After centrifugation at 12000 rpm for 15 min at 4°C, the upper aqueous phase was transferred into a new tube. The RNA was precipitated by adding 250 µl of isopropanol, incubated for 10 min at RT, and at centrifuged 12000 rpm at 4°C for 10 min. Finally, the RNA pellet was washed with 75% RNAse-free ethanol, dissolved in 20-50 µl of RNase-free water (DEPC H$_2$O), and stored at -80°C.

2.2.1.5 **Determination of nucleic acid concentration**

The concentration of nucleic acids was determined spectrophotometrically using a Nano Drop spectrophotometer. Prior to measurement, the instrument was calibrated with buffer used for the sample dilution. To evaluate the concentration, 1 µl of the solution was loaded on the pedestal arm. The concentration was determined automatically. The quality of nucleic acids, i.e. contamination with proteins, was estimated by the ratio of absorbance 260 nm/280 nm. The correct value of the ratio is between 1.8 and 2.0.

2.2.1.6 **Cloning techniques**

2.2.1.6.1 **Cleavage of DNA with restriction endonucleases**

Restriction enzyme digestions were performed by incubating double-stranded DNA with a restriction enzyme in a total volume of 10 µl. Per 1 µg DNA 7.5 U of restriction enzyme

was used, together with a buffer recommended by the supplier. The reaction was incubated at 37°C for 90 min.

2.2.1.6.2 Isolation of DNA fragments from agarose gels using the QIAquick Gel Extraction Kit (Qiagen)

The kit was used to extract and purify DNA of 70 bp to 10 kb in length from agarose gels. Up to 400 mg agarose could be processed during a single isolation. Three gel volumes (gel volume corresponds to the slice weight, 100 mg = 100 µl) of QG buffer were added to the agarose gel piece and incubated at 50°C for 10 min. After the gel slice was dissolved, one gel volume of isopropanol was added. The solution was applied to a QIAquick column, provided by the company, and centrifuged for 1 min at 13000 rpm. The flow through was discarded, and the column was washed with 0.75 ml of PE buffer. After 5 min of incubation, the column was centrifuged, and the flow through was discarded. The column was placed into a fresh microcentrifuge tube. DNA was eluted by application of 50 µl of EB buffer to the centre of the QIAquick membrane, and a subsequent centrifugation for 1 min.

2.2.1.6.3 Dephosphorylation of plasmid DNA

Dephosphorylation was performed to avoid self-religation of linearised plasmid DNA. To remove the terminal 5'-phosphate group of the vector, the DNA was incubated with 2 U of *Antarctic phosphatase* for 1 hour at 37°C.

2.2.1.6.4 Ligation of DNA fragments

The cloning of an insert DNA into a vector (digested with appropriate restriction enzyme(s)) was carried out in the following ligation reaction mix in a total volume of 10 µl for 3 hours at RT.

Ligation reaction	Ligase Buffer × 10	1 µl
	Vector DNA (digested)	25-50 ng
	Insert DNA	30-120 ng
	T4 DNA ligase (5 U/µl)	1 µl
	H_2O	up to 10 µl

2.2.1.6.5 TA-Cloning

Taq polymerase and other DNA polymerases have a terminal transferase activity that results in the non-template addition of a single nucleotide to the 3' ends of PCR products. In the presence of all four dNTPs, dATP is preferentially added. This terminal transferase activity is the basis of the TA-cloning strategy. For cloning of PCR products, a pGEMT-easy vector system that has 5'-dT overhangs was used. The reaction was incubated in a total volume of 10 µl for 3 hours at RT, or overnight at 16°C.

Cloning of PCR products using pGEMT-easy vector system	pGEMT-easy vector	50 ng
	PCR product	150 ng
	T4 DNA Ligase buffer (×10)	1 µl
	T4 DNA Ligase	1 µl
	H_2O	up to 10 µl

2.2.1.6.6 Transformation of competent bacteria (Hanahan, 1983)

Transformation of bacteria was done by gently mixing a 50 µl aliquot of DH5α competent bacteria with 10 µl of ligation reaction. After incubation for 30 min on ice, bacteria were heat-shocked for 45 sec at 42°C, and cooled down for 5 min on ice. After adding 950 µl of S.O.C. medium, the mixture was incubated at 37°C, at 600 rpm, for 1 hour. Finally, 150 µl of the transformed bacteria were plated out on LB-agar plates containing an appropriate antibiotic (50 µg/ml), and incubated overnight at 37°C.

2.2.1.7 Gel electrophoresis

Gel electrophoresis is the technique which enables the separation of nucleic acids and proteins in an electrical field according to their size, which is directly related to the number of nucleotides or amino acids in the molecule, charge and shape.

2.2.1.7.1 Agarose gel electrophoresis of DNA

Agarose gels were used to run nucleic acid molecules from 50 bases to more than 20 kb, depending on the concentration of the agarose. Usually, 1.2 g agarose was added to 100 ml of 0.5 × TBE buffer, and boiled in the microwave to dissolve the agarose. After cooling down the solution to approximately 60°C, 3 µl of ethidium bromide (10 mg/ml) or 5 µl of

Roti Safe were added to stain the gel. The prepared agarose gel was poured into a horizontal gel chamber. Gel electrophoresis was performed 5 min at 95 V, and further at 120 V for 40 min.

2.2.1.7.2 Length standard

For determination of DNA fragment length on agarose gels, length standards were loaded in parallel (100 bp, or 1Kb Plus DNA-ladder, Life Technologies)

2.2.1.8 Polymerase Chain Reaction (PCR)

2.2.1.8.1 Amplification of DNA fragment

The PCR is an *in vitro* method to amplify specific DNA fragments. The method uses high temperatures to denature double-stranded DNA, and to allow bindings of primers (annealing). After primers bind to the single-stranded DNA, oligonucleotides are extended by the polymerase (elongation). Denaturation, annealing and elongation are steps which are repeated certain time to increase exponentially the number of DNA fragments. The amplified products can be loaded on an agarose gel.

PCR reaction components	DNA	10 ng
	forward primer (10 pmol)	1 µl
	reverse primer (10 pmol)	1 µl
	10 mM dNTPs	1 µl
	10 × PCR buffer	5 µl
	50 mM MgCl$_2$	1.5 µl
	Taq DNA Polymerase (5 U/µl)	0.5 µl
	dH$_2$O	Up to 50 µl

The reaction mixture was performed in a 200 µl reaction tube and placed in a thermocycler. Thermal cycling was carried out for 25-35 cycles with denaturation at 94°C for 30 sec, annealing at 55-62°C for 30-45 sec and extension at 72°C for 30-90 sec. (depending on the product size).

2.2.1.8.2   cDNA synthesis

cDNA synthesis generates cDNA fragments from RNA templates and helps to determine the expression of genes in specific tissues or in different development stages. After DNAse digestion, 1-5 µg of total RNA was mixed with 1 µl of oligo (dT) (10 pmol/µl) in a total volume of 13 µl. For RNA denaturation, the mixture was heated to 65°C for 10 min and then quickly chilled on ice. After a brief centrifugation, 4 µl of 5x first strand buffer and 2 µl of 0.1 M DTT were added, mixed and incubated at 42°C for 2 min. Further, 1 µl of reverse transcriptase enzyme (Superscript II RT) was added and the mixture was incubated at 42°C for 50 min for first strand cDNA synthesis. The reaction was inactivated by heating at 70°C for 15 min. The quality of synthesised cDNA was checked by PCR using primers specific for the housekeeping gene *Hprt*, before it was subjected to further analysis.

2.2.1.8.3   Quantitative Real-Time PCR (qPCR or qRT-PCR)

The quantitative real-time PCR is a method that relies on the basic PCR principle; however, due to the presence of fluorescent dye in the mastermix, which binds unspecifically to double stranded DNA, provides very accurate and reproducible quantitation of gene copies. In the study we used the PCR mastermix including Platinum SYBR Green qPCR. SYBR-Green which is bound to double stranded DNA can be excited with light with a wavelength of 480 nm. Its emission spectrum is comparable to that of fluorescein with a maximum at 520 nm. The fluorescent intensity was measured after every PCR cycle using the HT7900 Fast Real-Time PCR System (Applied Biosystems), and a graph was generated. During the exponential phase the threshold value was determined. It defines the PCR cycle where the optimal conditions, with enough reaction materials and the maximal polymerase activity, are obtained. This value is used for further calculations (Ct value). The data were evaluated with the Sequence-detection system software (SDS Version 2.4, PE Applied Biosystems). The reaction was comprised of the following components:

Real-time PCR reaction components	SYBR-Green	5 µl
	Primer F (100 pmol/µl)	1 µl

	Primer R (100 pmol/ µl)	1 µl
	H$_2$0	1 µl
	cDNA (1:20)	2 µl

The following program was used on the HT7900 Fast Real-Time PCR System:

50°C	2 min	
95°C	15 min	*Taq* activation
94°C	15 sec	Denaturation
60°C	30 sec	Annealing
72°C	30 sec	Elongation
95°C	15 sec	
60°C	15 sec	
60°C- 95°C	2°C/min	melting curve

After measurement the data was transferred to MS Excel (Microsoft) for further calculations. Relative expression was determined by the ΔΔCt method based on the following formula:

$$\Delta Ct = Ct \text{ (gene of interest)} - Ct \text{ (reference gene)}$$
$$\Delta\Delta Ct = \Delta Ct \text{ (control)} - \Delta Ct \text{ (sample of interest)}$$
$$\text{Relative expression} = 2^{\Delta\Delta Ct}$$

For detection of the housekeeping gene *Gapdh*-specific primers were used.

2.2.1.8.4 Sequence analysis, Sanger DNA-sequencing

The non-radioactive sequencing is based on the principle of chain termination developed by Sanger and Coulson (Sanger and Coulson, 1975). The method uses four dideoxynucleotides that are labelled with different fluorescent dyes. These dideoxynucleotides lack a 3'-hydroxyl group required for the formation of

a phosphodiester bond between two nucleotides. Incorporation of such a dideoxynucleotide leads to a termination of the DNA extension.

The sequencing PCR reaction was performed using following components:

Sequencing PCR reaction components	DNA	1 µl
	Sequence-specific primer (10 pmol/ µl)	1 µl
	BigDye	1 µl
	5 × Buffer	2 µl
	ddH$_2$O	5 µl

Sequencing program:

95°C	5 min		Polymerase activation
95°C	30 sec		Denaturation
53°C	30 sec	25	Annealing
60°C	2 min	cycles	Elongation
72°C	5 min		Final elongation
8°C	∞		

After PCR completion, 10 µl of dH$_2$O (Ampuwa) were added to the reaction and gel electrophoresis was performed in the automatic sequencer 3500XL (Applied Biosystems, Life Technologies, Darmstadt, Germany).

2.2.1.9 Protein analysis methods

2.2.1.9.1 Isolation of total protein lysate from tissues

Approximately 100 mg of tissue was homogenised in 300-500 µl protein lysis buffer and incubated 1 hour on ice. Then, the samples were treated with ultrasound on ice with 3 x 15 impulses, centrifuged at 13000 rpm for 20 min at 4°C, and the supernatant was transferred to a fresh Eppendorf tube. To isolate the proteins from cells, $5×10^6$ cells/ml were washed with cold DPBS, and resuspended in 50-200 µl of protein lysis buffer. The cells were incubated on ice for 30 min, treated with ultrasound on ice with 3×10 impulses, and centrifuged at 13000 rpm for 20 min at 4°C. The supernatant was transferred to a

46

fresh Eppendorf tube. The protein extracts were either used immediately or stored at -80°C.

2.2.1.9.2 Determination of protein concentration (Bradford, 1976)

To determine the protein concentration, the Bradford assay was employed. The method uses the Brilliant Blue G dye which binds unspecifically to cationic and hydrophobic site chains of proteins. Upon binding the absorption maximum is shifted from 495 nm to 595 nm. The absorption of light, measured at 595 nm in a spectrophotometer is proportional to the protein concentration. The exact concentration of the proteins was calculated based on the standard curve.

Protein quantitation assay	Protein	2 µl
	PBS	798 µl
	Bradford reagent	200 µl

2.2.1.9.3 SDS-PAGE gel for separation of proteins

The NuPage Precast Gel System was used for the separation of proteins. NuPage 4-12% Bis-Tris gel is a SDS-PAGE polyacrylamide gel with 4-12% percentage gradient, what allows more efficient separation of proteins. It consists of NuPage Bis-Tris pre-cast gels and specifically optimised buffers which have an operating pH of 7.0. This neutral pH increases the stability in both proteins and gels, providing increased confidence in electrophoresis results.

2.2.1.9.4 Sodium Dodecyl Sulphate Polyacrylamide Gel Electrophoresis (SDS-PAGE)

Usually, 30 µg of protein were diluted in DPBS (total volume of 30 µl) and mixed with 10 µl of 4 × SDS loading dye, denatured at 70°C for 10 min, and chilled on ice. The protein samples and additionally 10 µl of protein marker (pre-stained protein standard) were loaded on the gel, placed in the chamber which was filled with 1 × MES Running Buffer. The gel was running 15 min at 80 V, and further 1-2 hours at 120 V

2.2.1.9.5   Semi-dry blotting of proteins (Gershoni and Palade, 1982)

After protein electrophoresis, the SDS PAGE gel, a PVDF membrane at the appropriate size, and six pieces of Whatman paper were moistured with transfer buffer. They were further placed on the lower plate of semi-dry blotter, 3 Whatman papers, membrane, gel and on the top 3 more Whatman papers, to form a sandwich model. The upper plate was placed over the sandwich and the transfer was carried out at 3.5 mA/cm^2 for 1 hr.

2.2.1.9.6   Incubation of protein-bound membranes with antibodies

To block unspecific binding sites, the membrane was incubated in blocking buffer (Western Blot) for 1 hour at RT. Further, the membrane was incubated with the primary antibody at a recommended antibody dilution at 4°C overnight in washing buffer (Western Blot). On the next day, the membrane was washed three times for 20 min with washing buffer to wash out unbound antibodies, and incubated with the appropriate secondary antibody in washing buffer (Western Blot) at RT for 1 hour. After the incubation step, the membrane was washed three times for 20 min with washing buffer (Western Blot). Next, the membrane was washed 3 × 5 min in DPBS, and placed on a plastic film. For the detection of the chemiluminescent signals, the detection solution was pipetted on the membrane and incubated for 2 min, before the signals were captured using the Western Blot detection system (FlourChem Q Alpha Innotech, Logan, USA). For the detection of proteins using alkaline phosphatase (AP), the secondary antibodies were conjugated to alkaline phosphatase. After the membrane was incubated three times for 20 min with washing buffer (Western Blot), the membrane was washed 3 x 10 min with AP Buffer at RT. Further, to visualise protein bands, the PVDF membrane was incubated in the darkness with the AP staining solution. The reaction was stopped by washing with DPBS, and the membrane was dried.

2.2.1.10   Histological techniques

2.2.1.10.1   Perfusion

The animal was anesthetised by intraperitoneal injection with 0.1 ml of animal anesthesia solution per 10 g of body weight. Once the mouse was sedated, the abdomen and chest were opened to free the heart and liver. The butterfly needle providing DPBS was placed

in the left ventricle very carefully and gentle to avoid penetration of the cardiac septum. To enable the drain of blood, the hole in the right atrium had to be done immediately (using an additional needle). DPBS was infused until the out-flow solution turned clear and the liver colour became light brown.

2.2.1.10.2 Tissue preparation for paraffin-embedding

The freshly prepared mouse tissues were fixed in 4% paraformaldehyde solution. The dehydration process was accomplished by passing the tissue through a series of increasing alcohol concentrations: 70%, 80%, 90%, 100% ethanol, and overnight in isopropanol. Later, the alcohol was removed from the tissue by incubation in 75%: 25%, 50%: 50%, 25%: 75% isopropanol-xylene solutions, and at the end in 100% xylene overnight. The next step was the incubation of the tissues in paraffin at 60°C. Before embedding, the paraffin was changed at least four times. Finally, the tissue was placed in the embedding mould and melted paraffin was poured into the mould to form a block. The paraffin block was incubated overnight at 4°C before sectioning.

Dehydration protocol:

overnight	4% Formaldehyde solution
overnight	70% EtOH
1 × 15 min	70% EtOH
3 × 20 min	80% EtOH
4 × 30 min	90% EtOH
5 × 20 min	100% EtOH
overnight	Isopropanol
30 min	75%: 25% isopropanol-xylene
30 min	50%: 50% isopropanol-xylene
30 min	25%: 75% isopropanol-xylene
overnight	Xylene
5 × 4 hours	Paraffin
	BLOCK EMBEDDING

2.2.1.10.3 Sections of the paraffin block

Paraffin blocks were clamped into the microtome (Leica Instruments GmbH, Nussloch, Germany). The thickness of the tissue section was 5 µm. The sections were floated on pre-warmed to 40°C water which helped to spread the sections out. Afterwards, sections were transferred onto glass slides. After complete drying of the sections at 37°C, slides were stored at 4°C for further analysis.

2.2.1.10.4 Immunofluorescence staining of paraffin sections

Tissue sections were incubated 3 × 3 min in xylene to remove the paraffin. Then, they were re-hydrated in a decreasing ethanol series (100%, 96%, 70%, 50%, and 30%) for 2 min each. For immunofluorescence staining, the sections were washed in DPBS, and fixed in 4% paraformaldehyde solution. After washing with DPBS, the slides were incubated with 50 mM NH_4Cl for 10 min, and again washed with DPBS. Next step was permeabilization of the tissue section using 0.2% Triton in DPBS, and a 1 hour incubation step with the primary antibody in a humidified chamber at RT. After washing with 0.2% Triton-DPBS, the slides were incubated with the secondary antibody in the humidified chamber also for 1 hour. Further, they were washed with 0.2% Triton-DPBS and DPBS. The nuclei were counterstained with DAPI. Immunostaining of the sections was examined using a fluorescence equipped microscope (Olympus, München, Germany).

Rehydration and staining protocol:

3 × 3 min	Xylene
2 min	100% EtOH
2 min	96% EtOH
2 min	70% EtOH
2 min	50% EtOH
2 min	30% EtOH
2 × 5 min	DPBS
15 min	4% Formaldehyde solution
2 × 5 min	DPBS
10 min	NH_4Cl (pre-warmed to 37^oC)

2 × 5 min	DPBS
3 × 4 min	0.2% Triton-DPBS
1 hour	Primary antibody in 0.2% Triton-DPBS
3 × 4 min	0.2% Triton-PBS
1 hour	Secondary antibody in 0.2% Triton-DPBS
3 × 4 min	0.2% Triton-DPBS
2 × 5 min	DPBS
	DAPI

2.2.1.10.5 Diaminobenzidine (DAB) immunohistochemistry

Tissue slides were incubated for 1 hour at 60°C to melt the paraffin, further dewaxed in xylol, hydrated in isopropanol, and washed in dH_2O. In the next step the slides were cooking for 30 min in a streamer: slides for NeuN and Iba-1 were boiled in citratbuffer 10 mM pH 6, while slides for Caspase-3 in Tris/EDTA Buffer pH 9 (10 mM Tris, 1 mM EDTA). After washing in dH_2O the slides were incubated for 30 min in the incubation box (with a wet milieu) with 100 µl FCS/PBS, and further incubated overnight at 4°C with primary antibody. On the next day, slides were washed in PBS, and incubated 1 hour with secondary antibody, and again washed with PBS. Further, each slide was incubated for 1 hour with 100 µl of Streptavidin (Sigma), diluted 1:1000. After washing in PBS, the signal was developed with DAB, washed with dH_2O, and the nuclei were stained *with Mayer's Hämalaun (Merck)*. After dehydration in isopropanol, the slides were put in xylol and embedded in DePex.

2.2.1.10.6 Hematoxylin-eosin (HE) staining of histological sections

Tissue sections were first incubated three times for 5 min in xylene, followed by incubation in 100%, 95%, 90%, 80%, 70%, and 50% ethanol for 3 min each. Thereafter, slides were washed in ddH_2O for 5 min, and stained for 5 min in hematoxylin. The staining was followed by rinsing with deionised water, and washing in tap water for 10 min. The treated slides were dipped fast in acid ethanol (1ml concentrated HCl in 400 ml 70% ethanol) for 8-12 times to destain the tissue sections, and in amonium water (0.25%). After rinsing in tap water for 2 min and further in deionised water for 2 min, the slides

were stained in eosin for 2 min, incubated in 70%, 80%, 90%, 95% and 100% ethanol for 2 min each, and 15 min in xylene. Finally, the stained tissue sections were incubated in xylene for 15 min and mounted with Eukitt-quick hardening mounting medium.

Rehydration and staining protocol:

3 × 5 min	Xylene
3 min	100% EtOH
3 min	95% EtOH
3 min	90% EtOH
3 min	80% EtOH
3 min	70% EtOH
3 min	50% EtOH
5 min	H_2O
5 min	Hematoxilin Mayers
wash	ddH$_2$O
5 ×	70% EtOH + HCl
wash	Ammonium ddH$_2$O
wash	ddH$_2$O
2 min 30 sec	Eosine
wash	ddH$_2$O
2 min	50% EtOH
2 min	70% EtOH
2 min	80% EtOH
2 min	95% EtOH
2 min	100% EtOH
15 min	Xelene
	Close with Eukitt-quick hardening mounting medium

2.2.1.10.7   Tissue preparation for cryomedium-embedding

After perfusion, the liver was dissected and dehydrated first in 15% sucrose for 3 hours, and further overnight in 30% sucrose. The liver samples were *embedded* in Cryo-Embedding Compound on dry ice, and stored overnight at -80°C.

52

2.2.1.10.8 Sections of the cryo-block

Cryo-tissue blocks were clamped into the cryotome (Leica Microsystems, Nussloch, Germany). The thickness of the tissue section was 5 µm. Tissue sections were collected on glass slides, and kept at -20°C for further analysis.

2.2.1.10.9 DAPI staining of cryo-sections

Slides were fixed for 15 min in 4% paraformaldehyde and washed three times for 5 min in DPBS. The nuclei were counterstained with DAPI. Sections were examined using a fluorescence equipped microscope (Olympus, München, Germany).

2.2.1.10.10 LacZ staining

Tissue slides were fixed in 0.2% glutaraldehyde for 10 min on ice. After 10 min of washing in DPBS, tissue sections were permeabilised 10 min by rinsing in detergent (Igepal) and immersed in 1 mg/ml X-gal staining solution overnight at 37°C in the dark. On the next day, the tissue sections were post-fixed for 10 min in 4% paraformaldehyde (PFA), rinsed in PBS for 10 min and washed 2 × 5 min in ddH_2O. Nuclei were counterstained with Nuclear Fast Red, subsequently; sections were rinsed in ddH_2O and washed for 2 min. The tissue sections were dehydrated, mounted with Eukitt-quick hardening mounting medium, and enclosed with coverslips.

2.2.1.11 Eukaryotic cell biological methods

The cells were cultured at 37°C in a humidified incubator (Sanyo, Japan) with 5% CO_2. All media and components (see paragraph 2.1.8.2) were always pre-warmed in the water bath.

2.2.1.11.1 Preparation of MEFs feeder layers

A frozen aliquot of MEFs was quickly thawed in the water bath at 37°C and transferred to 10 ml MEF medium. After centrifugation at 1000 rpm for 5 min, the cell pellet was gently resuspended in 10 ml MEFs medium and plated in 3 × T_{75} culture flasks. Cells were incubated at 37°C in 5% CO_2. When the cells formed a confluent monolayer, they were trypsinised (using TrypLE-Express), transferred to 24 × T_{75} flasks and grown until they reached confluency. Inactivation of mitotic activity was performed by treatment with

mitomycin C (1 mg/ml) for 3 hours. Afterwards, the cells were washed twice with 10 ml of DPBS, trypsinised, pelleted and stored at -80°C.

2.2.1.11.2 Trypsinisation of eukaryotic cells

Cells were washed twice with sterile DPBS and incubated in minimal amount of TrypLE-Express at 37°C until the cells detached from the bottom of the culture flask. Trypsin was inhibited by addition of culture medium, in which the cells were subsequently resuspended. The enzyme was removed by centrifugation at 1000 rpm for 5 min. Cells were resuspended in an appropriate volume of fresh cell culture medium, and transferred into a new flask/plate.

2.2.1.11.3 Cryopreservation and thawing of eukaryotic cells

Cells were grown to a confluency of > 80%, washed with DPBS, and trypsinised. They were spun down (1000 rpm for 5 min) in growth medium. The supernatant was aspirated, and the cells were resuspended in freezing medium. Aliquots of the cells were kept at -80°C. For revitalisation, frozen cells were quickly thawed in the water bath, inoculated in a suitable amount of growth medium, centrifuged and plated.

2.2.1.11.4 Growth of ES cells on feeder layer

An aliquot of frozen ES cells was quickly thawed at 37°C in the water bath. The cells were transferred to a 15 ml tube containing 6 ml of ES cell medium. After 5 min of centrifugation at 1000 rpm, the cell pellet was resuspended in 5 ml of ES cell medium and plated on 6 cm gelatine-coated dishes containing feeder layer. One day later, the medium was changed to a fresh one. On the next day, cells were washed with DPBS, trypsinised and pelleted. The cell pellet was resuspended in 10 ml ES cell medium and distributed either to 5-6 dishes (6 cm) or to 2 dishes (10 cm) covered with feeder layers. The cells were passaged every second day as described above.

2.2.1.11.5 Transfection of plasmids into eukaryotic cells

Eukaryotic cells were transfected with plasmids in order to induce an overexpression of gene of interest. The transfection was performed using the lipofectamine reagent. The day before transfection, cells were trypsinised and counted. The appropriate number of

cells was plated into a 6-well plate. On the day of transfection the confluency of cells should be around 85-90%. In two separate tubes two transfection cocktails were prepared. In the first tube plasmid DNA was placed in Opti-MEM, and in the second tube lipofectamine was put in Opti-MEM. After 5 min of incubation at RT, both mixtures were combined gently, and incubated for 20 min at RT. Subsequently, the medium from prepared cells was replaced with the transfection cocktail for 4 hours at 37°C and 5% CO_2. Afterwards, the medium was changed to the normal culture medium. Cells were either analysed under a fluorescent microscope, or cells were trypsinised after 1-2 days of growing and subjected for DNA, RNA or protein isolation.

2.2.1.12   Production of targeted embryonic stem (ES) cell clones

2.2.1.12.1   Electroporation of ES cells

ES cells, which have grown for two days in 10 cm dishes, were trypsinised. The cell pellet was washed in 20 ml DPBS, centrifuged and resuspended in 1 ml DPBS. Subsequently, 0.8 ml of cell suspension was mixed with 40 µg of a linearised DNA construct and transferred into an electroporation cuvette. The electroporation was performed at 240V, 500µF with the Bio-Rad gene pulserTM apparatus. After electroporation, the cuvette was placed on ice for 20 min. The cell suspension was transferred from the cuvette into 20 ml of ES cell medium and plated onto two 10 cm dishes containing feeder layers. The medium was changed every day. Two days after the electroporation, the puromycin for selection was added (2 µg/ml). Again, medium was changed every day. After approximately eight days of selection, drug resistant colonies had appeared and were genotyped.

2.2.1.13   Production of chimeras by injection of ES cells into blastocysts

The injection of the *Mocs2* knockout ES cells was performed in cooperation with Dr. Ursula Fünfschilling (Max Planck Institute of Experimental Medicine, Göttingen, Germany). The ES cells were injected into blastocysts, which were further transplanted into pseudopregnant foster mothers. The recipients gave birth to pups called chimeras.

2.2.1.14 Detection of chimerism and mice breeding

Chimerism of obtained animals was assessed based on the coat colour. Further, chimeric mice were bred with wild type animals to ascertain contribution of the ES cells to the germline. Additionally, the genotyping of spermatozoa was performed.

2.2.1.15 DNA preparation for microinjection

A large-scale preparation of the plasmids was performed using Endotoxin-free Qiagen Maxi Kit. Plasmids were linearised overnight in 37°C with the restriction enzyme *Xma*I. The samples were loaded on an EtBr-free 0.7% agarose gel as follows: 1 kb plus DNA ladder, undigested plasmid, 0.5 μg of digested plasmid, empty well, and 4.5 μg digested plasmid. The agarose gel electrophoresis was running for 15 min at 95 V, and further 1 hour at 120 V. In the next step, the gel was cut in the place of the empty well which separated small and large amount of the digested plasmid. The part of the agarose gel which contained the marker, undigested and 10 μl of digested plasmid was incubated for 20 min in 0.5 × TBE with EtBr. Both parts were recombined and the isolation of the unstained digested plasmid band was possible, since the corresponding 10 μl digested plasmid band was stained with EtBr. After gel extraction one volume DNA was precipitated with 10% volume of 2 M NaAc. Further, 2.2 × volume of ice-cold absolute 100% EtOH was added, mixed and centrifuged at 13000 rpm for 5 min at 4°C. The supernatant was discarded; the DNA pellet was washed with 0.5 ml of 70% EtOH, and centrifuged at 13000 rpm at 4°C for 5 min. Again, the supernatant was discarded, and to remove the ethanol completely, DNA samples were incubated for 5 min at 45°C. The DNA pellet was resuspended in TE buffer. The DNA concentration was estimated using a Nano Drop spectrophotometer. The final concentration should be 30 μg/ml. The microinjection was performed by Dr. Ursula Fünfschilling (Max Planck Institute of Experimental Medicine, Göttingen, Germany).

2.2.1.16 Determination of transgene integration with the DNA Walking Speed Up Kit

The DNA Walking Speed Up Kit is a method using a unique DNA Walking ACP (DW-ACP) primer designed to capture unknown target sites with high specificity. The optimised PCR

conditions allow obtaining unknown flanking regions of up to 3 kb in length. The subsequent nested PCR reactions using one primer provided by the company, and one transgene-specific primer, as well as the special composed PCR Master Mix allowed to obtained different PCR products, which indicated the integration site(s) of the transgene after sequencing. The procedure was performed according to manufacturer's protocol (DNA Walking SpeedUp Premix Kit, Seegene, USA).

2.2.1.17   Tattooing neonate animals

To identify the animals in the litter, foot tattoos were done using the MPI code. Tattoos are permanent and do not alter the physiology of animals. For the pigment injection a sterile syringe and needle were used.

2.2.1.18   rAAV production

The rAAV particles used in the study were produced by Vector Core from the Telethon Institute of Genetics and Medicine, Naples, Italy, by triple transfection of HEK293 cells. The viral particles were further purified by $CsCl_2$ ultracentrifugation. Physical titres (genome copies (GC)/mL) were determined using a real-time PCR-based assay and a dot blot analysis.

2.2.1.19   rAAV preparation and injection

The rAAV particles were stored at -80°C, and were always thawed on ice prior to injection. The appropriate amount of the viral particles was diluted in DPBS. The injection of neonatal mice was performed using a sterile 1 ml syringe, and a sterile, single-use 0.5 × 16 mm needle. The injections were performed directly into the liver (intrahepatic injection), or into the peritoneal cavity (intraperitoneal injection). Viral titres were calculated in GC/ml (number of viral genome copies per millilitre), or tu/ml (transfecting units per millilitre).

3   RESULTS

3.1   Generation of *Mocs2* knockout (KO) mice

**3.1.1   Generation of an isolated *Mocs2b* KO mouse**

One of the main aims of this study was to develop a therapy for patients suffering from molybdenum cofactor deficiency type B (or molybdenum cofactor deficiency, complementation group B (MOCODB; OMIM #252160), caused by mutations in the subunit B of the *MOCS2* gene (OMIM #603708). To achieve this goal, we decided to generate a KO mouse model of the disease. Taking the advantage of commercially available knockout embryonic stem cells (ESCs), we have purchased JM8A3 ESCs with a targeted mutation in the murine *Mocs2b* gene. Originally, JM8A3 cells are derived from the C57BL/6N mouse strain. These ES cells have been modified to correct the black mutation on the Agouti allele, therefore, mice derived from these ES cells have an agouti coat colour. In these ES cells one copy of the murine *Mocs2b* gene was targeted by a knockout first construct. A targeting vector was designed to insert a flippase recognition target (FRT) site followed by an En2-IRES-LacZ-pA trapping cassette. In the trapping cassette En2 (*engrailed 2*) the splice acceptor site is followed by an IRES (internal ribosome entry site), the *beta-galactosidase* (LacZ) gene and a pA (polyadenylation) signal. Additionally, a floxed β-actin-driven neomycin cassette, an FRT site and a loxP site (FRT-LacZ-loxP-Neo-FRT-loxP) are located upstream of the 4th exon of the murine *Mocs2b* gene, and a single loxP site is placed downstream of the 6th exon of the *Mocs2* gene. A knockout first allele is initially a non-expressed form, but can be converted to a conditional allele via flippase (Flp) recombination. **Figure 3.1** demonstrates a schematic representation of knock first and conditional alleles together with corresponding transcripts and proteins. Although the trapping cassette affects both, *Mocs2a* and *Mocs2b* transcripts, it has no effect on Mocs2a protein expression and disrupts only Mocs2b protein. This strategy enabled us to generate an isolated form of *Mocs2b* KO mice.
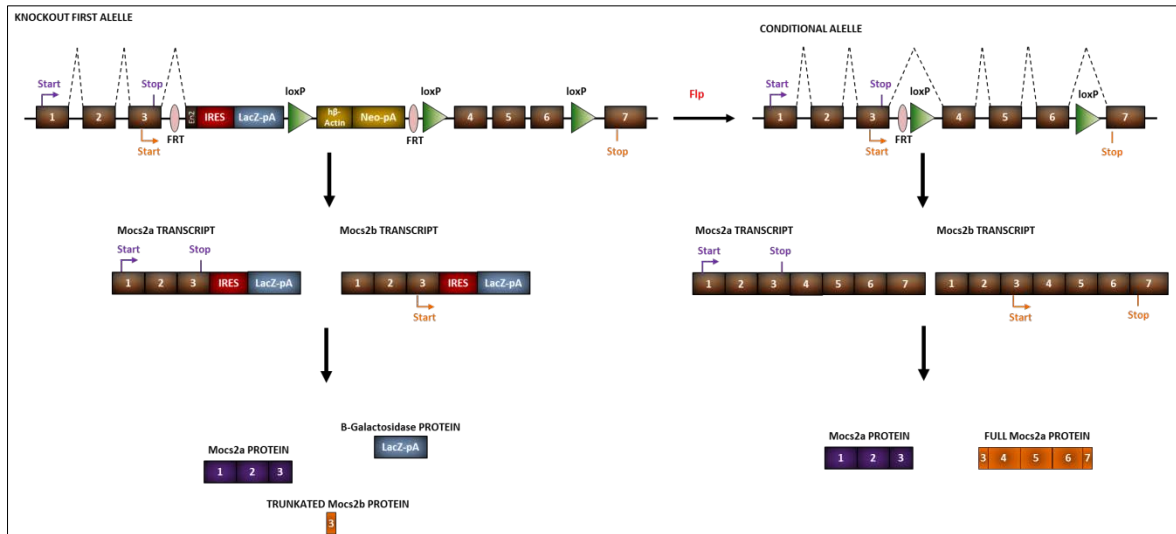
Fig. 3.1. Schematic representation of the *Mocs2b* knockout first and conditional constructs together with encoded transcripts and corresponding proteins. The knockout first construct incorporates the *engrailed 2* (En2) splice acceptor; internal ribosomal entry sites (IRES), the LacZ reporter gene with a polyadenylation signal (LacZ-pA), and the neomycin resistance gene (Neo-pA) under the control of the human β-actin promoter (hβ-Actin). The LacZ-Neo cassette is flanked by flippase recognition target (FRT) sites, and loxP sites are flanking the neomycin resistance gene and *Mocs2b* critical exons 4, 5 and 6. During the transcription process, exon 3 is spliced into the splice acceptor site of the En2-LacZ reporter gene truncating thereby both, *Mocs2a* and *Mocs2b* transcripts. Although trapping cassette affects both transcripts, open reading frame (ORF) of *Mocs2a* is intact allowing to normal translation. In contrast, truncated *Mocs2b* transcript leads to formation of short polypeptide, corresponding to part of exon 3. In parallel, the IRES sequence present in KO transcripts initiates translation of the LacZ protein **(left panel)**. In presence of the flippase (Flp) recombinase the LacZ-Neo cassette can be deleted, thus restoring Mocs2b expression and converting the knockout first to a conditional allele **(right panel)**.

The KO ESCs were propagated in our institute, and sent for the blastocyst injection to the Max Planck Institute (MPI) of Experimental Medicine, Göttingen (this experiment was performed in collaboration with Dr. Ursula Fünfschilling). *Mocs2b* KO JM8A3 ESCs were injected into C57BL/6N blastocysts, which were then transferred to pseudopregnant females. Chimerism of the obtained pups was assessed based on the coat colour. Unfortunately, the *Mocs2b* KO JM8A3 cells failed to contribute to chimera formation, as all pups obtained after the first injection were wild type (WT). To exclude that the presence of the LacZ-Neo cassette impaired chimera formation, it was removed from KO ESCs by expression of the Flp recombinase **(see Fig 3.1)**. For this reason, KO ESCs were transiently transfected with a pCAAG-FLPe vector to express FLP-recombinase, and to

remove the FRT-flanked reporter/selector (LacZ-Neo) cassette. The Flp transfection was performed in collaboration with Prof. Dr. Ibrahim Adham (Institute of Human Genetics, University Medical Center Göttingen (UMG)). Following the Flp transfection, KO JM8A3 ESCs were plated on Nanog-GFP feeder layer, and exposed to puromycin selection. The survived ESC colonies were picked manually from the selection dish, and transferred into 24-well plates where they were cultured to 70-80% confluency. Subsequently, one part of the cells was frozen, whereas the rest was used for DNA analysis. The efficiency of Flp recombination was tested by PCR using MOCS2-5'arm, LAR3 and MOCS2-3'arm primers, thus, allowing to distinguish between the knockout first (293 bp), conditional (621 bp) and WT allele (470 bp) **(Fig. 3.2a-c)**. Specificity of the designed strategy was verified by genotyping PCR of *Mocs2b* KO ESCs and WT cells **(Fig. 3.3a)**. The PCR analysis with KO DNA gave rise to two bands corresponding to knockout first and WT bands, while PCR with WT DNA resulted only in one band corresponding to the WT product. Next, we analysed genotypes of ES cell lines obtained after puromycin selection. In 3 out of 48 clones (No. 13, 16 and A) the knockout first allele was converted to a conditional one via Flp recombination **(Fig. 3.3b)**. The positive clones were then injected into the C57Bl/6N blastocyst to obtain chimeras. Blastocyst injection was performed in collaboration with Dr. Ursula Fünfschilling (MPI of Experimental Medicine, Göttingen).
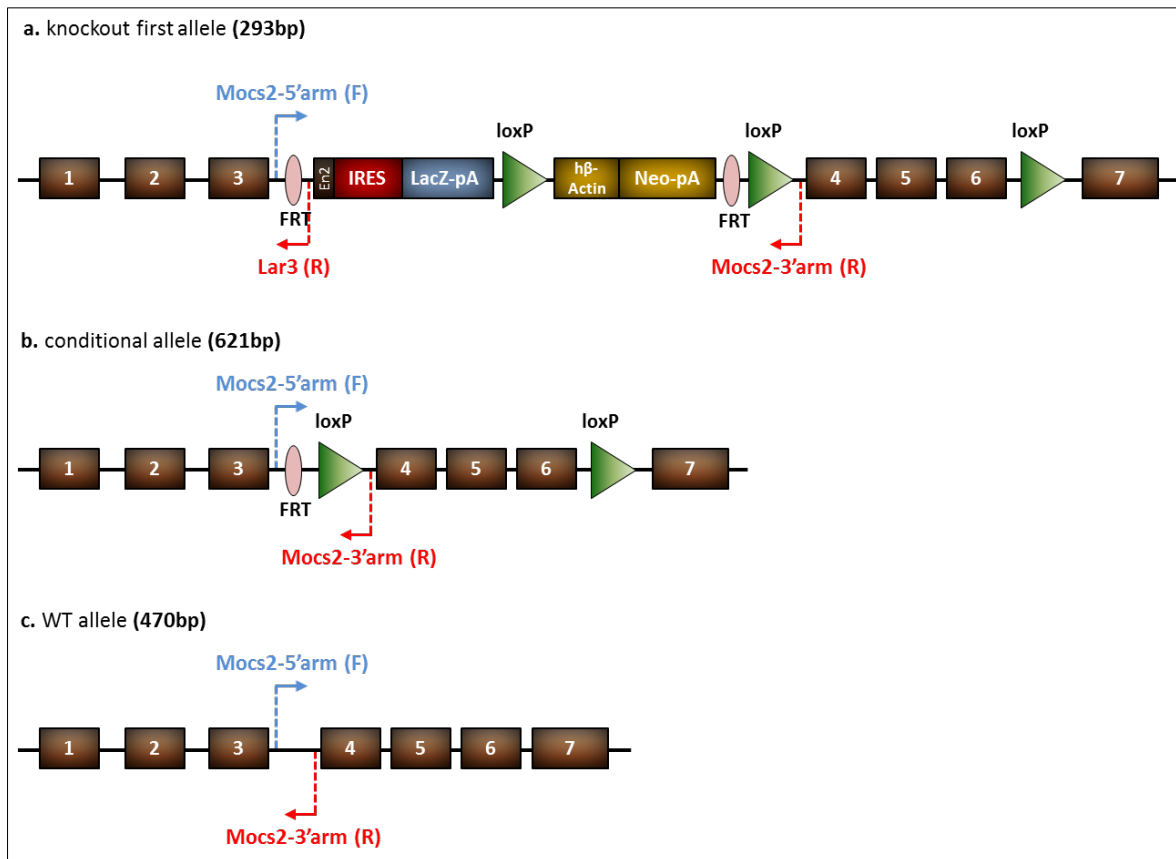
Fig. 3.2. Genotyping strategy used for the evaluation of Flp-recombination in *Mocs2b* KO ESCs. Schematic representation of the **(a)** knockout first, **(b)** conditional and **(c)** WT alleles, together with the corresponding PCR products amplified with Mocs2-5'arm (F), Lar3 (R) and Mocs2-3'arm (R) primers. The arrows depict the localisation and the direction of primers used for genotyping PCR (F = forward; R = reverse).
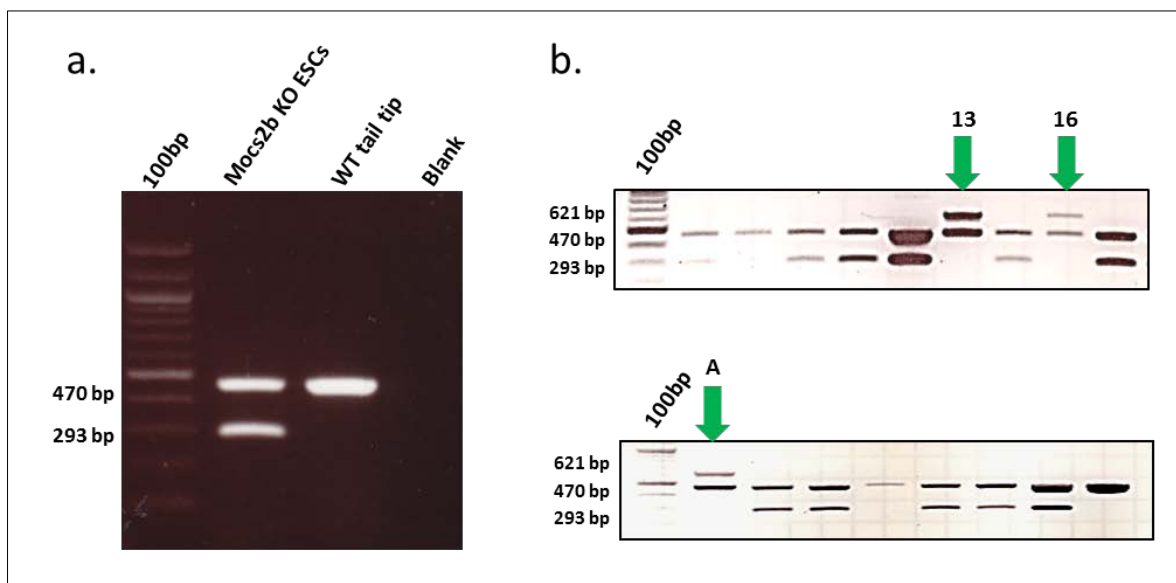

Fig. 3.3. Genotyping PCR of *Mocs2b* knockout first, conditional and WT allele. (a) Electrophoresis pattern of PCR products from *Mocs2b* KO ESCs, and wild type mouse tail (WT tail tip) DNA determined by

61

genotyping PCR. **(b)** Results of genotyping PCR performed with DNA extracted from *Mocs2b* KO ESCs transfected with the pCAAG-FLPe vector. In clone 13, 16 and A (marked with green arrows) Flp recombination has occurred successfully, thereby the knockout allele (corresponding to 293 bp) was converted to the conditional allele (621 bp). (100bp = 100 bp DNA ladder; Blank = negative control w/o DNA).

Blastocyst injections with conditional *Mocs2b* ESCs, derived from clones 13 and 16, gave rise to chimeras successfully, while the ESCs derived from clone A failed to contribute to chimera formation. Chimerism of obtained pups was next estimated based on the coat colour, and is presented in **Table 1.** At the age of 8 weeks, chimeric males were bred with C57Bl/6N females (n=10), nonetheless, the conditional allele was not transmitted to the F1 generation. Genotyping of spermatozoa of a 15% chimeric male confirmed impaired germline contribution **(Fig. 3.4)**. To collect the sperm, the chimeric male was bred with a WT female and vaginal plug was monitored to indicate insemination time. Following insemination, the female was sacrificed by cervical dislocation and sperm was flashed out from the uterus for genotyping PCR. To test the quality of the sperm DNA and to test for the gender, PCR analyses for two other genes, namely *Zfyve27* (chromosome 19-specific) and *Sry* (Y-chromosome-specific), were performed.

Tab. 1. Chimerism of the pups obtained after blastocyst injection with *Mocs2b* ESCs derived from clones 13 and 16.

Mocs2b KO JM8A3 ESCs			
CLONE 16		CLONE 13	
SEX	CHIMERISM (%)	SEX	CHIMERISM (%)
♀	80	♀	70
♂	20	♂	15
♂	5	♂	5-10
♂	5	♂	5-10
♂	5	♂	5-10
		♂	5-10
		♂	5-10
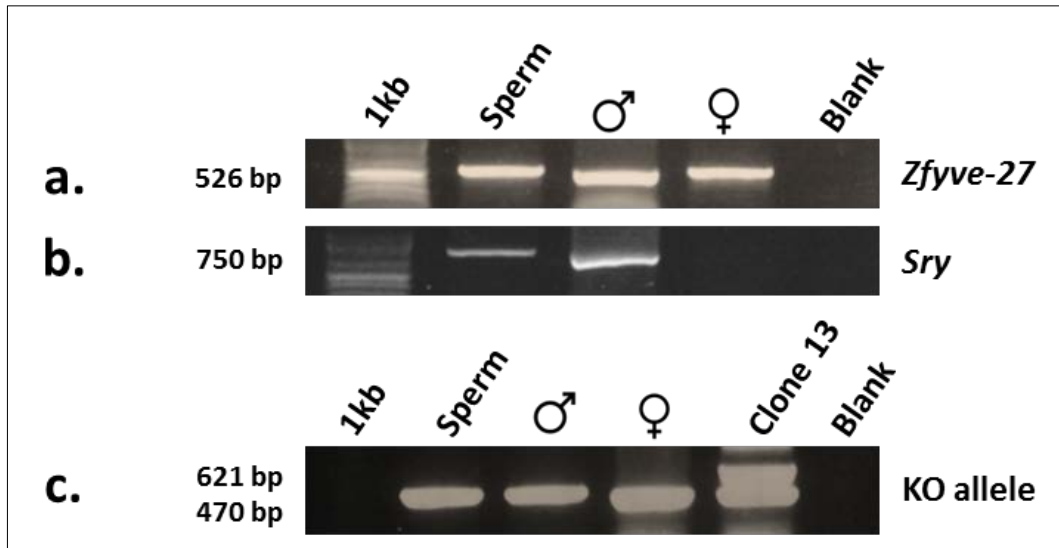
Fig. 3.4. Genotyping of sperm extracted from a 15% chimeric male. (a) Results of *Zfyve27* PCR showed good quality of DNA extracted from sperm, and DNA from male and female tail tips (♂ and ♀). **(b)** Results of *Sry*-specific PCR determined the male DNA. **(c)** Genotyping PCR could not detect the conditional allele in the examined sperm. Wild type male and female (♂ and ♀) DNA served as a control. (1kb = 1kb DNA plus ladder; Blank = negative control w/o DNA).

3.1.2   Generation of a knockout mouse of the complete *Mocs2* gene

To overcome the problem with the generation of the *Mocs2b* knockout mouse, we decided to purchase a commercially available knockout mouse model of the total *Mocs2* gene. The 95% male chimera was provided by the Knockout Mouse Project (KOMP) Repository at the University of California, Davis. The Mocs2[tm1(KOMP)Vlcg] targeting vector was designed to insert a *β-galactosidase* (lacZ) gene and a neomycin (Neo) resistance cassette downstream of the start codon of the *Mocs2* gene, abolishing gene function **(Fig. 3.5)**. Homologous recombination led to targeted deletion of 10.049 bp (NCBI Chr13: 114.818.308-114.828.357) encompassing almost the whole genomic sequence of the murine *Mocs2* gene. As a result, the LacZ reporter gene is under the control of the endogenous *Mocs2* promoter, and LacZ staining is observed where the deleted *Mocs2* gene is normally expressed.
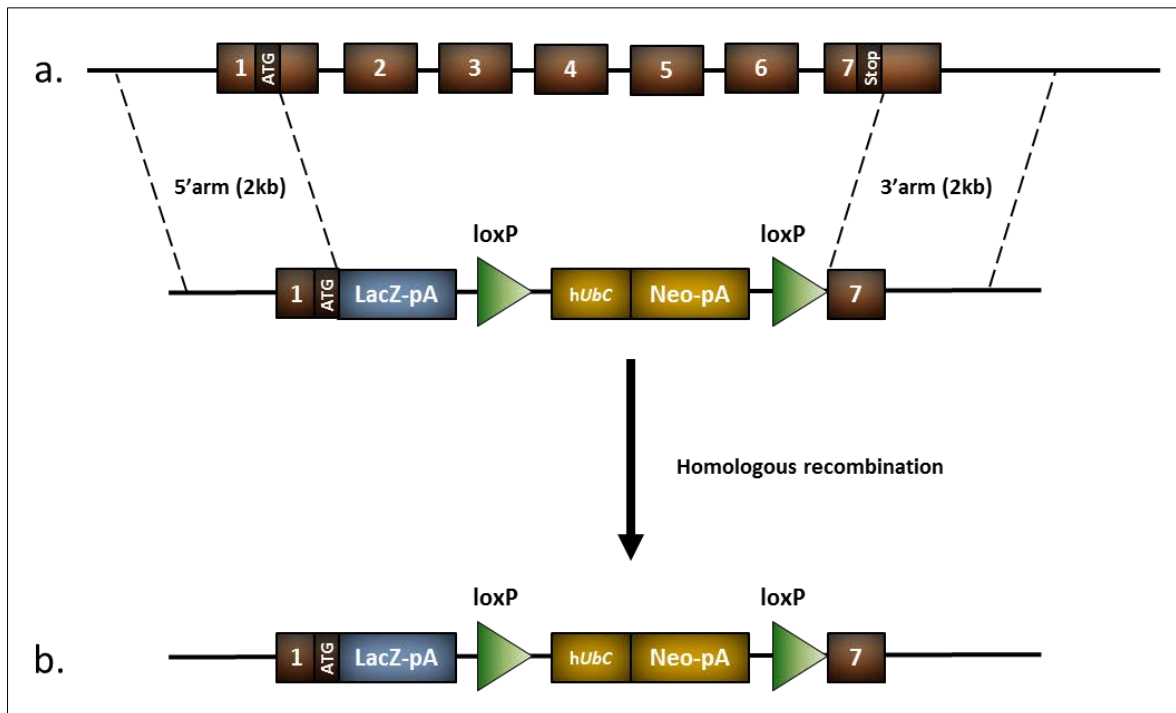
Fig. 3.5. Scheme of the strategy used for targeting of the complete *Mocs2* allele. (a) The targeting construct includes 5' and 3' homologous arms, a LacZ reporter gene (LacZ-pA) and neomycin cassette driven by a human Ubiquitin C promoter (hUbC-Neo-pA) flanked by two loxP sites. **(b)** Schematic representation of the homologous recombination product. Homologous recombination led to the deletion of almost the complete *Mocs2* gene. The gene trap cassette (LacZ-Neo) replaced the sequence downstream of the start codon (ATG) of *Mocs2a* up to stop codon (Stop) of *Mocs2b* isoform.

To establish a heterozygous *Mocs2* KO line (*Mocs2$^{+/-}$*), the 95% chimeric male was bred with a C57Bl/6N WT female, and transmission of the KO allele was confirmed in the F1 generation by PCR for 5' and 3' arms **(Fig. 3.6.)**. Next, *Mocs2$^{+/-}$* mice were bred with each other to obtain homozygous *Mocs2* knockout mice (*Mocs2* KO or *Mocs2$^{-/-}$*), where both alleles of the complete *Mocs2* gene were deleted. The strategy for genotyping the *Mocs2$^{-/-}$* and WT alleles to distinguish homo-and heterozygous animals was established using three primers: Mocs2KOGeno_F1, Neo_F and GeneSpec_R1. Predicted products correspond to 694 bp for the KO allele and 945 bp for the WT allele **(Fig. 3.7)**. After crossing of heterozygous mice, homozygous *Mocs2* deficient mice were obtained in accordance with Mendelian distribution **(Fig. 3.8)**.
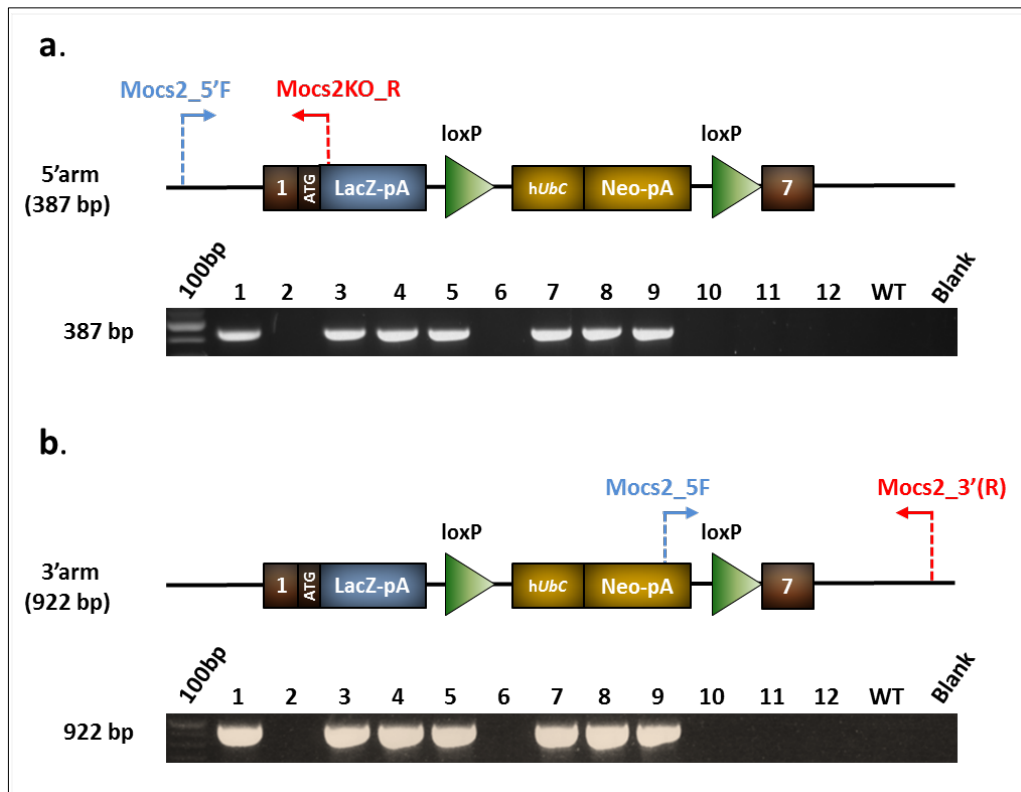
Fig. 3.6. The 95% male chimera transmitted the *Mocs2* KO allele to the F1 generation. PCR with Mocs2_5'F, Mocs2KO_R and Mocs2KO_F, Mocs2_3'R primers confirmed homologous recombination on the **(a)** 5' and **(b)** 3' site, respectively. The arrows indicate the localisation and the direction of primers used for genotyping PCR. (100bp = 100 bp DNA ladder; F = forward; R = reverse; Blank = negative control w/o DNA).
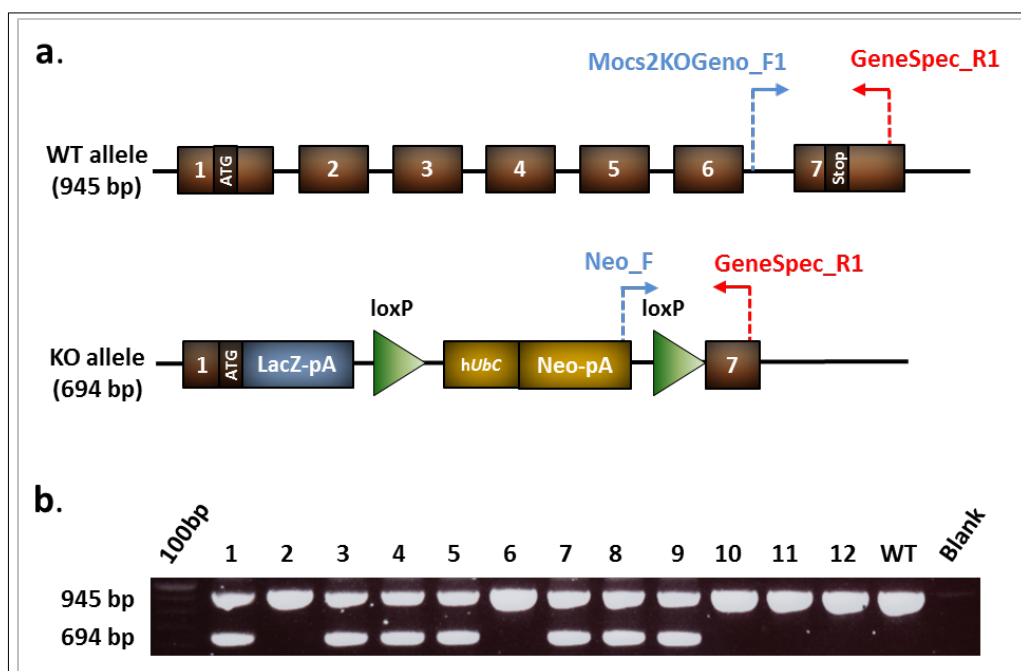

Fig. 3.7. Strategy of genotyping PCR to distinguish between homozygous and heterozygous *Mocs2* knockout mice. (a) Schematic representation of the *Mocs2* wild type (WT) and knockout (KO) alleles

65

together with primer arrangements. **(b)** Results of the genotyping PCR show that 7 out of 12 pups from the F1 generation were heterozygous (*Mocs2$^{+/-}$*). The arrows indicate the localisation and the direction of primers used for genotyping PCR. (100bp = 100 bp DNA ladder; F = forward; R = reverse; Blank = negative control w/o DNA)
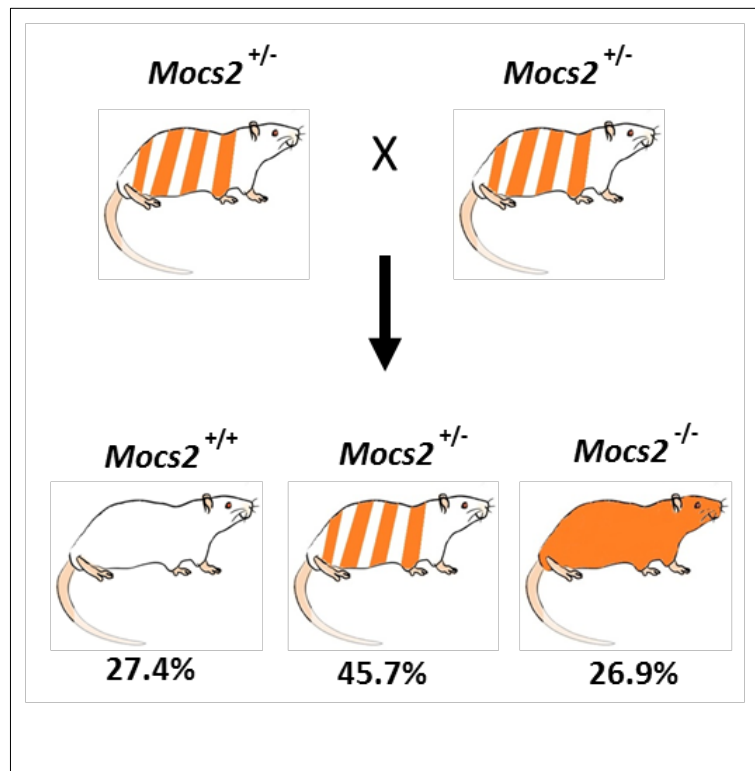
Fig. 3.8. Schematic diagram of the *Mocs2* KO allele inheritance. Breeding of heterozygous (*Mocs2$^{+/-}$*) mice resulted in 27% WT (*Mocs2$^{+/+}$*)-, 46% heterozygous (*Mocs2$^{+/-}$*)- and 27% homozygous *Mocs2* knockout (*Mocs2$^{-/-}$*) pups (n=413). Chi-square test did not show any statistically significant deviations from a 1:2:1 segregation ratio (Mendelian ratio).

### 3.1.3 Endogenous expression of murine *Mocs2* gene

In human the *MOCS2* gene is localised on the long arm of chromosome 5 (5q11.2). It is a unique example of a bicistronic gene, as it encodes two overlapping transcripts for *MOCS2A* and *MOCS2B*, respectively. Beside the function in molybdenum cofactor (MoCo) biosynthesis, there are not many informations regarding the genomic structure and tissue distribution of the *MOCS2* gene. For a better understanding of the clinical and pathomorphological aspects of MoCo deficiency we started with expression analysis of mouse *Mocs2* transcripts. For this reason, we extracted total RNA from different tissues of 12-day-old and adult WT mice, respectively. Subsequently, cDNA was synthesised and used as a template for quantitative RT-PCR (qRT-PCR) analysis. In contrast to human

MOCS2A and *MOCS2B* isoforms, mouse *Mocs2a* and *Mocs2b* transcripts cannot be distinguished via RT-PCR **(see Fig. 1.2)**, therefore, it was only possible to prove the global expression of *Mocs2* transcripts using *Mocs2a/b*-specific primers qF_Mocs2Ex4 and qR_Mocs2Ex5. The qRT-PCR analyses demonstrated ubiquitous expression of the *Mocs2a/b* transcripts in 12-day-old wild type mice, with the highest expression observed in the liver, kidney and skin. In tissues derived from adult wild type mice expression of *Mocs2a/b* decreased, but the tissue distribution patterns seemed to remain identical **(Fig. 3.9)**. Subsequently, these qRT-PCR results were confirmed by Western blot analysis using proteins extracted from tissues of 12-day-old wild type mice. Here, Mocs2b protein expression could be detected in the liver and brain using the Mocs2b-specific antibody EP113633 **(Fig. 3.10)**.
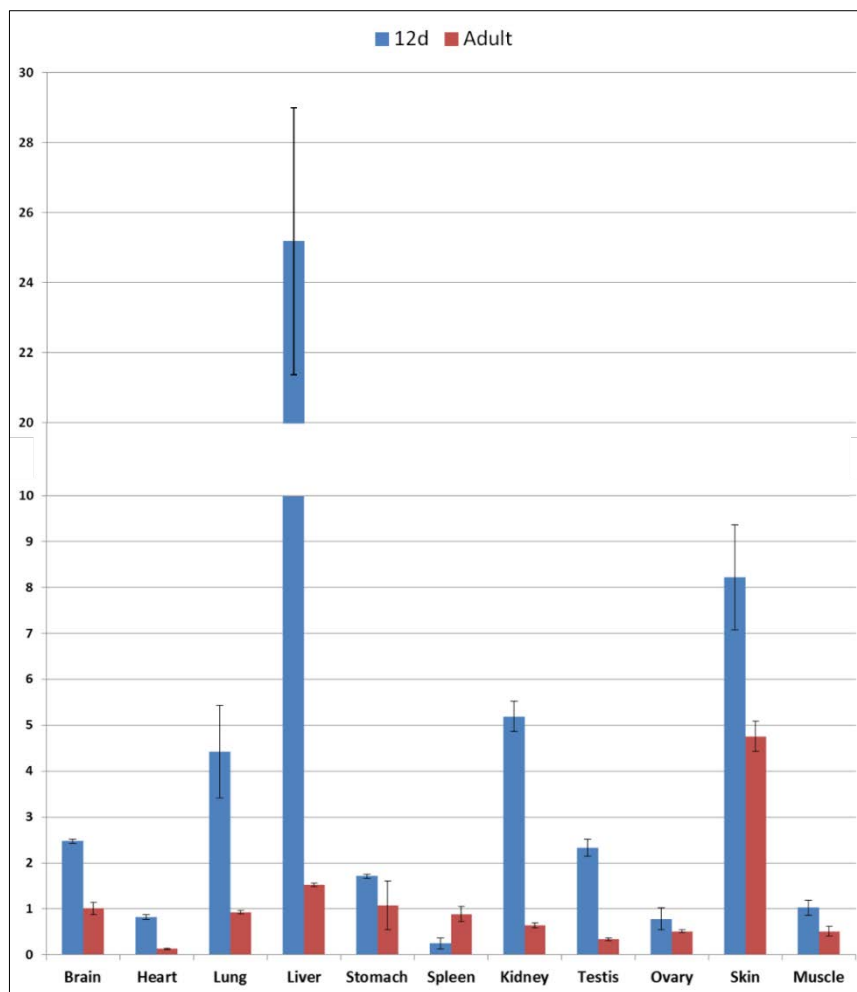
Fig. 3.9. *Mocs2a/b* expression in different tissues obtained from 12-day-old or adult wild type mice by qRT-PCR analyses. Real-time PCR results representing the expression of the endogenous *Mocs2a/b* gene in 12-day-old (blue bars) and adult wild type mice (red bars). In the majority of tissues analysed, 12-day-old

(12d) wild type mice showed significantly higher levels of *Mocs2a/b* gene expression than adult mice. The results were normalised to *Glyceraldehyde-3-phosphate dehydrogenase* (*Gapdh*) expression, and are presented as a relative value to the *Mocs2a/b* expression level in the brain derived from adult wild type mice. Values and associated error bars represent mean ± s.d. (n=3).
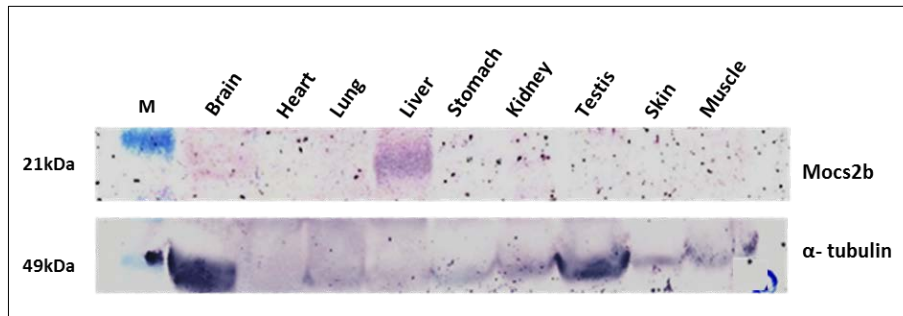

Fig. 3.10. Mocs2b protein expression in different tissues derived from a 12-day-old wild type mouse. Western blot analysis demonstrating robust expression of the Mocs2b protein in the liver and moderate expression in the brain of a 12-day-old wild type mouse. The α-tubulin antibody was used as a control for protein loading. M = SeeBlue Plus2 Pre-stained Protein Standard.

In order to visualise the cellular distribution of the murine *Mocs2a/b* gene in different tissues, we took advantage of the LacZ reporter gene included in the *Mocs2* knockout cassette **(see Fig. 3.5)**. Here, LacZ expression is driven by the endogenous murine *Mocs2* gene promoter, thereby an indirect expression of both *Mocs2* isoforms (*Mocs2a and Mocs2b*) can be followed by expression of β-galactosidase. Due to the problem that homozygous *Mocs2* knockout (*Mocs2$^{-/-}$*) mice die early after birth, LacZ staining was performed on tissue sections derived from heterozygous *Mocs2* knockout (*Mocs2$^{+/-}$*) mice. For this reason different tissues from 12-day-old *Mocs2$^{+/-}$*mice and adult *Mocs2$^{+/-}$* mice were extracted, respectively, and subjected to LacZ staining. In **Figure 3.11 and 3.13** results of LacZ staining performed on corresponding tissue sections from *Mocs2$^{+/-}$*mice are presented. LacZ positive cells were detected in each tissue analysed except spleen and adult muscle, and in contrast to the results obtained by qRT-PCR analysis, expression of β-galactosidase driven by the endogenous *Mocs2* gene promoter seemed to be age-independent. The most prominent LacZ signals were detected in the brain, with the highest intensity in the grey matter of the cortex, hippocampus and brainstem **(Fig. 3.11)**. Double staining with the neuron-specific nuclear protein NeuN confirmed the neuronal origin of LacZ positive cells **(Fig. 3.12)**. In the kidney, LacZ staining was restricted to the
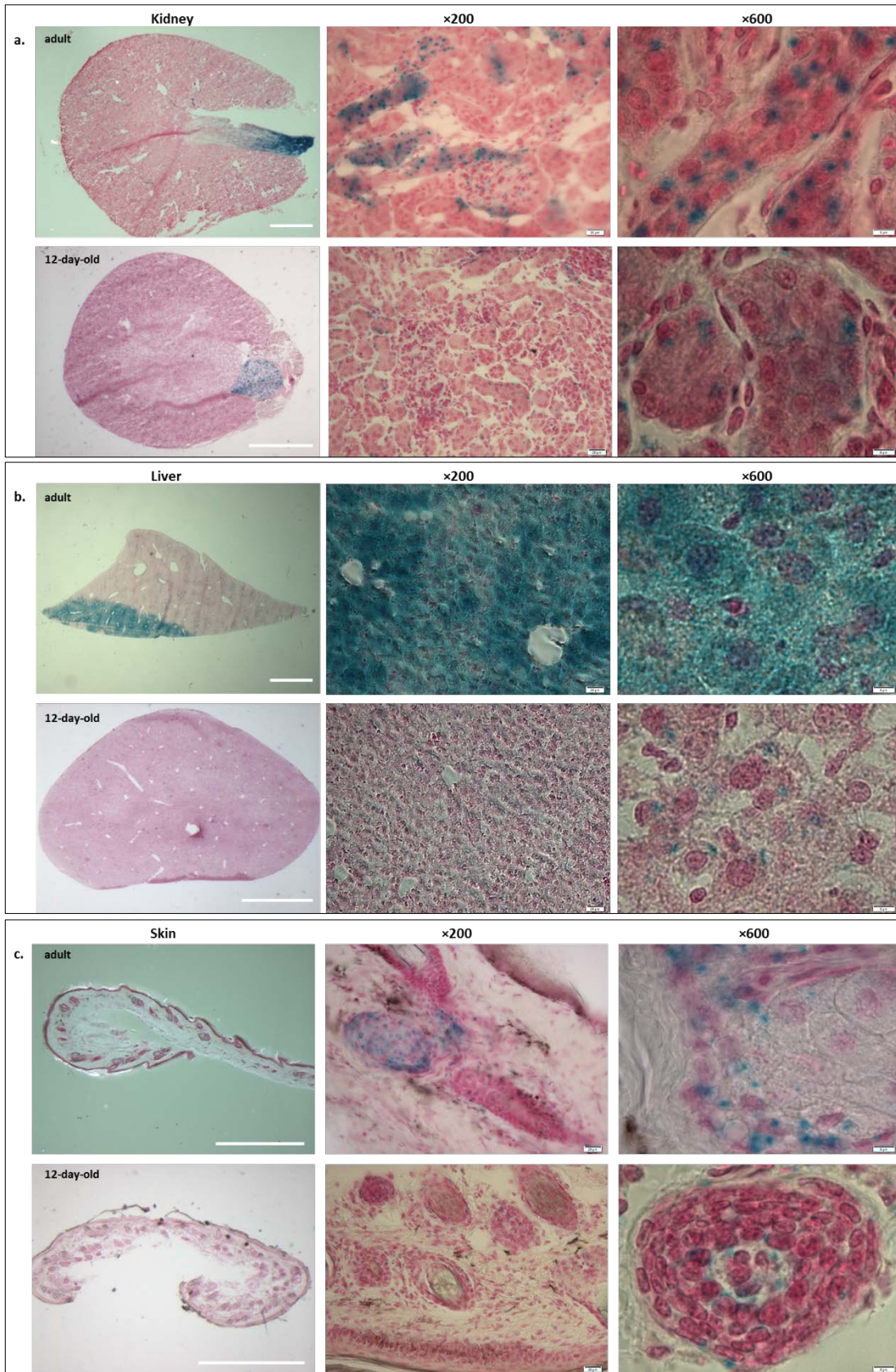
elements of the collecting system including collecting ducts, calyx and renal pelvis **(Fig. 3.13a)**. Moderate LacZ signal intensity was detected in the liver **(Fig. 3.13b)**. In the skin clear LacZ signals were detected in hair follicles **(Fig. 3.13c)**. Finally, intensive LacZ signals were detected in the gonads **(Fig. 3.13d, e)**. In the testis LacZ staining was restricted to germ cells, in particular to undifferentiated spermatogonia, as positive cells were detected as a single cell, paired cells or aligned cells inside the seminiferous tubules. A representative image from a 600× magnification revealed also the presence of a mitotic spindle, supporting our data. In contrast, in the ovary a week signal was detected in the stroma, however, the strongest LacZ staining was observed in oocytes.
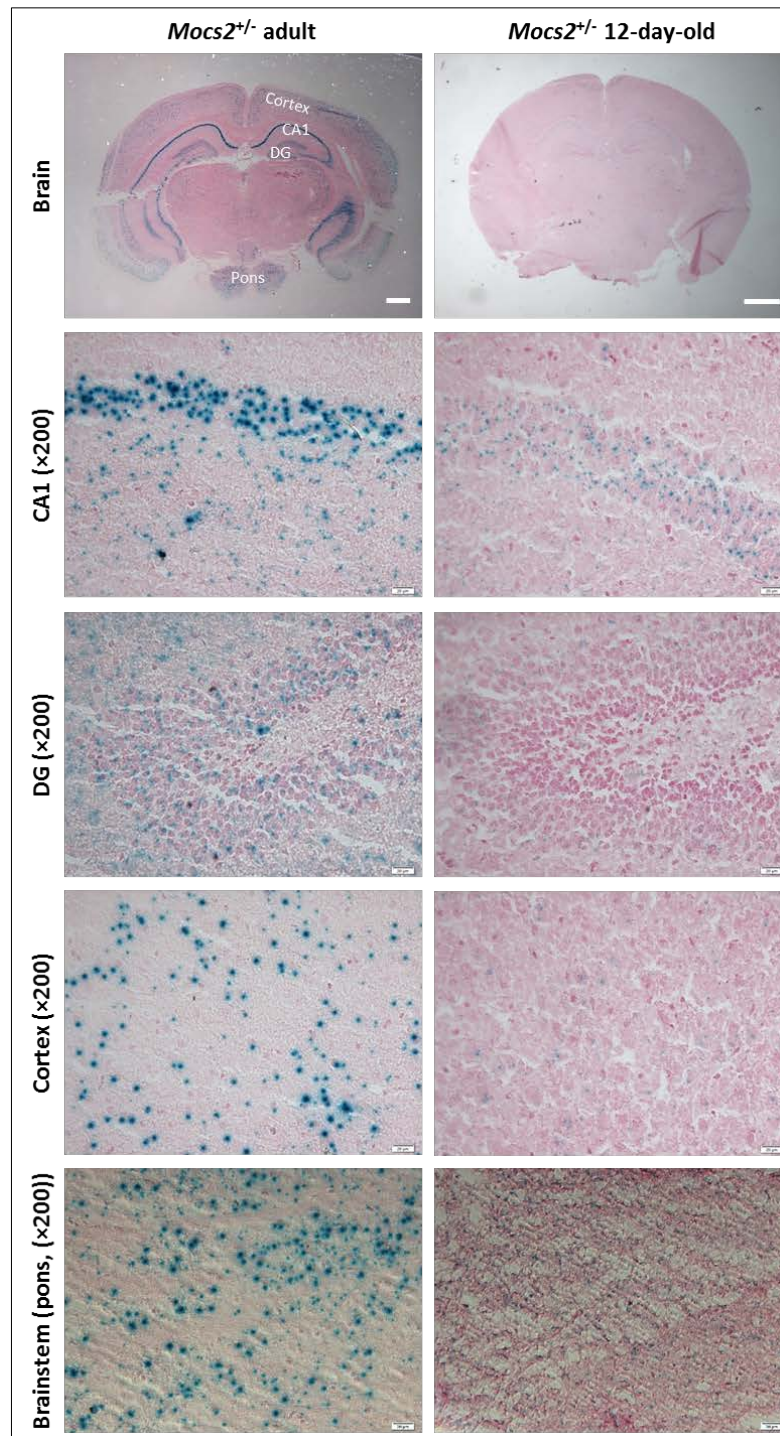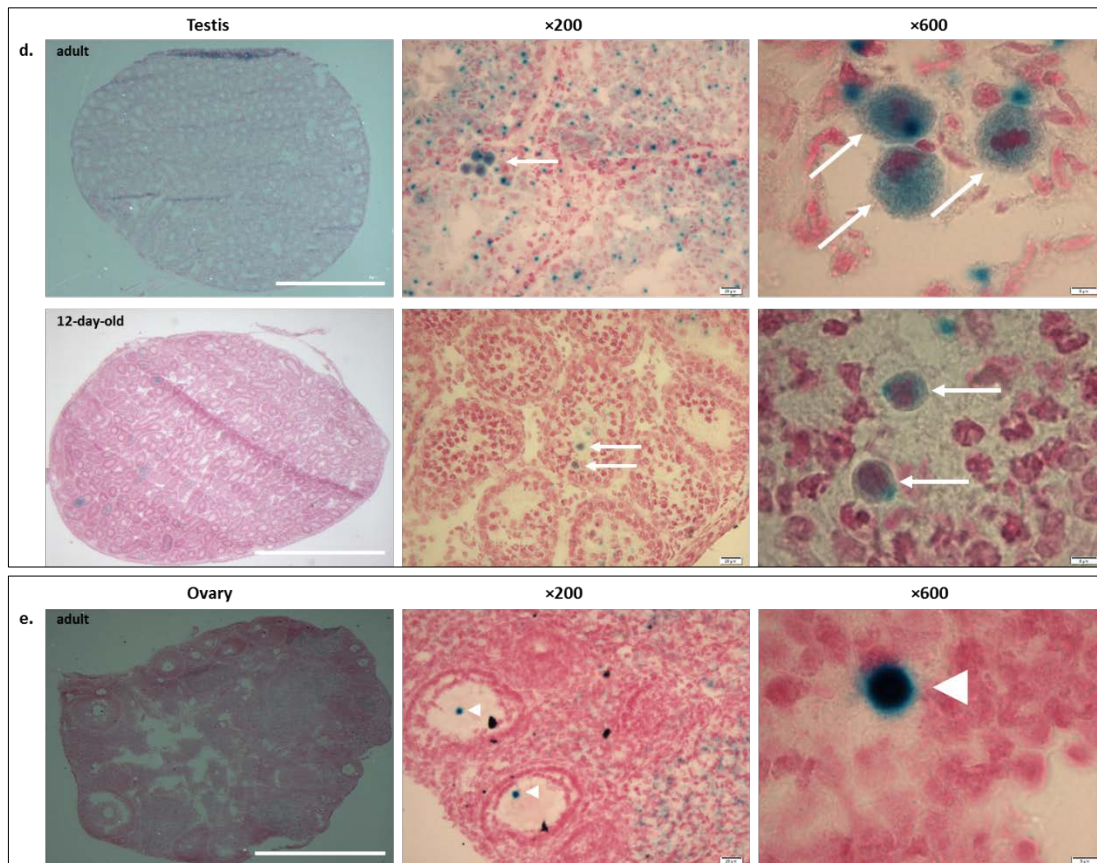
Fig. 3.11. LacZ images for *Mocs2a/b* expression in the brain of adult and 12-day-old *Mocs2*^{+/-} mice. LacZ staining of 10-μm brain sections from adult and 12-day-old *Mocs2*^{+/-} mice showing reporter gene activity in the hippocampus (CA1 and DG), cortex and brainstem. Nuclei were visualised by counterstaining with Nuclear Fast Red. Scale bars correspond to 1 mm for stereomacroscopic images, as well as 20 μm for images with ×200 magnification. CA1 = *Cornu Ammonis* 1, DG = Dentate gyrus.
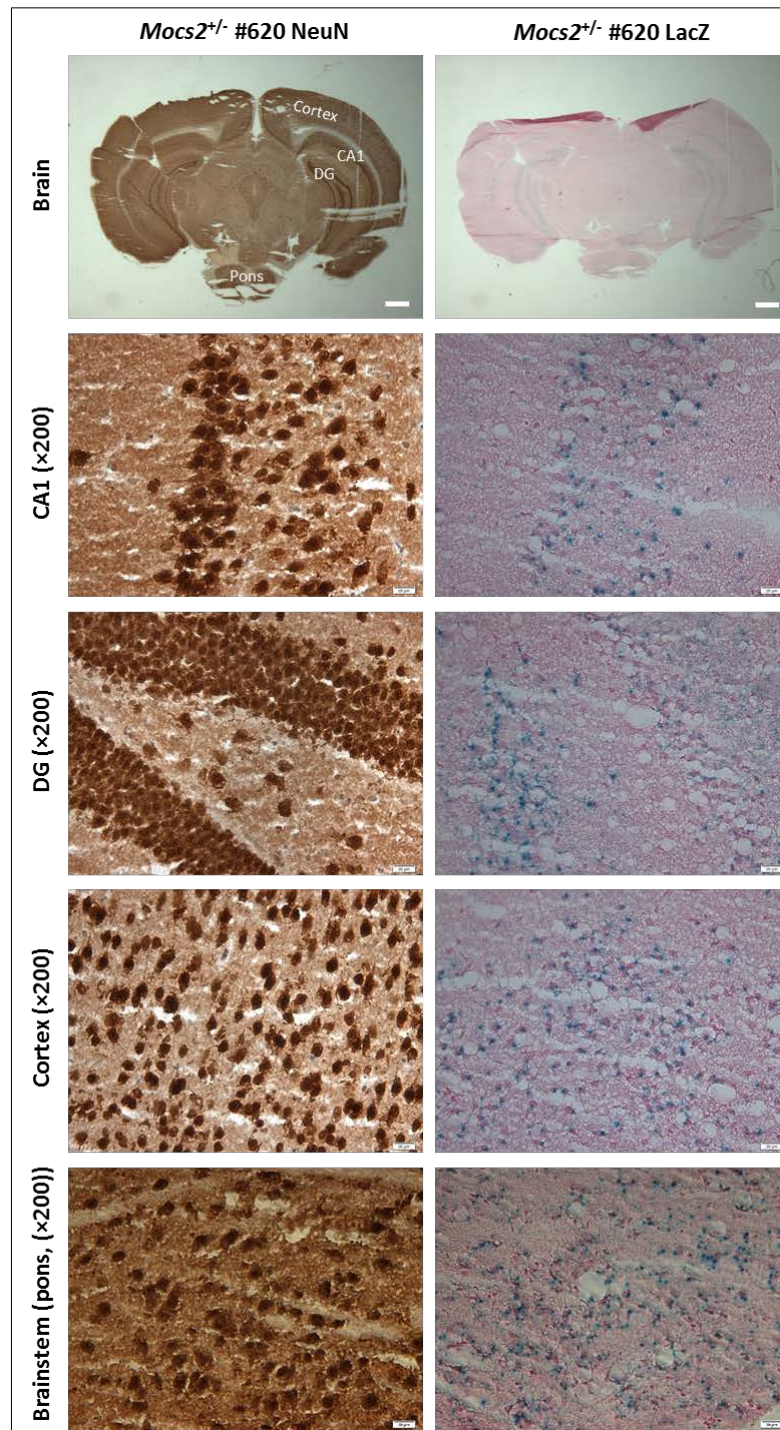
Fig. 3.12. Co-localisation of NeuN and LacZ signals in neurons from hippocampal, cortical and brainstem areas of adult *Mocs2*$^{+/-}$ #620 mouse. (Left column) Sections derived from an adult *Mocs2*$^{+/-}$ mouse brain were stained with a NeuN-specific antibody showing neuronal cell bodies stained in brown. **(Right column)** LacZ staining of the following brain sections showing *Mocs2* expressing cells in blue. Nuclei for LacZ staining were visualised by counterstaining with Nuclear Fast Red. Scale bars correspond to 1 mm for stereomacroscopic images, as well as 20 μm for images with ×200 magnification. CA1 = *Cornu Ammonis* 1, DG = *Dentate gyrus*.

	Kidney	×200	×600
a. adult			
12-day-old			

	Liver	×200	×600
b. adult			
12-day-old			

|	Skin	×200	×600
c. adult			
12-day-old			

Fig. 3.13. LacZ images for *Mocs2a/b* expression. LacZ staining of 10-μm tissue sections from adult and 12 day-old *Mocs2*^{+/-} mice shows reporter gene activity in **(a)** kidney's collecting duct system, **(b)** hepatocytes, **(c)** hair follicles of the skin and **(d, e)** germ cells, including undifferentiated spermatogonia **(arrows)** and oocytes **(arrowheads)**. Nuclei were visualised by counterstaining with Nuclear Fast Red. Scale bars correspond to 1 mm for stereomacroscopic images, as well as 20 μm and 5 μm for images with ×200 and ×600 magnifications, respectively.

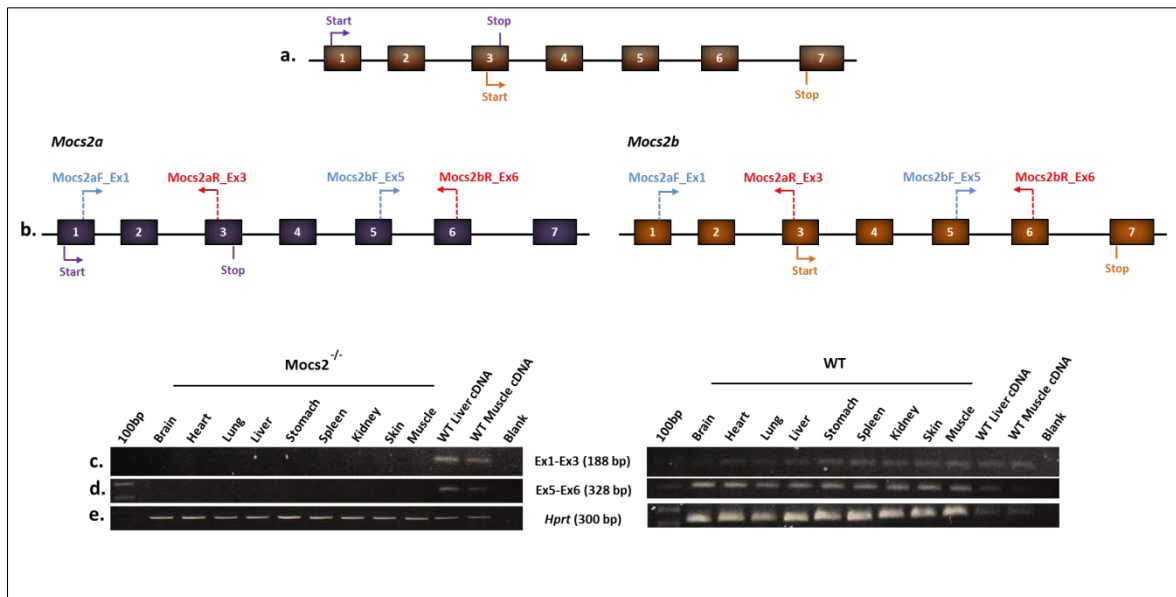### 3.1.4 Characterisation of *Mocs2* knockout mice

To begin with, we wanted to confirm on the genomic DNA level that the *Mocs2* gene was deleted in all examined tissues of *Mocs2* knockout (*Mocs2*^{-/-}) mice, and that it is present in corresponding tissues obtained from WT (*Mocs2*^{+/+}) mice. The PCR analyses were performed using primers Mocs2aF_In2-3 and Mocs2aR_In2-3 specific for the *Mocs2a* isoform*,* and primers Mocs2bF_Ex5 and Mocs2bR_In5-6 specific for the *Mocs2b* isoform. Primers specific for *Zfyve27* (Zfyve27_F and Zfyve27_R) were used to test the quality of extracted DNA samples **(Fig. 3.14)**.

73
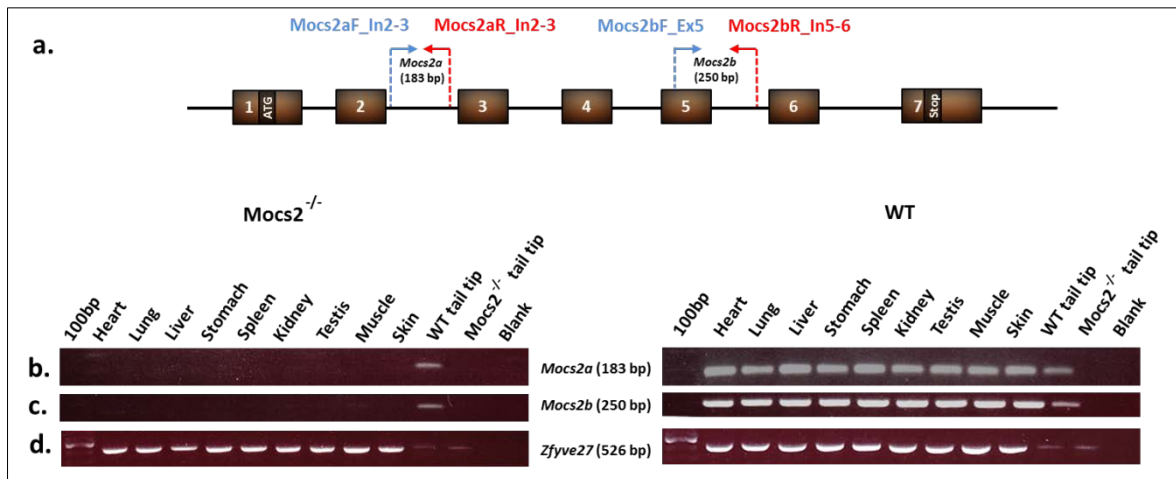
Fig. 3.14. Characterisation of *Mocs2*^{-/-} mice on the genomic DNA level. (a) Schematic representation of the *Mocs2* wild type (WT) allele together with primer arrangements. **(b, c)** PCR results showing the bands corresponding to *Mocs2a* and *Mocs2b* gene products (183 bp and 250 bp, respectively) in WT tissues, which are absent in *Mocs2*^{-/-} samples. **(d)** PCR analyses with primers specific for the *Zfyve27* sequence (526 bp) confirmed a good quality of isolated DNA. The arrows illustrate the localisation and the direction of primers used for genotyping PCR. (100bp = 100 bp DNA ladder; F = forward; R = reverse; Blank = negative control w/o DNA).

To confirm the successful deletion of the *Mocs2a/b* gene on the RNA level, we performed RT-PCR analyses. For this reason, we extracted total RNA from different tissues of *Mocs2*^{-/-} and *Mocs2*^{+/+} mice, respectively. Subsequently, cDNA was synthesised and used as a template for RT-PCR analysis. In contrast to human *MOCS2A* and *MOCS2B* isoforms, mouse transcripts cannot be distinguish via RT-PCR **(Fig. 3.15a)**, therefore, we were able to prove only global depletion of both, *Mocs2* transcripts. For this reason we designed two primer pairs, including Mocs2aF_Ex1, Mocs2aR_Ex3 and Mocs2bF_Ex5, Mocs2bR_Ex6 **(Fig. 3.15b)**. In agreement with results from the DNA study, we were unable to detect *Mocs2a/b* mRNA in any of *Mocs2*^{-/-} mouse tissues analysed, but it was detectable in corresponding tissues obtained from WT mice **(Fig. 3.15c, d)**. Primers specific for the housekeeping gene *Hprt* (HPRT_F, HPRT_R) were used to test the quality of synthesised cDNA samples **(Fig. 3.15e)**.

Fig. 3.15. Characterisation of *Mocs2*^{-/-} mice on the RNA level. (a) Schematic representation of the *Mocs2* wild type (WT) allele and **(b)** transcripts encoding *Mocs2a* and *Mocs2b* subunits**. (c, d)** RT-PCR results showing the bands corresponding to *Mocs2a/b* transcripts (188 bp and 328 bp) in WT tissues, while they are not present in the knockout samples. **(e)** RT-PCR analyses with primers specific for the *Hprt* gene (300 bp) confirmed a good quality of synthesised cDNA. The arrows illustrate the localisation and the direction of primers used for RT-PCR. (100bp = 100 bp DNA ladder; F = forward; R = reverse; Blank = negative control w/o DNA).

Furthermore, a qRT-PCR approach was employed to quantify *Mocs2a/b* expression in different tissues obtained from WT (*Mocs2*^{+/+}), heterozygous (*Mocs2*^{+/-}) and homozygous (*Mocs2*^{-/-}) mice. As expected, *Mocs2*^{-/-} mice did not express *Mocs2a/b* mRNA, and heterozygous mice showed reduced expression of both products compared to WT mice. Interestingly, in some tissues (e.g. lung or liver) no significant differences in *Mocs2a/b* expression could be observed between WT and heterozygous mice **(Fig. 3.16)**.
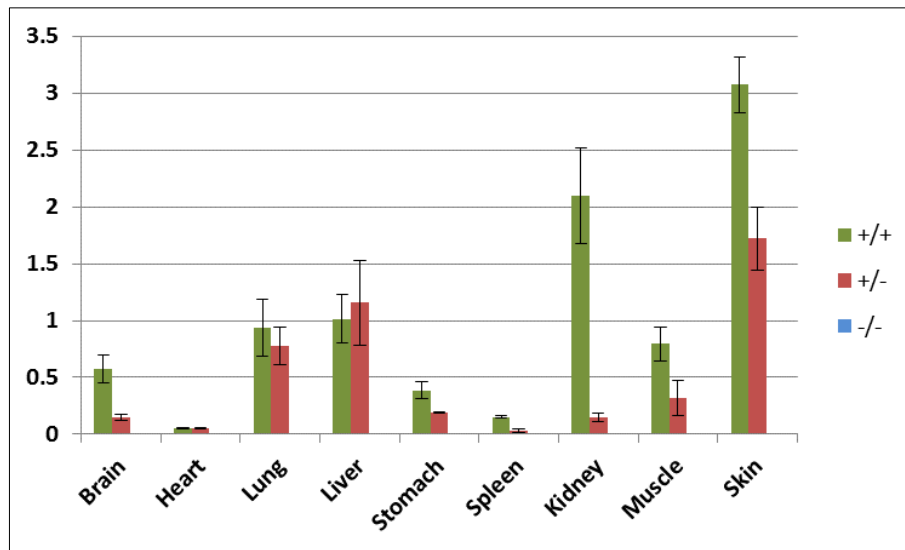
Fig. 3.16. Expression of *Mocs2a/b* gene in different tissues from *Mocs2*^{+/+} (wild type), heterozygous *Mocs2*^{+/-} and homozygous *Mocs2*^{-/-} mice. Quantitative RT-PCR data showing the expression of *Mocs2a/b* mRNA in different tissues from wild type (+/+ = green bars), heterozygous (+/- = red bars) and homozygous *Mocs2* knockout mice (-/- = blue bars). The results were normalised to *Gapdh* expression and are presented as a relative value to *Mocs2a/b* level in the WT liver. Values and associated error bars represent mean ± s.d. (n=3).

Finally, expression of Mocs2a and Mocs2b on the protein level should be analysed in WT and *Mocs2*^{-/-} animals. For this purpose, whole protein lysate was extracted from different tissues of *Mocs2*^{+/+} and *Mocs2*^{-/-} mice, respectively. From one part of each tissue, proteins were isolated for Western blot (WB), whereas the rest of the tissue specimens was prepared for immunohistochemical (IHC) analysis. Both experiments were performed by a Bachelor student, Ann-Christin Franke (Franke, 2014). For these purposes, specific antibodies for either Mocs2a (EP130014) or Mocs2b (EP113633) were used. Based on the molecular weight the Mocs2a protein should correspond to a 10 kDa band, while the Mocs2b protein to a 21 kDa band in WB analysis. Unfortunately, only the Mocs2b antibody was specific for WB analysis, and a strong expression of Mocs2b protein was detected exclusively in the WT liver and was not present in the *Mocs2*^{-/-} liver **(Fig. 3.17a)**. Immunohistochemical analyses using either a Mocs2a or Mocs2b-specific antibody showed a cytoplasmic localisation of both proteins in WT liver sections, while staining for Mocs2a and Mocs2b was undetectable in the *Mocs2*^{-/-} liver **(Fig. 3.17b, c)**.
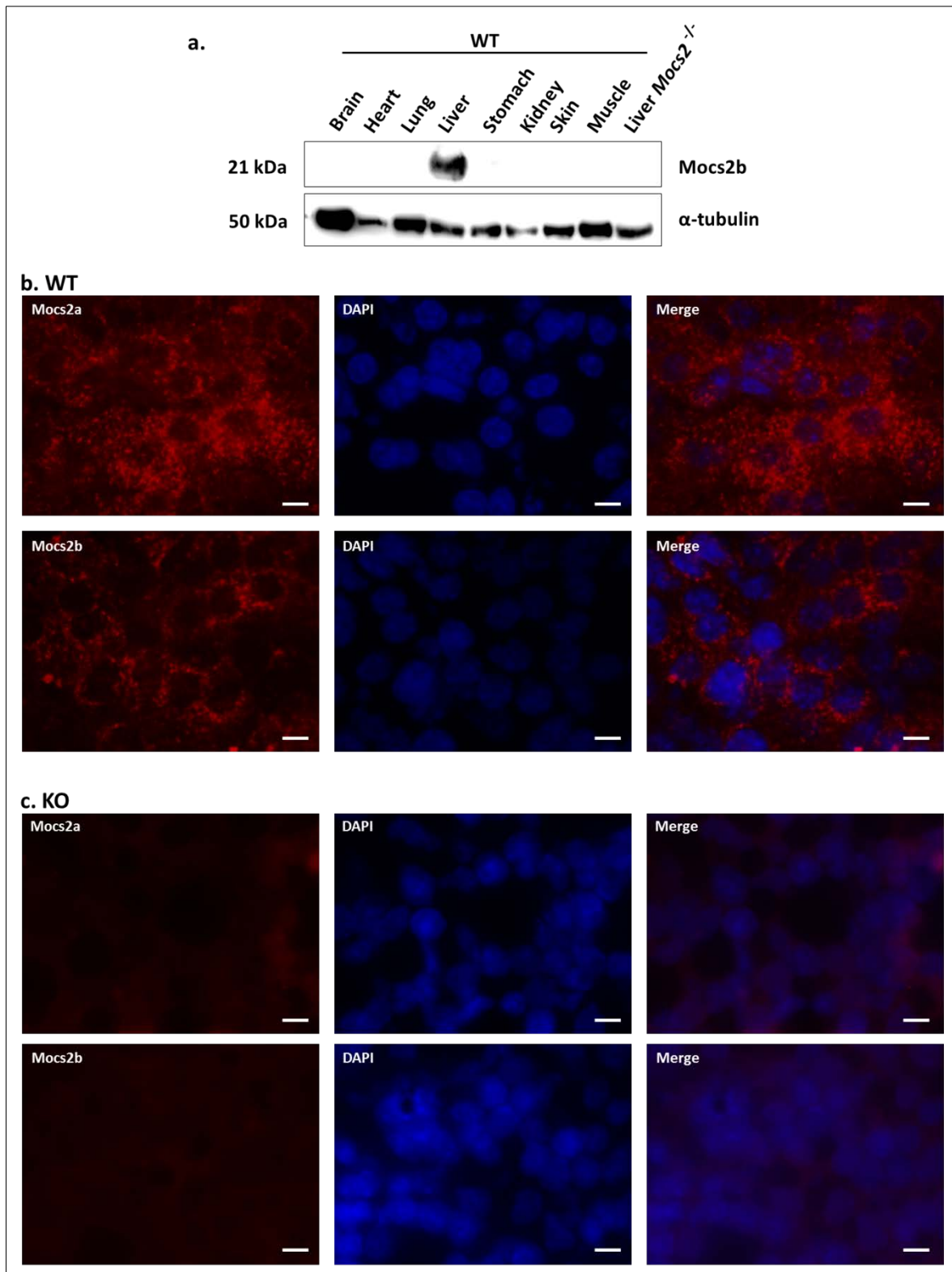
Fig. 3.17. Mocs2a/b protein expression in different tissues of adult wild type mice. (a) Western blot analysis revealed expression of Mocs2b in the liver derived from wild type (WT) mice, whereas expression of Mocs2b in other tissues could not be detected. In the liver of *Mocs2$^{-/-}$* mice Mocs2b expression was depleted. α-tubulin served as a loading control. Immunofluorescence staining with specific antibodies against Mocs2a and Mocs2b revealed Mocs2a and Mocs2b expression (red) **(b)** in liver cells of WT mice, but

not **(c)** in liver sections obtained from *Mocs2*$^{-/-}$ (KO) mice. Nuclei were counterstained with DAPI. Scale bars correspond to 10 μm.

3.1.5 Phenotypical analyses of *Mocs2*$^{-/-}$ mice

Mocs2 homozygous knockout (*Mocs2*$^{-/-}$) pups are much smaller in comparison to WT (*Mocs2*$^{+/+}$) and heterozygous (*Mocs2*$^{+/-}$) littermates **(Fig. 3.18 left)**. Additionally, *Mocs2*$^{-/-}$ mice present curly whiskers and a defect in the overall hair growth. They have flaky and wrinkled skin and are generally in a weaker health condition compared to *Mocs2*$^{+/+}$ and *Mocs2*$^{+/-}$ animals **(Fig. 3.18)**. *Mocs2*$^{-/-}$ mice appear normal at birth. During their first days of life *Mocs2*$^{-/-}$ mice increase their body weight, although at a significantly slower rate than their WT and heterozygous littermates **(Fig. 3.19)**. The mean life span of *Mocs2*$^{-/-}$ mice is 4.7 days, although most of them die at postnatal day 1, or between postnatal day 6 and 7 **(Fig. 3.20)**.
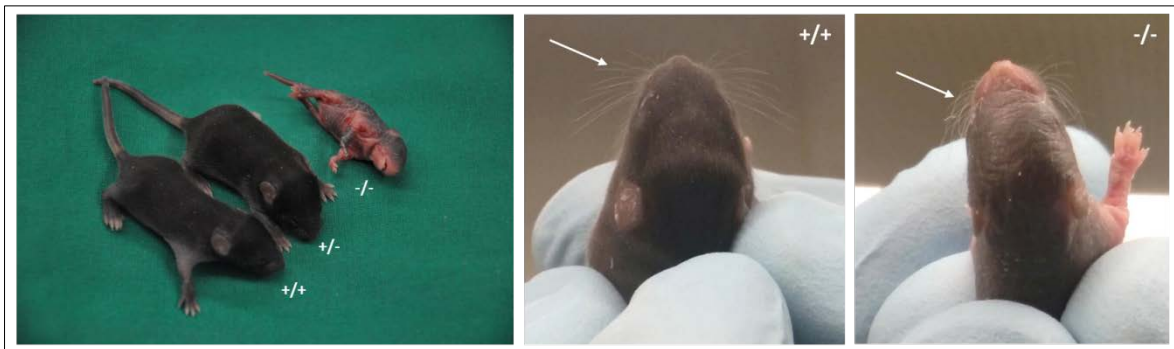
Fig. 3.18. *Mocs2*$^{-/-}$ **mice show growth retardation, abnormal shape of whiskers, a defect in the overall hair growth, as well as flaky and wrinkled skin compared to heterozygous and WT littermates. (Left image)** Exemplary picture of a 7-day-old *Mocs2*$^{-/-}$ mouse, in comparison to control animals from the same litter. **(Middle and right images)** Exemplary picture of a 7-day-old WT (*Mocs2*$^{+/+}$) and a knockout (*Mocs2*$^{-/-}$) mouse from the same litter. The WT mouse presented straight whiskers, while the *Mocs2*$^{-/-}$ animal whiskers appeared curly and flopped (shown by arrows).
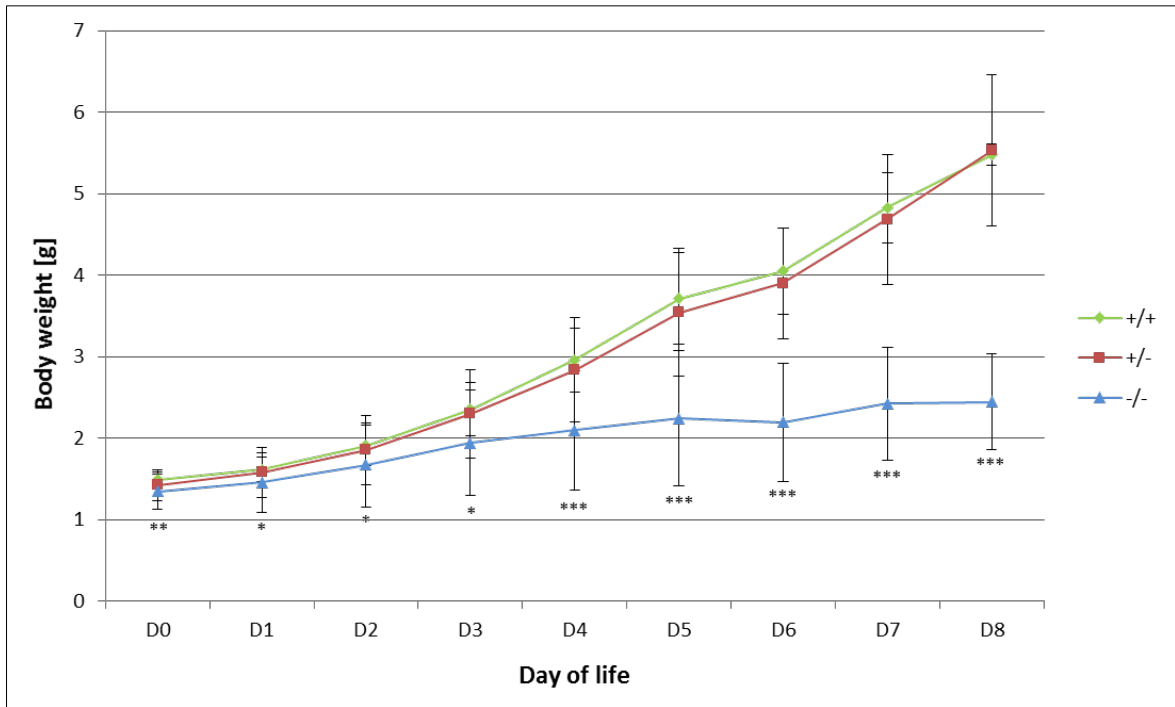
Fig. 3.19. Reduced postnatal body weight gain of *Mocs2*^{-/-} mice. Line graphs showing body weights of WT (+/+, green), heterozygous (+/-, red) and homozygous KO pups (-/-, blue). Body weight gain after birth of *Mocs2*^{-/-} mice was significantly slower as compared to WT (*Mocs2*^{+/+}) or heterozygous (*Mocs2*^{+/-}) littermates. Body weight and associated error bars representing mean ± s.d. from n = 35 for WT, n = 60 for heterozygous and n = 34 for homozygous KO pups. * p<0.05, ** p<0.01, *** p<0.001.
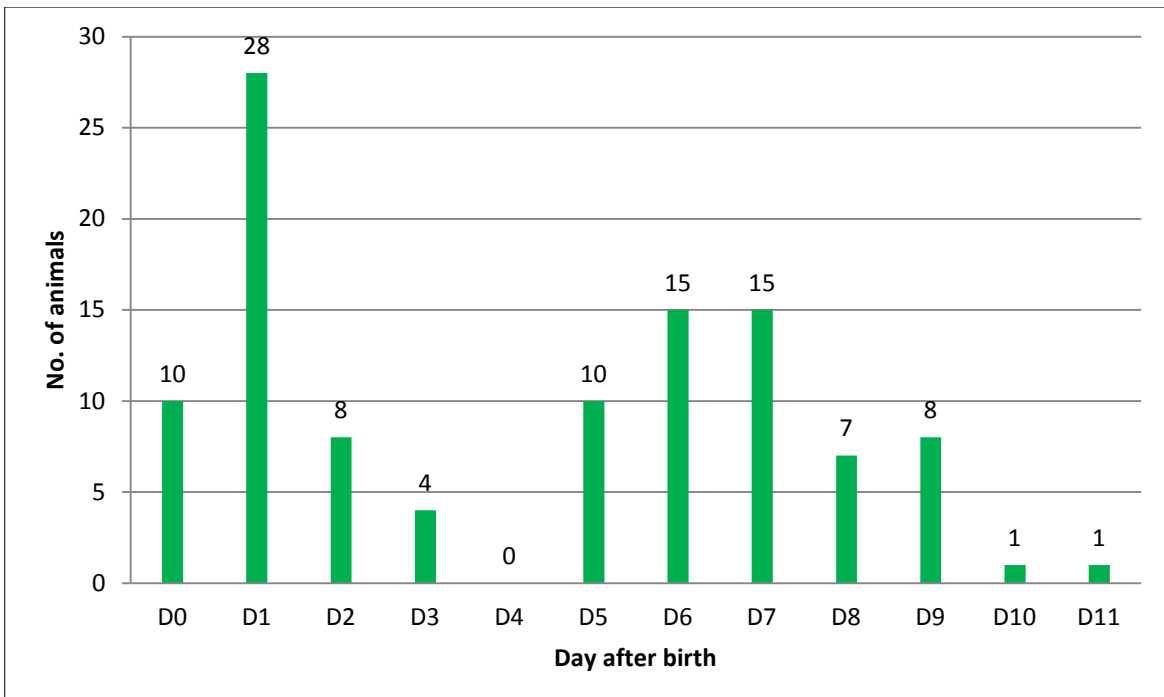
Fig. 3.20. Life span of *Mocs2*^{-/-} mice. The majority of homozygous *Mocs2*^{-/-} pups died shortly after birth. Bar graphs representing the life span of *Mocs2*^{-/-} mice. In total, 107 *Mocs2*^{-/-} mice were investigated. All of them

79

died within 11 days after birth, however, two important periods could be observed. The first critical time point was directly after birth (47% of animals died during this time), and a second time point between postnatal day 5 and 10 (52%), (n=107).

As presented above, *Mocs2*^{-/-} mice showed a reduced gain of their body weights compared to control animals, thereby *Mocs2*^{-/-} mice were significantly smaller. However, impaired growth did not completely explain the mortality of KO animals. Interestingly, shortly before death, all *Mocs2*^{-/-} mice presented a urinary retention. The *post-mortem* examination showed an accumulation of yellow deposits in the bladder **(Fig. 3.21a)**. These structures were most probably the underlying cause of the urinary track obstruction observed in *Mocs2*^{-/-} animals, however, biochemical analyses failed to identify the composition of these structures **(Fig. 3.21b)**.
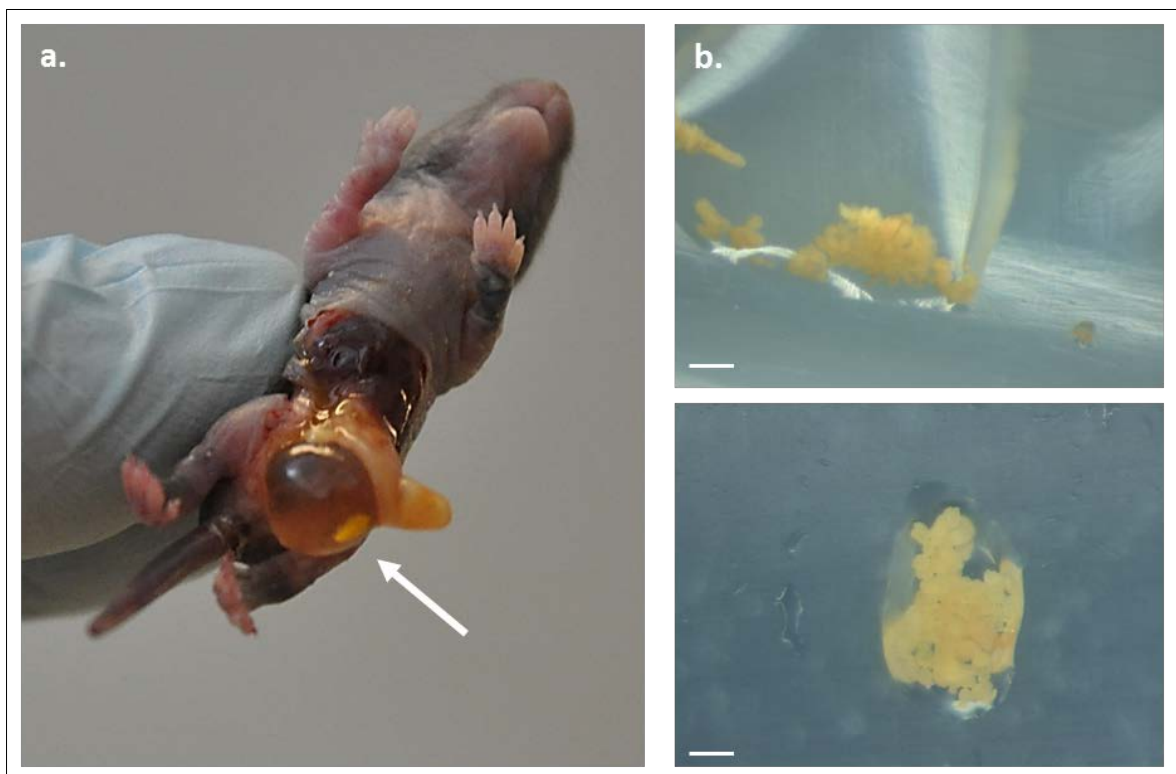
Fig. 3.21. *Mocs2*^{-/-} mice present a urinary retention and insoluble crystals in the bladder. (a) Exemplary picture of a 6-day-old *Mocs2*^{-/-} mouse. Arrow points to the presence of yellow deposits in the bladder. **(b)** Stereomicroscope images showing aggregates collected from the bladders of *Mocs2*^{-/-} animals. Scale bars correspond to 100 μm. (n = 50).

A reverse flow of the urine, i.e. from the bladder back into the kidneys, can result in hydronephrosis and cause permanent and severe damage to the kidneys, resulting in

kidney failure (Iravani *et al.*, 2014). In order to proof a possible renal involvement in the *Mocs2*^{-/-} phenotype, histopathological analyses of kidney sections was performed. The histological analysis of kidneys derived from *Mocs2*^{-/-} mice demonstrated the presence of crystals in the collecting duct system **(Fig. 3.22)**. This experiment was performed in cooperation with Dr. Samy Hakroush, Institute of Pathology, UMG. Consistent with these results, elevated level of proteins (proteinuria) and extremely high concentrations of haemoglobin and/or damaged erythrocytes (haemoglobinuria) in the *Mocs2*^{-/-} urine were identified **(Fig. 3.23)**. Both parameters are well-known indicators of kidney and urinary track diseases (House and Cattran, 2002).
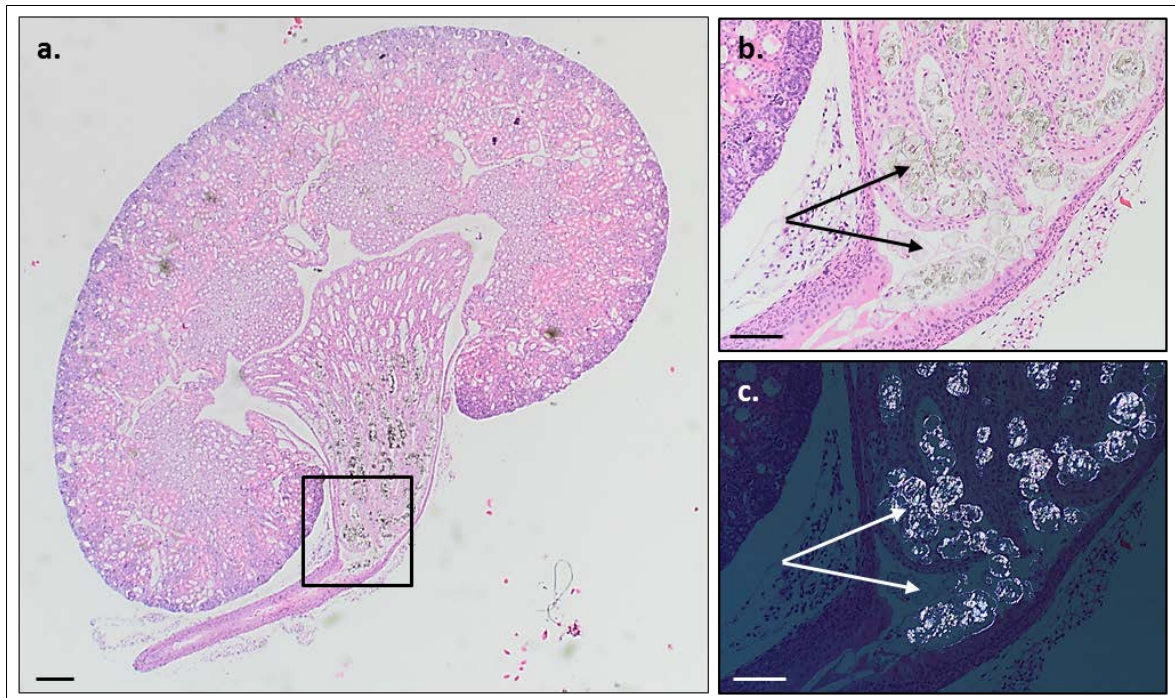
Fig. 3.22. *Mocs2*^{-/-} mice present kidney stones in the collecting duct system. (a) Exemplary images of HE-stained kidney sections from *Mocs2*^{-/-} mice show the localisation of stones. Black box in the kidney section indicates the region of renal pelvis seen in the higher magnification **(b and c)**. Arrows point to the presence of crystals in renal pelvis. To visualise stones, picture **(c)** was performed with reduced light intensity, which results in crystal flashing. Scale bars correspond to 200 μm. (n = 3).
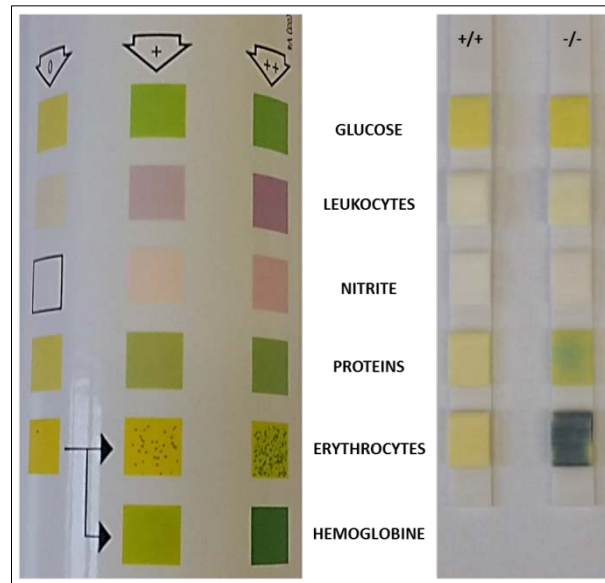
Fig. 3.23. _Mocs2_^{-/-} mice show elevated level of proteins and erythrocytes in the urine. Exemplary image demonstrating the results of colorimetric tests estimating the level of specific parameters, including glucose, leukocytes, nitrite, proteins and erythrocytes. In contrast to WT (_Mocs2_$^{+/+}$) animals, _Mocs2_$^{-/-}$ mice present elevated level of proteins (green colour in the test patch), and extremely elevated numbers of erythrocytes (dark-blue colour in the test patch) in the urine. (n = 3).

Furthermore, sulphite concentration, the substrate of sulphite oxidase, another molybdenum cofactor (MoCo)-dependent enzyme, was investigated. Using another colorimetric test, it was shown that _Mocs2_$^{-/-}$ mice presented an elevated concentration of urinary sulphite compared to WT control mice **(Fig. 3.24)**.
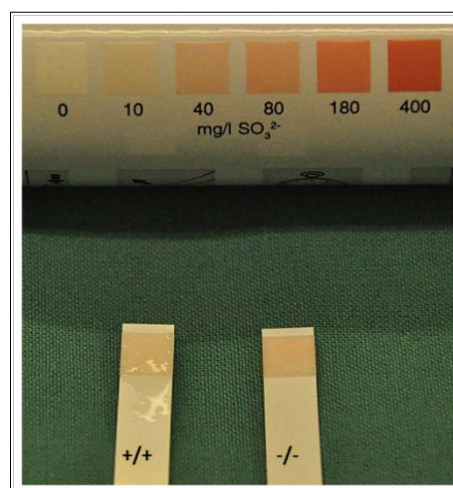

Fig. 3.24. _Mocs2_$^{-/-}$ mice present a higher concentration of urinary sulphite than WT littermates. Exemplary picture showing the results of a colorimetric test estimating the sulphite concentration. The level of urinary sulphite was higher in _Mocs2_$^{-/-}$ than in WT (_Mocs2_$^{+/+}$) control animals. (n = 10).

In rodents, an elevated level of sulphite leads to neuron loss in the hippocampus (Kocamaz *et al.*, 2012). To check the potential toxic effect of an increased sulphite level in the brain of *Mocs2*$^{-/-}$ mice, immunohistological analyses were performed. Brain sections from WT, *Mocs2*$^{+/-}$ and *Mocs2*$^{-/-}$ animals were either subjected to hematoxylin-eosin (HE) staining or stained with GFAP, NeuN, Casp3 and IBA1-specific antibodies. GFAP (glial fibrillary acidic protein) is an intermediate filament protein that is expressed in astrocytes (Reeves *et al.*, 1989). NeuN (RNA binding protein, fox-1 homolog (*C. elegans*) 3) is a neuronal nuclear antigen that is commonly used as a biomarker for neurons. Casp3 (Caspase 3 or apoptosis-related cysteine peptidase) plays a central role in the execution-phase of cellular apoptosis (Jeruc *et al.*, 2006) and is the predominant caspase involved in the cleavage of amyloid-beta 4A precursor protein, which is associated with neuronal death in Alzheimer's disease (Eimer and Vassar, 2013). IBA1 (ionising calcium-binding adaptor molecule) is specifically expressed in macrophages/microglia, and is up-regulated during the activation of these cells. IBA1 expression is up-regulated in microglia following nerve injury, central nervous system (CNS) ischemia and several other brain diseases (Ito *et al.*, 2001). Although the GFAP and NeuN stainings did not show any significant differences in astrocyte and neuron number (data not shown), HE staining revealed apoptosis in the hippocampus, cortex and brainstem (midbrain and pons) of *Mocs2*$^{-/-}$ and *Mocs2*$^{+/-}$ mice compared to brain sections from WT (*Mocs2*$^{+/+}$) mice **(Fig. 3.25)**. Typical apoptotic neurons show central aggregation and fragmentation of chromatin. To evaluate these results, *Mocs2*$^{-/-}$, *Mocs2*$^{+/-}$ and WT brain sections were stained with Casp3 **(Fig. 3.26a)**. *Mocs2*$^{-/-}$ and *Mocs2*$^{+/-}$ mice revealed elevated numbers of cells expressing Caspase 3 protein **(Fig. 3.26b)**. Surprisingly, increased number of Caspase 3 positive cells did not correlate with the number of IBA-1 positive cells **(Fig. 3.27).** These results indicate that apoptosis which occurs in the brain of *Mocs2*$^{-/-}$ mice may be one of the main factors responsible for severe somatic symptoms observed in these mice. These experiments were performed in collaboration with Dr. Imke Metz (Institute of Neuropathology, UMG).
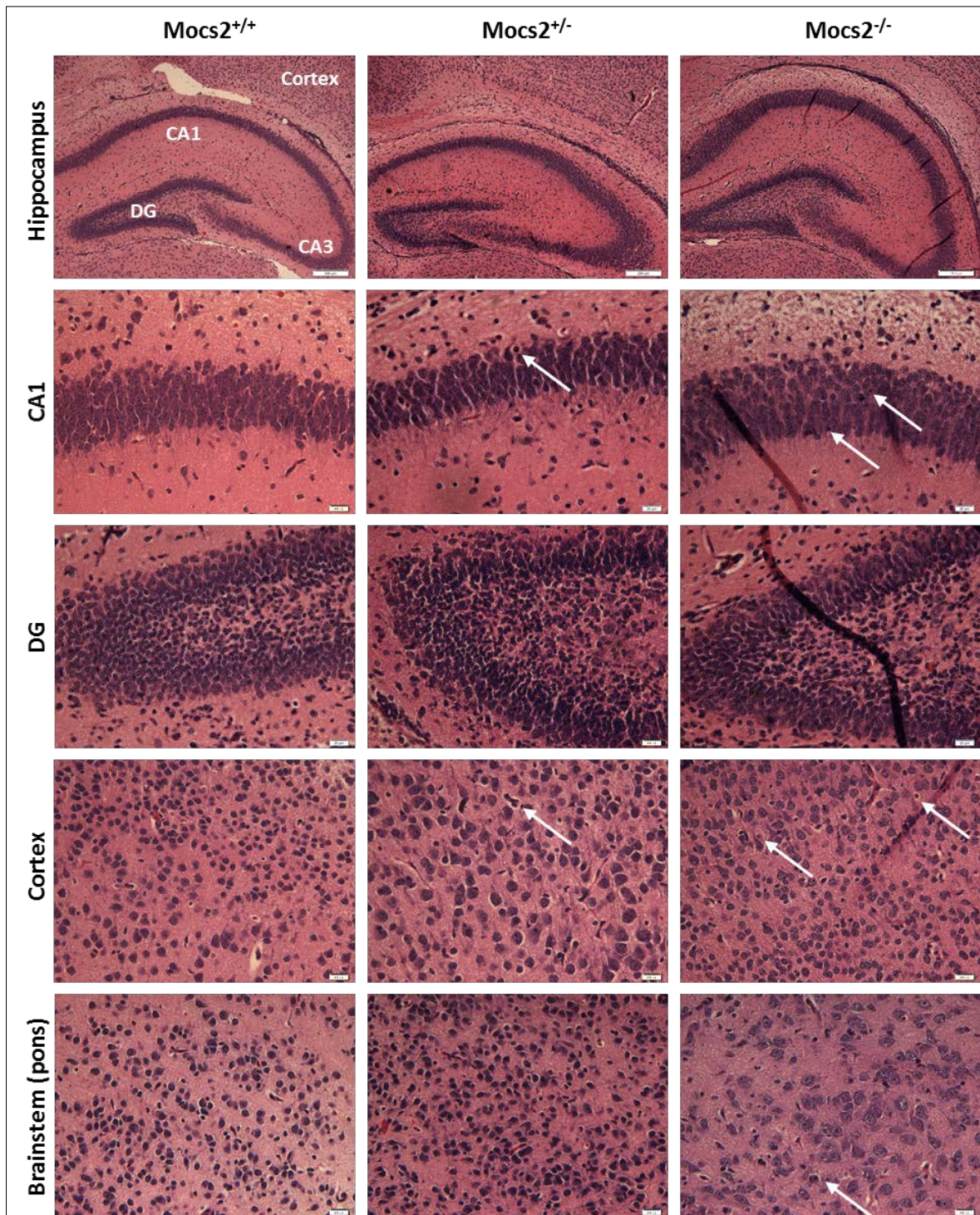
Fig. 3.25. *Mocs2*^{-/-} **animals presented apoptotic neurons in hippocampus, cortex and brainstem.** Exemplary images of hematoxylin-eosin (HE) staining of brain sections derived from *Mocs2*$^{+/+}$, *Mocs2*$^{+/-}$ and *Mocs2*$^{-/-}$ animals. Arrows point to the presence of apoptotic neurons. Scale bars correspond to 200 μm for hippocampus and 20 μm for CA1 (*Cornu Ammonis* 1), CA3 (*Cornu Ammonis* 3), DG (*Dentate gyrus*), cortex and brainstem (n = 2).
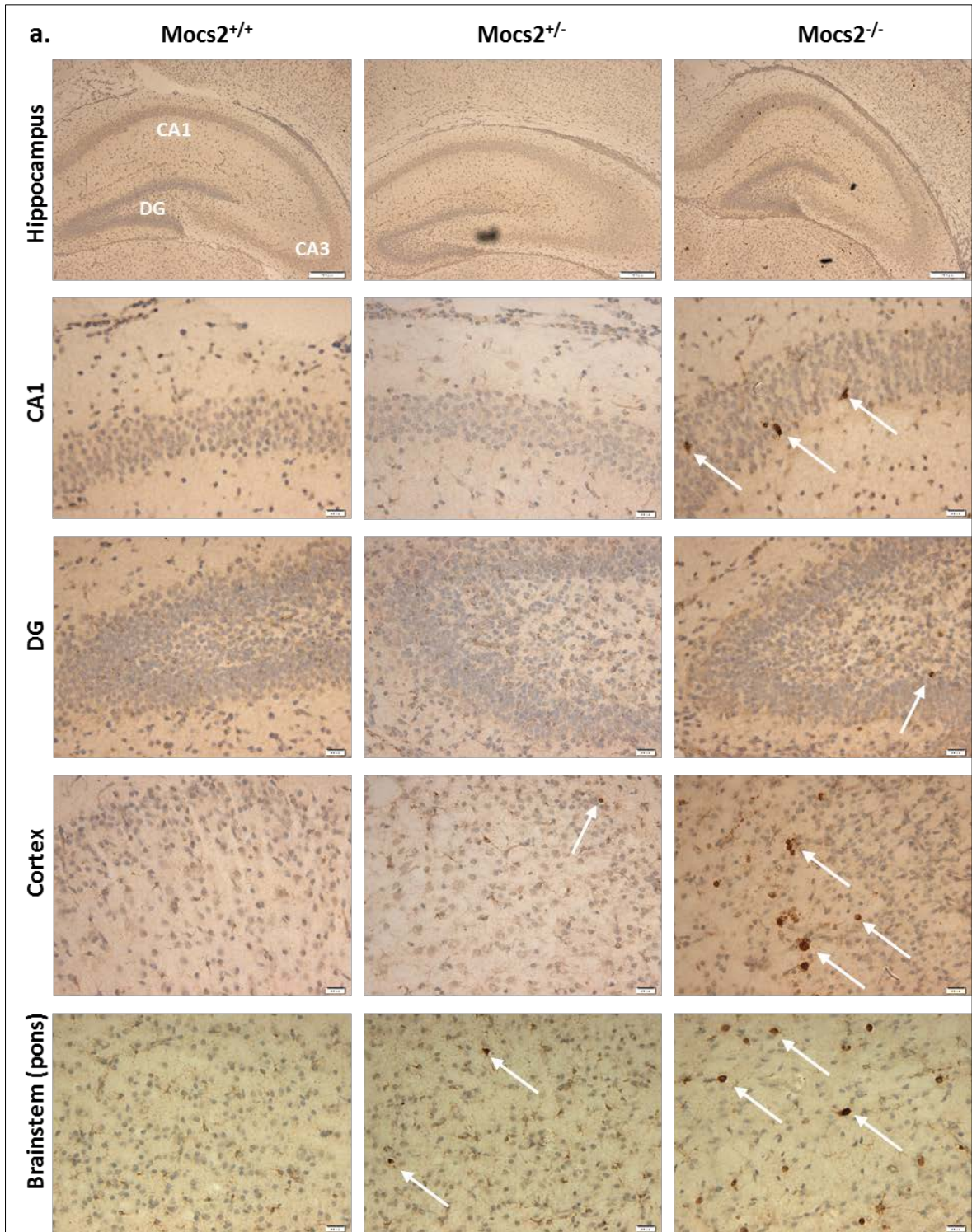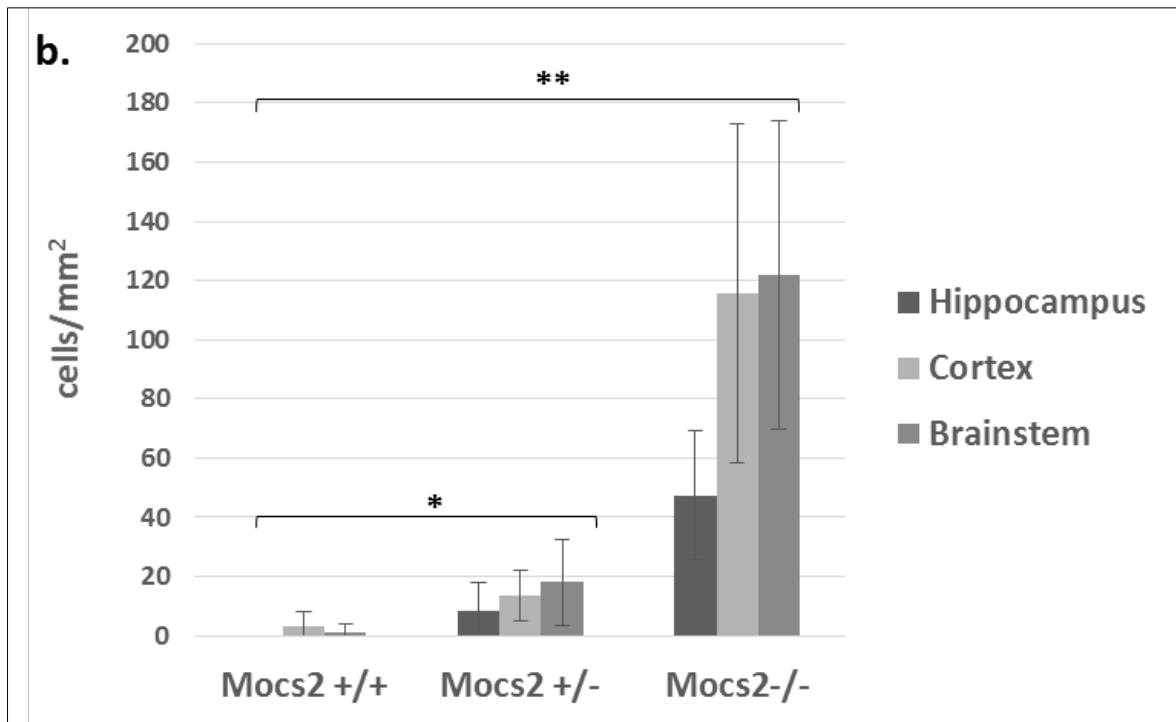
Fig. 3.26. *Mocs2^{-/-}* **animals presented massive apoptosis in hippocampus, cortex and brainstem. (a)** Exemplary images of Caspase 3 (Casp3) immunostaining of brain sections derived from *Mocs2^{+/+}*, *Mocs2^{+/-}* and *Mocs2^{-/-}* animals. Arrows point to the presence of Casp3 positive neurons. Nuclei were counterstained with hematoxylin. Scale bars correspond to 200 μm for hippocampus and 20 μm for CA1 (*Cornu Ammonis* 1), CA3 (*Cornu Ammonis* 3), DG (*Dentate gyrus*), cortex and brainstem (n = 2). **(b)** Bar graphs showing the number of apoptotic neurons in *Mocs2^{+/+}*, *Mocs2^{+/-}* and *Mocs2^{-/-}* brains. Values and associated error bars represent mean ± s.d. from 10 sections for each genotype (n = 2, * p<0.001, ** p<0.0001).
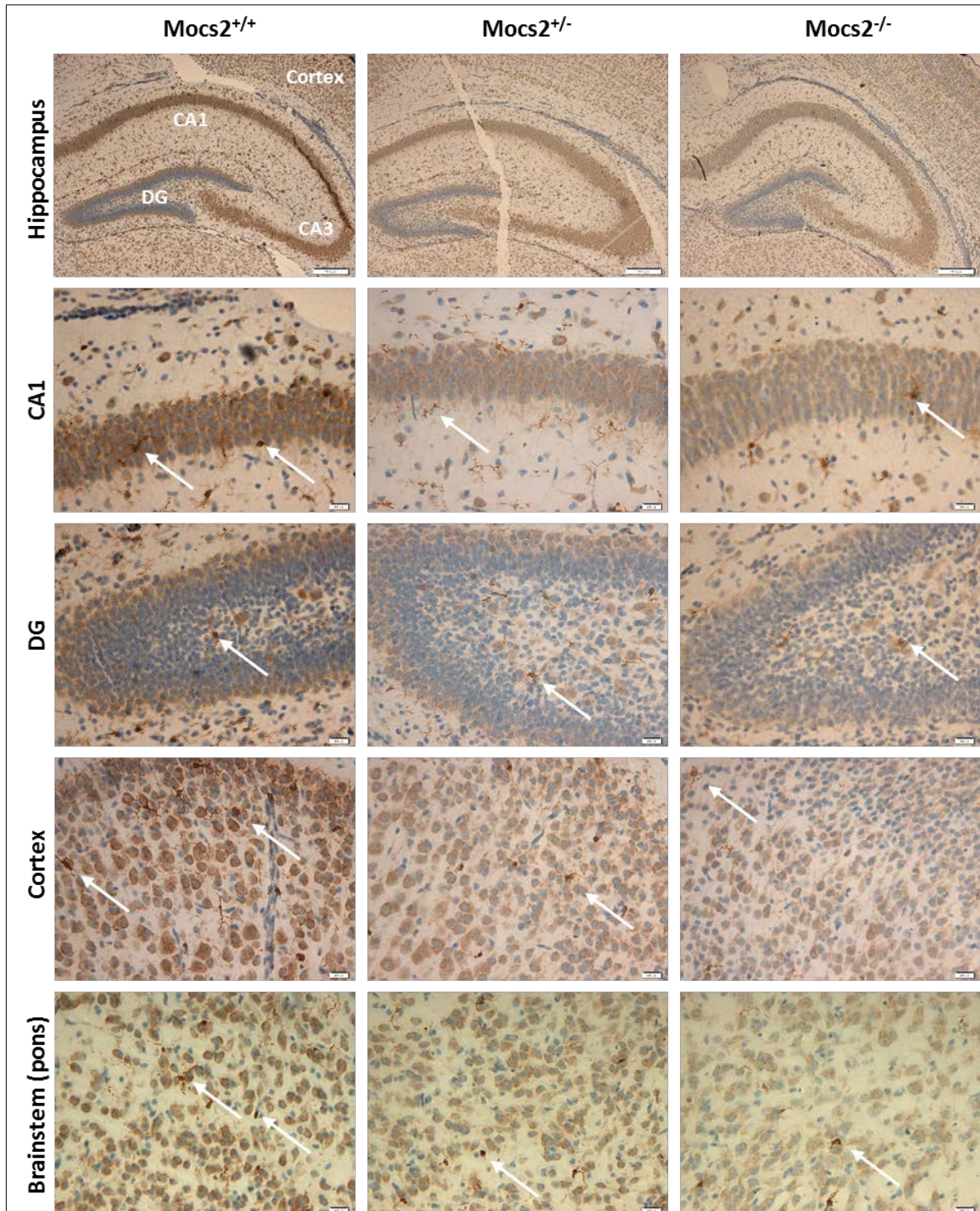
Fig. 3.27. Expression of IBA1 protein in hippocampus, cortex and brainstem of *Mocs2*^+/+^, *Mocs2*^+/-^ and *Mocs2*^-/-^ animals. Exemplary images of ionising calcium-binding adaptor molecule (IBA1) immunostaining of brain sections derived from *Mocs2*^+/+^, *Mocs2*^+/-^ and *Mocs2*^-/-^ animals. Arrows point to the presence of IBA1 positive neurons. Nuclei were counterstained with hematoxylin. Scale bars correspond to 200 μm for hippocampus and 20 μm for CA1 (*Cornu Ammonis* 1), CA3 (*Cornu Ammonis* 3), DG (*Dentate gyrus*), cortex and brainstem (n = 2).
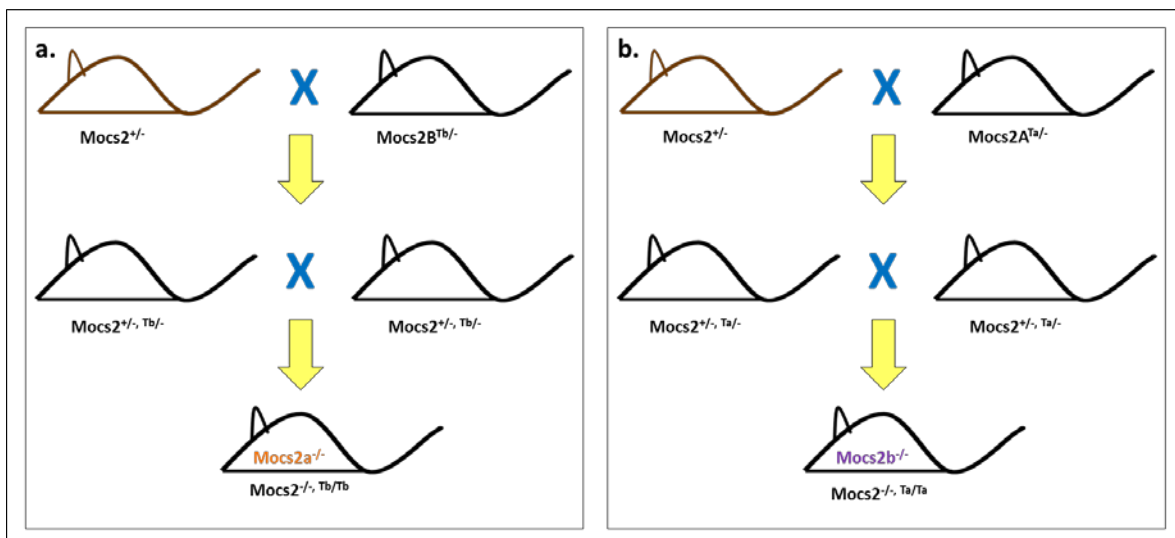
### 3.1.6 Generation of isolated *Mocs2a* and *Mocs2b knockout* mice

To generate the respective isolated forms of *Mocs2* knockout animals (either the knockout of the *Mocs2a* isoform or the knockout of the *Mocs2b* isoform) based on the knockout model of the complete *Mocs2* gene, we decided to breed these mice with MOCS2A or MOCS2B transgenic animals, respectively. **Figure 3.28** presents the strategy used for the generation of isolated *Mocs2a* and *Mocs2b* knockout mice.

Fig. 3.28. Schematic representation of the strategy used for the generation of a pure *Mocs2a* knockout or a *Mocs2b* knockout mouse model. **(a)** To obtain an isolated *Mocs2a* knockout mouse model, $Mocs2^{+/-}$ mice were crossed with transgenic *Mocs2B* animals expressing ubiquitously human MOCS2B protein ($Mocs2B^{Tb/-}$). Further, double heterozygous mice ($Mocs2^{+/-;Tb/-}$) were bred to each other to establish the *Mocs2a* knockout line with supplementation of the MOCS2B subunit ($Mocs2^{-/-;Tb/Tb}$). **(b)** The *Mocs2b* knockout line was generated by crossing $Mocs2^{+/-}$ mice with transgenic *Mocs2A* animals expressing ubiquitously human MOCS2A protein ($Mocs2A^{Ta/-}$). Next, double heterozygous mice ($Mocs2^{+/-;Ta/-}$) were bred to each other to give rise to the isolated form of *Mocs2b* knockout mice ($Mocs2^{-/-;Ta/Ta}$).

3.1.7 Generation of a *MOCS2A* transgenic mouse line

To generate a *MOCS2A* transgenic mouse model, the pronuclear injection with the construct pWajaIII was performed. The pWajaIII construct was generated by Dr. Waja Wegner (Wegner, 2007). The vector contains the complete human *MOCS2A* open reading frame driven by an enhanced *β-actin* promoter **(Fig. 3.29a)**. Before pronuclear injection, the construct was linearised with the restriction enzyme *Xma*I and subsequently purified **(Fig. 3.29b)**.
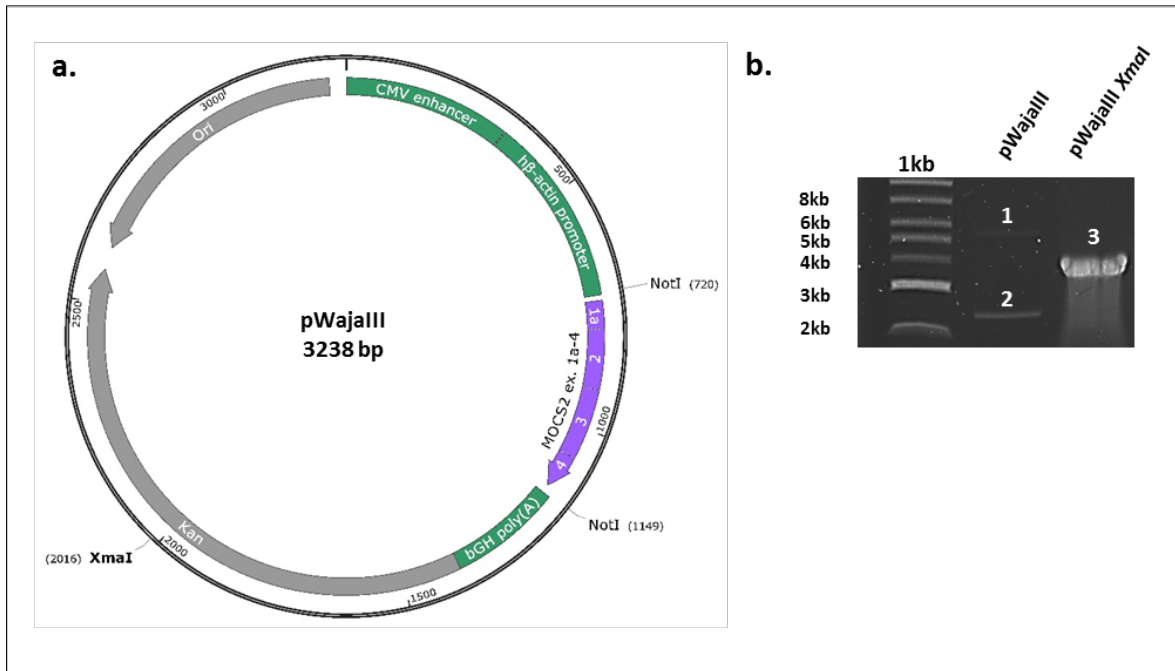
Fig. 3.29. Preparation of the MOCS2A transgene construct. (a) Schematic representation of the pWajaIII vector showing the human *MOCS2A* ORF under the control of the *Cytomegalovirus* (CMV) enhancer and *β-actin* promoter followed by a bovine growth hormone polyadenylation signal (bGH polyA), the kanamycin (Kan) resistance gene and the origin of replication (Ori). **(b)** Agarose gel electrophoresis revealed bands specific for the undigested and digested pWajaIII plasmid. Band 1 and 2 correspond to the undigested plasmid either in nicked circles (1) or supercoiled (2) conformation. Band 3 (3.3 kb) corresponds to the linearized plasmid after *Xma*I digestion.

Microinjections into the male pronuclei of fertilised oocytes, as well as the transfer of injected embryos to C57Bl/6N pseudopregnant foster mothers were performed in collaboration with Dr. Ursula Fünfschilling (MPI of Experimental Medicine, Göttingen). The first injection resulted in 37 pups. To identify potential founder animals, genotyping PCR experiments were performed using human *MOCS2A* transgene-specific primers qMOCS2AEx1a_F and qMOCS2AEx2_R **(Fig. 3.30a)**. In 6 out of 37 animals the *MOCS2A* transgene could be detected by PCR analyses **(Fig. 3.30b)**.
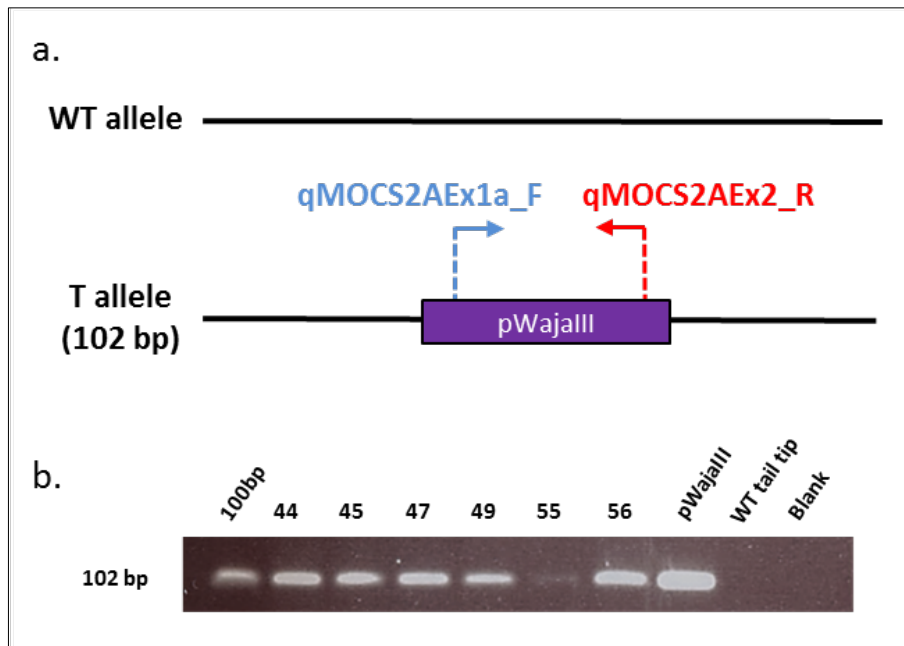
Fig. 3.30. Detection of the *MOCS2A* transgene in putative founder animals. (a) Scheme of the strategy used for the identification of founder animals. **(b)** Results of the genotyping PCR (102 bp) revealed six animals presenting the *MOCS2A* transgene. Results of the genotyping PCR for negative pups are not shown. The arrows indicate the localisation and the direction of primers used for genotyping PCR. (100bp = 100 bp DNA ladder; F = forward; R = reverse; Blank = negative control w/o DNA).

The number of transgene copies integrated in founder animals genome was estimated by real-time PCR experiments using *MOCS2A*-specific primers qMOCS2AEx1a_F and qMOCS2AEx2_R. Normalised results presented in **figure 3.31** revealed that all animals carried 2 copies of the *MOCS2A* transgene.
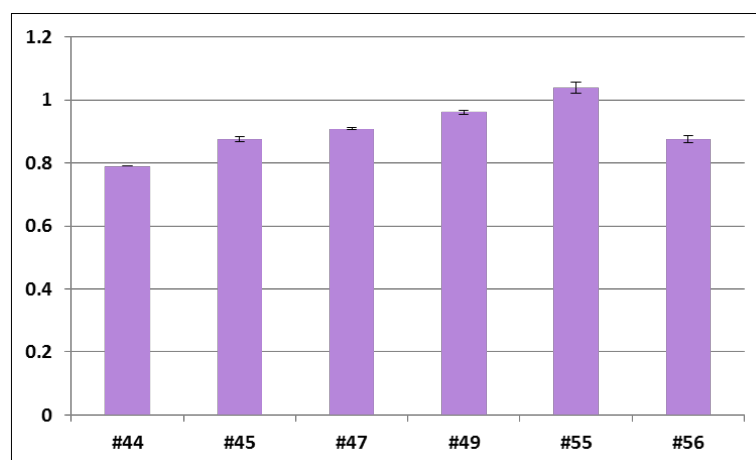
Fig. 3.31. Copy number evaluation of the *MOCS2A* transgene in founder animals. Bar graphs showing the results of qPCR analysis indicated that all investigated animals carried 2 copies of the *MOCS2A* transgene.

The results obtained from the *MOCS2A* transgene were normalised against a murine single copy gene, namely *acrosin* (*Acr*), and are presented as a relative value to another single copy gene, named pelota (Pelo). Values and associated error bars represent mean ± s.d. (n = 3).

To establish a *MOCS2A* transgenic line we bred founder animals with C57Bl/6N wild type mice. Due to several problems with *MOCS2A* founder animals (one animal died, one presented no germline contribution, and two other animals were infertile), we were able to establish only two transgenic lines, namely *MOCS2A* #44 (A6) and *MOCS2A* #56 (A5). To exclude that random transgene integration disturbed the function of other genes, the position of the transgene integration in the genome of the *MOCS2A* founder animal #56 was investigated. In agreement with previous findings, founder animal #56 had two integration sites on chromosome 2. The first transgene (Ta1) was integrated into the third intron of the *DnaJ (Hsp40) Homolog, Subfamily C, Member 24* (*Dnajc24*) gene (NCBI chr2:107210791-107210601). The integration site of the second transgene (Ta2) was localised in the second intron of the *Aven* gene (NCBI chr2: 112538459-112537983). In **Figure 3.32a** the strategy designed for genotyping of the WT and transgenic alleles is shown. For the identification of the first *MOCS2A* transgene Ta1 we used the following primers: Mouse#56_T1F, TransgeneA_F and Mouse#56_T1R, whereas, for the detection of the second *MOCS2A* transgene Ta2 primers Mouse#56_T2F, TransgeneA_F and Mouse#56_T2R were used **(Fig. 3.32b)**. Genotyping PCR revealed that only the first *MOCS2A* transgene Ta1 was transmitted to the offspring, giving rise to a *MOCS2A5* transgenic mouse line with a single copy of the *MOCS2A* transgene **(Fig. 3.32c)**. Both, integration and expression of the *MOCS2A* transgene, were confirmed in each tissue of heterozygous *MOCS2A* mouse (*MOCS2A*$^{Ta/-}$) by PCR analyses **(Fig. 3.33a-c)**. To check if the first MOCS2A transgene Ta1 integration has any influence on the murine *Dnajc24* host gene, *Dnajc24* expression was analysed in transgenic tissues in the F1 generation. Primers used for the detection of *Dnajc24* transcripts were localised in the 3rd and 4th exon of the *Dnajc24* gene, respectively, flanking the third intron containing the *MOCS2A* Ta1 transgene. Using qRT-PCR analyses a significant reduction in *Dnajc24* expression was observed in *MOCS2A*$^{Ta/-}$ mice compared to WT animals **(Fig. 3.34)**. Although heterozygous *MOCS2A*$^{Ta/-}$ animals were healthy and fertile, homozygous *MOCS2A*$^{Ta/Ta}$ mice were embryonically lethal. Therefore, heterozygous *MOCS2A*$^{Ta/-}$ mice were bred with

heterozygous *Mocs2*$^{+/-}$ knockout mice to obtain *Mocs2*$^{+/-, Ta/-}$ mice. Furthermore, double heterozygous *Mocs2*$^{+/-, Ta/-}$ mice were bred either to each other or with *Mocs2*$^{+/-}$ mice to obtain *Mocs2*$^{-/-, Ta/Ta}$ or *Mocs2*$^{-/-, Ta/-}$ (knockout mouse model corresponding to the *Mocs2b* isoform). Although ten breeding pairs were established, they have never given rise to living offspring. In most cases pregnancy finished with spontaneous abortion for unknown reason. In few cases, females had to be sacrificed due to delivery complications. For these reason this line was excluded from further experiments.
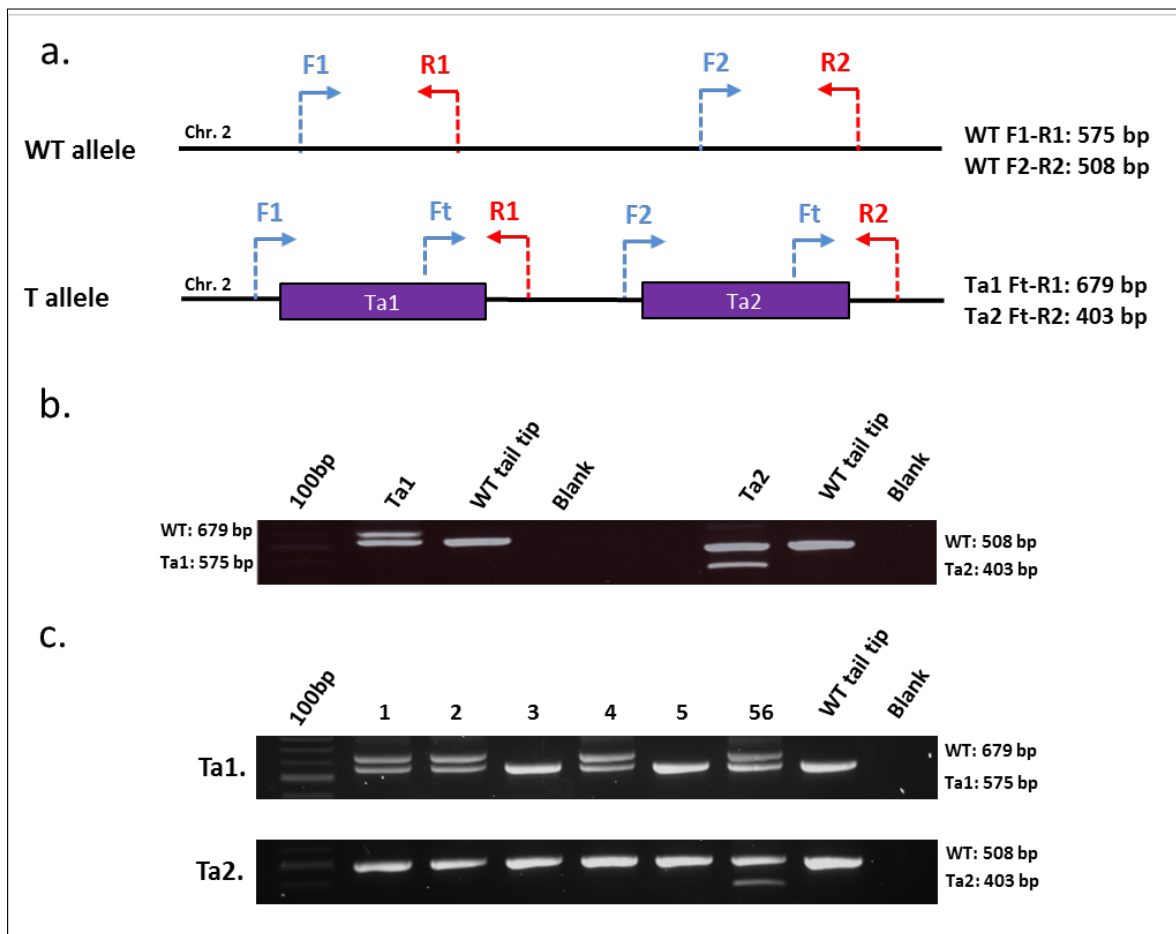
Fig. 3.32. The *MOCS2A* transgene Ta1 presented in the MOCS2A5 line is transmitted to the F1 generation. **(a)** Schematic representation of the strategy used for the identification of transgenic alleles *MOCS2* Ta1 and Ta2. **(b)** PCR results showing the integration of both transgenes (Ta1 and Ta2) in the genome of the founder mouse #56, and **(c)** segregation of the transgenes in the F1 generation. The arrows depict the localisation and the direction of primers used for genotyping PCR. (100bp = 100 bp DNA ladder; F1 = Mouse#56_T1F; R1 = Mouse#56_T1R; F2 = Mouse#56_T2F; R2 = Mouse#56_T2R; Ft= TransgeneA_F; Blank = negative control w/o DNA).
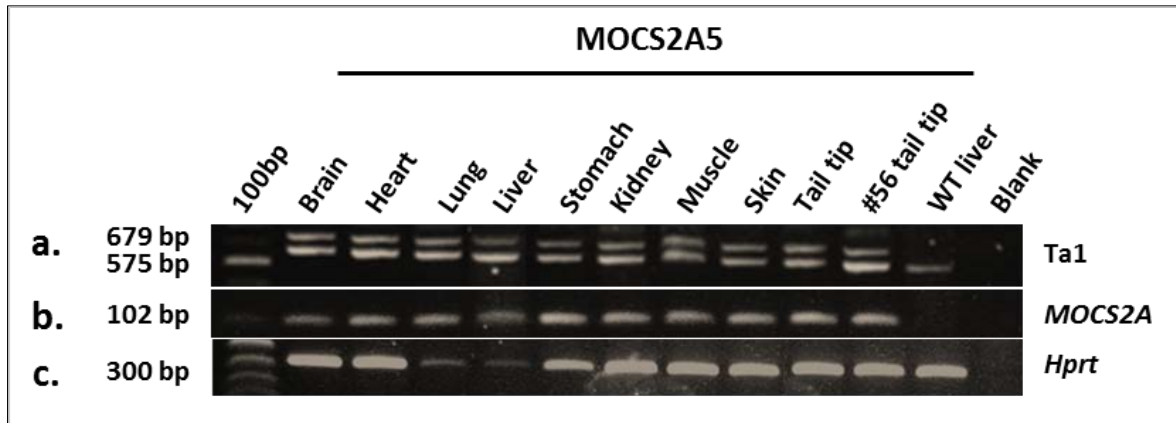
Fig. 3.33. The *MOCS2A* transgene Ta1 is present and expressed in each tissue of mice from the MOCS2A5 line. (a) Genotyping PCR results demonstrate the presence of the *MOCS2A* transgene Ta1 in all tissues investigated in mice from the F1 generation. A DNA sample derived from the tail of the *MOCS2A* founder mouse #56 was used as a positive control. **(b)** RT-PCR analyses demonstrated the expression of the human *MOCS2A* transcript in different tissues derived from a mouse of the F1 generation. A cDNA sample derived from the tail of the *MOCS2A* founder mouse #56 was used as a positive control. **(c)** PCR analysis of the housekeeping gene *Hprt* was performed as a control for cDNA quality. (100bp = 100 bp DNA ladder).
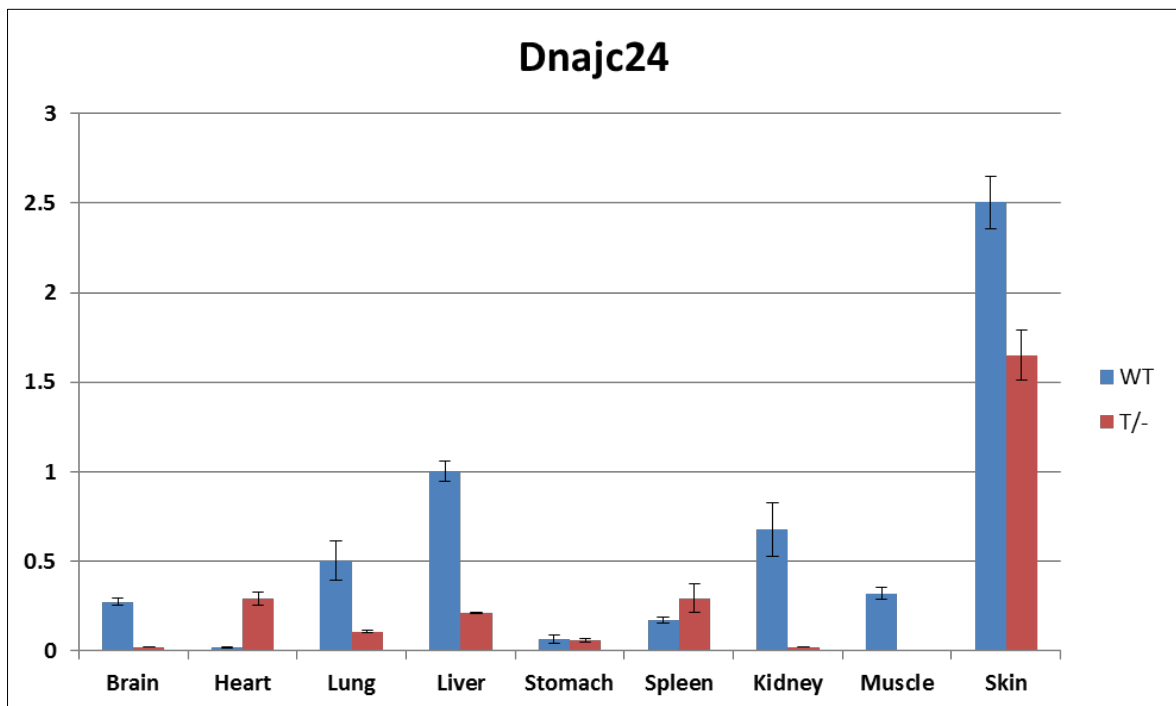
Fig. 3.34. Integration of the *MOCS2A* transgene impaired the expression of the *Dnajc24* host gene in several tissues. qRT-PCR experiments revealed reduced expression of the *Dnajc24* gene in several tissues of *MOCS2A* transgenic mice (*MOCS2A*$^{Ta/-}$) compared to WT tissues. The results were normalised to *Gapdh* expression, and are presented as a relative value to the *Dnajc24* expression level in the liver of a WT mouse. Values and associated error bars represent mean ± s.d. (n = 3).

In the second *MOCS2A* transgenic line (A6) the integration site of *MOCS2A* transgene was localised by employing a genome walker assay. By using this approach a single integration site of the *MOCS2A* transgene could be identified on murine chromosome 6 (NCBI chr6: 44712888) and no other gene is localised in this chromosomal region. **Figure 3.35a** represents the strategy used for the identification of *MOCS2A* transgene integration by genotyping PCR. For this reason the following primers were used: Mouse#44_F, TransgeneA_R and Mouse#44_R. Subsequently, the *MOCS2A* transgene integration could be shown in all tissues of founder animal #44. Moreover, the *MOCS2A* transgene was transmitted to the offspring, as PCR products with the right size were also detected in pups of the F1 generation (**Fig. 3.35b**). Heterozygous transgenic $MOCS2A^{Ta/-}$ mice were bred with heterozygous knockout $Mocs2^{+/-}$ mice to generate $Mocs2^{+/-,\ Ta/-}$ mice, which were further bred to each other. Using this breeding strategy, mice with the following genotypes were obtained: $Mocs2^{+/-,\ Ta/Ta}$, $Mocs2^{+/-,\ Ta/-}$, $Mocs2^{-/-,\ Ta/Ta}$, and $Mocs2^{+/+,\ -/-}$ (**Fig. 3.36**). All animals were healthy and appeared normally developed, but in comparison to the transgenic MOCS2A5 mouse line these mice did not express the *MOCS2A* transgene (**Fig. 3.37**). RT-PCR analyses with primers qMOCS2AEx1a_F and qMOCS2AEx2_R showed strong RT-PCR bands corresponding to the *MOCS2A* product only in tissues of founder animal #56, whereas *MOCS2A* expression could not be detected in tissues derived from founder animal #44 as well as in its progeny. Following the RT-PCR experiments, these results were confirmed by qRT-PCR analyses with the following primers: qMOCS2AEx1a_F and qMOCS2AEx2_R (**Fig. 3.37c**), therefore, the MOCS2A6 mouse line was excluded from further experiments.
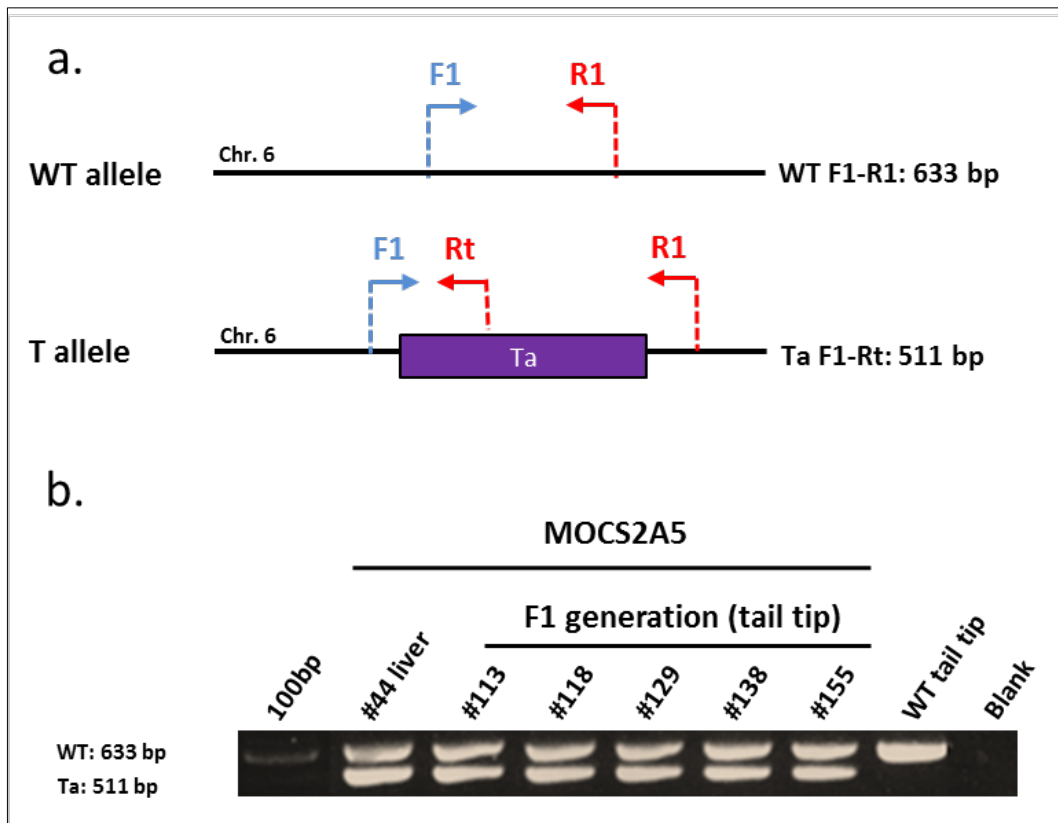
Fig. 3.35. The MOCS2A6 mouse line contained only one copy of the *MOCS2A* transgene. **(a)** Schematic representation of the strategy used for the identification of the *MOCS2A* transgene in mice from the MOCS2A6 mouse line. **(b)** Results of genotyping PCR with primers F1, R1 and Rt showed the presence of the *MOCS2A* transgene (Ta) in different tissues of founder animal #44 as well as its germline transmission to the progeny. Genomic DNA from tail tips of wild type (WT) mice was used as a negative control. The arrows illustrate the localisation and the direction of primers used for genotyping PCR. (100bp = 100 bp DNA ladder; F1 = Mouse#44_F; R1 = Mouse#44_R; Rt = TransgeneA_R; Blank = negative control w/o DNA).
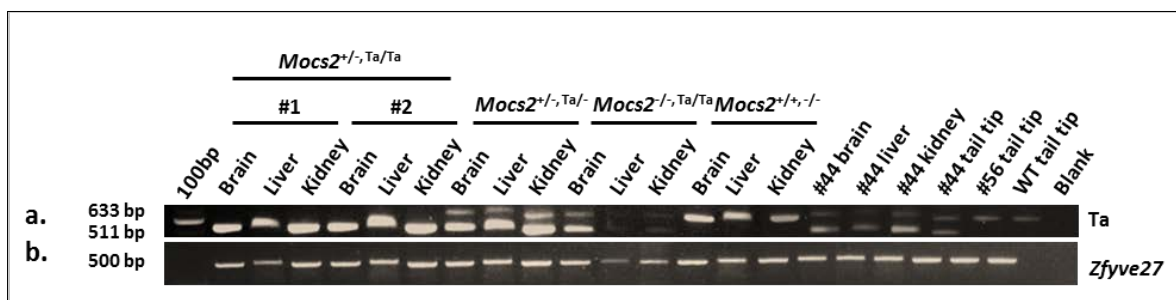
Fig. 3.36. The *MOCS2A* transgene Ta presented in the MOCS2A6 line is transmitted to the F1-generation. **(a)** Genotyping PCR results from different tissues demonstrating the presence of MOCS2A transgene or the wild type allele (WT) in pups derived from the breeding of *Mocs2*$^{+/-, Ta/-}$ mice. **(b)** PCR analyses specific for the murine *Zfyve27* gene was used as a quality control of extracted DNA samples. Genomic DNA samples from founder #44 and #56 were used as an internal control. (100bp = 100 bp DNA ladder; Blank = negative control w/o DNA).
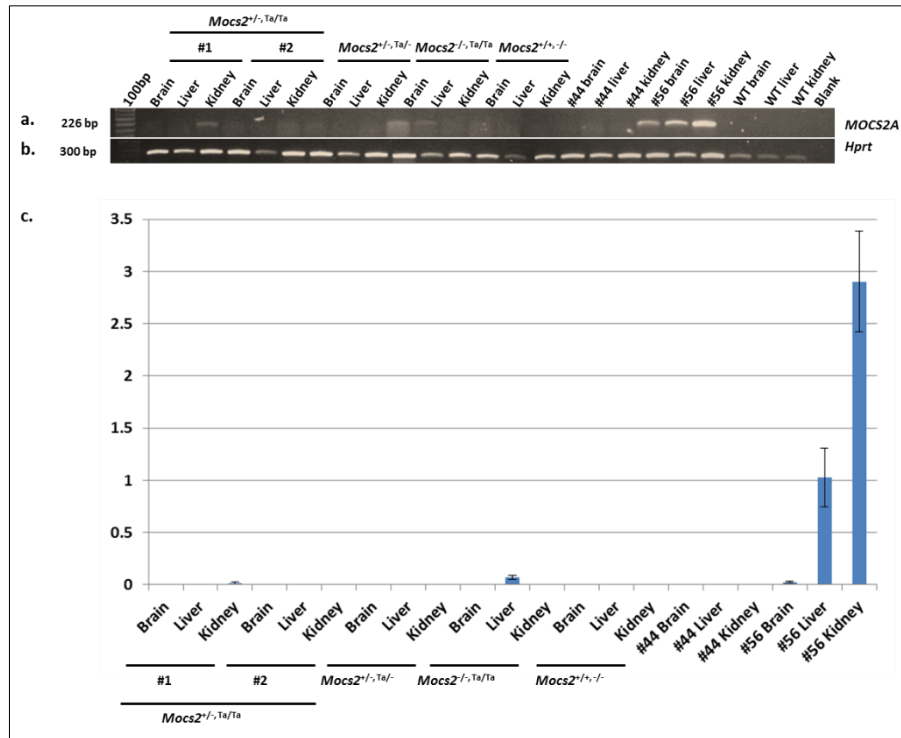
Fig. 3.37. Expression analyses of the *MOCS2A* transgene in different tissues of the MOCS2A5 mouse line.

(a) RT-PCR analyses demonstrating that the *MOCS2A* transgene was not expressed in tissues derived from founder animal #44 and its progeny compared to *MOCS2A* transgene expression observed in founder animal #56. **(b)** RT-PCR analyses for the murine housekeeping gene *Hprt* served as a quality control of synthesised cDNA. (100bp = 100 bp DNA ladder; Blank = negative control w/o DNA). **(c)** The results of qRT-PCR experiments confirmed the lack of *MOCS2A* transgene expression in tissues obtained from founder animal #44 and its progeny. The results were normalised to the expression of the murine housekeeping gene *Gapdh*, and are presented as a relative value to the *MOCS2A* transgene expression level in the liver from founder animal #56. Values and associated error bars represent mean ± s.d. (n = 3).

3.1.8 Generation of the *MOCS2B* transgenic mouse line

To generate *MOCS2B* transgenic mice, a pronuclear injection with the linearised pWajaII (Wegner, 2007) construct encoding the human *MOCS2B* gene was performed. The pWajaII construct carries the human *MOCS2B* gene under the control of the *β-actin* promoter **(Fig. 3.38a)**. Prior to injection, the pWajaII construct was linearised by *Xma*I digestion and purified **(Fig. 3.38b)**. Pronuclear injection of the pWajaII construct into mouse fertilised oocytes was performed in collaboration with Dr. Ursula Fünfschilling (MPI of Experimental Medicine, Göttingen).
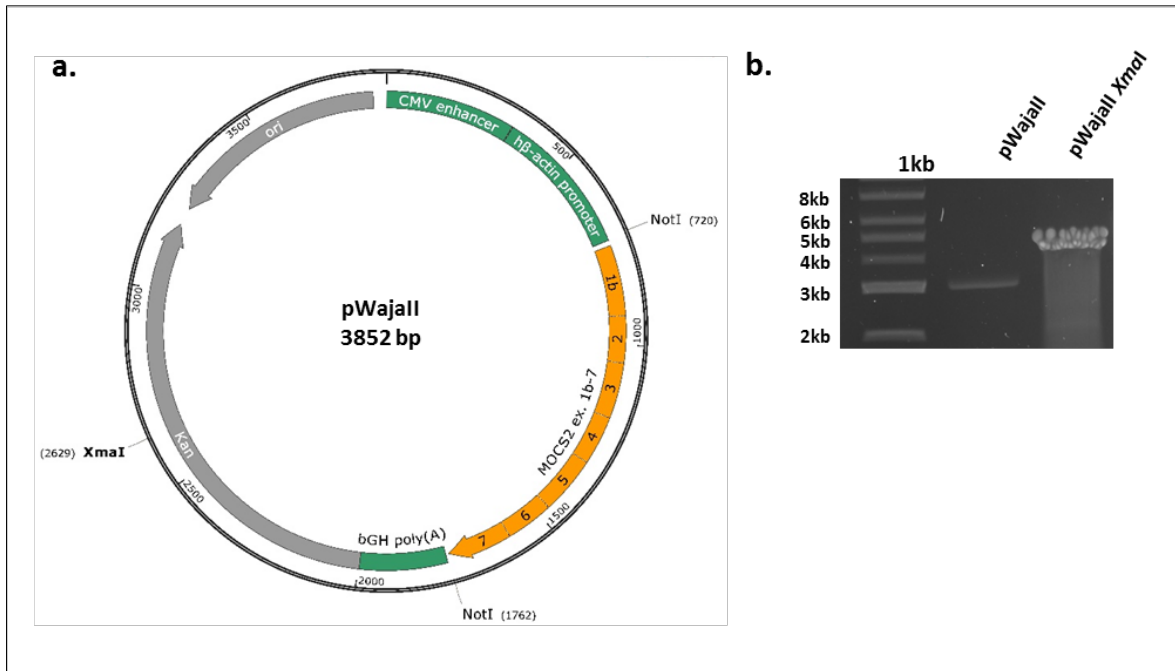
Fig. 3.38. Preparation of the *MOCS2B* transgene construct. (a) Schematic representation of the pWajaII vector showing the human *MOCS2B* ORF under the control of the *Cytomegalovirus* (CMV) enhancer and *β-actin* promoter followed by a bovine growth hormone polyadenylation signal (bGH polyA), the kanamycin (Kan) resistance gene and the origin of replication (Ori). **(b)** Agarose gel electrophoresis revealed bands specific for the undigested and digested pWajaII plasmid. Band 4.5 kb corresponds to the linearised plasmid after *Xma*I digestion.

To identify potential founder animals carrying the *MOCS2B* transgene genotyping PCR analyse with *MOCS2B*-specific primers qMOCS2BEx5_F and qMOCS2BEx6_R was performed **(Fig. 3.39a)**. In 5 out of 25 animals the *MOCS2B* transgene was observed **(Fig. 3.39b)**. In order to estimate the number of *MOCS2B* transgene copies in the respective founder animals, qPCR experiments were done with *MOCS2B* transgene-specific primers qMOCS2BEx5_F and qMOCS2BEx6_R. The qPCR results indicated that two copies of the *MOCS2B* transgene integrated into the genome of each founder animal **(Fig. 3.40).**
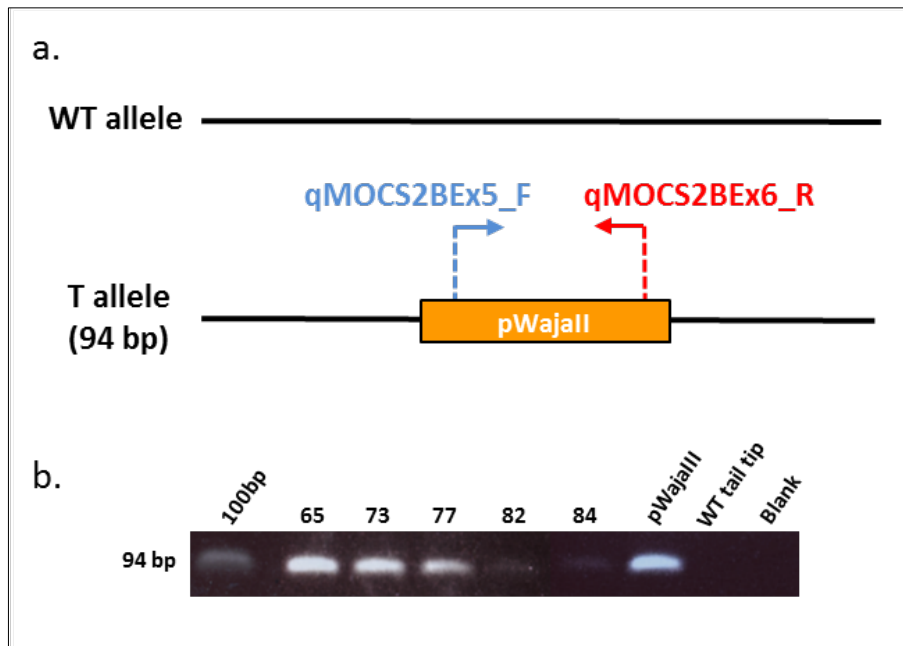
Fig. 3.39. Detection of the *MOCS2B* transgene in putative founder animals. (a) Schematic representation of the strategy used for the identification of founder animals. **(b)** Results of the genotyping PCR (94 bp) revealed five animals presenting the *MOCS2A* transgene. Results of the genotyping PCR for negative pups are not shown. The arrows indicate the localisation and the direction of primers used for genotyping PCR. (100bp = 100 bp DNA ladder; F = forward; R = reverse; Blank = negative control w/o DNA).
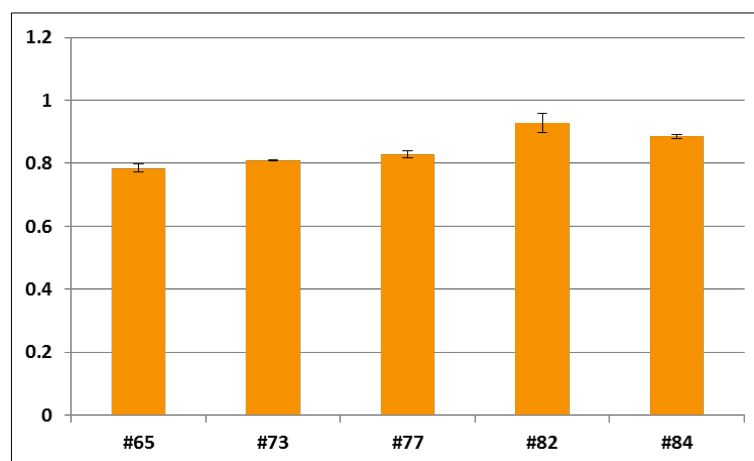
Fig. 3.40. Copy number evaluation of the *MOCS2B* transgene in founder animals. Bar graphs showing the results of qPCR analysis indicated that all investigated animals carried 2 copies of the *MOCS2B* transgene. The results obtained from the *MOCS2B* transgene were normalised against a murine single copy gene, namely *acrosin* (*Acr*) and are presented as a relative value to another single copy gene, named pelota (*Pelo*). Values and associated error bars represent mean ± s.d. (n = 3).

To exclude that the integration of the human *MOCS2B* transgene into the murine genome did not influence the expression of a murine gene in the vicinity of the integration site,

the *MOCS2B* transgene integration site was localised in founder animal #84 using the genome walker assay. In contradiction to the obtained qPCR results, only one integration site on mouse chromosome 5 could be identified (NCBI ch5: 139888374-139888100) and to date no other mouse gene was described in this chromosomal region. To establish a transgenic *MOCS2B* mouse line, founder animal #84 was crossed with C57BL/6N wild type mice. Genotyping PCR experiments of mice from the F1 generation with Mouse#84_F, Mouse#84_R and TransgeneB_F **(Fig. 3.41a)** demonstrated germline transmission of the *MOCS2B* transgene **(Fig. 3.41b)**. Heterozygous transgenic mice ($MOCS2B^{Tb/-}$) were healthy, fertile and gave rise to homozygous $MOCS2B^{Tb/Tb}$ animals with the predicted Mendelian ratio after breeding with $MOCS2B^{Tb/-}$ mice (data not shown). Thus, the transgenic MOCS2B4 mouse line could be established. Furthermore, expression of the human *MOCS2B* transgene was confirmed by RT-PCR experiments using human *MOCS2B*-specific primers Nest.hum.F1Ex3 and Nest.hum.R1Ex6 **(Fig. 3.42),** or by Western blot analysis with the human MOCS2B-specific antibody EP113635 **(Fig. 3.43)**.
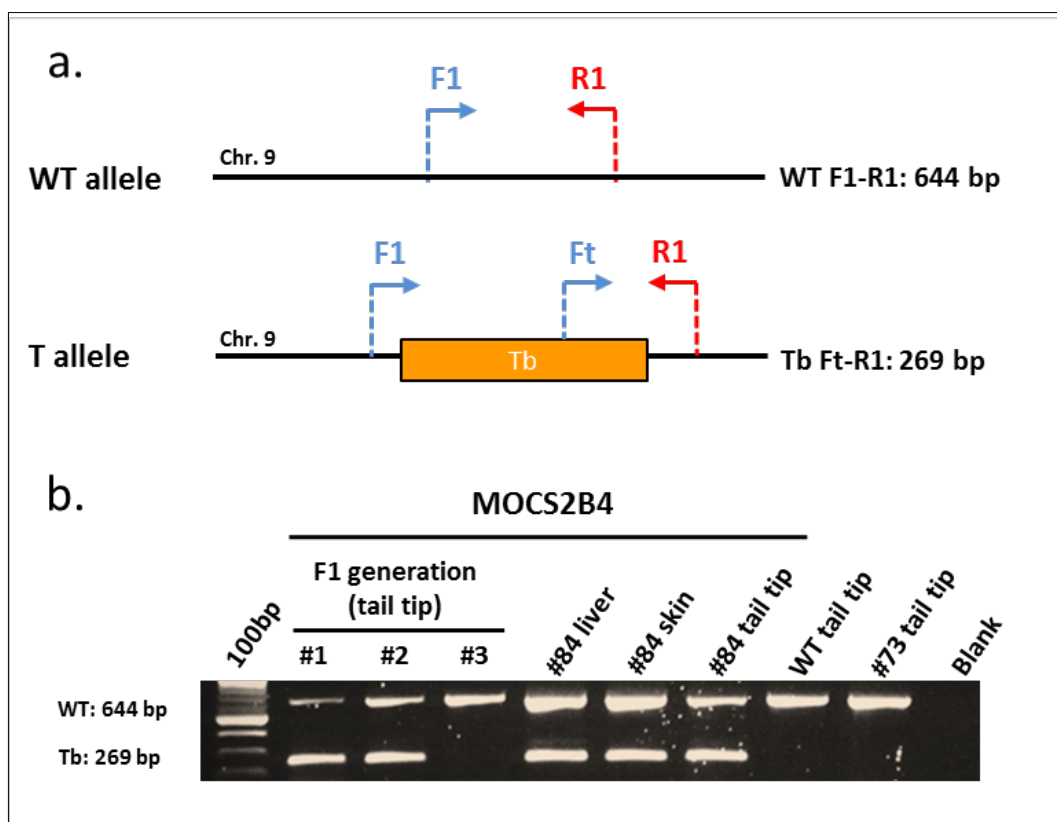
Fig. 3.41. The MOCS2B4 mouse line contained only one copy of the *MOCS2B* transgene. **(a)** Schematic representation of the strategy used for the identification of the *MOCS2B* transgene in mice from the

MOCS2B4 mouse line. **(b)** Results of genotyping PCR with primers F1, R1 and Rt showed the presence of the *MOCS2B* transgene (Tb) in different tissues of founder animal #84 as well as its germline transmission to the progeny (#1-3). Genomic DNA from tail tips of wild type (WT) and founder #73 mice was used as a negative control. The arrows illustrate the localisation and the direction of primers used for genotyping PCR. (100bp = 100 bp DNA ladder; F1 = Mouse#84_F; R1 = Mouse#84_R; Rt = TransgeneB_F; Blank = negative control w/o DNA).
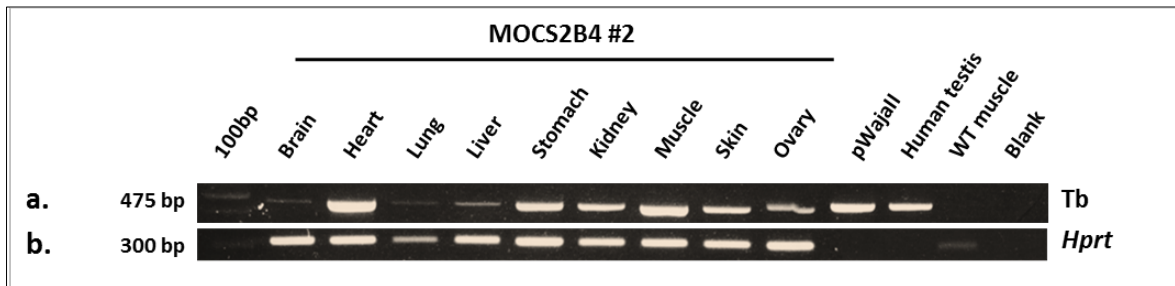
Fig. 3.42. The *MOCS2B* transgene (Tb) is expressed in each tissue of mice from the MOCS2B4 line. (a) RT-PCR analyses demonstrated the expression of the human *MOCS2B* transcript in different tissues derived from a mouse of the F1 generation. A pWajaII construct and cDNA sample derived from human testis was used as a positive control. A cDNA sample derived from mouse muscle served as a negative control. **(b)** PCR analysis of the murine housekeeping gene *Hprt* was performed as a control for cDNA quality. (100bp = 100 bp DNA ladder).
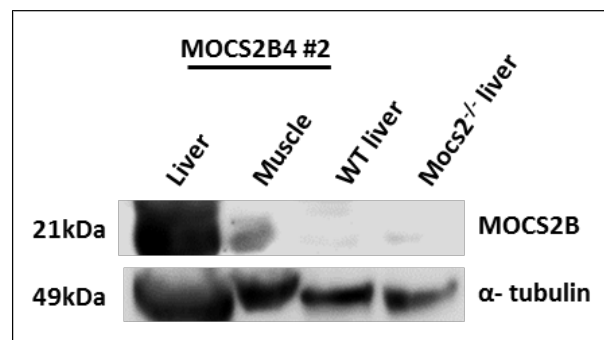
Fig. 3.43. Expression of the human *MOCS2B* transgene in tissues of the transgenic MOCS2B4 mouse. To analyse MOCS2B protein expression in different tissues of the transgenic MOCS2B4 mouse, whole proteins were isolated from liver and muscle, and subjected to Western blot analyses using a specific antibody against human MOCS2B. In the liver and muscle derived from MOCS2B4 #2 mouse a MOCS2B-specific signal of 21 kDa could be observed. Proteins extracted from livers of wild type (WT) or *Mocs2*$^{-/-}$ mice were loaded as a negative control. The anti α-tubulin antibody was used as a protein loading control.

In order to generate an isolated *Mocs2a* knockout mouse model, heterozygous transgenic *MOCS2B*$^{Tb/-}$ mice were bred with heterozygous *Mocs2*$^{+/-}$ mice to obtain *Mocs2*$^{+/-, Tb/-}$ mice which were further bred with each other to obtain *Mocs2*$^{-/-, Tb/-}$ (corresponding to a

knockout mouse model for the *Mocs2a* isoform). Similar to *Mocs2*^{-/-} offspring, *Mocs2*[-/-, Tb/-] (= *Mocs2a* knockout) pups died within the first 8 days after birth manifesting a related phenotype, i.e. *Mocs2*[-/-, Tb/-] mice exhibited a general poor health condition, curly whiskers and bladder obstructions (data not shown). In contrast to *Mocs2*^{-/-} mice, *Mocs2*[-/-, Tb/-] mice showed a significantly improved increase in body weight postnatally **(Fig. 3.44)**, however, it was still significantly lower than weight gain of WT animals. Additionally, *Mocs2*[-/-, Tb/-] mice extended their mean life span to 5.9 days, as most of them died between day 5 and 8 after birth **(Fig. 3.45)**.
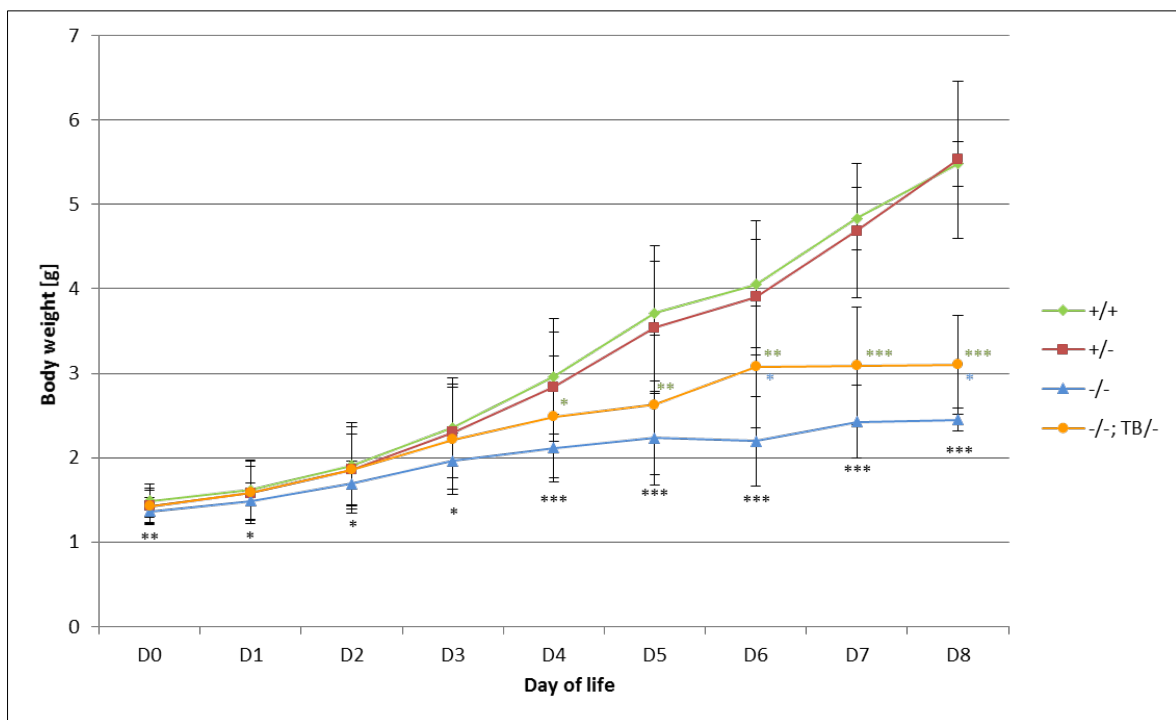
Fig. 3.44. Gain of weight of *Mocs2*[-/-, Tb/-] mice after birth. *Mocs2*[-/-, Tb/-] expressing the human *MOCS2B* transgene presented a significantly improved gain in weight postnatally as compared to *Mocs2*^{-/-} mice. Line graphs showing the body weight of WT (green, +/+), *Mocs2*^{+/-} (red, +/-), *Mocs2*[-/-, Tb/-] (orange, -/- Tb/-) and *Mocs2*^{-/-} (blue, -/-). Body weight and associated error bars representing mean ± s.d. (n = 35 for WT, n = 60 for *Mocs2*^{+/-}, n = 34 for *Mocs2*^{-/-} and n = 12 for *Mocs2*[-/-, Tb/-] pups). * p<0.05, ** p<0.01, *** p<0.001. Black stars indicate significant differences between WT and *Mocs2*^{-/-} mice, green stars showed the significance between WT and *Mocs2*[-/-, Tb/-] and blue stars represent significance between *Mocs2*[-/-, Tb/-] and *Mocs2*^{-/-}.
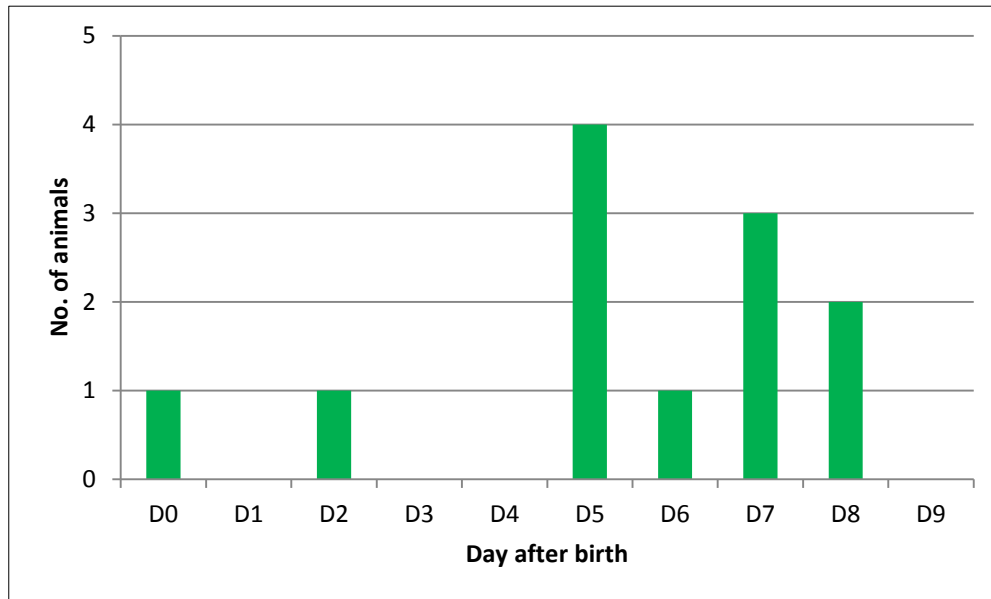
Fig. 3.45. Life span of *Mocs2*^{-/-, Tb/-} mice. Bar graphs represents the life span of *Mocs2*$^{-/-,\,Tb/-}$ mice. In total, 12 *Mocs2*$^{-/-,\,Tb/-}$ mice were investigated. All of them died within 8 days after birth with a critical time point between postnatal day 5 and 8 (83%), (n = 12).

3.1.9　　　　Rescue of the *Mocs2* knockout phenotype by supplementation with the transgenes encoding MOCS2A and MOCS2B proteins

In order to rescue the *Mocs2*$^{-/-}$ phenotype, both *Mocs2* subunits (human MOCS2A and MOCS2B) were supplemented by crossing *Mocs2*$^{+/-}$ animals with both transgenic MOCS2A5 and MOCS2B4 mice **(Fig. 3.46)**. Although the *MOCS2A* transgene was known to impair the expression of murine *Dnajc24* gene, heterozygous *MOCS2A*$^{Ta/-}$ animals were viable and expressed the *MOCS2A* transgene **(see Fig. 3.33)**. For this reason *MOCS2*$^{+/-,\,Ta/-}$ were bred with *MOCS2*$^{+/-,\,Tb/-}$ animals, however no offspring were obtained.
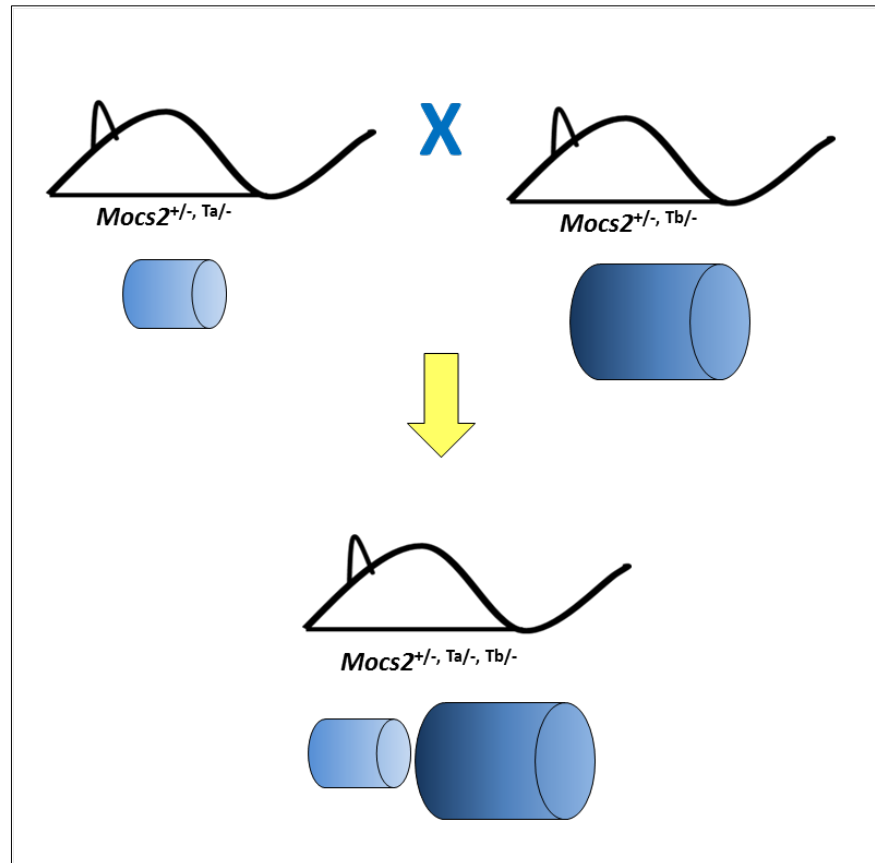
Fig. 3.46. Gene therapy approach designed for *Mocs2* knockout mice. Schematic representation of the mating strategy to rescue the phenotype of *Mocs2*$^{-/-}$ mice by complementation of the *Mocs2* gene with both *Mocs2* subunits expressed by the transgenic animals MOCS2A$^{Ta/-}$ and MOCS2B$^{Tb/-}$.

3.2 Gene therapy approach for molybdenum cofactor deficiency, supplementation group B

3.2.1 Generation of MOCS2B recombinant adeno-associated viruses (rAAVs)

Recombinant adeno-associated viruses (rAAVs) are currently among the most frequently used viral vectors for gene therapy approaches (Daya and Berns, 2008). The generation of rAAV serotype 2/8 was performed in collaboration with Prof. A. Auricchio (Telethon Institute of Genetics and Medicine, TIGEM, Italy). Briefly, the open reading frame (ORF) of the human *MOCS2B* gene was cloned into the pAAV2.1TBGeGFP3 plasmid (kindly provided by TIGEM, Italy). The pAAV2.1TBGeGFP3 plasmid contains the liver-specific *Thyroxine binding globulin* (*TBG*) promoter followed by a multiple cloning site, an eGFP reporter gene, and a polyA signal flanked by inverted terminal repeats (ITRs) **(Fig. 3.47).** The ORF of the human *MOCS2B* gene was amplified from a human cDNA library with two different pairs of *MOCS2B* gene-specific primers: F_NotIEx3, R_NotIEx7, or F_NotIEx3, R_

NotISTOPEx7 **(Fig. 3.48a)**. The first primer pair amplified the *MOCS2B* ORF, deprived of the stop codon in exon 7, while the second pair of primers amplified the complete *MOCS2B* transcript including the stop codon. *MOCS2B* and *MOCS2B*-STOP PCR products were cloned into the pGEMT-easy vector, transformed into DH5α competent *E.coli* and checked for the correct sequence, respectively. Furthermore, both inserts and the pAAV2.1TBGeGFP3 backbone plasmid were digested with the restriction enzyme *Not*I and ligated together **(Fig. 3.48b)**. The correct orientation of the inserts for *MOCS2B* and *MOCS2B-STOP* was confirmed by digestion with the restriction enzymes *Nde*I and *BamH*I, respectively **(Fig. 3.48c)**. Finally, both pAAV2.1TBG-MOCS2B-eGFP3 and pAAV2.1TBG-MOCS2B-STOP-eGFP3 constructs were purified and sent to TIGEM where they were used for the production of viral particles. In **Figure 3.48d** the structure of the final vectors pAAV2.1TBG-MOCS2B-eGFP3 and pAAV2.1TBG-MOCS2B-STOP-eGFP3 is represented. This cloning strategy let us to produce two types of viruses, encoding either the MOCS2B-eGFP fusion protein or only the MOCS2B protein.
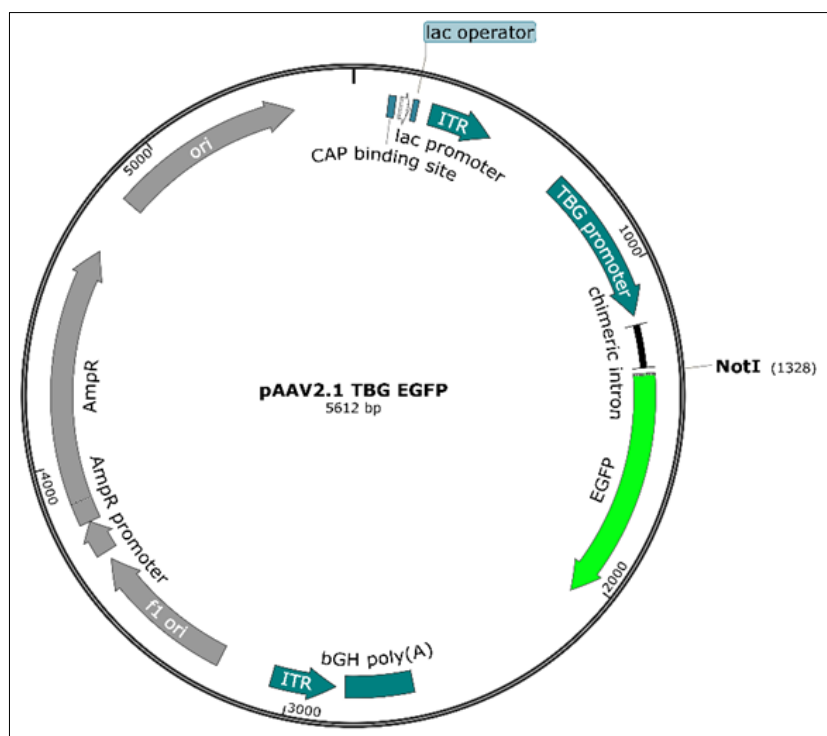
Fig. 3.47. Map of pAAV2.1TBGeGFP3 backbone vector. The pAAV2.1TBGeGFP3 vector contains Inverted Terminal Repeats (ITRs) flanking the *Thyroxine binding globulin* (TBG) promoter, followed by chimeric intron, eGFP and bovine growth hormone polyadenylation (bGH polyA) signal. The *Not*I restriction site is localised between the chimeric intron and eGFP sequence. (ori = origin of replication).
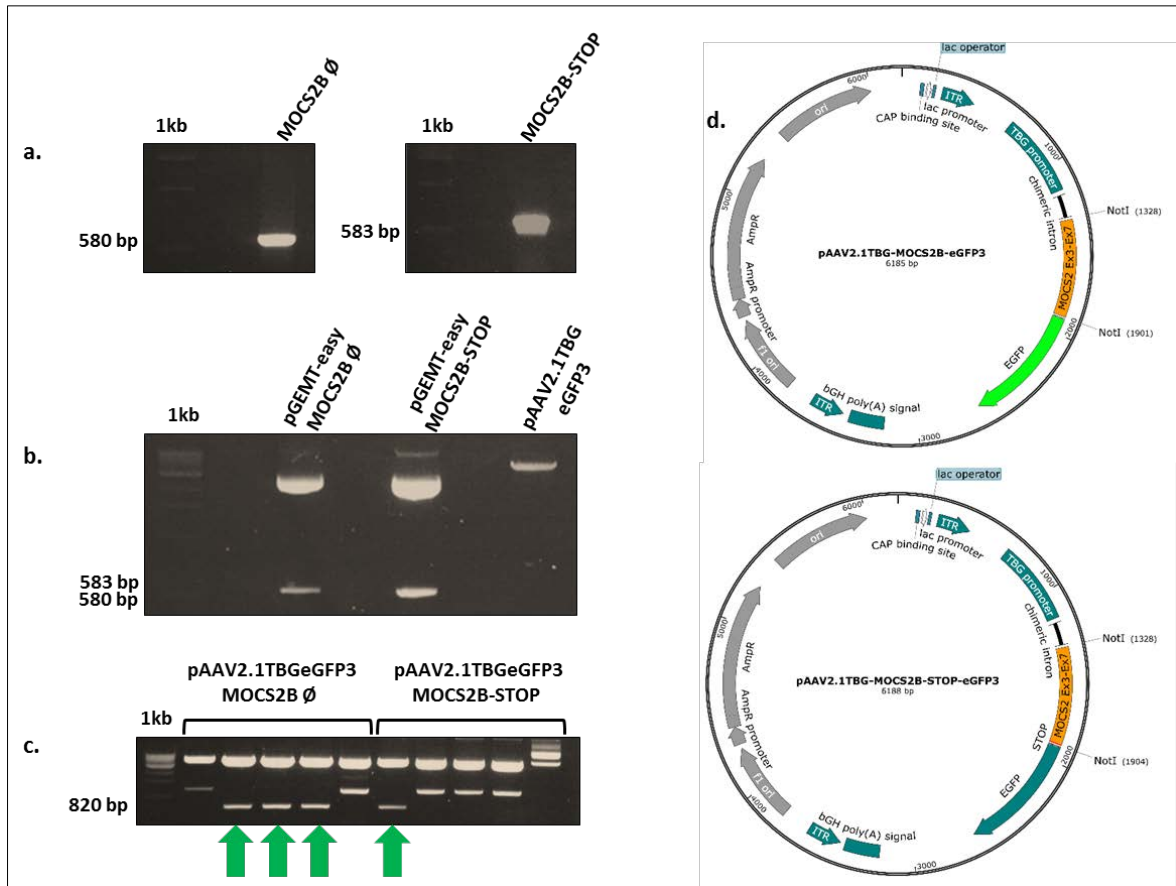
Fig. 3.48. Cloning of *MOCS2B* and *MOCS2B*-STOP into the pAAV2.1TBGeGFP3 backbone vector. (a) Agarose gel electrophoresis image showing PCR products of both human *MOCS2B* transcripts. Left panel presenting the 580 bp PCR product of *MOCS2B* transcript without the STOP codon (MOCS2B Ø), the right panel showing the 583 bp PCR product of the *MOCS2B* transcript with the STOP codon (MOCS2B-STOP). **(b)** Agarose gel electrophoresis image of cloned MOCS2B Ø and MOCS2B-STOP inserts and the pAAV2.1TBGeGFP3 backbone vector after *Not*I digestion. Restriction analyses revealed correct sizes of the MOCS2B (580 bp) and MOCS2B-STOP (583 bp) inserts, respectively, and the linearised backbone vector (5612 bp). **(c)** Agarose gel electrophoresis image of MOCS2B and MOCS2B-STOP inserts after cloning into the pAAV2.1TBGeGFP3 vector and *Nde*I, *BamH*I double digestion. To verify the correct orientation of cloned MOCS2B and MOCS2B-STOP sequences, inserts were cut out from the pAAV2.1TBGeGFP3 vector with *Nde*I, *BamH*I double digestion. Expected bands were: 5612 bp for the pAAV2.1TBGeGFP3 vector; 820 bp for the correctly orientated MOCS2B insert and 823 bp for the correctly orientated MOCS2B-STOP insert. Three positive clones for pAAV2.1TBG-MOCS2B-eGFP3 and one positive clone for pAAV2.1TBG-MOCS2B-STOP-eGFP3 were obtained (arrows indicate positive clones). **(d)** Schematic representation of the pAAV2.1TBG-MOCS2B-eGFP3 and pAAV2.1TBG-MOCS2B-STOP-eGFP3 plasmids encoding the MOCS2B-eGFP fusion protein (upper), and the MOCS2B protein (lower), respectively. (1kb = 1kb DNA plus ladder).

105

To check the functionality of generated constructs, human hepatocellular carcinoma cells (HepG2) were transfected with the pAAV2.1TBG-MOCS2B-eGFP3. Although the efficiency of transfection was very poor, eGFP-positive HepG2 cells have been found **(Fig. 3.49)**.
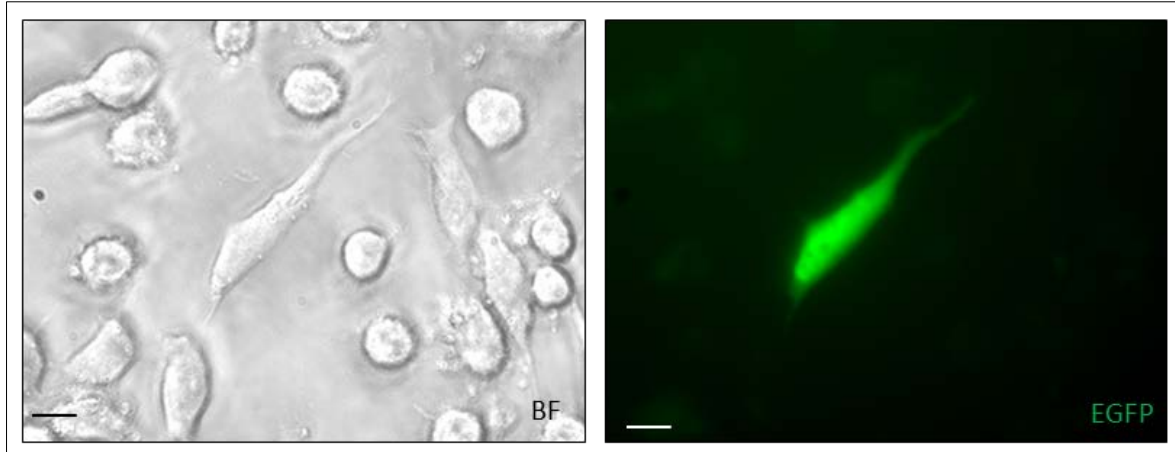
Fig. 3.49. TBG promoter-driven expression of the MOCS2B-eGFP fusion protein in HepG2 cells. HepG2 cells transfected with the pAAV2.1TBG-MOCS2B-eGFP3 vector presented an eGFP signal. Scale bars correspond to 10 μm. (BF = Bright field).

The production of recombinant adeno-associated virus required three different plasmids. Besides the plasmid encoding the therapeutic protein, a plasmid carrying the AAV2 Rep-Cap genes and a helper plasmid are involved. All three plasmids had to be co-transfected. After expression of Rep and Cap proteins, the ITR flanked transgene cassette was replicated, and the single-stranded DNA molecules were encapsulated. Thereafter, viral particles were harvested, purified and titred (AAV 1461 rAAV2/8TBG-MOCS2B-eGFP3 = $2,5\times10^{12}$ genome copies (GC)/ml, and AAV1460 rAAV2/8TBG-MOCS2B-STOP-eGFP3 = $4,6\times10^{12}$ GC/ml). To confirm that the rAAV was able to infect hepatocytes *in vivo*, intrahepatic (n = 2) or intraperitoneal injections (n = 2) with either 1×10^{10} GC of AAV1460 rAAV2/8TBG-MOCS2B-STOP-eGFP3 or with PBS as a control (n = 2) were performed in wild type mice. Nested PCR analysis using *MOCS2B*-specific primers nest.humF1_Ex3 and nest.hum.R1_Ex6 followed by a PCR with humF2_Ex3 and nest.hum.R2_Ex3 revealed the presence of AAV-delivered *MOCS2B* DNA into the liver, independent on the injection technique **(Fig. 3.50)**. However, at the RNA level, RT-PCR analyses showed *MOCS2B* expression only after intrahepatic injection **(Fig. 3.51)**.
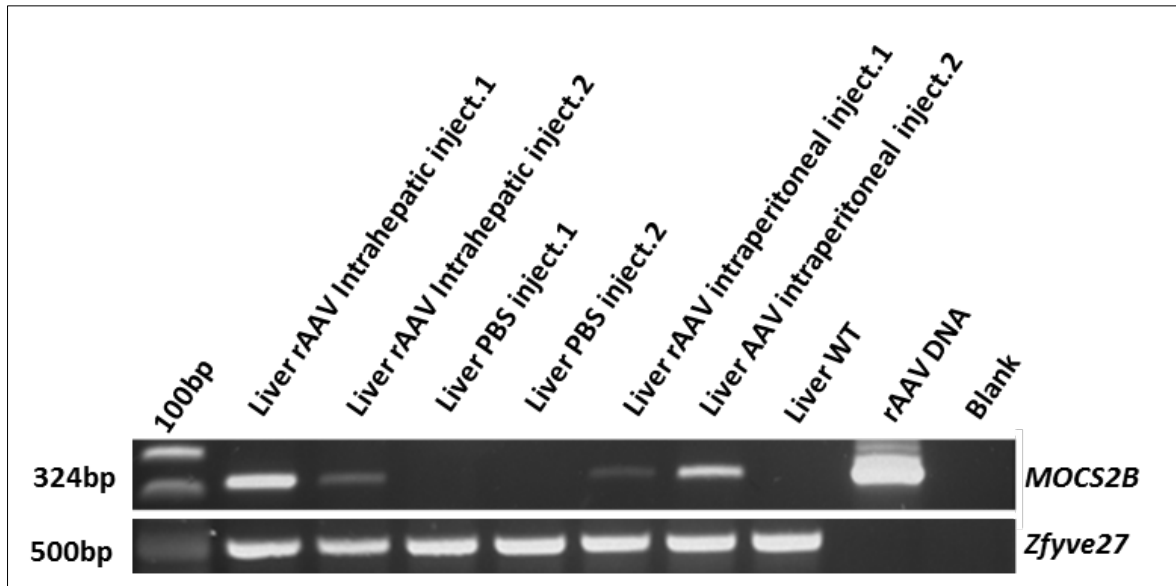
Fig. 3.50. Infection ability of rAAV 1460 (rAAV2/8TBG-MOCS2B-STOP-eGFP). (Upper panel) Agarose gel electrophoresis image of nested PCR experiments showing the presence of the *MOCS2B* transgene in the livers of wild type mice after intrahepatic or intraperitoneal injection with rAAV2/8TBG-MOCS2B-STOP-eGFP regardless of the type of injection. **(Lower panel)** PCR analyses specific for the murine *Zfyve27* gene was used as a quality control of extracted DNA samples from livers after intrahepatic or intraperitoneal injection with AAV or PBS, respectively. (100bp = 100 bp DNA ladder; Blank = negative control w/o DNA).
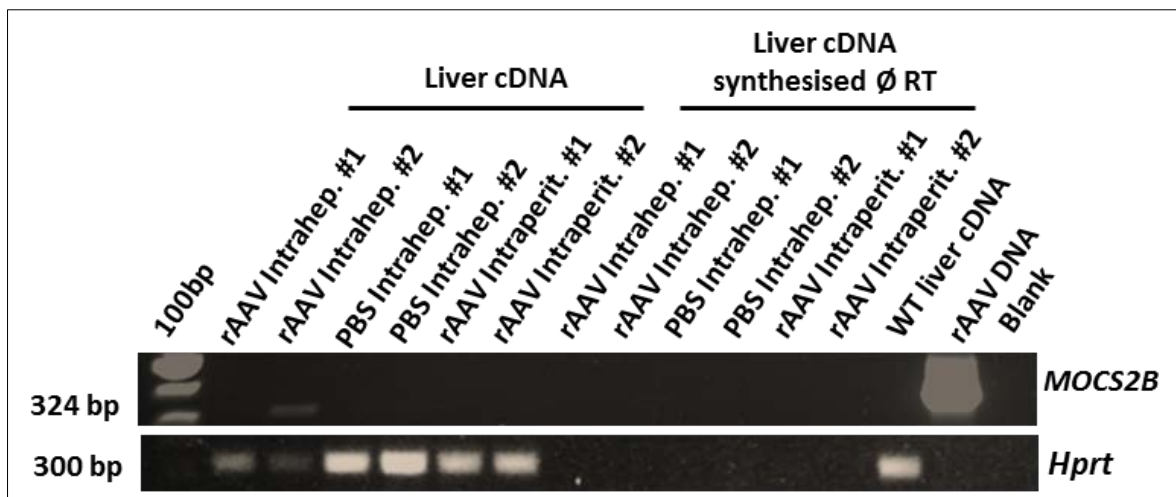
Fig. 3.51. Efficiency of *MOCS2B* expression after different routes of rAAV2/8TBG-MOCS2B-STOP-eGFP infections. RT-PCR analysis showed that *MOCS2B* is transcribed in the liver only after intrahepatic injection. PCR products amplified from cDNA synthesised without reverse transcriptase (Ø RT) served as a negative control. (100bp = 100 bp DNA ladder; Blank = negative control w/o cDNA).

To visualise the expression of the MOCS2B protein after viral infection *in vivo*, immunohistochemical analyses were performed. For this reason, wild type newborn pups

were injected intrahepatically with rAAV2/8TBG-MOCS2B-eGFP3 as well as with rAAV2/8TBG-MOCS2B-STOP-eGFP3 viruses, and 11 days after injection staining of liver sections were performed with a EP113635 MOCS2B-specific antibody. The results showed that hepatocytes transduced with the rAAV2/8TBG-MOCS2B-STOP-eGFP3 virus presented a cytoplasmic expression of the MOCS2B protein, while hepatocytes transduced with rAAV2/8TBG-MOCS2B-eGFP3 demonstrated a co-localisation of both MOCS2B as well as the MOCS2B-EGFP signal **(Fig. 3.52)**.
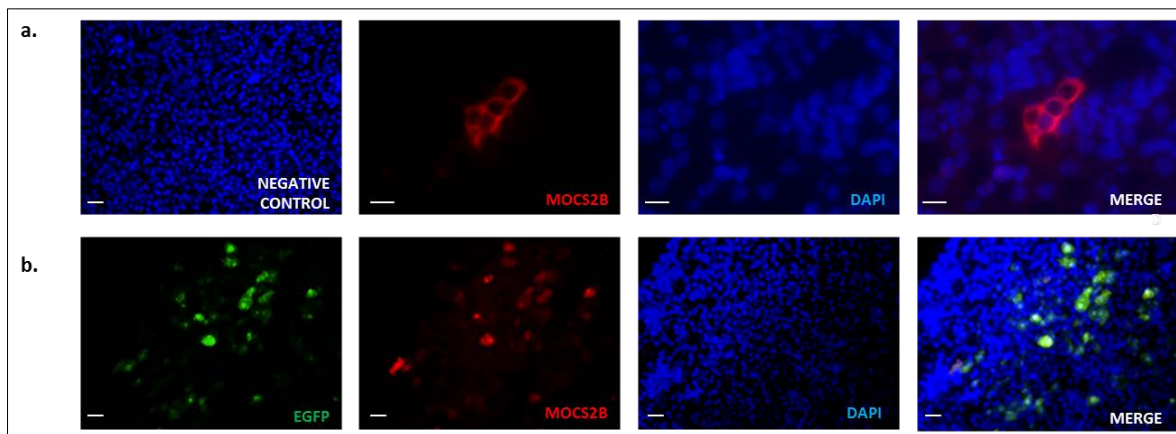
Fig. 3.52. Immunohistochemical analysis of mouse hepatocytes transduced either with the rAAV2/8TBG-MOCS2B-STOP-eGFP3 virus or with the rAAV2/8TBG-MOCS2B-EGFP virus. (a) After antibody staining the MOCS2B protein was shown to be expressed in the cytoplasm of hepatocytes after transduction with the rAAV2/8TBG-MOCS2B-STOP-eGFP. Non-injected livers from wild type mice served as a negative control. **(b)** MOCS2B expression co-localised with MOCS2B-EGFP fusion proteins after transduction with rAAV2/8TBG-MOCS2B-eGFP3. Scale bars correspond to 20 μm for the negative control and the lower panel, and to 10μm for the upper panel.

In order to study if intrahepatic injections could lead to infection of other tissues, wild type mice were injected with 1×10^{10} GC of AAV1460 rAAV2/8TBG-MOCS2B-STOP-eGFP3 or with PBS as a control. One week after injection, genomic DNA from several tissue samples was extracted and analysed by PCR using *MOCS2B*-specific primers F2nest.hum.F2Ex3 and R2nest.hum.R2Ex3 primers. PCR products specific for the *MOCS2B* transgene were detected in all tissues investigated except in the brain, however, *MOCS2B* was not present in DNA samples extracted from tissues of mice injected with PBS **(Fig. 3.53)**.
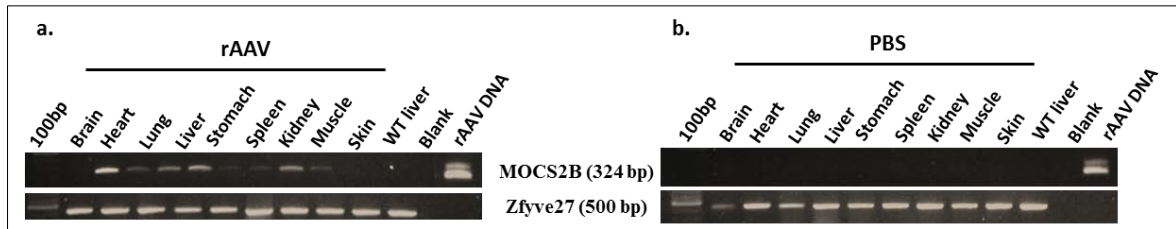
Fig. 3.53. Characterisation of rAAV (1460AAV2/8TBGMOCS2B-STOP-eGFP3) tropism. (a) *MOCS2B*-specific PCR products were detected in almost all tissues of rAAV2/8TBG-MOCS2B-STOP-eGFP (rAAV) injected mice except in the brain. **(b**) In contrast, in tissues of mice injected with PBS *MOCS2B*-specific PCR products were not observed. DNA extracted from 1460AAV2/8TBGMOCS2B-STOP-eGFP3 virus (rAAV DNA) was used as a positive control. **(Lower panels)** PCR analyses specific for the murine *Zfyve27* gene was used as a quality control of extracted DNA samples from different tissues of mice injected either with rAAV2/8TBG-MOCS2B-STOP-eGFP (rAAV) or with PBS (negative control). (100bp = 100 bp DNA ladder; Blank = negative control w/o DNA).

To examine the expression profile of human MOCS2B-EGFP fusion protein, wild type mice were injected with pAAV2/8TBG-MOCS2B-eGFP3 virus. To increase the efficiency of viral transduction animals received two intrahepatic injections with 1×10^{10} GC and 4×10^{10} GC, respectively. The first injection was applied at the day of birth, and the second injection at postnatal day 6. Mice were anesthetised 11 days or 6 months after the second injection and following perfusion, tissues from both animals were fixed and objected to cryosectioning. In both cases MOCS2B-EGFP signals were detected exclusively in liver sections **(Fig 3.54)**. At this stage we were in the position to conclude that intrahepatic injection with pAAV2/8TBG-MOCS2B-eGFP3 causes co-infection of other tissues, however, MOCS2B-EGFP expression was restricted exclusively to the liver.

a.
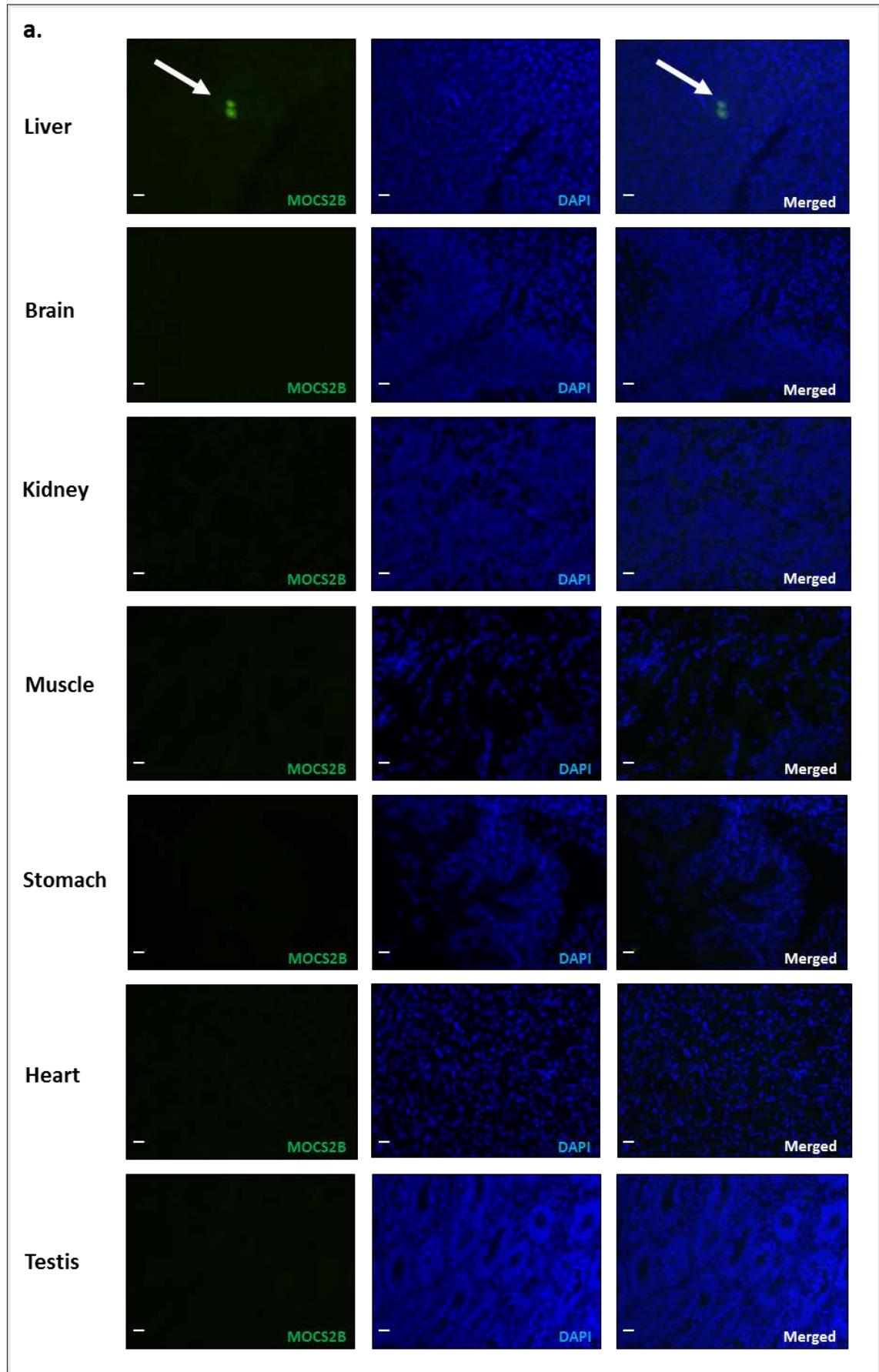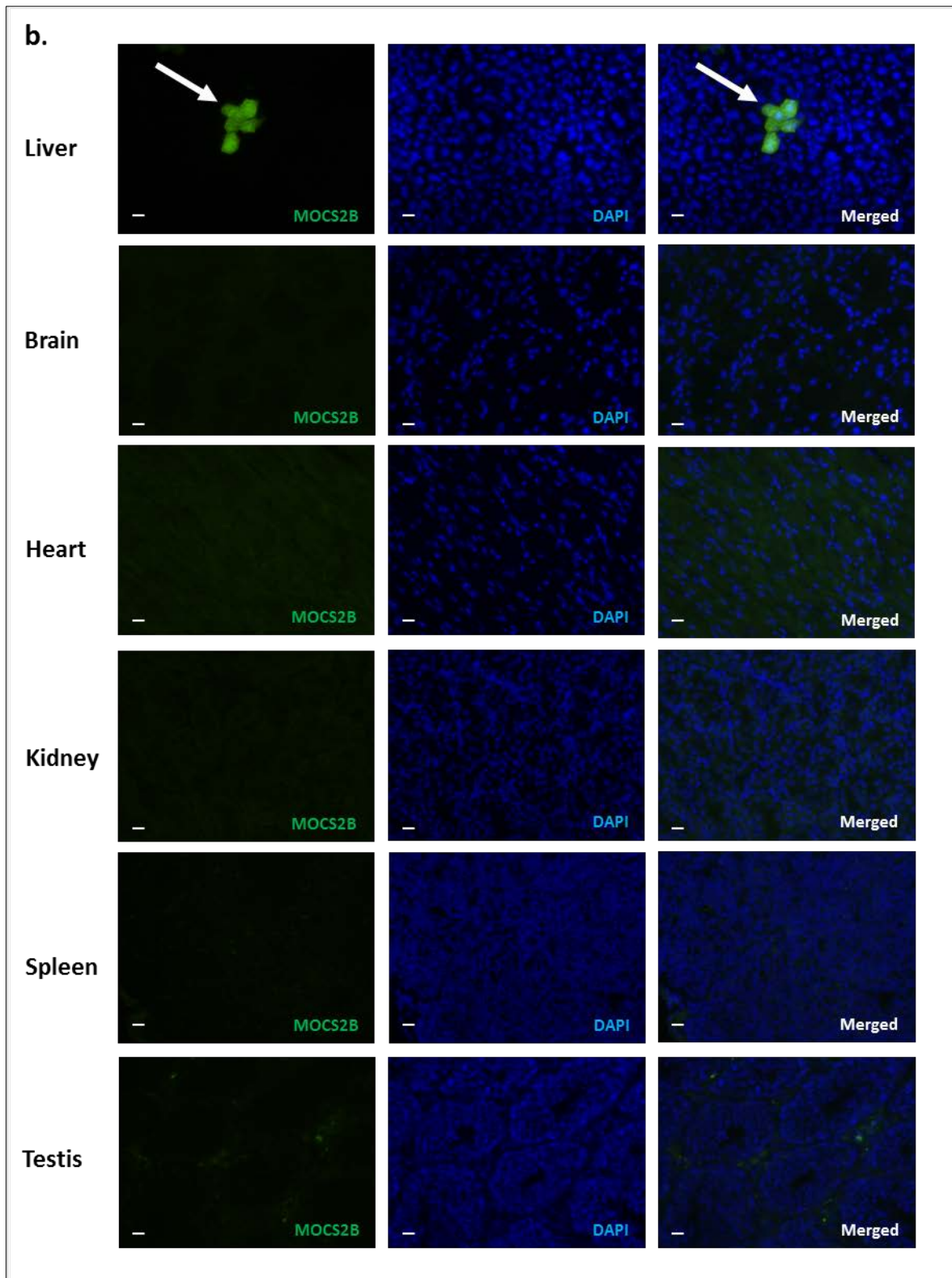
Fig. 3.54. Visualisation of MOCS2B-EGFP expression after injection with pAAV2/8TBG-MOCS2B-eGFP3. Fluorescence images showing the expression of TBG-driven MOCS2B-EGFP in different mouse tissues **(a)** 11 days and **(b)** 6 months after the second intrahepatic injection, respectively. Nuclei were counterstained with DAPI. Scale bars correspond to 20 µm.

3.2.2 Therapeutic potential of rAAV-*MOCS2B*-based gene therapy

In order to investigate the effect of a rAAV-*MOCS2B* gene therapy in homozygous *Mocs2^{-/-}* mice, we performed double intrahepatic injection of Mocs2^{-/-} animals with pAAV2/8TBG-MOCS2B-STOP-eGFP3 (first injection shortly after birth with 1×10^{10} GC in 20 ul PBS, and second injection at postnatal day 6 with 4×10^{10} GC of rAAV in 40 ul PBS). As expected, it did not rescue the phenotype, and the *Mocs2^{-/-}* animals died witin the first 8 days of life. However, in agreement with previous results **(see Fig. 3.44)**, the body weight of treated animals was higher as compared to untreated *Mocs2^{-/-}* pups **(Fig. 3.55)**. Because only three animals were treated with pAAV2/8TBG-MOCS2B-STOP-eGFP3 statistical analysis was not performed.
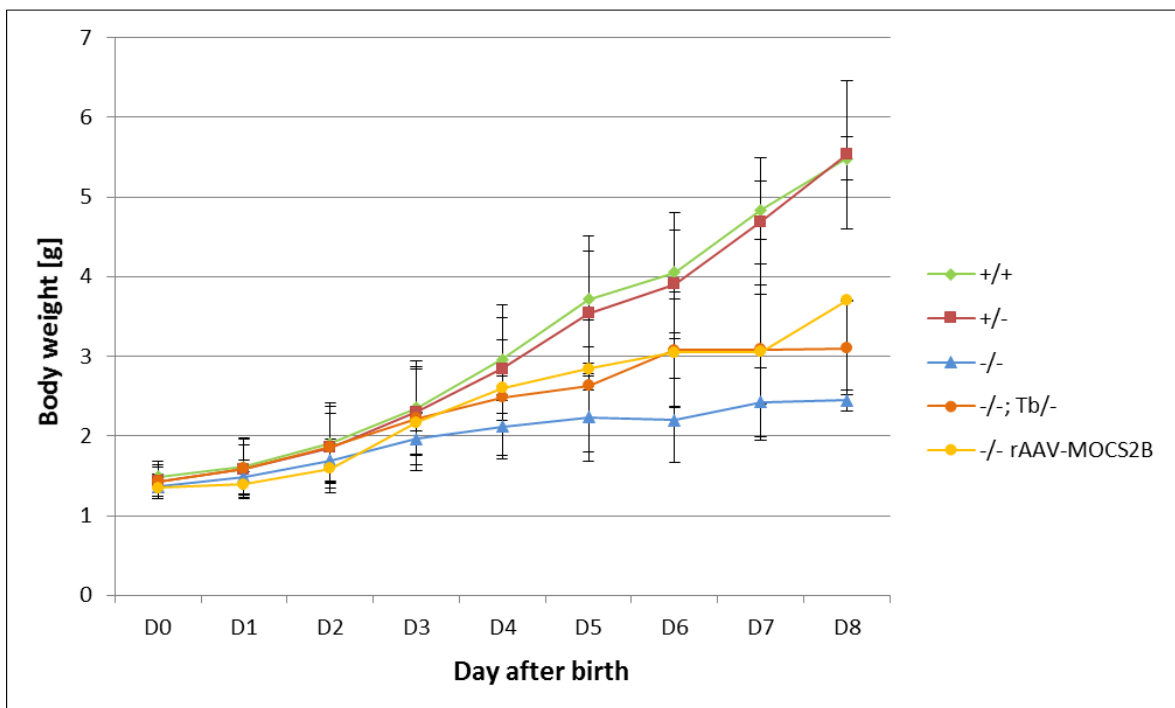
Fig. 3.55. *Mocs2^{-/-}* animals treated with rAAV-MOCS2B have higher body weight in comparison to non-treated *Mocs2^{-/-}* mice. Line graphs showing the body weight of WT (green), *Mocs2^{+/-}* (red), *Mocs2^{-/-}* (blue), *Mocs2^{-/-, Tb/-}* (orange), and *Mocs2^{-/-}* mice treated with rAAV-MOCS2B (yellow). Body weight and associated error bars representing mean ± s.d. (n = 35 for WT, n = 60 for *Mocs2^{+/-}*, n = 34 for *Mocs2^{-/-}*, n = 12 for *Mocs2^{-/-, Tb/-}* pups and n = 3 for *Mocs2^{-/-}* injected with rAAV-*MOCS2B* animals).

3.2.3 Long-term study designed to determine *MOCS2B* overtime expression after injection with rAAV

In the next step, we investigated expression efficiency of the transgene, delivered via rAAV infection. We injected animals at different time points using different amounts of rAAV. To visualise MOCS2B protein expression we used AAV2/8TBG-MOCS2B-eGFP3 which encodes for the fusion MOCS2B-eGFP protein. We divided animals into three groups. The first group (I) obtained single intrahepatic injection at the day of birth with 1×10^{10} GC of rAAV in 20 ul PBS. The second group (II) obtained a single injection at postnatal day 6 with 4×10^{10} GC of rAAV in 40 ul of PBS, and the last group (III) obtained a double injection, i.e. a first injection shortly after birth with 1×10^{10} GC in 20 ul PBS, and a second injection at postnatal day 6 with 4×10^{10} GC of rAAV in 40 ul of PBS. Animals treated in the same way with PBS were used as a negative control. **Table 2** shows an overview of the injection scheme for the long term study experiment.

Tab. 2. Strategy of rAAV injections used for investigation of rAAV gene therapy duration.

INVESTIGATION GROUP	1×10^{10}GC (day of birth)	4×10^{10}GC (day 6 after birth)
I	✓	
II		✓
III	✓	✓

Expression of the fusion protein MOCS2B-eGFP was analysed at different time points: 1 week-, 1 month-, 3 months-, 6 months-, 12 months- and 24 months after injection(s). The animals were anesthetised and perfused. Afterwards, the livers were isolated and fixed before cryosections were established. After nuclei staining, slides were analysed under a fluorescent microscope. The results showed that in all groups the expression of the therapeutic gene persists at least 12 months. Moreover, in the groups which obtained a single injection (at the day of birth or at postnatal day 6) we were able to detect MOCS2B-eGFP expression even 24 months after injections **(Fig. 3.56a, 3.57a and 3.58a)**. Quantitative analysis, evaluating the percentage of MOCS2B-eGFP positive cells, showed

the highest number of infected hepatocytes one week after the 1st injection. There were approximately 6.5% of all liver cells infected, however, one month after injection the number of eGFP-positive cells decreased to 2% **(Fig. 3.56b)**. In the two other groups, the number of eGFP-positive cells was approximately 2% **(Fig. 3.57b and 3.58b)**.
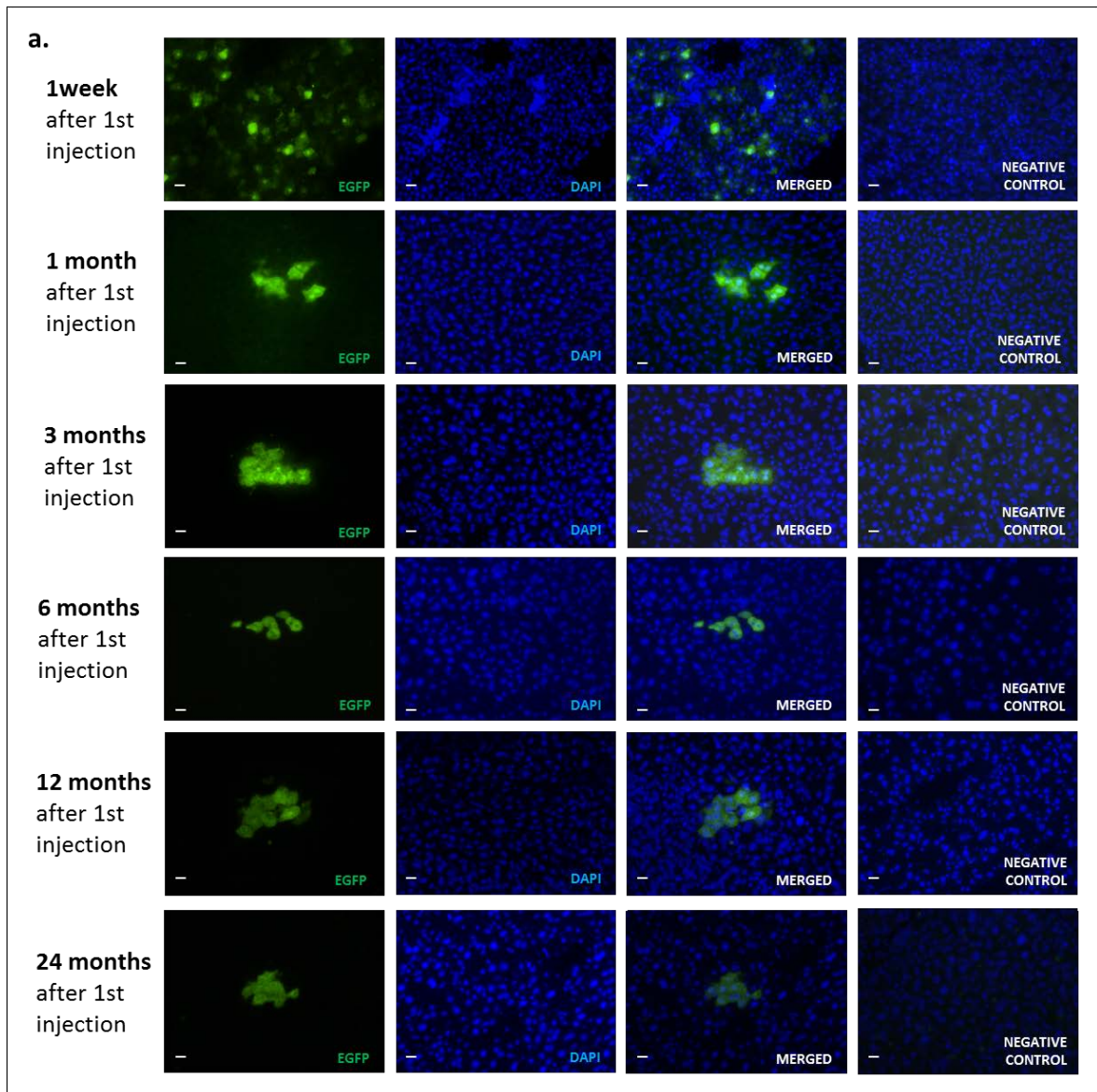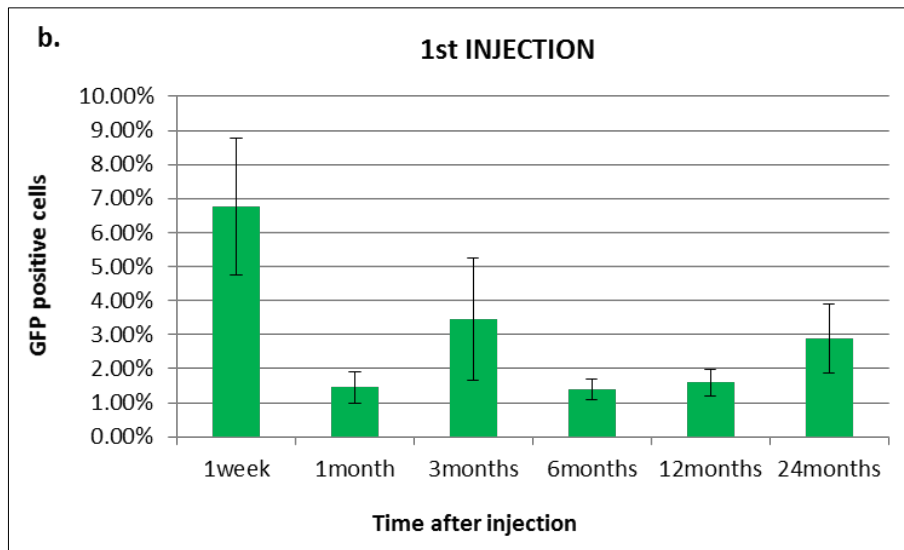
Fig 3.56. eGFP expression analysis at different time points after injection at the day of birth with 1×10^{10} GC of rAAV MOCS2B-eGFP in 20 ul PBS. (a) Fluorescent images showing eGFP expression after single injection at the day of birth. Liver sections from animals treated with PBS serve as a negative control. **(b)** Bar graphs showing the number of eGFP positive cells were normalised to the total number of liver cells. Values and associated error bars represent mean ± s.d. (n = 1).

a.

1 week after 2nd injection

1 month after 2nd injection

3 months after 2nd injection

6 months after 2nd injection

12 months after 2nd injection

24 months after 2nd injection
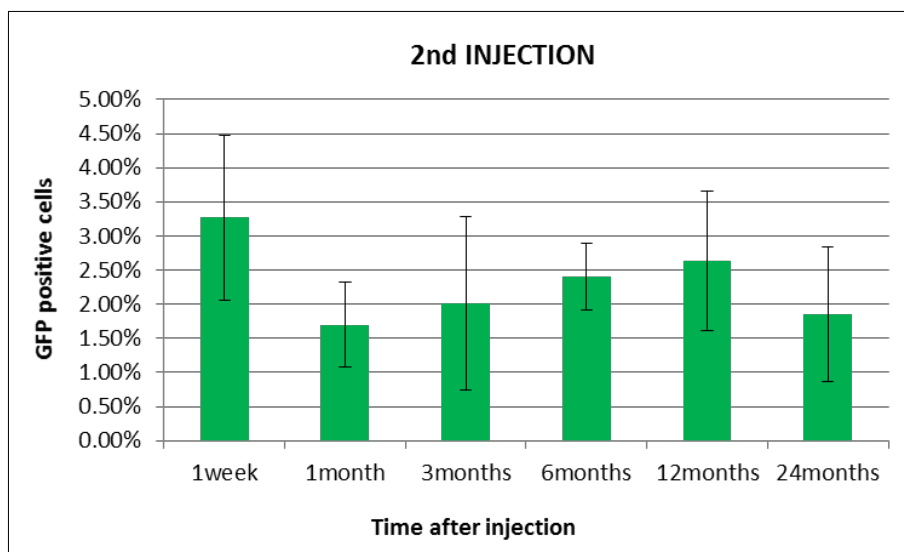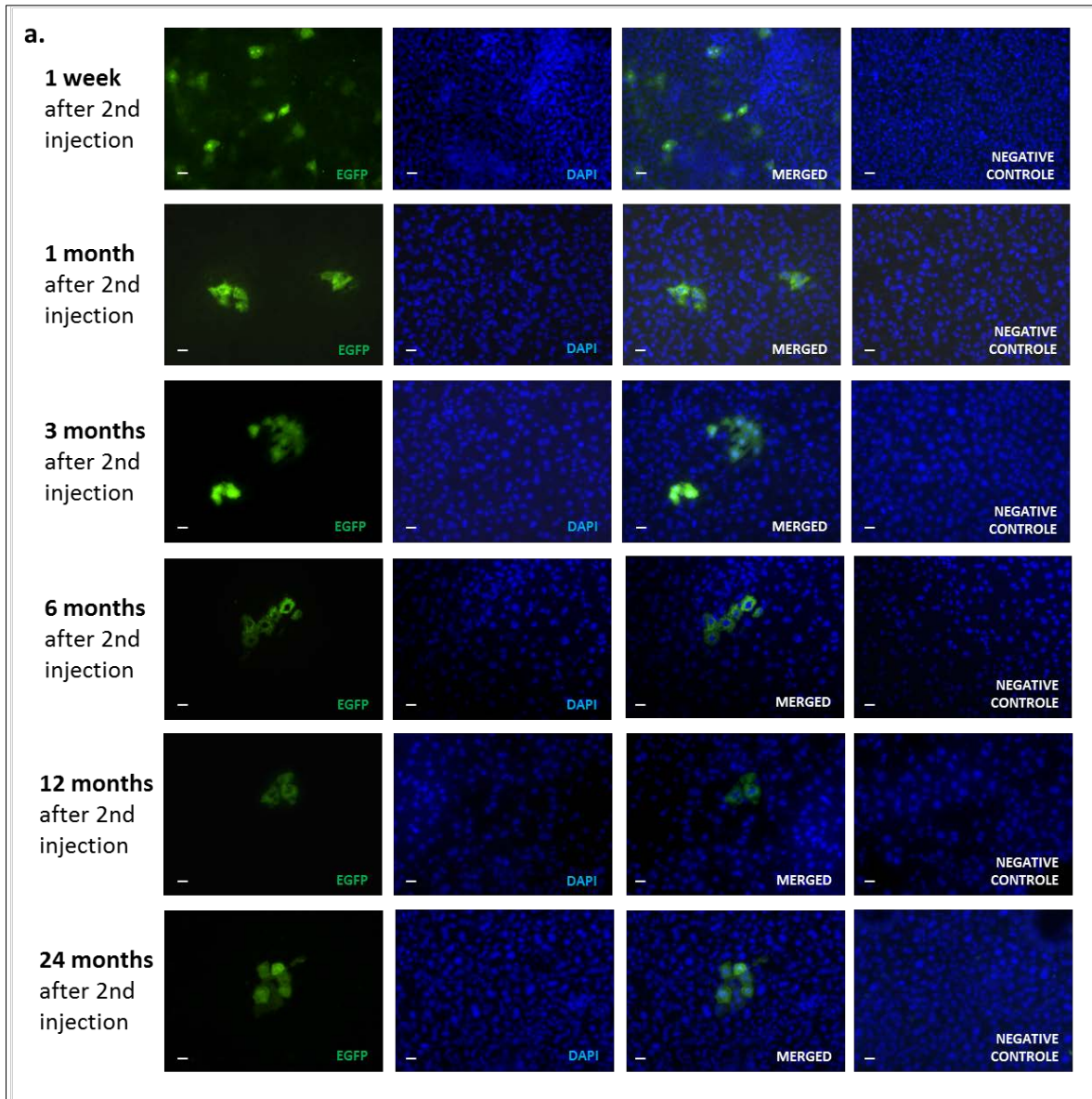
Fig. 3.57. eGFP expression analysis at different time points after injection at day 6 after birth with 4×10^{10} **GC of rAAV MOCS2B-eGFP in 40 ul PBS. (a)** Fluorescent images showing eGFP expression after single injection at postnatal day 6. Liver sections from animals treated with PBS served as a negative control. **(b)** Bar graphs showing the number of eGFP positive cells were normalised to the total number of liver cells. Values and associated error bars represent mean ± s.d. (n = 1).
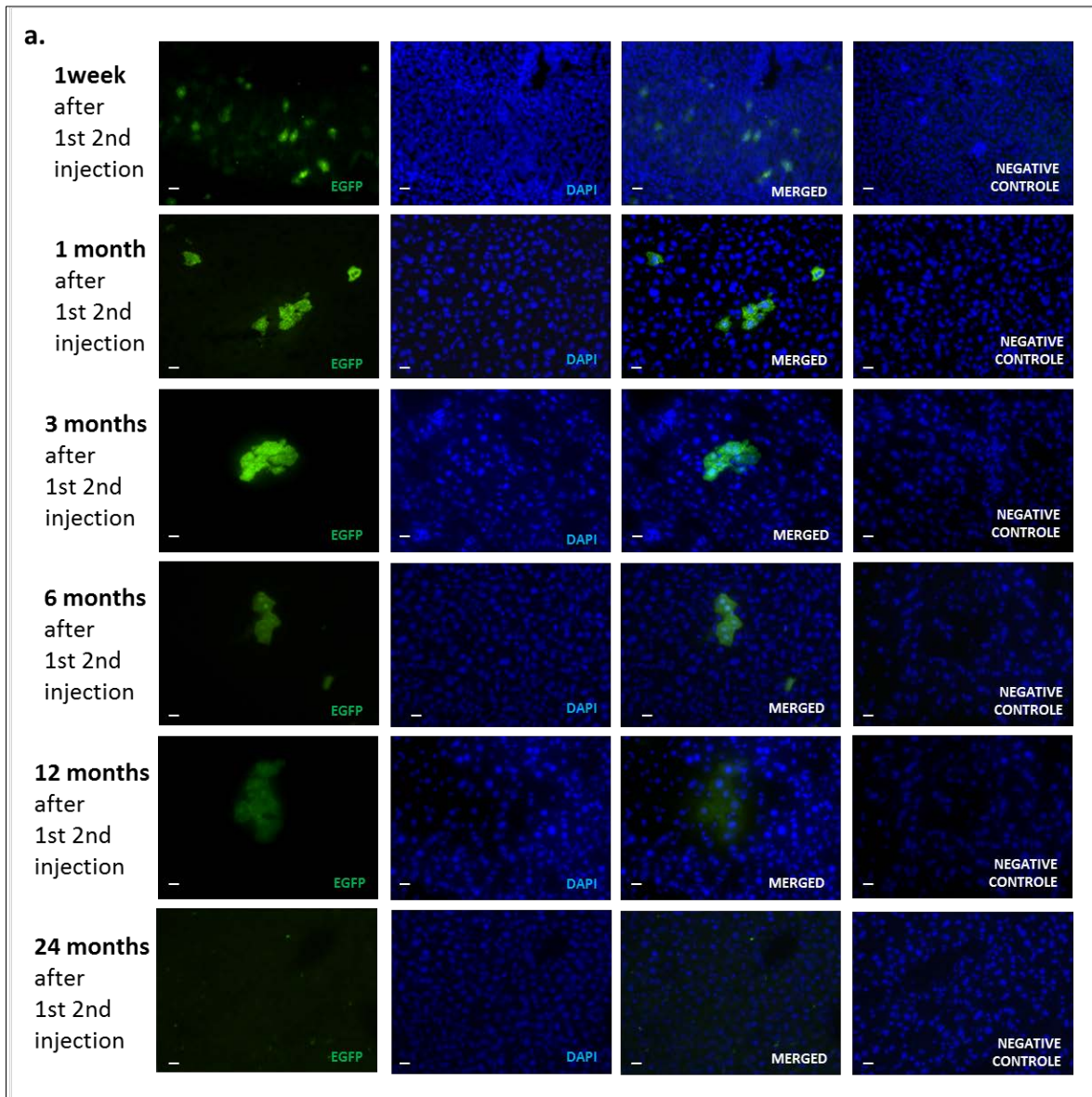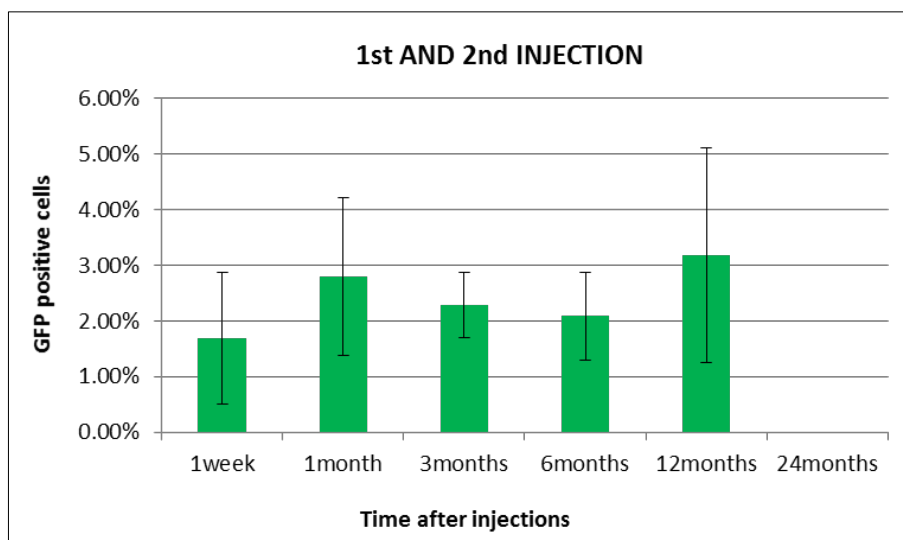
Fig. 3.58. eGFP expression analysis at different time points after injections at the day of birth with 1×10^{10} GC of rAAV MOCS2B-GFP in 20 ul PBS, and at postnatal day 6 with 4×10^{10} GC of rAAV MOCS2B-GFP in 40 ul PBS. (a) Fluorescent images showing eGFP expression after double injection. Liver sections from animals treated with PBS served as a negative control. **(b)** Bar graphs showing the number of eGFP positive cells were normalised to the total number of liver cells. Values and associated error bars represent mean ± s.d. (n = 1).

3.2.4   Long-term study of the tumorigenic potential of rAAV-based gene therapy

Although rAAV remains one of the most promising vector for gene therapy, its site specific integration is lost due to genetic modifications. It has been shown to either persist as episomes or integrate randomly into the host genome. Aim of this study was to check the tumorigenic potential of rAAV in different mouse genetic backgrounds, including C57Bl/6N and 129sv. A cohort of 50 animals from each strain received two intrahepatic injections with rAAV (1460 AAV2/8TBGMOCS2B-STOP-eGFP3). The first injection at the day of birth (1×10^{10} GC in 20 ul of PBS), and the second one at postnatal day 6 (4×10^{10} GC in 40 ul of PBS). At the same time, 50 animals from each background were injected in the same way with PBS and served as a control. Animals were kept in sterile conditions, and the underlying cause of each death was investigated in collaboration with pathologists, Dr. Ursula Kohlhofer, Dr. Klaudia Kloss, and PD Dr. Leticia Quintanilla-Martinez de Fend (Institute of Pathology, University of Tübingen,).

Animals treated with rAAV analysed from the C57Bl/6N strain were in average at an age of 11 to 30 months. In that cohort, 21 animals developed hepatic tumours, one animal a

primary intestine tumour with metastases, one mouse a malignant hematopoietic tumour (unclassifiable lymphoma), and one adenocarcinoma of the lung. Additionally to hepatocellular carcinoma (HCC), five animals presented also with hematopoietic tumours (one animal a histiocytic sarcoma, and four animals diffuse large B-cell lymphomas, DLBCL). One animal developed additionally a hemangiosarcoma **(Tab. 3)**. The first onset of HCCs was manifested quite late, as it was observed between 17-21 months. In younger mice no hepatic tumour was detected. Mice which developed a malignant hepatic tumour together with a hematopoietic tumour, were older than 22.5 months. From the group treated with PBS, analysed animals were in average at an age of 8 to 30 months. 22 animals with an age range of 9 to 28 months developed tumours. Four animals developed hemangiosarcoma, one together with leukaemia; one animal a sarcoma of the skin; three animals histiocytic sarcomas; five animals diffuse large B-cell lymphomas including two with plasmatic differentiation; one mouse a B-cell lymphoma of follicular centre cell type; one B-cells lymphoblastic lymphoma; one animal a plasma cell neoplasm; five animals hepatocellular carcinoma; and one animal both: i.e. a plasma cell neoplasm and a HCC. Mice that developed hemangiosarcomas were 14, 17, 18 and 22.5 months old, whereas mice that developed a hematopoietic neoplasia were 18 to 28 months old **(Tab. 3)**. Non-malignant causes of death are listed in the table **(Tab. 4)**.

Tab. 3 Summary of malignant reason of death of C57Bl/6N mice treated either with rAAV or with PBS (n = 50)

MALIGNANT DIAGNOSIS	C57Bl/6N rAAV	C57Bl/6N PBS
Primary intestine tumour with metastases to other organs	1 **(2%)**	-
Lymphoma unclassifiable	1**(2%)**	-
Hepatocellular carcinoma (HCC)	10 **(20%)**	5 **(10%)**
HCC with lung metastases	3 **(6%)**	-
HCC with lung metastases and diffuse large B-cell lymphoma (DLBCL)	1 **(2%)**	-
HCC, histiocytic sarcoma with questionable acute leukaemia with maturation	1 **(2%)**	-
HCC and DLBCL	1 **(2%)**	-

HCC, hemangiosarcoma of the spleen and ovary	1 **(2%)**	-
HCC, DLBCL, hemangiosarcoma	1 **(2%)**	-
HCC and DLBCL with plasmatic differentiation	1 **(2%)**	-
Hepatocellular adenoma (HCA)	1 **(2%)**	-
HCC vs (HCA)	1 **(2%)**	-
Adenocarcinoma of the lung with tubulopapillary growth formation	1 **(2%)**	-
Hemangiosarcoma of the spleen	-	2 **(4%)**
Hemangiosarcoma of the spleen and leukaemia with maturation	-	1 **(2%)**
Hemangiosarcoma of the liver	-	1 **(2%)**
Sarcoma of the skin	-	1 **(2%)**
Histiocytic sarcoma	-	1 **(2%)**
Histiocytic sarcoma, solid type	-	1 **(2%)**
Histiocytic sarcoma with liver metastases	-	1 **(2%)**
Diffuse large B-cell lymphoma	-	3 **(6%)**
Diffuse large B-cell lymphoma with plasmatic differentiation	-	2 **(4%)**
B-cells lymphoma of follicular centre cell type	-	1 **(2%)**
B-cells lymphoblastic lymphoma	-	1 **(2%)**
Plasma cells neoplasm and HCC	-	1 **(2%)**
Plasma cell neoplasm	-	1 **(2%)**
Σ	**24 (48%)**	**22 (44%)**

Tab. 4. Overview of non-malignant reason of death of C57Bl/6N mice treated either with rAAV or with PBS (n = 50)

NON-MALIGNANT DIAGNOSIS	C57Bl/6N rAAV	C57Bl/6N PBS
Skin injuries	2 **(4%)**	3 **(6%)**
Ulcerative dermatitis	9 **(18%)**	9**(18%)**
Gastrointestinal obstruction	1 **(2%)**	2 **(4%)**
Cardiac diseases	1 **(2%)**	1 **(2%)**

Kidney and cardiac diseases	1 **(2%)**	1 **(2%)**
Hydronephrosis or urinary track obstruction	3 **(6%)**	5 **(10%)**
Penis inflammation	1 **(2%)**	1 **(2%)**
Enlargement of seminal vesicles	1 **(2%)**	-
Dehydration	1 **(2%)**	-
Eye abnormalities	-	1 **(2%)**
Seminal vesicles abnormalities	-	3 **(6%)**
Hepatomegaly and splenomegaly	-	1 **(2%)**
Age	5**(14%)**	1 **(2%)**
Unknown	1 **(2%)**	-
Σ	**26 (52%)**	**28 (56%)**

In the 129sv strain the analysed animals after rAAV injections were 11 to 22.5 months old. Only seven animals developed tumours. HCC was found in three animals, one of these additionally developed a hemangiosarcoma of the uterus. In this group the youngest mouse that developed a hepatic lesion was 15 months, the oldest one 25 months. Four mice developed other malignant neoplasms (diffuse large B-cell lymphoma, marginal cell lymphoma and hemangiosarcoma of the uterus, uterine endometrial adenocarcinoma, and bronchoalveolar adenocarcinoma). The animals were 21-, 20-, 24- and 25.5 months old, respectively **(Tab. 5.)**. The youngest analysed animal injected with PBS from the 129sv line was 3 months old, the oldest one 26 months old. In contrast to the rAAV-injected mice, in that group only three mice developed tumours. One animal developed a HCC, and two other animals showed malignant neoplasms (urothelial carcinoma with squamous cell differentiation, and hemangiosarcoma of the uterus). The animal that developed a hepatocellular carcinoma was 19 months old; the mice with malignant neoplasms were 22.5 and 23 months, respectively **(Tab. 5)**. Non-malignant causes of death are listed in the table **(Tab. 6)**.

Tab. 5. Summary of malignant reason of death of 129sv mice treated either with rAAV or with PBS (n = 50)

MALIGNANT DIAGNOSIS	129sv rAAV	129sv PBS
Hepatocellular carcinoma (HCC)	2**(4%)**	1**(2%)**
HCC and uterus hemangiosarcoma	1**(2%)**	-
Diffuse large B-cell lymphoma	1**(2%)**	-
Uterine endometrial adenocarcinoma	1**(2%)**	-
Uterus hemangiosarcoma and marginal cell lymphoma	1**(2%)**	-
Bronchoalveolar adenocarcinoma	1**(2%)**	-
Hemangiosarcoma of the uterus and uterine endometrial adenocarcinoma	-	1**(2%)**
Urothelial carcinoma with squamous cell differentiation	-	1**(2%)**
Σ	7**(14%)**	3**(6%)**

Tab. 6. Overview of non-malignant reason of death of 129sv mice treated either with rAAV or with PBS (n = 50)

NON-MALIGNANT DIAGNOSIS	129sv rAAV	129sv PBS
Epilepsy	1 **(2%)**	-
Retrobulbar abscesses with periocular swelling	10 **(20%)**	4 **(8%)**
Gastrointestinal obstruction	3 **(6%)**	1 **(2%)**
Hydronephrosis, urinary track obstruction with stones in the bladder	3 **(6%)**	7 **(14%)**
Stones in the bladder	10 **(20%)**	8 **(16%)**
Penis inflammation	2 **(4%)**	1 **(2%)**
Uterus and uterine horn abnormalities	6 **(12%)**	5 **(10%)**
Hematometra	1 **(2%)**	-
Common bad condition	2 **(4%)**	-
Cardiac disease	-	1 **(2%)**
Lung infection	-	1 **(2%)**
Seminal vesicles abnormalities	-	2 **(4%)**
Obesity	-	2 **(4%)**

Age	5 **(10%)**	15 **(30%)**
Σ	**43 (86%)**	**47 (94%)**

There was no coincidence between results obtained from both strains, and they showed extremely different patterns. In the C57Bl/6N strain almost half of the animals from both groups, injected with rAAV or PBS, developed tumours (48% and 44%, respectively). However, animals from the 129sv strain died mostly because of other diseases, only 14% of animals injected with rAAV developed tumours and only 6% from the group which obtained injections with PBS. The results indicate, that there is a different potential of rAAV-based malignancy in different mouse strains. Additionally, 18% from each group of C57Bl/6N mice suffered from Ulcerative dermatitis. They were mostly females (16 females and 2 males, data not shown). In the 129sv strain were three non-malignant frequent causes of death: kidney obstruction, cystine stones formation, and retrobulbar abscess with periocular swelling. Except one animal, all mice which suffered from the first two diseases were males (data not shown) regardless of injection which they obtained. The retrobulbar abscess with periocular swelling was not gender-specific but it occurred more frequently in the rAAV than PBS treated mice (20% vs 8%).

4   DISCUSSION

4.1   Summary of results

Molybdenum cofactor (MoCo) deficiency type A is thus far only one curable type of MoCo deficiency. In the present study, a mouse model for MoCo deficiency type B ($Mocs2^{-/-}$) was generated, characterised and used for preclinical trials. To create pure knockouts of each $Mocs2$ isoform ($Mocs2a^{-/-}$ and $Mocs2b^{-/-}$), $Mocs2^{-/-}$ animals were crossed with generated transgenic mice expressing either the human $MOCS2A$ or human $MOCS2B$ isoform. In turn, the $Mocs2a^{-/-}$ animals were established. Due to several problems with $MOCS2A$ transgenic mice, we could not establish a $Mocs2b^{-/-}$ line.

The type of therapy relevant for MoCo deficiency is strictly dependent upon the type of the disease. The substitution therapy sufficient for rescuing MoCo deficiency type A is not effective in type B or C. In contrast to cyclic pyranopterin monophosphate (cPMP), other intermediate products of MoCo biosynthesis such as molybdopterin (MPT) and active MoCo, are unstable due to incorporated sulphur atoms. For this reason, we designed and developed a gene therapy approach using recombinant adeno-associated virus (rAAV). A single injection using relatively low doses of rAAV was able to drive expression of the MOCS2B therapeutic protein for at least two years. Additionally, a potential tumour formation risk caused by random integration of rAAV DNA into the host genome was analysed. Although the rAAV treatment increased the risk of tumour formation, it was highly dependent upon the genetic background of treated animals. Moreover, rAAV induced tumours did not occur earlier in treated animals compared with the onset of spontaneous tumours presented in untreated control animals. Finally, the rAAV encoding human MOCS2B protein was generated and its infection ability was evaluated in mice. Thus far, we have been unable to test therapeutic values of generated rAAV.

4.2   Expression pattern of *Mocs2a/b* isoforms

To date, the expression of *MOCS* genes has not been studied in detail. Besides northern blot analyses of *MOCS1* (Reiss *et al.*, 1998) and *MOCS2* (Stallmeyer *et al.*, 1999) transcripts, very little is known about the tissue distribution of *MOCS* genes. In the present study, the expression of *Mocs2* isoforms was investigated in mouse tissues using the quantitative real time PCR (qPCR) method. *Mocs2* isoforms were present in all

investigated tissues, with the highest expression in the skin, kidney, liver, lung, brain, and the lowest expression in the heart and spleen. Our data correlate with the previously described expression of *Mocs1* transcripts (Lee, 2003). In the study by Lee and co-workers, the highest expression of *Mocs1* transcripts was detected in the liver, brain and kidney, while a weak expression was found in muscles. To visualise the cellular distribution of *Mocs2* transcripts, we took advantage of the β-Galactosidase (LacZ) reporter cassette presented in the *Mocs2* knockout allele. In agreement with our qPCR results, LacZ signals (equivalent of *Mocs2a/b* expression) were detected in all investigated tissues, with the highest incidence in kidney, brain, skin and germ cells. In the present study, LacZ-positive cells were detected in the collecting system of the kidney, in the cortex, the hippocampus and the brainstem, as well as in the hair follicles of the skin. An interesting pattern was observed in the testes, with strong LacZ staining detected in undifferentiated spermatogonia. LacZ-positive cells resembled the morphology of the undifferentiated spermatogonia inside seminiferous tubules. They existed either as a single cell or as chains of two, three or four cells. Counterstaining of the chromatin revealed the presence of mitotic spindle in each LacZ positive spermatogonia-like cell. Moreover, these cells were identified in testes of 12-day-old *Mocs2*$^{+/-}$ mice, which do not contain later stages of germ cells (e.g. spermatocytes, spermatids), but rather only spermatogonia (Meikar *et al.*, 2011). In contrast to the qRT-PCR results, it was difficult to obtain reproducible LacZ-staining results in tissue sections of the liver, given that LacZ signals were either very week (as in 12-day-old pups) or uneven (as in liver sections of adult animals). It has been shown in rats that hepatocytes are responsible for the uptake and degradation of β-Galactosidase (Blomhoff *et al.*, 1985). Indeed, this finding could explain the discrepancy between qRT-PCR and LacZ staining results, as the β-Galactosidase protein is rapidly digested in the liver tissue and thus reproducible LacZ staining could not be detected. **Table 7** summarises the expression of *Mocs1* and *Mocs2* genes in murine tissues.

Tab. 7. Expression of *Mocs1* and *Mocs2* genes in murine tissues

Tissue	*Mocs1*	*Mocs2* (qPCR)	*Mocs2* (LacZ)
Brain	++	+++	+++
Heart	n.a.	+	+
Lung	n.a	+++	+++
Liver	+++	+++	+[*]
Stomach	n.a	++	++
Spleen	n.a	+	-
Kidney	+++	+++	+++
Testis	n.a	++	+
Ovary	n.a	+	+
Skin	n.a	+++	+++
Muscle	+	++	-

- = no expression, + = low expression, ++ = moderate expression, +++ = high expression, n.a. = not analysed.

* β-galactosidase is metabolised in the liver, thus LacZ staining does not correlate with *Mocs2* gene expression in the liver.

Here, the immunohistochemical analysis of WT mouse hepatocytes using a Mocs2b-specific antibody revealed a cytoplasmic localisation of Mocs2b protein with a punctuate expression pattern. One could expect that the expression of *MOCS* proteins correlates with the activity of molybdenum cofactor-dependent enzymes. In rat liver cells, aldehyde oxidase and sulphite oxidase are expressed in mitochondria (Williams, 1952; Cohen *et al.*, 1972), while xanthine oxidoreductase was shown to be localised in peroxisomes (Angermuller *et al.*, 1987; Frederiks and Vreeling-Sindelarova, 2002) and the amidoxime reducing component is expressed in both cellular compartments (Wahl *et al.*, 2010; Klein *et al.*, 2012). Additionally, it was shown in *Arabidopsis thaliana* that the MOT2 protein-

the putative homologue of human molybdate transporter - exhibits a vacuolar localisation (Wiese *et al.*, 2007; Gasber *et al.*, 2011). All such findings together support our results concerning a cytosolic, vesicle-like expression pattern of Mocs2 proteins in mouse hepatocytes.

4.3   Characterisation of *Mocs2* knockout mice

To date, 80 MoCo deficient patients have been diagnosed worldwide. The majority (50%) of the mutations leading to MoCo deficiency have been identified in the *MOCS1* gene (MoCo deficiency type A), while 32.5% of mutations have been described in the *MOCS2* gene (type B), and only 14 mutations (17.5%) have been reported in the *Gephyrin* (*GPHN*) gene (type C) (HGMD Professional 2015.1). Mouse models for type A and type C diseases have already been established (Feng *et al.*, 1998; Lee *et al.*, 2002). Although protein products of both *Mocs1* and *Gphn* genes are involved in the biosynthesis pathway of molybdenum cofactor, the *Gphn* knockout mice do not resemble the phenotype of *Mocs1* knockout mice. Besides its role in the MoCo biosynthesis pathway, *Gphn* protein has an additional function in glycin- and GABA$_A$ -receptors' localisation and anchoring. Gephyrin-deficient mice display a failure in inhibitory neurotransmission, which consequently prevents suckling. Accordingly, *Gphn*$^{-/-}$ animals die within the first day of their life. Since MoCo deficient mice show first symptoms at day 3-4 after birth, premature death of *Gphn*$^{-/-}$ mice is a result of impaired neurotransmission rather than MoCo deficiency (Reiss *et al.*, 2005).

In the present study, the mouse model for MoCo deficiency type B has been developed. Similar to *Mocs1*$^{+/-}$ (Lee *et al.*, 2002) and *Gphn*$^{+/-}$ (Feng *et al.*, 1998) mice, heterozygous *Mocs2*$^{+/-}$ animals are phenotypically normal and fertile. In all three KO mouse models, heterozygous matings lead to the birth of homozygous mutants in expected numbers (~25%). In contrast to *Gphn*$^{-/-}$ animals, *Mocs1*$^{-/-}$ and *Mocs2*$^{-/-}$ pups appear normal at birth and suckle; however, they failed to thrive and died between day of birth and day 12 after birth, with a mean life span of 6.3 ±3.7 and 4.7 ± 3.1 days for *Mocs1*$^{-/-}$ (n=28) and *Mocs2*$^{-/-}$ (n=107) pups, respectively. *Mocs2*$^{-/-}$ pups presented two critical periods after birth: between day 0-4 when 47% of *Mocs2*$^{-/-}$ neonates died; and later between day 5-10 when 51% of the animals died. *Mocs1*$^{-/-}$ animals present only one critical time point between

day 3-10 when 82% of the animals died (Lee *et al.*, 2002). **Figure 4.1** presents the survival rate of *Mocs2*^{-/-} mice in comparison to *Mocs1*^{-/-} mice. Discrepancies between the survival rates of *Mocs1*^{-/-} and *Mocs2*^{-/-} animals could result from different genetic backgrounds, given that *Mocs1* knockout mice were derived from a hybrid (C57Bl/6J × 129sv) strain, while *Mocs2* knockout mice were derived from a pure C57Bl/6N background. On the other hand, one can speculate that Mocs2 proteins can display additional function(s) shortly after birth. In turn, the depletion of Mocs2 proteins not only impaired the formation of molybdopterin synthase, but additionally essential physiological processes in newborn mice.
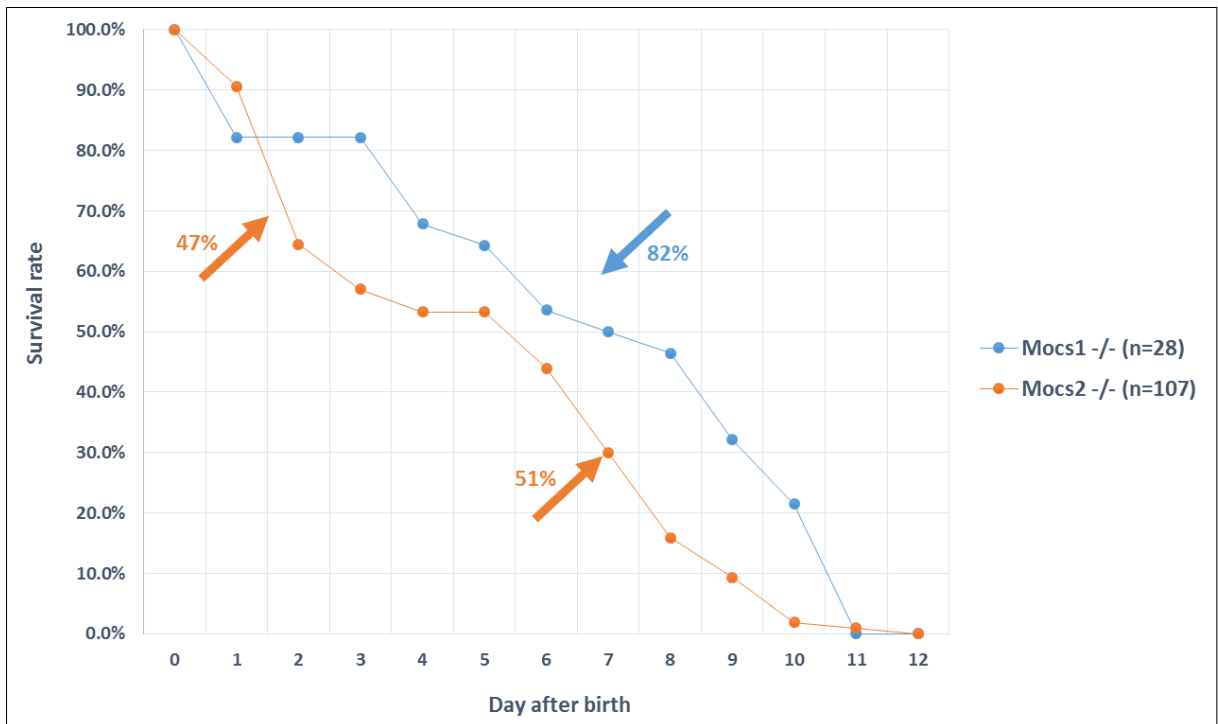
Fig. 4.1. Survival rate of *Mocs1*^{-/-} and *Mocs2*^{-/-} pups. Line graph showing the survival rate of *Mocs2*^{-/-} pups (orange) in comparison to *Mocs1*^{-/-} mice (blue). Arrows depict critical survival periods of knockout animals after birth. *Mocs2*^{-/-} mice present two critical periods (shown with orange arrows): the first between day of birth (0) and postnatal day 4 (47% of *Mocs2*^{-/-} pups died), and the second between postnatal day 5 and 10 (51% of *Mocs2*^{-/-} pups died). In contrast, *Mocs1*^{-/-} mice present only one critical point between postnatal day 3 and 10. During this time, 82% of *Mocs1*^{-/-} pups died. The results showing the survival of *Mocs1*^{-/-} mice were adopted from Lee *et al.*(2002).

Similar to *Mocs1*^{-/-} neonates, *Mocs2*^{-/-} appeared externally normal but failed to grow due to an impaired gain of weight. The intense weight loss of *Mocs1*^{-/-} and *Mocs2*^{-/-} mice may

be due to either hindered access to the milk - as stronger heterozygous ($Mocs2^{+/-}$) and wild type ($Mocs2^{+/+}$) littermates eliminate homozygous mutant mice from the mother - or simply a very severe systemic phenotype. Apart from their smaller size in comparison to $Mocs2^{+/+}$ and $Mocs2^{+/-}$ littermates, $Mocs2^{-/-}$ and $Mocs1^{-/-}$ mice present a poor skin condition, curly whiskers and an overall problem with hair growth **(Fig. 4.2)**. One could ask why their whiskers can grow whereas growing other types of hair is impaired. This may be explained by differences between development of whiskers and other hairs (Wrenn and Wessells, 1984; Maklad *et al.*, 2010). In rodents, whiskers develop prenatally and pups are born with an intact vibrissae, which is invisible to the naked eye (Landers *et al.*, 2006). By contrast, the last step of anagen (active growth phase of hair follicles) - when hair fibres emerge through the epidermis - occurs at day 5 postpartum and can be affected by MoCo deficiency (Hedrich, 2004). Surprisingly, skin and hair phenotypes seem more severe in $Mocs2^{-/-}$ mice compared with $Mocs1^{-/-}$ pups. As previously mentioned, the different genetic backgrounds can explain these differences, although I speculate that the more severe externally phenotype of $Mocs2^{-/-}$ mice is rather a result of impaired functions of Mocs2 isoforms.

Fig. 4.2. *Mocs1*^{-/-} and *Mocs2*^{-/-} mice show growth retardation, abnormal shape of whiskers, and defect in the overall hair growth as compared to healthy littermates. (Left) Exemplary picture of a 8-day-old *Mocs1*^{-/-} mouse, and **(right)** a 7-day-old *Mocs2*^{-/-} mouse, in comparison to control animals from the same litters. The picture of *Mocs1* animals was adopted from Lee *et al.* (2002).

Owing to the loss of MoCo, all molybdenum-dependent enzymes should be inactive in *Mocs1*- and *Mocs2*-deficient mice. In the study by Lee and colleagues, the activities of sulphite oxidase and xanthine dehydrogenase in *Mocs1*^{-/-} mice were measured directly from the liver extract (Lee *et al.*, 2002). In our study, we performed the semi-quantitative test showing an elevated level of sulphite in the fresh urine of *Mocs2*^{-/-} neonates compared to control littermates.

Despite a description of the general phenotype (i.e. smaller size and curly whiskers) and biochemical analyses, a previous study by Lee did not analyse *Mocs1*-deficient mice in detail (Lee *et al.*, 2002). The authors suggested that the phenotype presented in mice resembles the phenotype presented in patients. Since MoCo deficiency in patients leads to the loss of white matter (Endres *et al.*, 1988; Graf *et al.*, 1998; Johnson *et al.*, 2001), Lee and colleagues performed a morphological analysis of *Mocs1*^{-/-} brain sections. Nuclear staining of hippocampus, cortex and spinal cord derived from *Mocs1*^{-/-} mice showed no abnormalities in cell number or changes in the cellular layers in the brain. In agreement with these results, we could not show any changes in the cell number and morphology of *Mocs2*^{-/-} brains. In contrast to Lee's study, we performed a deep pathological analysis of HE, NeuN and GFAP stained *Mocs2*^{-/-} brain sections. Although NeuN and GFAP did not show any significant differences in the number of neurons and astrocytes, respectively, HE staining revealed the presence of apoptotic neurons in hippocampus, cortex and brainstem regions of *Mocs2*^{-/-} brains. Subsequently, we confirmed these findings by Caspase 3 immunostaining, showing massive apoptosis of neurons in *Mocs2*^{-/-} brains. Apoptotic neurons were also identified in *Mocs2*^{+/-} brains, albeit with lower incidence (5-6 fold lower than in *Mocs2*^{-/-} brains). These results support the previous study by Reiss and colleagues, showing massive cell death programme in the brain of *Mocs1*^{-/-} mice. Although the authors could not show any morphological changes in *Mocs1*^{-/-} brain, expression analysis with microarrays indicated the activation of a cell death programme (Reiss *et al.*, 2005). In light of these results, we showed for the first time that the mouse model for MoCo deficiency resembles not only biochemical but also pathological features observed in MoCo-deficient patients. In MoCo-deficient animals, the brain phenotype is milder than observed in patients, probably because the life span of MoCo-deficient animals (12 days) is too short to develop such severe abnormalities. Thus far, brain

dysmorphologies described in MoCo-deficient patients have been explained by sulphite toxicity to the central nervous system (CNS), whereby sulphite is endogenously generated during the metabolism of sulphur-containing amino acids and drugs **(Fig. 4.3)**. Zhang and colleagues analysed the sulphite toxicity in rat brains, in hepatocellular carcinoma (HepG2) and human foetal liver cell lines, as well as different neuronal cell lines derived from rodents. *In vivo*, sulphite induced a significant and dose-dependent decrease in ATP synthesis in rat brain mitochondria. Additionally, an *in vitro* study revealed a sulphite-mediated depletion of ATP in the investigated cell lines, although the accumulation of sulphite was more likely to occur in neuronal cells (Zhang *et al.*, 2004). Furthermore, Grings and colleagues showed in detail that sulphite disrupts brain mitochondrial energy homeostasis and induces mitochondrial permeability transition pore opening via thiol group modification (Grings *et al.*, 2014). Reiss and colleagues excluded sulphate deficiency as a potential trigger for neuronal death (Reiss *et al.*, 2005).
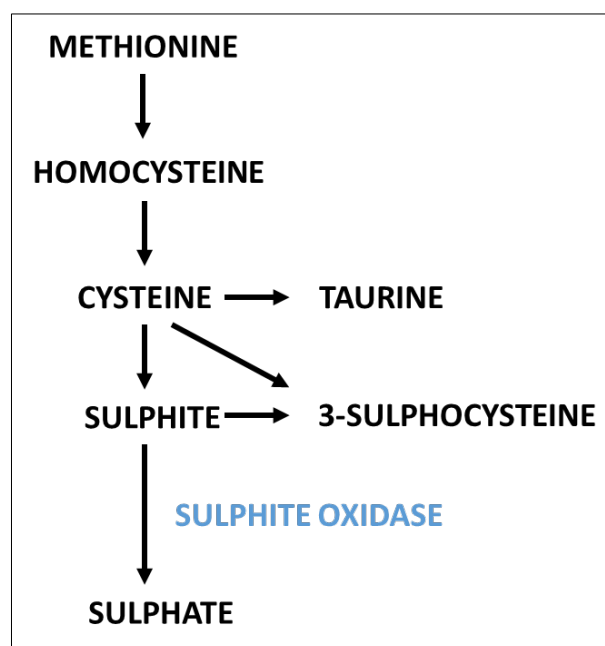
Fig. 4.3. Metabolism of sulphur-containing amino acids. Sulphite is generated during the metabolism of sulphur-containing amino acids, i.e. methionine. In the final step, sulphite is oxidised to sulphate by one of the MoCo-dependent enzymes, sulphite oxidase. Scheme adopted and modified from Tan *et al.* (2005).

During our study, I observed that all *Mocs2*^{-/-} pups manifested urinary obstruction associated with a presence of yellow deposits in the bladder. Subsequently, I also confirmed this phenotype in bladders of *Mocs1*^{-/-} mice (data not shown). Yellow deposits

have already been described in rescued $Mocs1^{-/-}$ mice (Hahnewald, 2009). During this study, Hahnewald tested the therapeutic potential of different cPMP concentrations, whereby the higher doses of cPMP were able to completely rescue the phenotype of MoCo deficiency type A, while the lower doses led to the precipitation of yellow deposits in kidneys **(Fig. 4.4)**. Hahnewald showed that the reconstitution of xanthine dehydrogenase activity in animals treated with lower cPMP doses was insufficient; thus, it was speculated that these deposits might have a xanthine composition. In agreement with this study, Ohtsubo and colleagues showed that the knockout of xanthine oxidoreductase (*Xor*) leads to premature death of $Xor^{-/-}$ mice due to the deposition of crystals and lipid-rich substances in renal tubes (Ohtsubo *et al.*, 2009) **(Fig. 4.4.)**. To check the ingredients of the deposits extracted from the $Mocs2^{-/-}$ bladder, I sent them for biochemical analysis, although their composition was not identified. Interestingly, crystal concretions were also present in the kidneys of $Mocs2^{-/-}$ neonates.
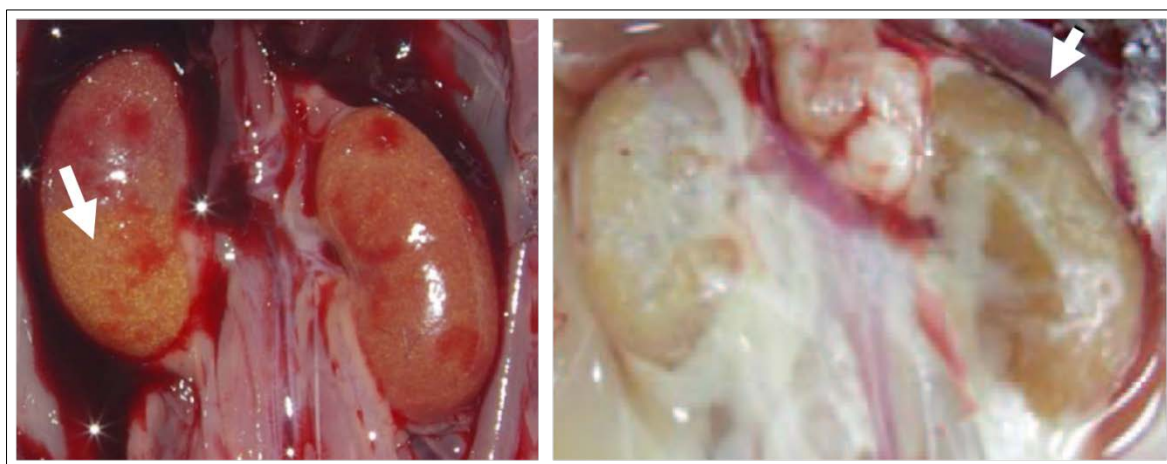
Fig. 4.4 Concretions presented in kidneys derived from $Mocs1^{-/-}$ and $Xor^{-/-}$ mice. (Left) Xanthine stones identified by Hahnewald and colleagues in adult kidneys of $Mocs1^{-/-}$ mice treated with lower doses of cPMP. **(right)** Examplary image of xanthine crystals and lipid-rich substances in kidneys of 4-week old $Xor^{-/-}$ mice. Arrows depict yellow deposits in kidneys. Images were adopted from Hahnewald (2009) and Ohtsubo *et al.* (2009).

To conclude, I characterised the phenotype of a mouse model for molybdenum cofactor deficiency type B and compared it with the mouse model for molybdenum cofactor deficiency type A **(Tab. 8)**. Briefly, $Mocs2^{-/-}$ mice shared most of the external features previously described in $Mocs1^{-/-}$ mice, including curly whiskers, poor skin condition and

overall hair growth abnormalities. *Mocs2*^{-/-} pups presented a shorter live span compared to *Mocs1*^{-/-} mice, with two critical postnatal periods during which almost 98% of the pups died. In addition to external changes, we also identified severe phenotypes in the brain, kidneys and in the skin. However, I could not point out which of these phenotypes is the primary cause of death, given that defects in one of these organs could result in secondary effects in other tissues. I can speculate that malformed hair follicles can trigger a wound-like condition of the skin, resulting in wrinkle formation and flakiness in the skin. The animals may undergo dehydration, which can occur due to a defective barrier function in the skin (Cartlidge, 2000; Rutter, 2000). If water and electrolyte are continuously lost, blood pressure can fall dangerously low and result in shock and severe damage to many internal organs, such as the kidneys, liver and brain. As dehydration is associated with renal dysfunction (Roncal Jimenez *et al.*, 2014), it can explain the phenotype observed in the kidney. We have shown that the *Mocs2*^{-/-} animals present crystals in the collecting duct system of kidneys, as well as in the bladder. Since *Mocs2* isoforms are highly expressed in kidney collecting system, the knockout of the *Mocs2* gene can be a primary cause of crystal formation (nephrolithiasis). On the other hand, dehydration caused by skin failure may increase the concentration of minerals in the urine, resulting in nephrolithiasis. The accumulation of such crystals can form a plug, which causes a complete blockage of the urethra. The bladder became full of urine, which starts to go back into the kidney. This backflow of urine (vesicoureteric reflux) leads to infection, hydronephrosis and finally kidney damage (Tullus, 2015). The presence of proteins and haemoglobin in the urine - evaluated by the colorimetric test - confirmed the severe degenerative changes in kidneys. The presence of proteins in the urine may indicate damage of the filtration apparatus and the red blood cells were a sign of bleeding in the urinary system, caused by e.g. kidney stones. In turn, renal failure may interrupt the blood flow through the brain (Sims and Zaidan, 1995). The brain is particularly vulnerable to ischaemia (inadequate blood supply to a local area). Only 5 minutes of interruption in the blood flow to the brain triggers the death of neurons in several brain regions, while for example 20-40 minutes of ischaemia is required to destroy kidney cells or cardiac myocytes (Lee *et al.*, 2000). Cerebral ischaemia is accompanied by a marked inflammatory reaction, which is initiated by ischaemia-induced expression of adhesion

molecules, cytokines and other inflammatory mediators, including prostanoides and nitric oxide (Iadecola and Alexander, 2001). These molecules activate the microglia, which is the resident macrophage population of the CNS responsible for the clearance of apoptotic neurons (Witting *et al.*, 2000; Ginhoux *et al.*, 2013). In light of this data, we performed immunostaining in $Mocs2^{-/-}$ brain sections using IBA1 (ionising calcium-binding adaptor molecule), a specific marker for microglia and macrophages (Ito *et al.*, 2001). Although immunostaining for Casp3 (marker of apoptosis) showed massive apoptosis of neurons in brain sections of $Mocs2^{-/-}$ mice, IBA1 staining did not show increased activation of microglia. The rapid microglial response to local brain injury is mediated by extracellular ATP (Davalos *et al.*, 2005). It can be hypothesised that the loss of mitochondria function due to the toxic effect of sulphite reduced the amount of extracellular ATP and thus abolished the over-activation of microglial cells. Finally, the observed phenotype may be an additive effect of the phenotypes observed in each tissue. Thus far, the brain phenotype has been considered the most severe, as the CNS is predominantly affected in patients. Indeed, this hypothesis was further confirmed in our study. Although $Mocs2^{+/-}$ mice do not present any abnormalities, we could identify slight neuron apoptosis in the hippocampus, cortex and brainstem. Since only the brain phenotype has been presented in $Mocs2^{+/-}$ mice, it seems to be a primary cause of premature death of $Mocs2^{-/-}$ animals.

Tab. 8. Comparison of the phenotypes presented by *Mocs1*- and *Mocs2*- deficient mice

Analysed features	$Mocs1^{-/-}$	$Mocs2^{-/-}$
Genetic background	C57Bl/6J × 129sv	C57Bl/6N
Heterozygous animals	Normal and fertile	Normal and fertile
Number of homozygous mutant (-/-) mice	~25%	~25%
-/- pups	Normal at birth	Normal at birth
Suckling	Normal	Normal
Survival rate	1-11 days	1-12 days
Critical survival points	1 (82% died)	2 (47% and 51%)

Mean life span	6.3	4.7
Impaired growth	Yes	Yes
Curly whiskers	Yes	Yes
Impaired hair growth	Yes	Yes
Neuron apoptosis	Yes (microarray)	Yes (immunostaining)
Activity of MoCo-dependent enzymes	Diminished	Diminished
Sulphite level in the fresh urine	Elevated	Elevated
Convulsions and ataxia	No	No
Yellow deposits in the bladder	Yes	Yes
Stones in kidney collecting ducts	Not analysed	Yes

In contrast to MoCo-deficient mice, patients present only progressive neurological damages. To date, the phenotype of isolated forms of aldehyde oxidase- and mitochondrial amidoxime reducing component-deficiency have not been described in humans. In most cases, xanthine oxidoreductase deficiency (xanthinuria) does not present any severe clinical symptoms and there is no specific treatment beyond maintaining a high fluid intake and avoiding foods that are high in purines (Gargah *et al.*, 2010). Xanthinuria is sometimes accompanied with xanthine deposition, which may rarely lead to renal failure (Ichida *et al.*, 2012). In light of these findings, the phenotype observed in MoCo-deficient patients is mostly restricted to sulphite oxidase deficiency. In the first week of life, patients present feeding difficulties with tonic/clonic seizures. Additionally, they present symptoms such as metabolic acidosis, intracranial haemorrhage, exaggerated startle reaction, axial hypotonia and limb hypertonia (van der Knaap and Valk, 2005). Neuron damages are severe and progressive as a result of the accumulation of sulphite in the brain (Mechler *et al.*, 2015). Magnetic resonance imaging (MRI) studies revealed a diffused pattern of brain atrophy with the arrested development of myelination (Appignani *et al.*, 1996). Other observed features of MoCo deficiency in patients include dilated ventricles, hydrocephalus, brain hypodensity, spastic paraplegia,

myoclonus, ophisthotonus and ocular abnormalities (i.e. lens dislocation, spherophakia, iris coloboma, nystagmus or enophthalmos) (van der Knaap and Valk, 2005).

4.4   Generation of isolated *Mocs2a* and *Mocs2b* knockout mice

Although a *Mocs2a* knockout mouse line was successfully generated, it was not possible to establish a *Mocs2b* knockout, given that both *MOCS2A* transgenic lines failed to supplement the *Mocs2a* subunit in *Mocs2*$^{-/-}$ mice. In the first *MOCS2A* transgenic line (MOCS2A5) derived from the MOCS2A founder mouse #56, the *MOCS2A* transgene was expressed ubiquitously, although it was integrated in the third intron of the *DnaJ (Hsp40) Homolog, Subfamily C, Member 24* (*Dnajc24*) gene (NCBI chr2:107210791-107210601). Heterozygous animals (*MOCS2A*$^{Ta/-}$) were fertile and had a normal appearance, while homozygous animals (*MOCS2A*$^{Ta/Ta}$) were embryonically lethal. qRT-PCR analyses showed a significant reduction of *Dnajc24* expression in *MOCS2A*$^{Ta/-}$ tissues in comparison to WT tissues. To date, the function of *Dnajc24* gene is not well studied. *Dnajc24*^{m1Jkn} mice (a chemically induced knockout mouse model of *Dnajc24* gene) are retarded in growth and development and die before embryonic day 14 (E14) (Mouse Genome Informatics (MGI)). In the presented study, mating of heterozygous *Dnajc24*$^{+/-}$ mice with *Mocs2*$^{+/-}$ mice led to a formation of double heterozygous animals. The breeding of double heterozygous mice failed to generate offspring, although several females were pregnant. In accordance with the Mendelian ratio, approximately 6.25% of pups from the F1 generation should be born with a WT genotype. Most probably a cumulative effect of double knockout (DKO: *Mocs2*$^{-/-}$*Dnajc24*$^{-/-}$, or *Mocs2*$^{-/-}$*Dnajc24*$^{+/-}$) caused severe malformation of DKO embryos, preventing the normal growing of other embryos and finally leading to abortion. In light of these results, a second transgenic line (MOCS2A6) was derived from the founder mouse MOCS2A #44. In this case, the integration site was identified on chromosome 6 (NCBI chr6: 44712888). To date, no gene has been described in this area, although *MOCS2A* transgene expression was silenced. This problem seems to be common for transgenic mice generated via random transgene integration. A so-called position effect can influence the expression of the transgene (Robertson *et al.*, 1995). The integration of foreign DNA into the heterochromatin region of genomic DNA often results in silencing of

the transgene. No additional *MOCS2A* founder animals were available to generate a *Mocs2b* knockout mouse model.

By contrast, a *MOCS2B* transgenic line was successfully established, providing us the opportunity to generate a *Mocs2a* knockout mouse model. For this reason, *Mocs2*$^{+/-}$ mice were bred with *MOCS2B* transgenic animals and subsequently double heterozygous animals *Mocs2*$^{+/-, Tb/-}$ were selected and bred with each other. As expected, the *Mocs2*$^{-/-, Tb/Tb}$ and *Mocs2*$^{-/-, Tb/-}$ animals presented the same phenotype as *Mocs2*$^{-/-}$ mice, although the body weight during the postnatal period was higher compared to that presented by complete knockout mice. Additionally, most of the *Mocs2*$^{-/-, Tb/Tb}$ and *Mocs2*$^{-/-, Tb/-}$ presented only one critical time point and died between postnatal day 5 and 10, with a mean survival time of 5.9 ± 2.4 days. In light of these results, we can speculate that the Mocs2b protein has a dual function: besides the function which it performs together with the Mocs2a protein as a molybdopterin synthase, it may play additional role(s) that shortly after birth contributed to the reduction of growth retardation of *Mocs2*$^{-/-, Tb/Tb}$ and *Mocs2*$^{-/-, Tb/-}$ pups.

4.5   Therapy for molybdenum cofactor deficiency

The molybdenum cofactor deficiency is an example of a disease caused by a loss-of-function mutation. There are three types of MoCo deficiency, namely A, B and C, which are distinguished based upon the mutations in genes regulating MoCo biosynthesis pathway. The type A of deficiency is attributed to the mutation in the *MOCS1* gene, which protein products (MOCS1A and MOCS1B) are involved in the conversion of a guanosine triphosphate (GTP) to the cyclic pyranopterin monophosphate (cPMP). The cPMP is only one stable intermediate in the entire MoCo biosynthesis pathway (Schwarz *et al.*, 2004). Schwarz and colleagues purified cPMP from *Escherichia coli* and used it for the substitution therapy in a mouse model of MoCo deficiency type A. Intrahepatic cPMP injection was sufficient to rescue the MoCo deficiency type A (Schwarz *et al.*, 2004). Four years later (in year 2008), Veldman and colleagues used the cPMP for the treatment of a MoCo deficiency type A patient for the first time. Intravenous injections led to an efficient uptake of the cPMP, resulting in the restoration of activity of molybdenum cofactor-dependent enzymes. It was not possible to rewind damages caused by the toxic sulphite,

137

although further neurodegeneration was retained (Veldman *et al.*, 2010). This year, the patient will celebrate her 7th birthday. By contrast, substitution therapy cannot be employed for other types of MoCo deficiency, since other intermediates in the MoCo biosynthesis pathway are very unstable and purification is not possible. Therefore, development of potential therapy for MoCo deficiency type B and C is required. **Figure 4.5** presents a MoCo biosynthesis pathway in the context of possible therapy approaches for each type of MoCo deficiency.
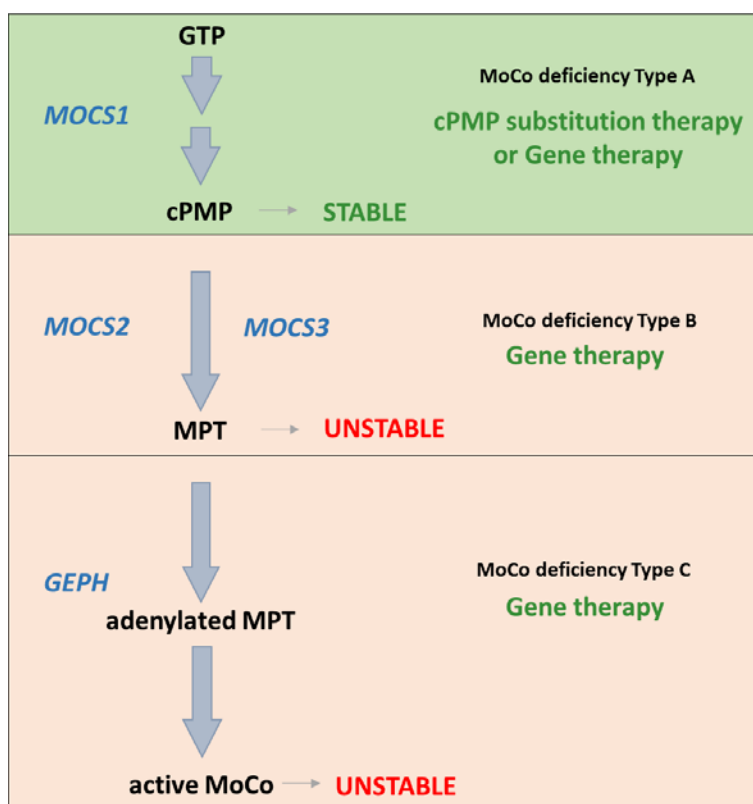
Fig. 4.5. Schematic representation of the molybdenum cofactor (MoCo) biosynthesis pathway together with potential therapies for the MoCo deficiency type A, B and C. A therapy for each type of MoCo deficiency depends on the biochemical character of missing intermediates. The green square represents MoCo deficiency type A, while the squares below present type B and C, respectively. Type A of the disease can be effectively cured by substitution therapy with purified bacterial cyclic pyranopterin monophosphate (cPMP), which is relatively stable in the lower pH. In contrast to cPMP, following intermediates, molybdopterin (MTP) and active MoCo are unstable. In this case, gene therapy is required to supplement mutated protein and restore the MoCo biosynthesis pathway.

4.5.1   Recombinant adeno-associated virus (rAAV)-based gene therapy

Several considerations must be taken into account when designing a viral vector-based gene therapy, including a) infection efficiency, b) long-time expression of the therapeutic gene and c) a lack of toxicity (Daya and Berns, 2008). A growing body of evidence has shown that rAAV vectors fulfil all of these criteria.

4.5.2   rAAV engineering and the route of delivery

The first pre-clinical trials for MoCo deficiency gene therapy using recombinant adeno-associated virus (rAAV) have been performed on a *Mocs1$^{-/-}$* mouse model (Kugler *et al.*, 2007). Kugler and colleagues rescued the phenotype of a mouse model of MoCo deficiency type A by intrahepatic injections with rAAV serotype 1/2 carrying a *MOCS1* therapeutic gene under a ubiquitous CMV promoter. Based upon their results - as well as those obtained by Hahnewald and colleagues (Hahnewald *et al.*, 2009) - we designed the rAAV-based gene therapy for MoCo deficiency type B. In order to increase the efficiency of viral infection and in turn the expression of the therapeutic gene, we used rAAV serotype 2/8 carrying the human *MOCS2B* gene under the control of a liver-specific, tyroxine binding globulin (TBG) promoter. To characterise the transduction efficiency and potential risk of rAAV induced tumour formation, we performed a long-term study. **Table 9** presents a summary of the strategy used in the present study in comparison to the strategy used by Kugler and colleagues (Kugler *et al.*, 2007).

Tab. 9: Comparison of strategies designed for the rAAV therapy of *Mocs1* (Kugler *et al.*, 2007) and *Mocs2* deficient mice

GENE THERAPY PARAMETERS	*Mocs1$^{-/-}$* (Kugler *et al.*, 2007)	*Mocs2$^{-/-}$* (Present study)
SEROTYPE	rAAV1/2	rAAV2/8
PROMOTER	CMV-ß-actin	TBG
EXPRESSION CASSETTE	MOCS1	MOCS2B
SCHEME OF INJECTIONS	Day 1: 1×10^9 tu	Day 1: 2×10^8 tu

	Day 4: 3×10^9 tu	Day 6: 8×10^8 tu
ROUTE OF INJECTION	Intrahepatic	Intrahepatic
PHENOTYPE RESCUE	Yes	n.a.
PERSISTENCE	n.a.	24 months
RATE OF LIVER CELLS WITH TRANSGENE EXPRESSION	100% to 5%	6.5% to 2%
PATTERN OF EXPRESSION	Ubiquitous	Liver
TUMORIGENIC POTENTIAL	n.a.	Strain dependent

CMV = Cytomegalovirus, TBG = Tyroxine binding globulin, tu = transfecting units, n.a. = not analysed

In the presented study, we chose the liver as a target organ for the gene therapy approach. Our choice was dictated by several factors: [1] all molybdenum cofactor (Moco)-dependent enzymes are active in the liver; [2] the liver is a highly vascularised organ, and thus a newly synthesised therapeutic protein can easily and efficiently gain access to the systemic circulation; [3] a growing number of studies have demonstrated that a liver-directed transfer can induce transgene product-specific immune tolerance (Mingozzi and High, 2007; LoDuca *et al.*, 2009); and finally [4] the skin of newborn mice is transparent, which simplifies direct injection to the liver. Before the rAAV preparation, the appropriate tropism (viral affinity for specific tissue(s)) should be defined, since different serotypes of the virus interact with tissue-specific surface molecules (Rabinowitz and Samulski, 2000). A liver-specific tropism has been shown for serotype 8 of rAAV (rAAV8). This virus has been derived from the rhesus monkey (Gao *et al.*, 2002) and the rAAV8 capsid has 82.8% homology with the capsid of best studied serotype 2 (AAV2) (Grieger and Samulski, 2005). Although the AAV2 is able to transduce hepatocytes, the expression of the therapeutic protein is low (Grimm and Kay, 2003). Most researchers employ so-called hybrid virions, which encode ITRs from the best described AAV2, as well as cap proteins derived from the AAV8, whose receptors appear highly prevalent in murine liver cells. It has been shown that such a hybrid virus achieves a 10- to 100-fold improvement in gene transfer efficiency compared with other vectors (Gao *et al.*, 2002).

Many studies have shown successful gene transfer to the liver using rAAV2/8 (Cunningham *et al.*, 2008; Flageul *et al.*, 2009; Laurence *et al.*, 2009; Torres-Torronteras *et al.*, 2014). Additionally, specific expression of a therapeutic gene can be triggered by an appropriate promoter (Papadakis *et al.*, 2004). Kugler and colleagues showed that intrahepatic injection of neonatal mice with rAAV1/2 encoding EGFP under a CMV promoter leads to EGFP expression in different tissues, including the brain (Kugler *et al.*, 2007). In our study, we used a liver-specific tyrosine-binding globulin (TBG) promoter. It was shown that the TBG promoter-driven gene expression was restricted to the liver, with minimal invasion to other tissues (Yan *et al.*, 2012). In agreement with this study, intrahepatic injection with rAAV2/8TBGMOCS2B-STOP-eGFP3 resulted in the expression of the MOCS2B protein exclusively in the liver of WT mice. At the same time, viral DNA could be detected in all other tissues analysed, except the brain. Although viral particles could be transported through blood vessels to different tissues, rAAV2/8 was unable to cross the blood-brain barrier.

One of the drawbacks of intrahepatic injection is its restriction to a small volume injectable into a newborn liver. In order to test other routes of viral delivery, we performed intraperitoneal injection (IP). Although IP was sufficient to transduce the liver, it was not efficient enough to induce expression of the therapeutic gene. In light of these results, intrahepatic injection seems the most efficient route to deliver viral particles to the liver. These two aspects - rAAV engineering as well as the route of transduction - are very important to induce transgene expression for a long time in a tissue-specific manner. Modification of the strategy used by Kugler (Kugler *et al.*, 2007), by changing the serotype and promoter and reducing the viral doses, was supposed to reduce the potential risk of the host immune response, which remains the greatest challenge facing AAV gene delivery. The host defence mechanism at the adaptive level comprises cell-mediated and humoral immunity. The cell-mediated response at the cellular level, eliminating the transduced cells using cytotoxic T cells, whereas the humoral response produces neutralising antibodies (NAb), preventing the re-administration of vector (Zaiss *et al.*, 2002). This first issue may be influenced by the route of viral administration (Brockstedt *et al.*, 1999) and AAV serotype (Wang *et al.*, 2007). Additionally, the cell-specific promoter might reduce the cellular response to rAAV (Cordier *et al.*, 2001). A different route of

injection (intraperitoneal, intravenous, subcutaneous or directly to the tissue of interest) and packaging of a transgene to the distinct serotype of the rAAVs (Halbert *et al.*, 2000) serve as potential factors that may allow re-administration of the virus. To overcome the problem of immune response in rodents, it is possible to use the window of vulnerability that encompasses the first days after birth, when the mature pattern of immune response to antigen is not yet achieved (Landreth, 2002). In contrast to human development, mice are born at an immunologically immature stage with few B cells and almost no T cells in the peripheral lymphoid tissues (Fadel and Sarzotti, 2000). Hahnewald and Hu showed in their studies that gene therapy in the neonatal period in mice avoid the development of immune responses and prolonged expression of the therapeutic gene (Hahnewald *et al.*, 2009; Hu and Lipshutz, 2012). In terms of human, AAV-based gene therapy seems more complicated, given that humans do not present a window of vulnerability. Moreover, most human beings are serologically positive for antibodies against AAV particles (Boutin *et al.*, 2010), thus significantly limiting rAAV gene transfer. However, it was shown that there might also exist in humans an ideal age interval for gene therapy intervention. Calcedo and colleagues studied the NAb titers to AAV2 and AAV8 in a cohort of 752 anonymous human subjects from different age groups (1 day to 18 years), showing that NAb prevalence is moderate at birth, decreases markedly from 7 to 11 months - probably due to a drop in maternal antibody levels - and subsequently progressively increases through childhood and adolescence (Calcedo *et al.*, 2011). In light of this data, the age between 7 to 11 months seems the best period for rAAV treatment in humans. In case of patients who present the phenotype of disease earlier, an alternative strategy must be considered. Possible solutions to reduce the immune response include the administration of a short-term immunosuppression regimen concomitant with gene transfer or the development of more efficient vectors that can be administered at lower doses (Mingozzi and High, 2007).

4.5.3 Efficiency of rAAV transduction

The present long-term study has shown that a single injection of AAV2/8TBG-MOCS2B-eGFP3 is sufficient to activate and maintain expression of the therapeutic gene for at least two years. As previously mentioned, several parameters (e.g. serotype, promoter or route

of viral delivery) should be considered before starting treatment. Another important issue includes the right time and amount of the virus used for injection. To optimise these parameters, we treated the animals with different virus concentrations with two temporally separated doses, both in the neonatal period. Through this strategy, we tried to find the balance between the injection volume restricted by the size of the animal and the potential immune response increasing with age. Three groups of animals obtained injection/injections with AAV2/8TBG-MOCS2B-eGFP3: the first group (I) obtained a single intrahepatic injection at the day of birth with 1×10^{10} GC (2×10^8 transfecting units (tu)); the second group (II) obtained a single injection at postnatal day 6 with 4×10^{10} GC (8×10^8 tu); and the last group (III) received a double injection, the first injection at the day of birth with 1×10^{10} GC, and a second injection at day 6 after birth with 4×10^{10} GC. The doses were chosen based upon the previous gene therapy study for molybdenum cofactor deficiency type A (Hahnewald *et al.*, 2009). In this study, Hahnewald and colleagues showed that 4×10^8 tu (corresponding to 1×10^7 tu per g of body weight) is the minimal dosage required to rescue the phenotype of molybdenum cofactor deficiency type A. Under normal conditions, the AAV DNA can be detected in the cell nucleus as early as 2 hours post-infection (Sanlioglu *et al.*, 2000), and the AAV-mediated transgene expression is typically detected 2 to 3 weeks after vector infection (Miao *et al.*, 1998). In our system, we were able to detect the MOCS2B-EGFP expression in hepatocytes as early as one week after injection, although the number of GFP-positive cells differed between different mouse groups. A single injection with 2×10^8 tu of AAV2/8TBG-MOCS2B-eGFP3 at the day of birth provided the best results, as 6.5% of liver cells were GFP-positive one week after injection. The number of positive cells gradually declined and maintained at 2%. In the other two groups (II and III) the initial efficiency was between 2-3% one week after injection and slightly decreased afterwards. In contrast to animals from group I and II (single injection), those from group III (double injection) did not present GFP-positive cells after 24 months. Because only one animal for each time point was used for the intrahepatic injection, technical problems during AAV injection cannot be ruled out. Therefore, it will be important to repeat this experiment with more animals to perform a solid statistical analysis. Interestingly, the first attempt to use AAV therapy for MoCo deficiency type A led to a transduction rate close to 100% one week after injection (Kugler

et al., 2007). In comparison to our study, Kugler and colleagues injected approximately 60-fold more virus (5×10^9 tu) than we did. Unfortunately, there was no correlation between transduction efficiency and the number of GFP-positive cells, as only 5% of liver cells were GFP-positive one month after viral injection. The reason for such a dramatic decline of transgene expressing cells is due to the episomal nature of the rAAV genome, which can be easily lost during mitotical cell division (Beer *et al.*, 2010). However, rAAV-mediated gene therapy in a mouse model of molybdenum cofactor deficiency type A revealeds promising results after intrahepatic injection of newborn mice. Although less than 5% of hepatocytes expressed the therapeutic gene, most of the animals survived for 20 weeks (Kugler *et al.*, 2007). There are currently several clinical trials using AAVs for gene therapy approaches for the treatment of human disease. The long-term expression of the therapeutic gene was shown for example in a human haemophilia B patient, who obtained injection of rAAV encoding factor IX (F.IX) (Buchlis *et al.*, 2012). Although the F.IX levels did not rise >1% and remained at a sub-therapeutic level, the patient survived 10 years post-injection and died owing to causes unrelated to the gene transfer. The RT-PCR analysis confirmed the expression of the F.IX transcript in the injected muscle tissue, reflecting an example of the longest transgene expression from a parenterally administered AAV vector and thus confirming that long-time expression is possible; rather, only the dosage has to be optimised to make the entire therapy approach highly efficient.

4.5.4 Tumorigenic potential of rAAV-based gene therapy in mouse

As mentioned at the beginning of this chapter, the ideal gene therapy approach should present a general lack of toxicity. In case of rAAV therapy, this aspect still prompts controversy. The wild type (WT) AAV is neutral for humans as it presents a site-specific integration on chromosome 19. This process is mediated by Rep proteins (Balague *et al.*, 1997). Unfortunately, the rAAV lost such ability during the process of its production, as all viral genes (including Rep) are replaced by the therapeutic gene (Linden *et al.*, 1996). Although AAV vectors are predominantly non-integrating extrachromosomal episomes that serve as the major source for transgene expression, Nakai and colleagues showed in mice that after tail vein injection of recombinant AAV2 vectors expressing hF-IX at doses

of 2.4×10^{11} to 3.0×10^{11} vector genomes per mouse less than 10% of double-stranded rAAV genomes can be found inserted in the host chromosomal DNA (Nakai *et al.*, 2001). Furthermore, a significant proportion of rAAV DNA integration events took place in transcriptionally active regions, as shown in the mouse liver (Nakai *et al.*, 2003). We cannot exclude the possibility that long-term expression of the therapeutic gene in our study comes from integrated viral DNA rather than episomes. These findings prompt the question of whether there is any risk of insertional mutagenesis after rAAVs administration. The universal safety of rAAV was first questioned by a single study that described the development of hepatocellular carcinoma (HCC) in mice after rAAV-based gene therapy (Donsante *et al.*, 2007). Using a murine model of β-glucuronidase deficiency, Donsante and colleagues identified an increased rate of HCC in mice treated with rAAV in the neonatal period. Subsequently, several groups investigated rAAV-mediated genotoxicity in mice and failed to reproduce these results (Bell *et al.*, 2005; Li *et al.*, 2011). To investigate this issue, we performed the longitudinal study in which mice from two different strains - namely C57Bl/6N and 129sv mice - obtained two intrahepatic injections (first at the day of birth with 1×10^{10} GC, and second at the day 6th with 4×10^{10} GC) with 1460 AAV2/8TBGMOCS2B-STOP-eGFP3 (n=50) or PBS (n=50) and were kept under sterile conditions to eliminate the risk of other infections (e.g. hepatitis virus infection). The cause of death of each animal was investigated by animal pathologists. The groups treated with PBS were used as a control showing a spontaneous tumour rate specific for each strain. We measured a tumour rate of 44% (22 mice, including 7 HCC) and 6% (3 mice, with 1 HCC) in C57Bl/6N and 129sv strain, respectively. Our results are in contradiction with previously published data showing the tumour incidences of 86% and 14% in strain C57Bl/6 and 129sv, respectively (Smith *et al.*, 1973; Blackwell *et al.*, 1995). These discrepancies could be caused by differences in the housing condition (e.g. diet or SPF status) between experimental animal groups (Turturro *et al.*, 2002). In contrast to previous studies, we also showed the differences in the frequency of spontaneous hepatocellular carcinoma (HCC). 10% and 2% of control animals from C57Bl/6N and 129sv strains developed HCC, respectively, which is significantly higher than <5% and 0% cited in the literature for the C57Bl/6N and 129sv strain, respectively (Smith *et al.*, 1973; Drinkwater and Ginsler, 1986). Since the first onset of HCCs was manifested quite late

(17-27 months), they could not be due to premature experiment termination. Taken together, both studies present the same trend, whereby the C57Bl strain is considered susceptible to many tumours, including HCC. Compared to control groups, our experimental cohorts (mice treated with rAAV) showed slight increase in their tumour rate (48% and 14% in C57Bl/6N and 129sv strain, respectively). Based upon these results, it is extremely difficult to assess an influence of the rAAV infection on the global tumour formation. The differences became clearer when taking a closer look to tumour composition presented in each group. As expected, the highest differences were observed in the frequency of HCC, as 20% of C57Bl/6N and 6% of 129sv animals develop HCC after rAAV treatment. An increase of HCC frequency did not correlate with their earlier onset after rAAV infection, as the HCC latency period in rAAV treated mice was similar as in control mice (17-21 months). In agreement with our study, Chandler and colleagues showed that rAAV-mediated gene therapy activates genotoxicity. They found that rAAV integrate into the Rian (RNA imprinted and accumulated in nucleus) locus, resulting in overexpression of microRNAs and retrotransposon-like 1 (Rtl1), leading to HCC formation (Chandler *et al.*, 2015). However, they described factors that may influence the frequency of HCC formation. They injected mice intrahepatically with 1×10^{11}GC to 2×10^{11}GC or 1×10^{9}GC to 1×10^{10}GC and revealed that there is a relationship between AAV dose and frequency of HCC following injection. They found that reducing AAV dose reduced the aggregate incidence of HCC at 22 months from 84% to 12%. Another factor that may trigger HCC formation is a promoter-driven therapeutic gene. They showed that AAV carrying a TBG or chicken β-actin (CBA) promoter developed HCC more frequently than those that contained a human alpha 1-antitrypsin (hAAT) promoter. Finally, they showed that the serotype may also modulate the hepatic tumour formation, as more mice presented HCC after treatment with AAV8 than after treatment with AAV2 (Chandler *et al.*, 2015). In light of these results, the dose of the virus as well as the serotype and promoter should be taken into consideration in future studies. Although Chandler and colleagues showed that the serotype 8 of AAV or usage of the TBG promoter are factors that increase genetoxicity, they only performed their analysis in mice with the C57Bl/6 background. Since I showed that background is a key factor that influences the HCC frequency - with C57Bl/6N mice developing HCC more frequently than

129sv mice (48% vs 14%) - a study of such factors as serotype, promoter or doses of the virus should be repeated in different mouse strains. From the non-malignant cause of death, the most frequent disease in the C57Bl/6N background was ulcerative dermatitis, whereby 18% animals from the group injected with rAAV and 18% from the group treated with PBS developed this disease. It is known from the literature that in some colonies from C57Bl/6N strain > 20% of animals may develop this skin lesion, while both the incidence and severity is higher in females (Kastenmayer *et al.*, 2006; Brayton, 2009; Hampton *et al.*, 2012). This trend was also observed in our colony (data not shown). Affected mice usually had pruritic leading to self-mutilation, disease progression and often euthanasia for ethical reasons. In the 129sv strain, the most frequent non-malignant causes of death were retrobulbar abscesses with periocular swelling and urinary track obstruction with stones localised in the bladder. There is no information concerning the incidence of the eye lesion in the 129sv strain. Since the frequency was higher in the rAAV treated group than PBS (20% vs 8%), it can indicate that the virus may have an influence on the development of the disease. By contrast, urinary obstruction has been already described in animals from the 129sv strain (Brayton, 2009). Typically, it occurs in males and is a frequent non-malignant contributor to death.

In conclusion, I have shown that the administration of rAAV2/8 carrying the MOCS2B therapeutic gene under the control of the TBG promoter can predispose to HCC formation, although the genetic background is a main factor that can influence the frequency of rAAV-mediated insertional mutagenesis and subsequent genotoxicity.

4.6   Perspectives

Therapies for most of the orphan diseases are challenging for the clinical study, given that the development of such therapy is extremely expensive and does not give sufficient profits for the pharmaceutical industry. A rAAV-based gene therapy seems a very promising tool for treatment of several diseases and it has been successfully used in many clinical trials, i.e. for haemophilia B (Hasbrouck and High, 2008), cystic fibrosis (Moss *et al.*, 2004) or Leber's congenital amaurosis (Simonelli *et al.*, 2010).

Deep knowledge about the exact expression of the *Mocs2* gene will help to improve the strategy used for therapy. To date, very little is known about the exact expression pattern

of *Mocs2* genes in the cell compartments. Although we showed that Mocs2 proteins are expressed in vesicle-like structures in the cytoplasm, an exact subcellular localisation should be performed. To identify the specific localisation of Mocs2 proteins, immunohistochemical analysis using a specific Mocs2 antibodies and organelle-specific marker antibodies should be conducted. This experiment can be performed for example in the neuronal cell line e.g. Neuro-2a or in liver sections.

In the present study, I established the knockout mouse model for the complete *Mocs2* gene. The most severe phenotype caused by *Mocs2* ablation was observed in the brain, kidney and skin. However, I was unable to point out the primary cause of the premature death of *Mocs2*$^{-/-}$ mice, given that damage occurring in one tissue may lead to a secondary effect in other organs, i.e. dehydration caused by impaired skin barrier can lead to stone formation in the urinary tract and parallel to kidney damage, resulting in decreased blood pressure, ischaemia and apoptosis in the brain. On the other hand, apoptosis in the brain can lead to kidney dysfunction, leading in turn to stone formation, etc. In future work, one should concentrate on the detailed characterisation of *Mocs2* knockout animals. To gain an overview of the general health condition of the knockout animals, basic examination of the blood and urine parameters should be performed. The analysis of the blood parameter should include the measurement of the blood activity of MoCo-dependent enzymes (aldehyde oxidase, xanthine oxidoreductase, sulphite oxidase and mitochondrial amidoxime reducing component (mARC), as well as level of liver transaminases (AST and ALT), triglycerides, glucose, total cholesterol, total protein, albumin and urea). Moreover, biochemical analysis of urine should include the specific gravity, pH, presence of proteins, bacteria, inflammatory markers, nitrite, ketones, leukocyte esterase, as well as the number of blood cells and the level of bilirubin, urobilinogen, sulphite, cystine, uric acid and xanthine. It will give the overall impression regarding the condition of all organs.

Thus far, we have taken a closer look at the brain and kidney. In future studies, a histopathological analysis of the liver should be conducted. Since all MoCo-dependent enzymes are expressed in the liver, a severe phenotype in this organ is also expected. Furthermore, precise skin analysis should be performed. HE staining followed by histopathological analysis will show changes in the skin morphology. Identification of

severe changes could suggest that the skin barrier may be disturbed in $Mocs2^{-/-}$ pups. To measure the epidermal permeability barrier (EPB), simple techniques that monitor the diffusion of dyes (X-Gal or Lucifer Yellow) through the upper epidermis and measurement of transepidermal water loss (TEWL) resulting from a defective skin barrier could be performed. Finally, studying the influence of *Mocs2* isoforms on mice fertility - especially in context of spermatogenesis - should be investigated. For this reason, a spermatogonial stem cell (SSC) culture from testis of $Mocs2^{-/-}$ mice should be established and transplanted to busulfan treated males. Busulfan treatment eliminates dividing cells from seminiferous tubules and only injected cells can colonise them. This technique is routinely used for testing the development potential of germ cells. After injection into recipient males, the spermatogenesis reconstitution should be investigated. Taking advantage of the LacZ reporter, one could easily identify cells derived from knockout mice.

Although we detected crystal-like structures in the kidney and bladder of $Mocs2^{-/-}$ mice during phenotypical characterisation, the biochemical analysis failed to describe the composition of these structures. The analysis should be repeated using combined samples from more $Mocs2^{-/-}$ animals.

To gain some ideas concerning whether *Mocs2* depletion is able to induce neuron apoptosis, the siRNA approach to knockdown the *Mocs2* gene in a neuronal cell line, e.g. Neuro-2a cells (ATCC), could be engaged. If *Mocs2* knockdown will not induce massive apoptosis of Neur-2a cells, it means that apoptosis is rather a secondary effect caused by damages observed in the skin or the kidney. In parallel, an inducible conditional *Mocs2* knockout could be generated. Activation of the Cre-recombination in adult $Mocs2^{flox/flox}$ mice followed by pathological analysis of the skin, kidney and brain could give a clue about which tissue is first affected. If the primary phenotype will be present in the kidney, the symptoms can be cured and the condition of the brain and skin can be investigated. Moreover, the premature death of $Mocs2^{-/-}$ mice can be a result of the general weak condition of knockout animals, which hinders access to milk. To check whether the animals have an appropriate food intake, the stomach content should be measured in comparison to the wild type littermates.

Gene therapy approaches for MoCo deficiency type B remain questionable due to the bicistronic structure of *Mocs2* genes. It is unknown whether re-expression of *Mocs2*

genes in trans-configuration will lead to the production of functional subunits of Mocs proteins and finally to the formation of a molybdopterin synthase complex. To investigate this, we decided to supplement both Mosc2a and Mocs2b subunits by crossing a *Mocs2* knockout with transgenic animals. For this reason, I generated transgenic mouse lines overexpressing human MOCS2A or MOCS2B proteins. I obtained a *MOCS2B* transgenic line and successfully created a double transgenic mouse line *Mocs2*[-/-, Tb/-] (or *Mocs2a*^{-/-}). As expected, double transgenic animals presented a similar phenotype to *Mocs2*^{-/-} mice and died within the first 9 days after birth. Surprisingly, the re-expression of the *MOCS2B* gene significantly improved the body weight and mean life span of *Mocs2*[-/-, Tb/-] pups. In light of this result, I speculate that the Mocs2b protein can execute another function, independent from the Mocs2a protein function. As mentioned in the introduction section, there are at least three isoforms of the *Mocs2b* gene leading to translation of two different proteins: with complete or truncated (Mocs2bΔ) products encoded by exon 5. The part of exon 5 that is missing in Mocs2bΔ isoform is a part of the catalytic domain of Mocs2b protein. Thus far, Mocs2bΔ protein has not been detected in mice. In future studies, the characterisation of the tissue distribution on the RNA and protein level and its potential function should be elucidated.

To rescue the phenotype of MoCo deficiency, double transgenic mice *Mocs2*[-/-, Tb/-] should be bred with a *MOCS2A* transgenic line. Since both established *MOCS2A* transgenic lines failed to express the transgene, generation of an additional *MOCS2A* transgenic line will be necessary. Furthermore, the *MOCS2A* mice should be crossed with *Mocs2* knockout mice to generate the isolated form of *Mocs2b* knockout (*Mocs2b*^{-/-}). For this model of the disease, we have already established a rAAV-based therapy.

In the long-term study performed on wild type animals, we have shown that the virus can efficiently transduce hepatocytes, whereby around 2% of cells express the MOCS2B-eGFP fusion protein at least 2 years after injection. However, the efficiency of this therapy must be elucidated in isolated form of *Mocs2b* knockout. The process of transgenic line generation as well as the breeding of animals is time-consuming experiment. Since the isolated knockout of *Mocs2a* isoform has already been established, the viral particles encoding *MOCS2A* should be generated to check whether the design viral therapy will rescue the phenotype. Another possibility is viral treatment of complete *Mocs2*^{-/-} mice,

although the virus encoding both Mocs2a and Mocs2b proteins is required. Essentially, these proteins are encoded from two different yet overlapping open reading frames (ORF). One option to produce two distinct proteins from the transcript delivered by the virus is to use a 2A peptide-based strategy for the therapeutic gene designing (Szymczak and Vignali, 2005). The 2A peptide is a self-processing peptide from the Foot-and-Mouth Disease Virus (FMDV). These peptides allow multiple proteins to be encoded as polyproteins, which dissociate into component proteins on translation. Using this technique, it will be possible to express both subunits of Mocs2 proteins from a single vector.

In a final step, the phenotypical analyses of *Mocs1* knockout animals in the context of the phenotype identified in *Mocs2* knockout animals should be performed. In a previous study it was shown that the *Mocs1* deficient mice die at postnatal day 0-11 and presented a phenotype with growth retardation, as well as curly whiskers. However, the histological analysis of the brain in *Mocs1* deficient mice did not reveal any abnormalities. Because only nuclear staining of neuronal tissue of *Mocs1* deficient mice was used in the previous study, precise immunohistochemical analyses of the brain as well as all other organs should be conducted and compared to the phenotype observed in *Mocs2* deficient mice.

5   SUMMARY

Main aims of this study were the generation of a mouse model for the molybdenum cofactor deficiency type B disease as well as the development of a potential recombinant adeno-associated virus (rAAV) gene therapy approach. The molybdenum cofactor deficiency type B disease occurs as a result of an impairment in the second step of the molybdenum cofactor (MoCo) biosynthesis pathway, including mutations in the *MOCS2A*, *MOCS2B* or *MOCS3* genes (to date, no mutations have been found in the *MOCS3* gene) (Reiss *et al.*, 1999; Reiss and Hahnewald, 2011). Thus far, 26 cases of MoCo deficiency type B have been reported worldwide (HGMD Professional 2015.1). In 12 of these patients, the *MOCS2A* gene was mutated and in the rest of the patients the *MOCS2B* gene was affected. Accordingly, we decided to generate a knockout mouse model for the murine *Mocs2b* gene (*Mocs2b$^{-/-}$*). In the first trial, *Mocs2b* knockout was generated using commercially available mouse embryonic stem cells (ESCs), in which one copy of the *Mocs2b* gene was targeted by a knockout first construct. Although ESC injections into C57Bl/6N blastocysts gave rise to chimeras, they did not transmit the knockout allele to the progeny. To overcome this problem, a knockout model of the entire mouse *Mocs2* gene was established. In this model, both *Mocs2a* and *Mocs2b* isoforms were deleted. Although *Mocs2$^{-/-}$* mice were born in accordance with the Mendelian ratio and appeared normal at birth, a few hours later the body weights of *Mocs2$^{-/-}$* mice were significantly reduced compared to their heterozygous (*Mocs2$^{+/-}$*) and WT (*Mocs2$^{+/+}$*) littermates. Moreover, during the first days of life, *Mocs2$^{-/-}$* mice increased their body weights at a significantly slower rate than their WT and heterozygous littermates. Additionally, *Mocs2$^{-/-}$* mice presented skin problems, a defect in the overall hair growth and generally they were in a weaker health condition than *Mocs2$^{+/+}$* and *Mocs2$^{+/-}$* pups. The *Mocs2$^{-/-}$* animals died within 12 days after birth with a mean survival rate of 4.7 days. To select for potential tissues affected by the depletion of *Mocs2a/b* isoforms, *Mocs2a/b* expression analyses in different tissues of WT animals were performed. The results revealed ubiquitous expression of *Mocs2a/b* isoforms, with the highest expression levels detected in the mouse skin, liver, brain, lung and kidney. These findings can partially explain the skin phenotype observed in *Mocs2$^{-/-}$* pups. Similar correlations were identified in the kidney and brain. All *Mocs2$^{-/-}$* pups presented a urinary retention caused by the

accumulation of yellow deposits in the bladder. The histological analysis of kidneys derived from *Mocs2*$^{-/-}$ mice demonstrated the presence of crystals in the collecting duct system. Urine analysis revealed an elevated level of sulphite, proteins and extremely high concentrations of haemoglobin and/or damaged erythrocytes. The histopathological analysis of the brain showed severe neuronal apoptosis in the hippocampus, cortex and brainstem of *Mocs2*$^{-/-}$ mice. Despite being reduced as compared to the *Mocs2*$^{-/-}$ animals, *Mocs2*$^{+/-}$ mice also presented a statistical significant number of apoptotic neurons in the aforementioned brain regions, although *Mocs2*$^{+/-}$ animals developed normally and were fertile. I speculate that depletion of *Mocs2* genes has a direct effect on the normal function of tissues presenting with high *Mocs2a/b* expression levels. In order to rescue the phenotype of *Mocs2*$^{-/-}$ mice, we decided to supplement missing proteins Mocs2a and Mocs2b through a transgenic mouse approach. For this reason, two different transgenic mouse lines expressing either the *MOCS2A* or the *MOCS2B* isoform were generated. The rescue experiment was designed to check whether both subunits expressed in trans-configuration are able to form a functional complex. On the other hand, the generation of separate transgenic lines for *MOCS2A* and *MOCS2B* isoforms offered the possibility to breed them with *Mocs2*$^{-/-}$ mice and generate a pure knockout model for each isoform. The isolated knockout of either the *Mocs2a* or *Mocs2b* isoform could further serve as a model for testing a potential therapy approach. Unfortunately, due to several problems with transgenic *MOCS2A* mouse lines, it was not possible to create a rescue model for *Mocs2b*$^{-/-}$ knockout animals. To date, *MOCS2B* transgenic mice were successfully generated and subsequently bred with *Mocs2*$^{+/-}$ mice, giving rise to a mouse line corresponding to a knockout of the *Mocs2a* isoform. As expected, supplementation of *Mocs2*$^{-/-}$ mice with the transgenic MOCS2B protein (*Mocs2*$^{-/-, Tb/-}$ mice) did not rescue the phenotype of *Mocs2*$^{-/-}$ mice, although the body weight of *Mocs2*$^{-/-, Tb/-}$ pups and their mean life span significantly increased compared to their *Mocs2*$^{-/-}$ littermates. In parallel to the generation of an isolated form of the *Mocs2* knockout model, a potential gene therapy approach was developed. Among many available vectors, we decided to use the recombinant adeno-associated virus (rAAV)-based vector system. rAAVs are currently among the most frequently used viral vectors for gene therapy approaches. We used the viral particles with serotype 2/8 encoding either the human MOCS2B protein or the

MOCS2B-EGFP fusion protein under the control of the liver-specific *thyroxine-binding globulin (*TBG) promoter. The virus was administered via intrahepatic injection, as we showed that this route results in the highest transduction efficiency. Using this system, we were able to transduce approximately 2-7% of mouse liver cells and maintain *MOCS2B* transgene expression for at least two years after a single injection into the mouse liver. In agreement with previous results, infection with rAAV2/8TBG-MOCS2B-STOP-eGFP3 did not rescue the phenotype of *Mocs2*$^{-/-}$ mice, but it was sufficient to increase the body weight of *Mocs2* knockout pups after birth and prolong the mean life span of *Mocs2*$^{-/-}$ mice to 8 ± 0.7 days. Using a long-term study, we also investigated the potential malignancy risk of a viral-based gene therapy approach. We could demonstrate that the presence of tumours - and particularly hepatocellular carcinomas (HCC) - was mouse strain-specific, because HCC occurred more frequently in C57Bl/6N mice compared to the 129sv mouse strain. Moreover, only in C57Bl/6N mice did rAAV administration into the liver significantly increase the incidence of HCC compared to control animals treated with PBS.

6   LITERATURE

Abadeh, S., Killacky, J., Benboubetra, M., and Harrison, R. (1992). Purification and partial characterization of xanthine oxidase from human milk. Biochim Biophys Acta *1117*, 25-32.

Acland, G.M., Aguirre, G.D., Bennett, J., Aleman, T.S., Cideciyan, A.V., Bennicelli, J., Dejneka, N.S., Pearce-Kelling, S.E., Maguire, A.M., Palczewski, K., Hauswirth, W.W., and Jacobson, S.G. (2005). Long-term restoration of rod and cone vision by single dose rAAV-mediated gene transfer to the retina in a canine model of childhood blindness. Mol Ther *12*, 1072-1082.

Al-Salmy, H.S. (2002). Inter-strain variability in aldehyde oxidase activity in the mouse. Comp Biochem Physiol C Toxicol Pharmacol *132*, 341-347.

Angermuller, S., Bruder, G., Volkl, A., Wesch, H., and Fahimi, H.D. (1987). Localization of xanthine oxidase in crystalline cores of peroxisomes. A cytochemical and biochemical study. Eur J Cell Biol *45*, 137-144.

Appignani, B.A., Kaye, E.M., and Wolpert, S.M. (1996). CT and MR appearance of the brain in two children with molybdenum cofactor deficiency. AJNR Am J Neuroradiol *17*, 317-320.

Arenas, M., Fairbanks, L.D., Vijayakumar, K., Carr, L., Escuredo, E., and Marinaki, A.M. (2009). An unusual genetic variant in the MOCS1 gene leads to complete missplicing of an alternatively spliced exon in a patient with molybdenum cofactor deficiency. J Inherit Metab Dis *32*, 560-569.

Atchison, R.W., Casto, B.C., and Hammon, W.M. (1965). Adenovirus-Associated Defective Virus Particles. Science *149*, 754-756.

Auscher, C., Amory, N., van der Kemp, P., and Delbarre, F. (1979). Xanthine oxidase activity in human intestines. Histochemical and radiochemical study. Adv Exp Med Biol *122B*, 197-201.

Baba, T., Damke, H., Hinshaw, J.E., Ikeda, K., Schmid, S.L., and Warnock, D.E. (1995). Role of dynamin in clathrin-coated vesicle formation. Cold Spring Harb Symp Quant Biol *60*, 235-242.

Balague, C., Kalla, M., and Zhang, W.W. (1997). Adeno-associated virus Rep78 protein and terminal repeats enhance integration of DNA sequences into the cellular genome. J Virol *71*, 3299-3306.

Basheer, S.N., Waters, P.J., Lam, C.W., Acquaviva-Bourdain, C., Hendson, G., Poskitt, K., and Hukin, J. (2007). Isolated sulfite oxidase deficiency in the newborn: lactic acidaemia and leukoencephalopathy. Neuropediatrics *38*, 38-41.

Beedham, C. (1985). Molybdenum hydroxylases as drug-metabolizing enzymes. Drug Metab Rev *16*, 119-156.

Beer, S., Bellovin, D.I., Lee, J.S., Komatsubara, K., Wang, L.S., Koh, H., Borner, K., Storm, T.A., Davis, C.R., Kay, M.A., Felsher, D.W., and Grimm, D. (2010). Low-level shRNA cytotoxicity can contribute to MYC-induced hepatocellular carcinoma in adult mice. Mol Ther *18*, 161-170.

Bell, P., Wang, L., Lebherz, C., Flieder, D.B., Bove, M.S., Wu, D., Gao, G.P., Wilson, J.M., and Wivel, N.A. (2005). No evidence for tumorigenesis of AAV vectors in a large-scale study in mice. Mol Ther *12*, 299-306.

Bittner, F., Oreb, M., and Mendel, R.R. (2001). ABA3 is a molybdenum cofactor sulfurase required for activation of aldehyde oxidase and xanthine dehydrogenase in Arabidopsis thaliana. J Biol Chem *276*, 40381-40384.

Blackwell, B.N., Bucci, T.J., Hart, R.W., and Turturro, A. (1995). Longevity, body weight, and neoplasia in ad libitum-fed and diet-restricted C57BL6 mice fed NIH-31 open formula diet. Toxicol Pathol *23*, 570-582.

Blomhoff, R., Blomhoff, H.K., Tolleshaug, H., Christensen, T.B., and Berg, T. (1985). Uptake and degradation of bovine testes beta-galactosidase by parenchymal and nonparenchymal rat liver cells. Int J Biochem *17*, 1321-1328.

Bortels, H. (1930). Molybdan als Katalysator bei der biologischen Stickstoffbindung. Archiv für Mikrobiologie *1*, 333-342.

Boutin, S., Monteilhet, V., Veron, P., Leborgne, C., Benveniste, O., Montus, M.F., and Masurier, C. (2010). Prevalence of serum IgG and neutralizing factors against adeno-associated virus (AAV) types 1, 2, 5, 6, 8, and 9 in the healthy population: implications for gene therapy using AAV vectors. Hum Gene Ther *21*, 704-712.

Bradford, M.M. (1976). A rapid and sensitive method for the quantitation of microgram quantities of protein utilizing the principle of protein-dye binding. Anal Biochem *72*, 248-254.

Brayton, C. (2009). Spontaneous Diseases in Commonly Used Mouse Strains/Stocks.

Brockstedt, D.G., Podsakoff, G.M., Fong, L., Kurtzman, G., Mueller-Ruchholtz, W., and Engleman, E.G. (1999). Induction of immunity to antigens expressed by recombinant adeno-associated virus depends on the route of administration. Clin Immunol *92*, 67-75.

Buchlis, G., Podsakoff, G.M., Radu, A., Hawk, S.M., Flake, A.W., Mingozzi, F., and High, K.A. (2012). Factor IX expression in skeletal muscle of a severe hemophilia B patient 10 years after AAV-mediated gene transfer. Blood *119*, 3038-3041.

Calcedo, R., Morizono, H., Wang, L., McCarter, R., He, J., Jones, D., Batshaw, M.L., and Wilson, J.M. (2011). Adeno-associated virus antibody profiles in newborns, children, and adolescents. Clin Vaccine Immunol *18*, 1586-1588.

Carmi-Nawi, N., Malinger, G., Mandel, H., Ichida, K., Lerman-Sagie, T., and Lev, D. (2011). Prenatal brain disruption in molybdenum cofactor deficiency. J Child Neurol *26*, 460-464.

Cartlidge, P. (2000). The epidermal barrier. Semin Neonatol *5*, 273-280.

Chandler, R.J., LaFave, M.C., Varshney, G.K., Trivedi, N.S., Carrillo-Carrasco, N., Senac, J.S., Wu, W., Hoffmann, V., Elkahloun, A.G., Burgess, S.M., and Venditti, C.P. (2015). Vector design influences hepatic genotoxicity after adeno-associated virus gene therapy. J Clin Invest *125*, 870-880.

Chung, H.Y., Baek, B.S., Song, S.H., Kim, M.S., Huh, J.I., Shim, K.H., Kim, K.W., and Lee, K.H. (1997). Xanthine dehydrogenase/xanthine oxidase and oxidative stress. Age (Omaha) *20*, 127-140.

Clark, K.R., Sferra, T.J., Lo, W., Qu, G., Chen, R., and Johnson, P.R. (1999). Gene transfer into the CNS using recombinant adeno-associated virus: analysis of vector DNA forms resulting in sustained expression. Journal of drug targeting *7*, 269-283.

Cohen, H.J., Betcher-Lange, S., Kessler, D.L., and Rajagopalan, K.V. (1972). Hepatic sulfite oxidase. Congruency in mitochondria of prosthetic groups and activity. J Biol Chem *247*, 7759-7766.

Cohen, H.J., Fridovich, I., and Rajagopalan, K.V. (1971). Hepatic sulfite oxidase. A functional role for molybdenum. J Biol Chem *246*, 374-382.

Cordier, L., Gao, G.P., Hack, A.A., McNally, E.M., Wilson, J.M., Chirmule, N., and Sweeney, H.L. (2001). Muscle-specific promoters may be necessary for adeno-associated virus-mediated gene transfer in the treatment of muscular dystrophies. Hum Gene Ther *12*, 205-215.

Cunningham, S.C., Dane, A.P., Spinoulas, A., Logan, G.J., and Alexander, I.E. (2008). Gene delivery to the juvenile mouse liver using AAV2/8 vectors. Mol Ther *16*, 1081-1088.

Daniels, J.N., Wuebbens, M.M., Rajagopalan, K.V., and Schindelin, H. (2008). Crystal structure of a molybdopterin synthase-precursor Z complex: insight into its sulfur transfer mechanism and its role in molybdenum cofactor deficiency. Biochemistry *47*, 615-626.

Davalos, D., Grutzendler, J., Yang, G., Kim, J.V., Zuo, Y., Jung, S., Littman, D.R., Dustin, M.L., and Gan, W.B. (2005). ATP mediates rapid microglial response to local brain injury in vivo. Nat Neurosci *8*, 752-758.

Daya, S., and Berns, K.I. (2008). Gene therapy using adeno-associated virus vectors. Clin Microbiol Rev *21*, 583-593.

De Renzo, E.C., Heytler, P.G., and Kaleita, E. (1954). Further evidence that molybdenum is a cofactor of Xanthine oxidase. Arch Biochem Biophys *49*, 242-244.

Dent, C.E., and Philpot, G.R. (1954). Xanthinuria, an inborn error (or deviation) of metabolism. Lancet *266*, 182-185.

Donsante, A., Miller, D.G., Li, Y., Vogler, C., Brunt, E.M., Russell, D.W., and Sands, M.S. (2007). AAV vector integration sites in mouse hepatocellular carcinoma. Science *317*, 477.

Douar, A.M., Poulard, K., Stockholm, D., and Danos, O. (2001). Intracellular trafficking of adeno-associated virus vectors: routing to the late endosomal compartment and proteasome degradation. J Virol *75*, 1824-1833.

Drinkwater, N.R., and Ginsler, J.J. (1986). Genetic control of hepatocarcinogenesis in C57BL/6J and C3H/HeJ inbred mice. Carcinogenesis *7*, 1701-1707.

Eagleson, M. (1993). Concise Encyclopedia Chemistry. de Gruyter.

Eimer, W.A., and Vassar, R. (2013). Neuron loss in the 5XFAD mouse model of Alzheimer's disease correlates with intraneuronal Abeta42 accumulation and Caspase-3 activation. Mol Neurodegener *8*, 2.

Endres, W., Shin, Y.S., Gunther, R., Ibel, H., Duran, M., and Wadman, S.K. (1988). Report on a new patient with combined deficiencies of sulphite oxidase and xanthine dehydrogenase due to molybdenum cofactor deficiency. Eur J Pediatr *148*, 246-249.

Escors, D., and Breckpot, K. (2010). Lentiviral vectors in gene therapy: their current status and future potential. Arch Immunol Ther Exp (Warsz) *58*, 107-119.

Fadel, S., and Sarzotti, M. (2000). Cellular immune responses in neonates. Int Rev Immunol *19*, 173-193.

Fay, A.W., Hu, Y., Schmid, B., and Ribbe, M.W. (2007). Molecular insights into nitrogenase FeMoco insertion--the role of His 274 and His 451 of MoFe protein alpha subunit. J Inorg Biochem *101*, 1630-1641.

Feng, G., Tintrup, H., Kirsch, J., Nichol, M.C., Kuhse, J., Betz, H., and Sanes, J.R. (1998). Dual requirement for gephyrin in glycine receptor clustering and molybdoenzyme activity. Science *282*, 1321-1324.

Flageul, M., Aubert, D., Pichard, V., Nguyen, T.H., Nowrouzi, A., Schmidt, M., and Ferry, N. (2009). Transient expression of genes delivered to newborn rat liver using recombinant adeno-associated virus 2/8 vectors. J Gene Med *11*, 689-696.

Flotte, T.R., and Ferkol, T.W. (1997). Genetic therapy. Past, present, and future. Pediatr Clin North Am *44*, 153-178.

Franke, A.-C. (2014). Phänotyp der Molybdän-Cofaktor-Defizienz Typ B bei Patienten und im Tiermodell. Bachelor thesis, Georg-August University, Goettingen.

Frederiks, W.M., and Vreeling-Sindelarova, H. (2002). Ultrastructural localization of xanthine oxidoreductase activity in isolated rat liver cells. Acta Histochem *104*, 29-37.

Gao, G.P., Alvira, M.R., Wang, L., Calcedo, R., Johnston, J., and Wilson, J.M. (2002). Novel adeno-associated viruses from rhesus monkeys as vectors for human gene therapy. Proc Natl Acad Sci U S A *99*, 11854-11859.

Garattini, E., Fratelli, M., and Terao, M. (2008). Mammalian aldehyde oxidases: genetics, evolution and biochemistry. Cell Mol Life Sci *65*, 1019-1048.

Garattini, E., and Terao, M. (2012). The role of aldehyde oxidase in drug metabolism. Expert Opin Drug Metab Toxicol *8*, 487-503.

Gargah, T., Essid, A., Labassi, A., Hamzaoui, M., and Lakhoua, M.R. (2010). Xanthine urolithiasis. Saudi J Kidney Dis Transpl *21*, 328-331.

Gasber, A., Klaumann, S., Trentmann, O., Trampczynska, A., Clemens, S., Schneider, S., Sauer, N., Feifer, I., Bittner, F., Mendel, R.R., and Neuhaus, H.E. (2011). Identification of an Arabidopsis solute carrier critical for intracellular transport and inter-organ allocation of molybdate. Plant Biol (Stuttg) *13*, 710-718.

Gauttier, V., Pichard, V., Aubert, D., Kaeppel, C., Schmidt, M., Ferry, N., and Conchon, S. (2013). No tumour-initiating risk associated with scAAV transduction in newborn rat liver. Gene Ther *20*, 779-784.

Gershoni, J.M., and Palade, G.E. (1982). Electrophoretic transfer of proteins from sodium dodecyl sulfate-polyacrylamide gels to a positively charged membrane filter. Anal Biochem *124*, 396-405.

Ginhoux, F., Lim, S., Hoeffel, G., Low, D., and Huber, T. (2013). Origin and differentiation of microglia. Front Cell Neurosci *7*, 45.

Goncalves, M.A. (2005). Adeno-associated virus: from defective virus to effective vector. Virol J *2*, 43.

Graf, W.D., Oleinik, O.E., Jack, R.M., Weiss, A.H., and Johnson, J.L. (1998). Ahomocysteinemia in molybdenum cofactor deficiency. Neurology *51*, 860-862.

Grieger, J.C., and Samulski, R.J. (2005). Adeno-associated virus as a gene therapy vector: vector development, production and clinical applications. Adv Biochem Eng Biotechnol *99*, 119-145.

Grimm, D., and Kay, M.A. (2003). From virus evolution to vector revolution: use of naturally occurring serotypes of adeno-associated virus (AAV) as novel vectors for human gene therapy. Curr Gene Ther *3*, 281-304.

Grimm, D., Kern, A., Rittner, K., and Kleinschmidt, J.A. (1998). Novel tools for production and purification of recombinant adenoassociated virus vectors. Hum Gene Ther *9*, 2745-2760.

Grings, M., Moura, A.P., Amaral, A.U., Parmeggiani, B., Gasparotto, J., Moreira, J.C., Gelain, D.P., Wyse, A.T., Wajner, M., and Leipnitz, G. (2014). Sulfite disrupts brain mitochondrial energy homeostasis and induces mitochondrial permeability transition pore opening via thiol group modification. Biochim Biophys Acta *1842*, 1413-1422.

Hagen, W.R. (2011). Cellular uptake of molybdenum and tungsten. . Coordination Chemistry Reviews
255.

Hahnewald, R. (2009). Tiermodelle der Molybdän-Cofaktor-Defizienz und ihre Therapie Universität in Köln.

Hahnewald, R., Wegner, W., and Reiss, J. (2009). AAV-mediated gene therapy for metabolic diseases: dosage and reapplication studies in the molybdenum cofactor deficiency model. Genet Vaccines Ther *7*, 9.

Halbert, C.L., Rutledge, E.A., Allen, J.M., Russell, D.W., and Miller, A.D. (2000). Repeat transduction in the mouse lung by using adeno-associated virus vectors with different serotypes. J Virol *74*, 1524-1532.

Hampton, A.L., Hish, G.A., Aslam, M.N., Rothman, E.D., Bergin, I.L., Patterson, K.A., Naik, M., Paruchuri, T., Varani, J., and Rush, H.G. (2012). Progression of ulcerative dermatitis lesions in C57BL/6Crl mice and the development of a scoring system for dermatitis lesions. J Am Assoc Lab Anim Sci *51*, 586-593.

Hanahan, D. (1983). Studies on transformation of Escherichia coli with plasmids. J Mol Biol *166*, 557-580.

Hanzelmann, P., Hernandez, H.L., Menzel, C., Garcia-Serres, R., Huynh, B.H., Johnson, M.K., Mendel, R.R., and Schindelin, H. (2004). Characterization of MOCS1A, an oxygen-sensitive iron-sulfur protein involved in human molybdenum cofactor biosynthesis. J Biol Chem *279*, 34721-34732.

Hartmann, T., Terao, M., Garattini, E., Teutloff, C., Alfaro, J.F., Jones, J.P., and Leimkuhler, S. (2012). The impact of single nucleotide polymorphisms on human aldehyde oxidase. Drug Metab Dispos *40*, 856-864.

Hasbrouck, N.C., and High, K.A. (2008). AAV-mediated gene transfer for the treatment of hemophilia B: problems and prospects. Gene Ther *15*, 870-875.

Havemeyer, A., Grunewald, S., Wahl, B., Bittner, F., Mendel, R., Erdelyi, P., Fischer, J., and Clement, B. (2014). Reduction of N-hydroxy-sulfonamides, including N-hydroxy-valdecoxib, by the molybdenum-containing enzyme mARC. Drug Metab Dispos *38*, 1917-1921.

Hedrich, H. (2004). The Laboratory Mouse. Elsevier Academic Press.

Heidenreich, T., Wollers, S., Mendel, R.R., and Bittner, F. (2005). Characterization of the NifS-like domain of ABA3 from Arabidopsis thaliana provides insight into the mechanism of molybdenum cofactor sulfuration. J Biol Chem *280*, 4213-4218.

Hermonat, P.L., and Muzyczka, N. (1984). Use of adeno-associated virus as a mammalian DNA cloning vector: transduction of neomycin resistance into mammalian tissue culture cells. Proc Natl Acad Sci U S A *81*, 6466-6470.

Hille, R., and Nishino, T. (1995). Flavoprotein structure and mechanism. 4. Xanthine oxidase and xanthine dehydrogenase. FASEB J *9*, 995-1003.

Hille, R., Nishino, T., and Bittner, F. (2011). Molybdenum enzymes in higher organisms. Coord Chem Rev *255*, 1179-1205.

Hinshaw, J.E., and Schmid, S.L. (1995). Dynamin self-assembles into rings suggesting a mechanism for coated vesicle budding. Nature *374*, 190-192.

House, A.A., and Cattran, D.C. (2002). Nephrology: 2. Evaluation of asymptomatic hematuria and proteinuria in adult primary care. CMAJ *166*, 348-353.

Hu, C., and Lipshutz, G.S. (2012). AAV-based neonatal gene therapy for hemophilia A: long-term correction and avoidance of immune responses in mice. Gene Ther *19*, 1166-1176.

Hu, H., Gomero, E., Bonten, E., Gray, J.T., Allay, J., Wu, Y., Wu, J., Calabrese, C., Nienhuis, A., and d'Azzo, A. (2012). Preclinical dose-finding study with a liver-tropic, recombinant AAV-2/8 vector in the mouse model of galactosialidosis. Mol Ther *20*, 267-274.

Huttner, N.A. (2003). Adeno-associated virus type 2 as vector for human gene therapy: Characterization of virus-host interactions Ludwig-Maximilians-Universität München.

Iadecola, C., and Alexander, M. (2001). Cerebral ischemia and inflammation. Curr Opin Neurol *14*, 89-94.

Ichida, K., Amaya, Y., Okamoto, K., and Nishino, T. (2012). Mutations associated with functional disorder of xanthine oxidoreductase and hereditary xanthinuria in humans. Int J Mol Sci *13*, 15475-15495.

Ichida, K., Matsumura, T., Sakuma, R., Hosoya, T., and Nishino, T. (2001). Mutation of human molybdenum cofactor sulfurase gene is responsible for classical xanthinuria type II. Biochem Biophys Res Commun *282*, 1194-1200.

Inagaki, K., Lewis, S.M., Wu, X., Ma, C., Munroe, D.J., Fuess, S., Storm, T.A., Kay, M.A., and Nakai, H. (2007). DNA palindromes with a modest arm length of greater, similar 20 base pairs are a significant target for recombinant adeno-associated virus vector integration in the liver, muscles, and heart in mice. J Virol *81*, 11290-11303.

Iravani, O., Tay, E.W., Bay, B.H., and Ng, Y.K. (2014). Unilateral ureteric stone associated with gross hydronephrosis and kidney shrinkage: a cadaveric report. Anat Cell Biol *47*, 267-270.

Ito, D., Tanaka, K., Suzuki, S., Dembo, T., and Fukuuchi, Y. (2001). Enhanced expression of Iba1, ionized calcium-binding adapter molecule 1, after transient focal cerebral ischemia in rat brain. Stroke *32*, 1208-1215.

Jakobs, H.H., Mikula, M., Havemeyer, A., Strzalkowska, A., Borowa-Chmielak, M., Dzwonek, A., Gajewska, M., Hennig, E.E., Ostrowski, J., and Clement, B. (2014). The N-reductive system composed of mitochondrial amidoxime reducing component (mARC), cytochrome b5 (CYB5B) and cytochrome b5 reductase (CYB5R) is regulated by fasting and high fat diet in mice. PLoS One *9*, e105371.

Jeruc, J., Vizjak, A., Rozman, B., and Ferluga, D. (2006). Immunohistochemical expression of activated caspase-3 as a marker of apoptosis in glomeruli of human lupus nephritis. Am J Kidney Dis *48*, 410-418.

Johnson, J.L. (2003). Prenatal diagnosis of molybdenum cofactor deficiency and isolated sulfite oxidase deficiency. Prenat Diagn *23*, 6-8.

Johnson, J.L., Coyne, K.E., Rajagopalan, K.V., Van Hove, J.L., Mackay, M., Pitt, J., and Boneh, A. (2001). Molybdopterin synthase mutations in a mild case of molybdenum cofactor deficiency. Am J Med Genet *104*, 169-173.

Kaji, E.H., and Leiden, J.M. (2001). Gene and stem cell therapies. JAMA *285*, 545-550.

Kastenmayer, R.J., Fain, M.A., and Perdue, K.A. (2006). A retrospective study of idiopathic ulcerative dermatitis in mice with a C57BL/6 background. J Am Assoc Lab Anim Sci *45*, 8-12.

Kaufholdt, D., Gehl, C., Geisler, M., Jeske, O., Voedisch, S., Ratke, C., Bollhoner, B., Mendel, R.R., and Hansch, R. (2013). Visualization and quantification of protein interactions in the biosynthetic pathway of molybdenum cofactor in Arabidopsis thaliana. J Exp Bot *64*, 2005-2016.

King, J.A., Dubielzig, R., Grimm, D., and Kleinschmidt, J.A. (2001). DNA helicase-mediated packaging of adeno-associated virus type 2 genomes into preformed capsids. EMBO J *20*, 3282-3291.

Kitamura, S., Sugihara, K., Nakatani, K., Ohta, S., Ohhara, T., Ninomiya, S., Green, C.E., and Tyson, C.A. (1999). Variation of hepatic methotrexate 7-hydroxylase activity in animals and humans. IUBMB Life *48*, 607-611.

Kitamura, S., Sugihara, K., and Ohta, S. (2006). Drug-metabolizing ability of molybdenum hydroxylases. Drug Metab Pharmacokinet *21*, 83-98.

Klein, J.M., Busch, J.D., Potting, C., Baker, M.J., Langer, T., and Schwarz, G. (2012). The mitochondrial amidoxime-reducing component (mARC1) is a novel signal-anchored protein of the outer mitochondrial membrane. J Biol Chem *287*, 42795-42803.

Kocamaz, E., Adiguzel, E., Er, B., Gundogdu, G., and Kucukatay, V. (2012). Sulfite leads to neuron loss in the hippocampus of both normal and SOX-deficient rats. Neurochem Int *61*, 341-346.

Kramer, S.P., Johnson, J.L., Ribeiro, A.A., Millington, D.S., and Rajagopalan, K.V. (1987). The structure of the molybdenum cofactor. Characterization of di-(carboxamidomethyl)molybdopterin from sulfite oxidase and xanthine oxidase. J Biol Chem *262*, 16357-16363.

Krompholz, N., Krischkowski, C., Reichmann, D., Garbe-Schonberg, D., Mendel, R.R., Bittner, F., Clement, B., and Havemeyer, A. (2012). The mitochondrial Amidoxime Reducing Component (mARC) is involved in detoxification of N-hydroxylated base analogues. Chem Res Toxicol *25*, 2443-2450.

Kucera, J., Bulkova, T., Rychla, R., and Jahn, P. (1997). Bilateral xanthine nephrolithiasis in a dog. J Small Anim Pract *38*, 302-305.

Kugler, S., Hahnewald, R., Garrido, M., and Reiss, J. (2007). Long-term rescue of a lethal inherited disease by adeno-associated virus-mediated gene transfer in a mouse model of molybdenum-cofactor deficiency. Am J Hum Genet *80*, 291-297.

Kurosaki, M., Bolis, M., Fratelli, M., Barzago, M.M., Pattini, L., Perretta, G., Terao, M., and Garattini, E. (2013). Structure and evolution of vertebrate aldehyde oxidases: from gene duplication to gene suppression. Cell Mol Life Sci *70*, 1807-1830.

Kurosaki, M., Terao, M., Barzago, M.M., Bastone, A., Bernardinello, D., Salmona, M., and Garattini, E. (2004). The aldehyde oxidase gene cluster in mice and rats. Aldehyde oxidase homologue 3, a novel member of the molybdo-flavoenzyme family with selective expression in the olfactory mucosa. J Biol Chem *279*, 50482-50498.

Lai, C.M., Lai, Y.K., and Rakoczy, P.E. (2002). Adenovirus and adeno-associated virus vectors. DNA Cell Biol *21*, 895-913.

Lam, C.W., Li, C.K., Lai, C.K., Tong, S.F., Chan, K.Y., Ng, G.S., Yuen, Y.P., Cheng, A.W., and Chan, Y.W. (2002). DNA-based diagnosis of isolated sulfite oxidase deficiency by denaturing high-performance liquid chromatography. Mol Genet Metab *75*, 91-95.

Landers, M., Haidarliu, S., and Philip Zeigler, H. (2006). Development of rodent macrovibrissae: effects of neonatal whisker denervation and bilateral neonatal enucleation. Somatosens Mot Res *23*, 11-17.

Landreth, K.S. (2002). Critical windows in development of the rodent immune system. Hum Exp Toxicol *21*, 493-498.

Laurence, J.M., Wang, C., Zheng, M., Cunningham, S., Earl, J., Tay, S.S., Allen, R.D., McCaughan, G.W., Alexander, I.E., Bishop, G.A., and Sharland, A.F. (2009). Overexpression of indoleamine dioxygenase in rat liver allografts using a high-efficiency adeno-associated virus vector does not prevent acute rejection. Liver Transpl *15*, 233-241.

Lee, H. (2003). Functional Analysis of the Murine Genes, *MOCS1* and *Sox15*, Georg-August University, Göttingen.

Lee, H.J., Adham, I.M., Schwarz, G., Kneussel, M., Sass, J.O., Engel, W., and Reiss, J. (2002). Molybdenum cofactor-deficient mice resemble the phenotype of human patients. Hum Mol Genet *11*, 3309-3317.

Lee, J.M., Grabb, M.C., Zipfel, G.J., and Choi, D.W. (2000). Brain tissue responses to ischemia. J Clin Invest *106*, 723-731.

Li, H., Malani, N., Hamilton, S.R., Schlachterman, A., Bussadori, G., Edmonson, S.E., Shah, R., Arruda, V.R., Mingozzi, F., Wright, J.F., Bushman, F.D., and High, K.A. (2011). Assessing the potential for AAV vector genotoxicity in a murine model. Blood *117*, 3311-3319.

Linden, R.M., Ward, P., Giraud, C., Winocour, E., and Berns, K.I. (1996). Site-specific integration by adeno-associated virus. Proc Natl Acad Sci U S A *93*, 11288-11294.

Llamas, A., Mendel, R.R., and Schwarz, G. (2004). Synthesis of adenylated molybdopterin: an essential step for molybdenum insertion. J Biol Chem *279*, 55241-55246.

Llamas, A., Otte, T., Multhaup, G., Mendel, R.R., and Schwarz, G. (2006). The Mechanism of nucleotide-assisted molybdenum insertion into molybdopterin. A novel route toward metal cofactor assembly. J Biol Chem *281*, 18343-18350.

LoDuca, P.A., Hoffman, B.E., and Herzog, R.W. (2009). Hepatic gene transfer as a means of tolerance induction to transgene products. Curr Gene Ther *9*, 104-114.

Macaya, A., Brunso, L., Fernandez-Castillo, N., Arranz, J.A., Ginjaar, H.B., Cuenca-Leon, E., Corominas, R., Roig, M., and Cormand, B. (2005). Molybdenum cofactor deficiency presenting as neonatal hyperekplexia: a clinical, biochemical and genetic study. Neuropediatrics *36*, 389-394.

Mahler, H.R., Mackler, B., and Green, D.E. (1954). Studies on metalloflavoproteins. III. Aldehyde oxidase: a molybdoflavoprotein. J Biol Chem *210*, 465-480.

Maklad, A., Conway, M., Hodges, C., and Hansen, L.A. (2010). Development of innervation to maxillary whiskers in mice. Anat Rec (Hoboken) *293*, 1553-1567.

Matthies, A., Rajagopalan, K.V., Mendel, R.R., and Leimkuhler, S. (2004). Evidence for the physiological role of a rhodanese-like protein for the biosynthesis of the molybdenum cofactor in humans. Proc Natl Acad Sci U S A *101*, 5946-5951.

McLaughlin, S.K., Collis, P., Hermonat, P.L., and Muzyczka, N. (1988). Adeno-associated virus general transduction vectors: analysis of proviral structures. J Virol *62*, 1963-1973.

McManaman, J.L., Palmer, C.A., Wright, R.M., and Neville, M.C. (2002). Functional regulation of xanthine oxidoreductase expression and localization in the mouse mammary gland: evidence of a role in lipid secretion. J Physiol *545*, 567-579.

Mechler, K., Mountford, W.K., Hoffmann, G.F., and Ries, M. (2015). Ultra-orphan diseases: a quantitative analysis of the natural history of molybdenum cofactor deficiency. Genet Med.

Meikar, O., Da Ros, M., Korhonen, H., and Kotaja, N. (2011). Chromatoid body and small RNAs in male germ cells. Reproduction *142*, 195-209.

Mendel, R.R. (2013). The molybdenum cofactor. J Biol Chem *288*, 13165-13172.

Mendel, R.R., and Bittner, F. (2006). Cell biology of molybdenum. Biochim Biophys Acta *1763*, 621-635.

Merten, O.W., Geny-Fiamma, C., and Douar, A.M. (2005). Current issues in adeno-associated viral vector production. Gene Ther *12 Suppl 1*, S51-61.

Miao, C.H., Snyder, R.O., Schowalter, D.B., Patijn, G.A., Donahue, B., Winther, B., and Kay, M.A. (1998). The kinetics of rAAV integration in the liver. Nat Genet *19*, 13-15.

Mingozzi, F., and High, K.A. (2007). Immune responses to AAV in clinical trials. Curr Gene Ther *7*, 316-324.

Mingozzi, F., and High, K.A. (2013). Immune responses to AAV vectors: overcoming barriers to successful gene therapy. Blood *122*, 23-36.

Miranda, M., Rigueira, L., Suarez, M.L., Carbajales, P., Moure, P., Fidalgo, L.E., Failde, D., and Vazquez, S. (2010). Xanthine nephrolithiasis in a galician blond beef calf. J Vet Med Sci *72*, 921-923.

Miyazaki, M., Obata, Y., Abe, K., Furusu, A., Koji, T., Tabata, Y., and Kohno, S. (2006). Gene transfer using nonviral delivery systems. Perit Dial Int *26*, 633-640.

Moriwaki, Y., Yamamoto, T., Takahashi, S., Tsutsumi, Z., and Hada, T. (2001). Widespread cellular distribution of aldehyde oxidase in human tissues found by immunohistochemistry staining. Histol Histopathol *16*, 745-753.

Moss, R.B., Rodman, D., Spencer, L.T., Aitken, M.L., Zeitlin, P.L., Waltz, D., Milla, C., Brody, A.S., Clancy, J.P., Ramsey, B., Hamblett, N., and Heald, A.E. (2004). Repeated adeno-associated virus serotype 2 aerosol-mediated cystic fibrosis transmembrane regulator gene transfer to the lungs of patients with cystic fibrosis: a multicenter, double-blind, placebo-controlled trial. Chest *125*, 509-521.

Mulligan, R.C. (1993). The basic science of gene therapy. Science *260*, 926-932.

Nakai, H., Montini, E., Fuess, S., Storm, T.A., Grompe, M., and Kay, M.A. (2003). AAV serotype 2 vectors preferentially integrate into active genes in mice. Nat Genet *34*, 297-302.

Nakai, H., Yant, S.R., Storm, T.A., Fuess, S., Meuse, L., and Kay, M.A. (2001). Extrachromosomal recombinant adeno-associated virus vector genomes are primarily responsible for stable liver transduction in vivo. J Virol *75*, 6969-6976.

Nichols, J., and Rajagopalan, K.V. (2002). Escherichia coli MoeA and MogA. Function in metal incorporation step of molybdenum cofactor biosynthesis. J Biol Chem *277*, 24995-25000.

Niemeyer, G.P., Herzog, R.W., Mount, J., Arruda, V.R., Tillson, D.M., Hathcock, J., van Ginkel, F.W., High, K.A., and Lothrop, C.D., Jr. (2009). Long-term correction of inhibitor-prone hemophilia B dogs treated with liver-directed AAV2-mediated factor IX gene therapy. Blood *113*, 797-806.

Nonnenmacher, M., and Weber, T. (2012). Intracellular transport of recombinant adeno-associated virus vectors. Gene Ther *19*, 649-658.

Ohtsubo, T., Matsumura, K., Sakagami, K., Fujii, K., Tsuruya, K., Noguchi, H., Rovira, II, Finkel, T., and Iida, M. (2009). Xanthine oxidoreductase depletion induces renal interstitial fibrosis through aberrant lipid and purine accumulation in renal tubules. Hypertension *54*, 868-876.

Ohtsubo, T., Rovira, II, Starost, M.F., Liu, C., and Finkel, T. (2004). Xanthine oxidoreductase is an endogenous regulator of cyclooxygenase-2. Circ Res *95*, 1118-1124.

Ott, G., Havemeyer, A., and Clement, B. (2014). The mammalian molybdenum enzymes of mARC. J Biol Inorg Chem.

Papadakis, E.D., Nicklin, S.A., Baker, A.H., and White, S.J. (2004). Promoters and control elements: designing expression cassettes for gene therapy. Curr Gene Ther *4*, 89-113.

Pereira, D.J., McCarty, D.M., and Muzyczka, N. (1997). The adeno-associated virus (AAV) Rep protein acts as both a repressor and an activator to regulate AAV transcription during a productive infection. J Virol *71*, 1079-1088.

Peretz, H., Naamati, M.S., Levartovsky, D., Lagziel, A., Shani, E., Horn, I., Shalev, H., and Landau, D. (2007). Identification and characterization of the first mutation (Arg776Cys) in the C-terminal domain of the Human Molybdenum Cofactor Sulfurase (HMCS) associated with type II classical xanthinuria. Mol Genet Metab *91*, 23-29.

Prokop, A., and Davidson, J.M. (2007). Principles of Tissue Engineering (Third Edition). In: Gene delivery into cells and tissues, ed. R.L.a.J.V. Robert Lanza.

Pryde, D.C., Dalvie, D., Hu, Q., Jones, P., Obach, R.S., and Tran, T.D. (2010). Aldehyde oxidase: an enzyme of emerging importance in drug discovery. J Med Chem *53*, 8441-8460.

Qing, K., Mah, C., Hansen, J., Zhou, S., Dwarki, V., and Srivastava, A. (1999). Human fibroblast growth factor receptor 1 is a co-receptor for infection by adeno-associated virus 2. Nat Med *5*, 71-77.

Rabinowitz, J.E., and Samulski, R.J. (2000). Building a better vector: the manipulation of AAV virions. Virology *278*, 301-308.

Rajagopalan, K.V., and Johnson, J.L. (1992). The pterin molybdenum cofactors. J Biol Chem *267*, 10199-10202.

Reeves, S.A., Helman, L.J., Allison, A., and Israel, M.A. (1989). Molecular cloning and primary structure of human glial fibrillary acidic protein. Proc Natl Acad Sci U S A *86*, 5178-5182.

Reiss, J., Bonin, M., Schwegler, H., Sass, J.O., Garattini, E., Wagner, S., Lee, H.J., Engel, W., Riess, O., and Schwarz, G. (2005). The pathogenesis of molybdenum cofactor deficiency, its delay by maternal clearance, and its expression pattern in microarray analysis. Mol Genet Metab *85*, 12-20.

Reiss, J., Cohen, N., Dorche, C., Mandel, H., Mendel, R.R., Stallmeyer, B., Zabot, M.T., and Dierks, T. (1998). Mutations in a polycistronic nuclear gene associated with molybdenum cofactor deficiency. Nat Genet *20*, 51-53.

Reiss, J., Dorche, C., Stallmeyer, B., Mendel, R.R., Cohen, N., and Zabot, M.T. (1999). Human molybdopterin synthase gene: genomic structure and mutations in molybdenum cofactor deficiency type B. Am J Hum Genet *64*, 706-711.

Reiss, J., and Hahnewald, R. (2011). Molybdenum cofactor deficiency: Mutations in GPHN, MOCS1, and MOCS2. Hum Mutat *32*, 10-18.

Reiss, J., and Johnson, J.L. (2003). Mutations in the molybdenum cofactor biosynthetic genes MOCS1, MOCS2, and GEPH. Hum Mutat *21*, 569-576.

Riario-Sforza, G., Carcassi, A., Bayeli, P.F., Marcolongo, R., Marinello, E., and Montagnani, M. (1969). [Xanthine oxidase activity in the jejunal mucosa of patients with gout]. Boll Soc Ital Biol Sper *45*, 785-786.

Robertson, G., Garrick, D., Wu, W., Kearns, M., Martin, D., and Whitelaw, E. (1995). Position-dependent variegation of globin transgene expression in mice. Proc Natl Acad Sci U S A *92*, 5371-5375.

Roncal Jimenez, C.A., Ishimoto, T., Lanaspa, M.A., Rivard, C.J., Nakagawa, T., Ejaz, A.A., Cicerchi, C., Inaba, S., Le, M., Miyazaki, M., Glaser, J., Correa-Rotter, R., Gonzalez, M.A., Aragon, A., Wesseling, C., Sanchez-Lozada, L.G., and Johnson, R.J. (2014). Fructokinase activity mediates dehydration-induced renal injury. Kidney Int *86*, 294-302.

Rudolph, M.J., Johnson, J.L., Rajagopalan, K.V., and Kisker, C. (2003). The 1.2 A structure of the human sulfite oxidase cytochrome b(5) domain. Acta Crystallogr D Biol Crystallogr *59*, 1183-1191.

Rutter, N. (2000). Clinical consequences of an immature barrier. Semin Neonatol *5*, 281-287.

Sagi, M., Scazzocchio, C., and Fluhr, R. (2002). The absence of molybdenum cofactor sulfuration is the primary cause of the flacca phenotype in tomato plants. Plant J *31*, 305-317.

Samulski, R.J., Sally, M., and N., M. (1999). Development of Human Gene Therapy. In: Adeno-associated viral vectors.

Sanger, F., and Coulson, A.R. (1975). A rapid method for determining sequences in DNA by primed synthesis with DNA polymerase. J Mol Biol *94*, 441-448.

Sanlioglu, S., Benson, P.K., Yang, J., Atkinson, E.M., Reynolds, T., and Engelhardt, J.F. (2000). Endocytosis and nuclear trafficking of adeno-associated virus type 2 are controlled by rac1 and phosphatidylinositol-3 kinase activation. J Virol *74*, 9184-9196.

Sarnesto, A., Linder, N., and Raivio, K.O. (1996). Organ distribution and molecular forms of human xanthine dehydrogenase/xanthine oxidase protein. Lab Invest *74*, 48-56.

Schwarz, G., Santamaria-Araujo, J.A., Wolf, S., Lee, H.J., Adham, I.M., Grone, H.J., Schwegler, H., Sass, J.O., Otte, T., Hanzelmann, P., Mendel, R.R., Engel, W., and Reiss, J. (2004). Rescue of lethal molybdenum cofactor deficiency by a biosynthetic precursor from Escherichia coli. Hum Mol Genet *13*, 1249-1255.

Sever, S., Damke, H., and Schmid, S.L. (2000). Dynamin:GTP controls the formation of constricted coated pits, the rate limiting step in clathrin-mediated endocytosis. J Cell Biol *150*, 1137-1148.

Sharma, R., Khajuria, R., Sharma, C.L., Kapoor, B., Goswami, K.C., and Kohli, K. (2004). Gene Therapy: Current Concepts. JK Science *6*.

Simonelli, F., Maguire, A.M., Testa, F., Pierce, E.A., Mingozzi, F., Bennicelli, J.L., Rossi, S., Marshall, K., Banfi, S., Surace, E.M., Sun, J., Redmond, T.M., Zhu, X., Shindler, K.S., Ying, G.S., Ziviello, C., Acerra, C., Wright, J.F., McDonnell, J.W., High, K.A., Bennett, J., and Auricchio, A. (2010). Gene therapy for Leber's congenital amaurosis is safe and effective through 1.5 years after vector administration. Mol Ther *18*, 643-650.

Sims, N.R., and Zaidan, E. (1995). Biochemical changes associated with selective neuronal death following short-term cerebral ischaemia. Int J Biochem Cell Biol *27*, 531-550.

Smith, G.S., Walford, R.L., and Mickey, M.R. (1973). Lifespan and incidence of cancer and other diseases in selected long-lived inbred mice and their F 1 hybrids. J Natl Cancer Inst *50*, 1195-1213.

Smuda, J.W., and Carter, B.J. (1991). Adeno-associated viruses having nonsense mutations in the capsid genes: growth in mammalian cells containing an inducible amber suppressor. Virology *184*, 310-318.

Sonntag, F., Bleker, S., Leuchs, B., Fischer, R., and Kleinschmidt, J.A. (2006). Adeno-associated virus type 2 capsids with externalized VP1/VP2 trafficking domains are generated prior to passage through the cytoplasm and are maintained until uncoating occurs in the nucleus. J Virol *80*, 11040-11054.

Stallmeyer, B., Drugeon, G., Reiss, J., Haenni, A.L., and Mendel, R.R. (1999). Human molybdopterin synthase gene: identification of a bicistronic transcript with overlapping reading frames. Am J Hum Genet *64*, 698-705.

Summerford, C., Bartlett, J.S., and Samulski, R.J. (1999). AlphaVbeta5 integrin: a co-receptor for adeno-associated virus type 2 infection. Nat Med *5*, 78-82.

Summerford, C., and Samulski, R.J. (1998). Membrane-associated heparan sulfate proteoglycan is a receptor for adeno-associated virus type 2 virions. J Virol *72*, 1438-1445.

Szymczak, A.L., and Vignali, D.A. (2005). Development of 2A peptide-based strategies in the design of multicistronic vectors. Expert Opin Biol Ther *5*, 627-638.

Tan, W.H., Eichler, F.S., Hoda, S., Lee, M.S., Baris, H., Hanley, C.A., Grant, P.E., Krishnamoorthy, K.S., and Shih, V.E. (2005). Isolated sulfite oxidase deficiency: a case report with a novel mutation and review of the literature. Pediatrics *116*, 757-766.

Tejada-Jimenez, M., Galvan, A., and Fernandez, E. (2011). Algae and humans share a molybdate transporter. Proc Natl Acad Sci U S A *108*, 6420-6425.

Tejada-Jimenez, M., Llamas, A., Sanz-Luque, E., Galvan, A., and Fernandez, E. (2007). A high-affinity molybdate transporter in eukaryotes. Proc Natl Acad Sci U S A *104*, 20126-20130.

Terao, M., Kurosaki, M., Demontis, S., Zanotta, S., and Garattini, E. (1998). Isolation and characterization of the human aldehyde oxidase gene: conservation of intron/exon boundaries with the xanthine oxidoreductase gene indicates a common origin. Biochem J *332 (Pt 2)*, 383-393.

Teschner, J., Lachmann, N., Schulze, J., Geisler, M., Selbach, K., Santamaria-Araujo, J., Balk, J., Mendel, R.R., and Bittner, F. (2010). A novel role for Arabidopsis mitochondrial ABC transporter ATM3 in molybdenum cofactor biosynthesis. Plant Cell *22*, 468-480.

Tomatsu, H., Takano, J., Takahashi, H., Watanabe-Takahashi, A., Shibagaki, N., and Fujiwara, T. (2007). An Arabidopsis thaliana high-affinity molybdate transporter required for efficient uptake of molybdate from soil. Proc Natl Acad Sci U S A *104*, 18807-18812.

Torres-Torronteras, J., Viscomi, C., Cabrera-Perez, R., Camara, Y., Di Meo, I., Barquinero, J., Auricchio, A., Pizzorno, G., Hirano, M., Zeviani, M., and Marti, R. (2014). Gene therapy using a liver-targeted AAV vector restores nucleoside and nucleotide homeostasis in a murine model of MNGIE. Mol Ther *22*, 901-907.

Tratschin, J.D., Miller, I.L., and Carter, B.J. (1984). Genetic analysis of adeno-associated virus: properties of deletion mutants constructed in vitro and evidence for an adeno-associated virus replication function. J Virol *51*, 611-619.

Tsuchida, S., Kagi, A., Koyama, H., and Tagawa, M. (2007). Xanthine urolithiasis in a cat: a case report and evaluation of a candidate gene for xanthine dehydrogenase. J Feline Med Surg *9*, 503-508.

Tullus, K. (2015). Vesicoureteric reflux in children. Lancet *385*, 371-379.

Turturro, A., Duffy, P., Hass, B., Kodell, R., and Hart, R. (2002). Survival characteristics and age-adjusted disease incidences in C57BL/6 mice fed a commonly used cereal-based diet modulated by dietary restriction. J Gerontol A Biol Sci Med Sci *57*, B379-389.

van der Knaap, M.S., and Valk, J. (2005). Magnetic Resonance of Myelination and Myelin Disorders.

van Zuilen, C.D., Nickel, R.F., van Dijk, T.H., and Reijngoud, D.J. (1997). Xanthinuria in a family of Cavalier King Charles spaniels. Vet Q *19*, 172-174.

Veldman, A., Santamaria-Araujo, J.A., Sollazzo, S., Pitt, J., Gianello, R., Yaplito-Lee, J., Wong, F., Ramsden, C.A., Reiss, J., Cook, I., Fairweather, J., and Schwarz, G. (2010). Successful treatment of molybdenum cofactor deficiency type A with cPMP. Pediatrics *125*, e1249-1254.

Vorbach, C., Scriven, A., and Capecchi, M.R. (2002). The housekeeping gene xanthine oxidoreductase is necessary for milk fat droplet enveloping and secretion: gene sharing in the lactating mammary gland. Genes Dev *16*, 3223-3235.

Wahl, B., Reichmann, D., Niks, D., Krompholz, N., Havemeyer, A., Clement, B., Messerschmidt, T., Rothkegel, M., Biester, H., Hille, R., Mendel, R.R., and Bittner, F. (2010). Biochemical and spectroscopic characterization of the human mitochondrial amidoxime reducing components hmARC-1 and hmARC-2 suggests the existence of a new molybdenum enzyme family in eukaryotes. J Biol Chem *285*, 37847-37859.

Wang, L., Figueredo, J., Calcedo, R., Lin, J., and Wilson, J.M. (2007). Cross-presentation of adeno-associated virus serotype 2 capsids activates cytotoxic T cells but does not render hepatocytes effective cytolytic targets. Hum Gene Ther *18*, 185-194.

Wegner, W. (2007). Molekulare Charakterisierung der Molybdän-Cofaktor-Defizienz vom Typ B. Master thesis, Georg-August University, Goettingen.

Westerlinck, H., Meylaerts, L., Van Hoestenberghe, M.R., and Rossi, A. (2014). Sulfite oxidase deficiency in a newborn. JBR-BTR *97*, 113-114.

Wiese, S., Gronemeyer, T., Ofman, R., Kunze, M., Grou, C.P., Almeida, J.A., Eisenacher, M., Stephan, C., Hayen, H., Schollenberger, L., Korosec, T., Waterham, H.R., Schliebs, W., Erdmann, R., Berger, J., Meyer, H.E., Just, W., Azevedo, J.E., Wanders, R.J., and Warscheid, B. (2007). Proteomics characterization of mouse kidney peroxisomes by tandem mass spectrometry and protein correlation profiling. Mol Cell Proteomics *6*, 2045-2057.

Williams, J.N., Jr. (1952). Intracellular distribution of betaine aldehyde oxidase. J Biol Chem *195*, 37-41.

Witting, A., Muller, P., Herrmann, A., Kettenmann, H., and Nolte, C. (2000). Phagocytic clearance of apoptotic neurons by Microglia/Brain macrophages in vitro: involvement of lectin-, integrin-, and phosphatidylserine-mediated recognition. J Neurochem *75*, 1060-1070.

Woo, W.H., Yang, H., Wong, K.P., and Halliwell, B. (2003). Sulphite oxidase gene expression in human brain and in other human and rat tissues. Biochem Biophys Res Commun *305*, 619-623.

Wrenn, J.T., and Wessells, N.K. (1984). The early development of mystacial vibrissae in the mouse. J Embryol Exp Morphol *83*, 137-156.

Wright, J.F. (2009). Transient transfection methods for clinical adeno-associated viral vector production. Hum Gene Ther *20*, 698-706.

Xiong, L., Ishitani, M., Lee, H., and Zhu, J.K. (2001). The Arabidopsis LOS5/ABA3 locus encodes a molybdenum cofactor sulfurase and modulates cold stress- and osmotic stress-responsive gene expression. Plant Cell *13*, 2063-2083.

Yan, Z., Yan, H., and Ou, H. (2012). Human thyroxine binding globulin (TBG) promoter directs efficient and sustaining transgene expression in liver-specific pattern. Gene *506*, 289-294.

Young, S.M., Jr., McCarty, D.M., Degtyareva, N., and Samulski, R.J. (2000). Roles of adeno-associated virus Rep protein and human chromosome 19 in site-specific recombination. J Virol *74*, 3953-3966.

Zaiss, A.K., Liu, Q., Bowen, G.P., Wong, N.C., Bartlett, J.S., and Muruve, D.A. (2002). Differential activation of innate immune responses by adenovirus and adeno-associated virus vectors. J Virol *76*, 4580-4590.

Zhang, B., Penagaricano, F., Driver, A., Chen, H., and Khatib, H. (2011). Differential expression of heat shock protein genes and their splice variants in bovine preimplantation embryos. J Dairy Sci *94*, 4174-4182.

Zhang, X., Vincent, A.S., Halliwell, B., and Wong, K.P. (2004). A mechanism of sulfite neurotoxicity: direct inhibition of glutamate dehydrogenase. J Biol Chem *279*, 43035-43045.

Zhang, Y., and Gladyshev, V.N. (2008). Molybdoproteomes and evolution of molybdenum utilization. J Mol Biol *379*, 881-899.

ACKNOWLEDGEMENTS

CURRICULUM VITAE

Personal details

Name: Joanna Jakubiczka-Smorag

Date of birth: 23rd June 1984

Place of birth: Czestochowa, Poland

Nationality: Polish

Educational background

1991-1999   Primary School Czestochowa, Poland

1999-2003   Secondary School Czestochowa, Poland

2003-2008   Studies of Biology, Faculty of Biology and Earth Sciences at the Jagiellonian University in Krakow, Poland

                          Master of Science study in Genetics and Biology of Reproduction, Faculty of Biology and Earth Sciences at the Jagiellonian University in Krakow, Poland

                          Master Thesis at the Department of Endocrinology, Faculty of Biology and Earth Sciences at the Jagiellonian University in Krakow, Poland

2011-2015   Experimental studies for the doctoral thesis in the Institute of Human Genetics at the Georg-August University in Göttingen, Germany